COUPLED HEAT AND MASS TRANSFER IN CONCRETE EXPOSED TO FIRE

BAHJAT HUSAYN KHALAFALLAH

Doctor of Philosophy

THE UNIVERSITY OF ASTON IN BIRMINGHAM

March 2001

THE UNIVERSITY OF ASTON IN BIRMINGHAM

COUPLED HEAT AND MASS TRANSFER IN CONCRETE EXPOSED TO FIRE

Bahjat Husayn Khalafallah, BEng, MSc, MPhil

Thesis submitted for the degree of Doctor of Philosophy, 2001

SUMMARY

Spalling can be a very serious problem that occurs on concrete members in fires. The mechanisms proposed to explain spalling suggest that it is due to thermal stresses, high pore pressures, or both. As far as high pore pressures are concerned, several mathematical models have been developed, but the computed pressures show large variations. The reason is that some of the assumptions adopted are questionable. In particular, the very occurrence of diffusion of water vapour in concrete has been debateable. Also, due to the lack of a diffusivity equation that is specific for heated concrete, researchers who consider diffusion either assume that the diffusivities of vapour and air are constant or use molecular diffusivity equations the appropriateness of which for concrete is questionable.

The first investigation of this study is concerned with the reasonableness of the assumptions related to diffusion of water vapour in concrete and with the development of a diffusivity equation for heated concrete. It has been demonstrated that diffusion of water vapour does occur in concrete at all temperatures and that the type of diffusion in concrete is Knudsen diffusion. Neglecting diffusion leads to underestimating the pressure. It results in a maximum pore pressure of less than 1 MPa. It has also been shown that the assumption that diffusion in concrete is molecular is unreasonable even when the tortuosity is considered. Molecular diffusivity leads to overestimating the pressure. It results in a maximum pore pressure of 2.7 MPa of which the vapour pressure is 1.5 MPa while the air pressure is 1.2 MPa. Also, the first diffusivity equation, appropriately named 'concrete diffusivity', has been developed specifically for concrete that determines the effective diffusivity of any gas in concrete at any temperature. In thick walls and columns exposed to fire, concrete diffusivity leads to maximum pore pressures of 1.5 and 2.2 MPa (along diagonals), respectively, that are almost entirely due to water vapour pressure.

Also, spalling is exacerbated, and thus higher pressures may occur, in thin heated sections, since there is less of a cool reservoir towards which vapour can migrate. Furthermore, the reduction of the cool reservoir is affected not only by the thickness, but also by the time of exposure to fire and by the type of exposure, i.e. whether the concrete member is exposed to fire from one or more sides.

The second investigation is concerned with examining the effects of thickness and exposure time and type. It has been demonstrated that the build up of pore pressure is low in thick members, since there is a substantial cool zone towards which water vapour can migrate. Thus, if surface and/or explosive spalling occur on a thick member, then such spalling must be due to high thermal stresses, but corner spalling is likely to be pore pressure spalling. However, depending on the exposure time and type, the pore pressures can be more than twice those occurring in thick members and thought to be the maximum that can occur so far, and thus the enhanced propensity of pore pressure spalling occurring on thin sections heated on opposite sides has been conclusively demonstrated to be due to the lack of a cool zone towards which moisture can migrate. Expressions were developed for the determination of the maximum pore pressures that can occur in different concrete walls and columns exposed to fire and of the corresponding times of exposure.

Keywords: Concrete, Heat, Mass, Diffusion, Molecular, Knudsen, Thin, Fire, Pressure, Spalling.

To my Mother

ACKNOWLEDGEMENTS

I would like to thank my Supervisors, and indeed friends, Dr. J.A. Purkiss and Dr. L.Y. Li for their continuous help, invaluable advice, patience, and exceptional support without which it would have been much more difficult to complete this research.

I also thank King Abdulaziz University for giving me the opportunity to undertake this research, and for the financial, and personal, support. In particular, I would like to thank Professor F.F. Wafa of the Civil Engineering Department at KAU for his continuous support.

I would also like to express my thanks and deepest gratitude to Mr. A.M. Al-Nasser, the Saudi Arabian Cultural Attaché in the UK, for his invaluable, and unforgettable, support. Without his support, this research would not have been undertaken in the first place.

Thanks also to Dr. R.T. Tenchev for his support and for being a friend. I also thank my friend and officemate Y. Wang for his friendship. These two dear friends have made the work more enjoyable and less stressful.

Finally, thanks to everyone who helped or cared.

CONTENTS

PAGE

NOTATIONS

A constant equals to 0.6323 (noncarbonated material) and 0.2968 (carbonated material)

a permeability, in m/s;

concrete section thickness, in mm

C BET-constant;

heat capacity of concrete (per kilogram of concrete) including the chemically bound water, but excluding the free water

C_a heat of sorption of free water (per kilogram of free water)

C_i specific heat of phase i, in J/kg °C, where $i = a, v, s, l$

C_w mass density and heat capacity of bulk (liquid) water

c mass of anhydrous cement per m^3 of concrete

D molecular or Knudsen diffusivity in the gaseous phase, in m^2/s;

molecular diffusivity of water vapour and air through each other, in m^2/s

D_{AB} molecular diffusivity of gas A through gas B, in m^2/s

D_{av} molecular diffusivity of air through water vapour in the gaseous mixture, in m^2/s

D_{Conc} concrete diffusivity, in m^2/s

D'_{Conc} partial concrete diffusivity, in m^2/s

D_e effective (or totally effective) molecular or Knudsen diffusivity ($= \varepsilon_g D / \tau$), in m^2/s

D'_e partially effective molecular or Knudsen diffusivity ($= D / \tau$), in m^2/s

D_{e,CO_2} effective diffusivity of CO_2 in concrete at ambient temperature, in m^2/s

$D_{e,VA}$ effective molecular diffusivity of water vapour through air, in m^2/s

D_{Kn} Knudsen diffusivity, in m^2/s

D_{va} molecular diffusivity of water vapour through air in the gaseous mixture, in m^2/s, ($D_{va} = D_{av}$)

d pore diameter, in m, μm, or Å

d_k Kelvin diameter, in μm

d_m mean pore diameter, in Å

d_w molecular diameter of water, in μm

$\dot{E}$ rate of evaporation of free water per unit volume of concrete, in kg/m^3s

g the acceleration of gravity (= 9.806 m/s^2)

h humidity ($= P \leq P_s(T)$)

h_c transition humidity (= 0.75)

J moisture flux per unit volume of concrete, in kg/m^{3}s

J_i mass flux of phase i per unit area of concrete, in kg/m^{2}s, where $i = a, v, l$

K intrinsic permeability of dry concrete, in m^2

K_i relative permeability of phase i through dry concrete, in %, where $i = g, l$

Kn Knudsen number ($= \lambda / d$), dimensionless

k Boltzmann constant (= 1.38×10^{-23} kg-m^2/s^2-°K)

k_i thermal conductivity of phase i, in J/m^{2}s°C/m, where $i = a, v, s, l$

M_i molecular weight (or molar mass) of species i, in kg/kmol

m molecular mass, in kg

n molecular concentration

P pore water pressure, in Pa;

pressure, in Pa or atm

P_g pressure of a binary gaseous mixture, in Pa

P_i partial pressure of phase i, in Pa, where $i = a, v$;

pressure of phase i, in Pa, where $i = g, l$

P_{or} porosity, in %

P_s, P_{sat} saturation pressure of water vapour, in Pa

Q obstruction factor ($= \varepsilon_s / \tau$);

activation energy for water migration along the adsorption layers in the necks

R universal gas constant

R_i gas constant of phase i, in J/kg°K, where $i = a, v$

RH ambient relative humidity, in %

S saturation (=volume of free liquid water/porosity), in %

T temperature, in °C or °K

T_0 = 25°C

t_{crit} critical time at which the cool zone is eliminated, in min

t_{max} maximum time at which the very maximum pore pressure occurs, in min

v molecular velocity, in m/s

v_i velocity of phase i, in m/s, where $i = g, l$

w mass of free liquid water, in kg/m^3;

thickness of film of free water covering the wall of a pore, in μm

x RH/100

ε_i volume fraction of phase i per unit volume of concrete, in %, where $i = s,l,g.d$:

volume fraction of phase i per unit volume of the gaseous mixture, in %, where $i = a.v$

ε_p porosity of the paste

ε_s surface porosity of the porous medium

λ mean free path, in m or Å

λ_D specific heat of dehydration of bound water, in J/kg

λ_E specific heat of evaporation, in J/kg

μ_i dynamic viscosity of phase i, in kg/ms, where $i = a,v,g,l$

ρ_i density of phase i, in kg/m^3, where $i = s,l$;

mass of phase i per unit volume of the gaseous mixture, in kg/m^3, where $i = a,v$

ρ_{cem} mass of anhydrous cement per unit volume of concrete, in kg/m^3

$\overline{\rho C}$ effective heat capacity of concrete, in J/m^3 °C

$\overline{\rho Cv}$ vector of energy transport by fluid flow, in J/m^{2}s°C

σ Stefan Boltzman constant, in W/m^{2}K^4

σ_i collision diameter of species i, in Å, where $i = 1,2$

σ_{12} arithmetic average of the collision diameters of the species present, in Å

Ω collision integral, dimensionless

τ tortuosity

Subscripts

a air phase in the gaseous mixture

d dehydrated water phase

g phase of the gaseous mixture of water vapour and air

l free liquid water phase

v water vapour phase in the gaseous mixture

∞ environment

Left Superscript

0 initial condition at ambient temperature

CHAPTER 1

INTRODUCTION

1.1 FIRE SAFETY

Purkiss (1996) suggested that an acceptable definition of fire safety engineering could be taken as *'the application of scientific and engineering principles to the effects of fire in order to reduce the loss of life and damage to property by quantifying the risks and hazards involved and to provide an optimal solution to the application of preventive or protective measures'*.

The largest area of risk from fire damage is low-rise domestic housing that does not require sophisticated design methods, since the problem is not due to structural collapse but the spread of smoke and toxic gases and the resulting inability of the occupants to escape (Malhotra, 1987). Also, Purkiss reported that, within the UK for a long period, there have been very few, if any, recorded cases of death of the occupants in a fire caused directly by the collapse of the structure. Nevertheless, this relatively low incidence of deaths resulting from collapse does not imply that structural integrity is unimportant.

In fire safety engineering, the considerations to be dealt with can be assigned to two categories: active and passive provisions (Malhotra, 1986). The active provisions include provision of alarm systems, provision of smoke control systems, provision of in-built fire-fighting of fire control systems, control of hazardous contents, provision of access for external fire-fighting, and provision of fire safety management system. The passive measures are adequate compartmentation, control of flammability of the structure fabric, provision of fixed escape routes, and provision of adequate structural performance. Of course, the structural engineer's area of concern is the provision of adequate structural performance, or structural fire safety engineering.

Purkiss discussed the elements within the discipline of fire safety engineering that relate both to life safety and property safety. He identified the following key areas:

1) **Control of ignition.** Ignition can be controlled by:

(a) Controlling the flammability of materials within the structure by ensuring that materials used in the finishes are such that flammability is limited, ensuring that materials used in the contents of the structure produce a minimum hazard, and maintenance of the structure fabrics and finishes.

(b) Control of growth of fire by the use of vertical or horizontal fire compartments such that there is no possible route for smoke or flame through the compartment boundary.

(c) Fire safety management such as setting up procedures to ensure that all occupants are aware of the proper procedures in the event of a fire and banning smoking or naked flames.

2) **Control of means of escape.** Measures to control the means of escape can be forced by imposing statutory requirements for the provision of escape routing based on the maximum length of escape route, number of fire-escapes, and dimensions of escape routes, and by educating the occupants to respond to the warnings.

3) **Detection and control of the fire.** This can be done by ensuring the installation of systems for detection, which may be manual, automatic, or a combination of these, at the earliest possible stage, and control of the fire. Also, it is necessary to ensure clear visibility by controlling the build up of smoke either by forced venting or smoke curtains.

4) **Control of spread of fire.** Control of the spread of fire within a building may be achieved by in-built features, such as compartmentation, or by mechanical means, such as venting, smoke screens, or sprinklers. Control of the spread of fire between structures is done by controlling the lateral spacing between buildings.

5) **Prevention of structure collapse.** This area covers the imposition of stability and integrity on the structure as a whole or in part during a fire. Of course, there must be no total collapse of the structure during the evacuation stage nor, preferably, during the fire-fighting stage. Since the escape routes either to protected staircases or directly out of the building are designed to permit complete evacuation in about 2.5 minutes, evacuation should be relatively fast. However, there should be a sufficiently long period before the structure shows any sign of collapse, since fire-fighting may extend over a substantial period.

There are two approaches to avoid collapse of the structure before a given period, conventionally defined as the fire resistance of the structure: the passive and the active approaches. The passive approach is to design the structure such that, despite being weakened and deformable, it can sustain a reasonable level of applied load for the whole period. The active approach is to design measures to ensure that the fire is contained or that temperatures do not reach a level that will cause mechanical distress to the structure. A structure is designed to have both approaches operative. as the two systems are interdependent, and one can be used to reduce or modify the needs of the other.

Spalling of concrete in fires can be a very serious problem that affects the stability and integrity of concrete structures, and thus is a major factor in determining the fire resistance of these structures. It is a natural phenomenon whereby forces are generated within a concrete's body that cause disintegration of its surface, and involves the breaking up and dislodging, often violently, of particles or lumps of various sizes from the surface (Connolly, 1995). The consequences of spalling depend on the application. For example, in most applications, aggregate spalling (Section 1.2) may be an insignificant form of surface damage. Nevertheless, it is a major problem in concrete pavements used for military aircrafts (Austin *et al.*, 1992). All forms of spalling may result in reducing the period of fire resistance of a concrete member in fire. Spalling may lead to loss of load-bearing capacity and/or loss of integrity, and thus to fire resistance failure.

Spalling may lead to the loss of load-bearing capacity, since it may reduce the cross-sectional area of the concrete member to such an extent that it cannot sustain the imposed compressive stresses. Load-bearing failure may also occur when spalling of the concrete cover to the reinforcement occurs, which leads to the reinforcement reaching excessive temperatures, and thus to reducing the yield strength of steel that may result in flexural failure of the concrete member. Connolly (1995) reported that this form of spalling failure is quite commonly found in practice, since tension in the extreme fibres governs the design of most members of concrete structures. Flexural failure may be enhanced by the loss of bond, and thus load-bearing failure may result from the loss of composite action. Connolly showed that explosive spalling may be sufficiently violent to blow holes through a concrete member, and reported that thin slabs are particularly susceptible to such integrity failure.

The crucial effect spalling has on the fire resistance of concrete columns using analytical methods was confirmed by Mustapha (1994). Based on the work of Anderberg (1976), Lie (1984), and Schneider (1986), Mustapha calculated the structural response of concrete columns in fire, and

found that the amount of spalling a column suffers is more critical in fire resistance determination than the patterns of heating and loading.

Connolly *et al.* (1994) showed that ignoring spalling could render mathematical models of heat and mass transfer in concrete members in fire useless, and thus argued that, while spalling remains unpredictable, fire engineering calculations and computerised simulations of fire resistance tests will not be reliable. They argued that, by ignoring the effects of spalling, it is possible that current models used to predict the fire resistance of concrete members may produce unsafe results.

The consequences of spalling are such that, in 1994, during the construction of the Storebaelt Tunnel in Denmark, the 400 mm thick tunnel lining that was designed to achieve the appropriate fire resistance rating was reduced to a mere 100 mm in places due to spalling that occurred when a fire in a boring machine exposed the concrete to severe heating (Bolton, 1994). On 18 November 1996, spalling due to a fire of 10 h duration in the Channel Tunnel destroyed 100-200 mm of the 450 mm concrete rings over a length of thousands of meters (Ulm *et al.*, 1999a and b).

1.2 SPALLING

1.2.1 Types of Spalling

Gary (1916) suggested that spalling could be grouped into four categories: aggregate, corner, surface, and explosive spalling.

1.2.1.1 Aggregate Spalling

Aggregate spalling, splitting, or flaking is the bursting or splitting of aggregates at the concrete's heated surface. It occurs on or near the heated surface within the first 20 minutes of exposure to fire. It causes blistering of the surface of heated concrete where split aggregate particles and some surrounding cement matrix are moved but not ejected. Gary suggested that splitting is due to mineralogical characteristics of aggregate. Dougill (1971) and Austin *et al.* (1992) attributed

aggregate spalling to thermal shock. Aggregate spalling neither removes large amounts of concrete nor exposes the reinforcement, and thus has little, if any, effect on the fire resistance.

1.2.1.2 Corner Spalling

Corner spalling is due to the gradual disintegration of heated concrete, and occurs at the arrises or corners of such concrete members as beams and columns. Due to its progressive nature, it is also called corner separation or sloughing-off. It occurs in the later stages of exposure to fire (after 30 minutes). Dougill (1971) and Malhotra (1984) attributed corner spalling to the loss of tensile strength of concrete at high temperatures. Concrete at the corners or arrises becomes weakened and cracked until bond failure occurs and the concrete cover to the reinforcement can no longer supports its self-weight. Thus, corner spalling removes relatively large amounts of concrete. Dougill and Sertmehemetoglu (1977) suggested that the coincidence of strains at the arrises or corners and the bursting effects of heated reinforcement are contributory factors. The curvature of members such as loaded beams can also be a contributing factor to the occurrence of corner spalling.

Corner spalling is serious, since it generally involves the removal of the concrete cover to the reinforcement, and thus can lead to global failure. Malhotra (1972) showed that provision of a supplementary reinforcing mesh within the depth of the concrete cover reduces the amount of concrete that may be lost by corner spalling.

1.2.1.3 Surface Spalling

Surface spalling is a violent form of spalling that involves dislodging of lumps of concrete of sizes up to 100× 100 mm. The depth of these lumps is in the order of 25 to 50 mm. Thus, surface spalling can lead to the exposure of the reinforcement to fire and can significantly affects the fire resistance. The severity of surface spalling can also be enhanced, since this type of spalling may occur progressively. Dougill (1971) suggested that surface spalling is due to bursting stresses (pore pressure) created by super-heated water vapour trapped beneath the surface. He referred to surface spalling as local destructive spalling. Shorter and Harmathy (1965) and Copier (1979) considered surface spalling as minor explosive spalling due to its violent nature and cracking sound.

1.2.1.4 Explosive Spalling

Explosive spalling is a very violent form of spalling that involves explosive failure of heated concrete. It is differentiated from surface spalling by its magnitude. Gary (1916) referred to explosive spalling as the bursting of entire surfaces of wall slabs up to 1 m^2, and observed the ejection of parts of concrete slabs up to 12 m. Explosive spalling is extremely dangerous, and is recognisable, since it is accompanied by a large release of energy. It may result in a sudden failure of the concrete member, and produces an explosive sound.

1.2.2 Theories of Spalling

Since 1935, when Hassenjaeger inferred that spalling of heated concrete could be attributed to the influence of thermal stresses or high pore pressures, the mechanism of explosive spalling has been debateable, but the mechanisms proposed have fallen into one or the other of these two categories; they suggest that it is due to either thermal stresses (Saito, 1965; Dougill, 1972; Bažant, 1997; Ulm *et al.*, 1999a and b), high pore pressures (Harmathy, 1965; Shorter and Harmathy, 1965; Akhtaruzzaman and Sullivan, 1970; Meyer-Ottens, 1972; Bažant and Thonguthai, 1979, Abdel-Rahman and Ahmed, 1996; Anderberg, 1997; Connolly, 1997), or both (Zhukov, 1975; 1994).

Saito attributed spalling to the surface compressive stresses that result from the non-uniform distribution of temperature exceeding the compressive strength of concrete. Saito' theory suggested that spalling would occur within 30 minutes of exposure to a standard BS 476:Part 20:1987 standard fire resistance test, which is in agreement with experimental observations. Imposition of load or prestress reduces the magnitude of the thermal stresses necessary to cause compressive failure. The test programmes of Nisugi *et al.* (1959), Ehm (1966), and England (1971) confirmed this fact. A serious shortcoming of Saito's theory is that it implies that spalling is more likely to occur in thicker sections, while Meyer-Ottens showed that spalling is less likely in these sections.

Dougill enhanced Saito's theory, and explained the observed behaviour of thick sections, by proposing that heating a concrete section is analogous to subjecting it to a BS:1881:Part 4:1970 tensile splitting test, that is designed to assess the tensile strength of concrete by subjecting it to compressive loading, in that the stress distribution is similar in both cases. He suggested that explosive spalling is similar to the failure that occurs when concrete specimens fail violently at

loads greater than those corresponding to the peak stress. Dougill explained why spalling is less likely in thick members by considering that the cool zone provides a stiff restraint to counterbalance the face stiffness loss, and thus maintains the overall stiffness of the member.

Predicting spalling based on thermal stresses is relatively simple; estimation of the magnitudes of these stresses may be made using elastic theory. Also, non-linear constitutive models have been investigated, and accurate models for estimating thermal stresses were developed. However, the theory contradicts experimental observations of the susceptibility of water-cured, low moisture, high strength, and thick sections.

On the other hand, many researchers proposed that, on heating concrete, high pore pressures develop within its water-containing pores that impose bursting stresses on the concrete. Shorter and Harmathy suggested that spalling due to thermal stresses is possible, but they proposed that spalling may be due to a different phenomenon called "moisture clog" spalling. The moisture clog is a fully saturated layer that may develop due to condensation of water vapour as it travels into the cooler zone. A well-defined front separates the dry and fully saturated zones, and migrates into the concrete as further evaporation of water takes place. The vapour developed at the front is prevented from travelling into the cooler depths due to the full saturation, and thus is acted upon by opposing forces of temperature and pressure gradients. Thus, high pore pressure develops at the evaporation front, and spalling takes place when the pore pressure exceeds the tensile strength of concrete.

Meyer-Ottens proposed that the bursting stresses that cause spalling are due to drag forces induced by the vapour travelling from the moisture clog to the heated surface. He suggested that the friction between the escaping vapour and pore walls subjects the concrete to a tensile stress. Like Shorter and Harmathy, Meyer-Ottens assumed that spalling occurs when this stress exceeds the tensile strength of concrete. Also, Akhtaruzzaman and Sullivan and Bažant and Thonguthai (1979) proposed that the tensile strength of concrete is the correct parameter against which pore pressure is to be compared. However, comparing stresses cannot be correct since, unlike the strength, the pressure is confined to the pores; forces should be compared.

Shorter and Harmathy and Meyer-Ottens also related the location of the moisture clog (evaporation front) to the 100°C isotherm regardless of the built-up pressure. However, the saturation temperature increases when the pressure increases; water starts boiling at 100°C only when the pressure is atmospheric (Abbot and Van Ness, 1976; McGovern, 1996; Çengel and Boles, 1998).

Evidently, thus, many researchers acknowledged the significance of pore pressures to the phenomenon of spalling; experimental attempts were carried out and several mathematical models were developed to predict the pressure. The significance of the pressure can also be inferred from the fact that spalling is more likely to occur in thin concrete sections exposed to elevated temperatures, even though thermal stresses are greater in thicker sections; thus, the relation between the pore pressure and the likelihood of spalling, at least in heated thin sections, seems to be evident.

1.3 OBJECTIVES OF THE STUDY

The magnitudes of the pore pressure in heated concrete calculated by various existing models show large variations. The reason is that some of the assumptions adopted are questionable. In particular, the very occurrence of diffusion of water vapour in concrete has been debateable. Also, researchers who consider diffusion have had to either assume that the diffusivities of water vapour and air through concrete are constant or use molecular diffusivity equations the appropriateness of which for concrete is questionable due to the lack of a diffusivity equation that is specific for heated concrete. Furthermore, spalling is exacerbated, and thus higher pressures may occur, in heated thin sections. Moreover, the reduction of the cool reservoir is affected not only by the thickness, but also by the time and type of exposure. Thus, the objectives of this study are:

- To provide a better understanding of the behaviour of concrete structures subjected to fire.
- To investigate the reliability of the assumptions related to diffusion of water vapour through concrete subjected to high temperatures.
- To develop a diffusivity equation specifically for concrete at any temperature.
- To investigate the failure mechanisms of thin concrete walls and columns in fires.
- To provide some guidance for the determination of the maximum pore pressures that can occur in different walls and columns in fire and of the corresponding exposure times.

In Chapter 2, spalling theories will be discussed in detail. Also, pore pressure measurements and calculations will be reviewed. The mathematical models developed to predict the pressure in heated concrete range in complexity from the simple use of Steam Tables to full solution of the equations of state using the finite element method. Since different assumptions regarding whether diffusion of water vapour occurs in concrete are adopted, the pore structure of concrete and diffusion of gases will be reviewed in Chapter 2.

CHAPTER 2

LITERATURE REVIEW

2.1 INTRODUCTION

Hassenjaeger (1935) studied the experimental data available at that time, and concluded that spalling of heated concrete could be attributed to: the rapid heating of concrete, the thermally induced stresses that exceed the tensile strength of concrete, the sudden changes in the structure and volume of the aggregate, and the bursting pressures that result from the water vapour released by evaporation of the free water and from other gases released by the aggregate and the hardened cement paste. These reasons can be grouped into the influence of: (a) thermal stresses, (b) high pore pressures, and (c) both categories of reasons.

Following Hassenjaeger's work, the mechanisms of spalling proposed have fallen into one or the other of these categories with greater concentration on the influence of the high pore pressures. Thus, pore pressure measurements in heated concrete have been carried out by several researchers, and an artificial attempt to induce spalling has been undertaken by Sertmehemetoglu (1977). Also, several mathematical models of heat and mass transfer in heated concrete have been developed to attempt to calculate the maximum pore pressures.

In developing mathematical models, two main approaches are commonly adopted. In the first approach, diffusion of water vapour and air through concrete is neglected. This approach was introduced by Bažant and Thonguthai (1978) in the development of their model, and was adopted by, e.g., Bažant *et al.* (1981), Dhatt *et al.* (1986), Gong and Mujumdar (1993; 1995), and Majumdar *et al.* (1994; 1995). In the second approach, diffusion is considered, but researchers who adopt this approach, e.g. Chen and Pei (1989), Ahmed and Huang (1990), Irudayaraj and Wu (1994), Šelih *et al.* (1994), and Tenchev *et al.* (2001), have had to either assume constant values for the diffusivities of vapour and air or rely on molecular diffusivity equations intended for systems without walls, due to the lack of a diffusivity equation that is specific for concrete at various temperatures.

2.2 SPALLING THEORIES

2.2.1 Spalling Due to Thermal Stresses

2.2.1.1 Saito (1965)

Saito (1965) proposed that spalling occurs when the surface compressive stresses that result from the non-uniform distribution of temperature across a concrete section exceed the compressive strength of concrete. Due to temperature gradients, thermal stresses occur in a heated concrete section that are affected by the nature of heating, thermal properties of concrete, and time of exposure to heat. The distribution of temperature in a concrete slab heated for 60 minutes according to the BS 476:part 20:1987 standard heating regime is shown in Fig. 2.1. A thermal deformation occurs at every point of the concrete section that is proportional to the temperature at that point.

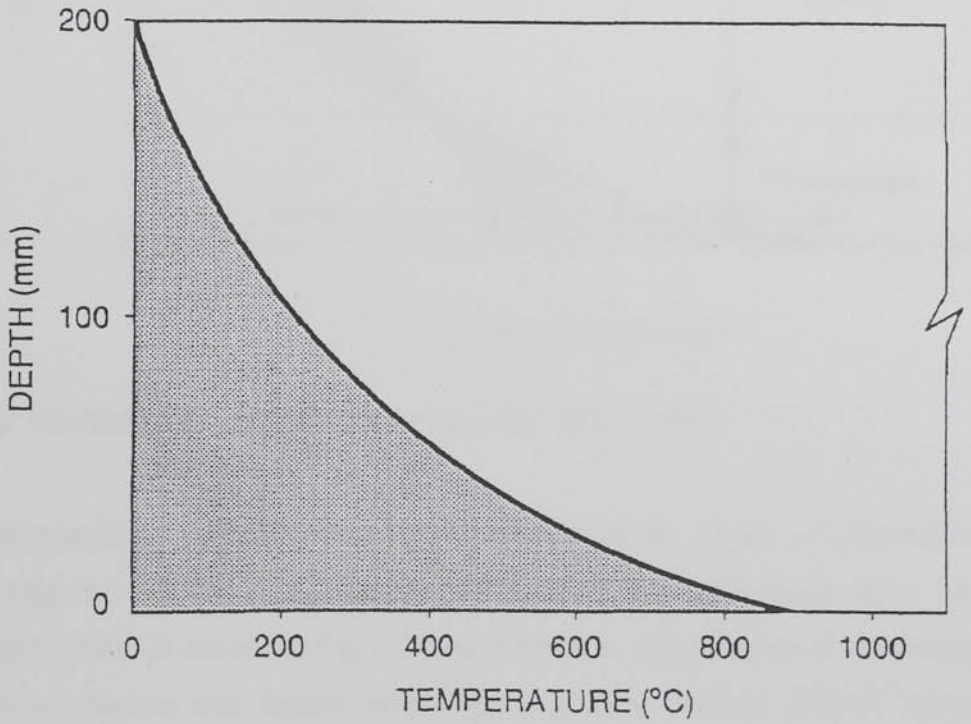

Fig. 2.1: Typical temperature distribution in concrete heated for 60 minutes according to BS476:Part 20:1987

According to Saito, the thermal deformation (total thermal strain) $\alpha\theta$ consists of a longitudinal thermal expansion δ, a curvature $1/\rho$, and a thermal strain $\varepsilon_{thermal}$, as demonstrated in Fig. 2.2. Fig. 2.2 shows that compressive stresses occur at both the exposed and unexposed faces of the heated section, and that tensile stresses occur in the cooler interior regions that counterbalance the compressive stresses. The temperature reduces the strength of concrete, and thus the susceptibility of concrete to spalling increases, but with continued heating, the temperature gradients, and thus the susceptibility of concrete to spalling, are reduced.

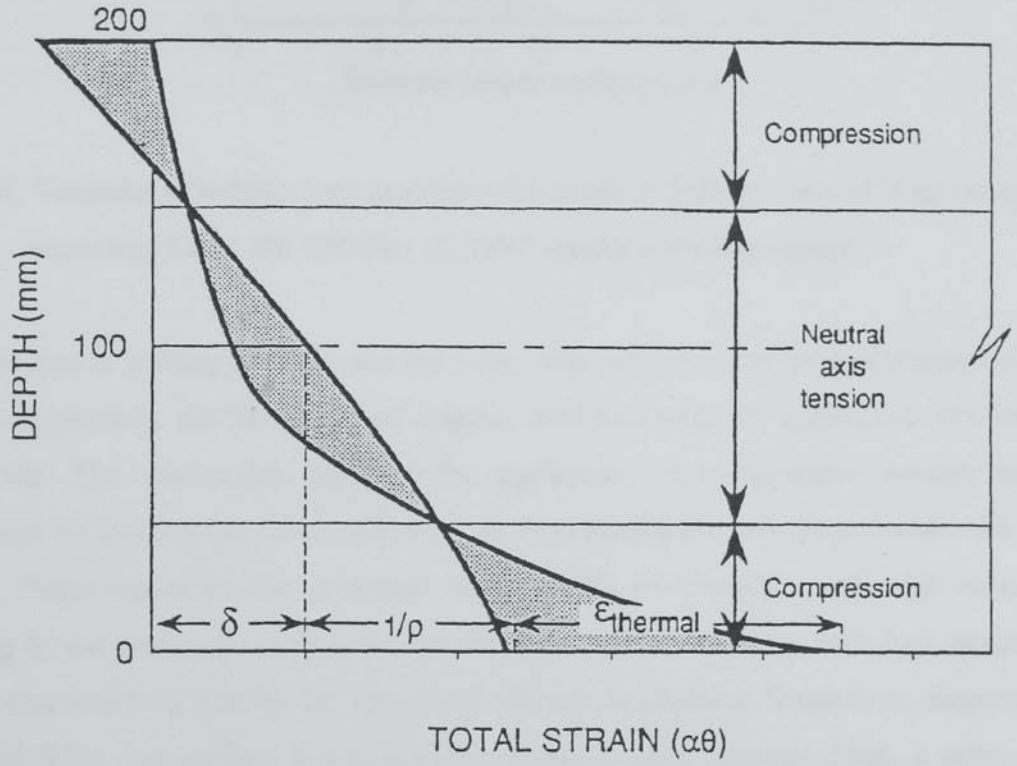

Fig. 2.2: Thermal strain in heated concrete (after Saito, 1965)

Saito calculated the maximum compressive stresses at the surface of a heated concrete section using elastic analysis. The thermal gradients, and thus the thermal stresses, are a function of the time of exposure to heat as shown in Fig. 2.3 that illustrates the variation of the temperature gradient with time for a concrete slab heated according to the BS 476:Part 20:1987 standard heating regime. Thus, Saito predicted that the maximum compressive stresses at the surface increase for some time and then decrease. The maximum temperature gradients, and thus spalling, occur within the first 30 minutes of the standard BS 476:Part 20:1987 standard fire resistance test. Saito's prediction is in agreement with experimental observations.

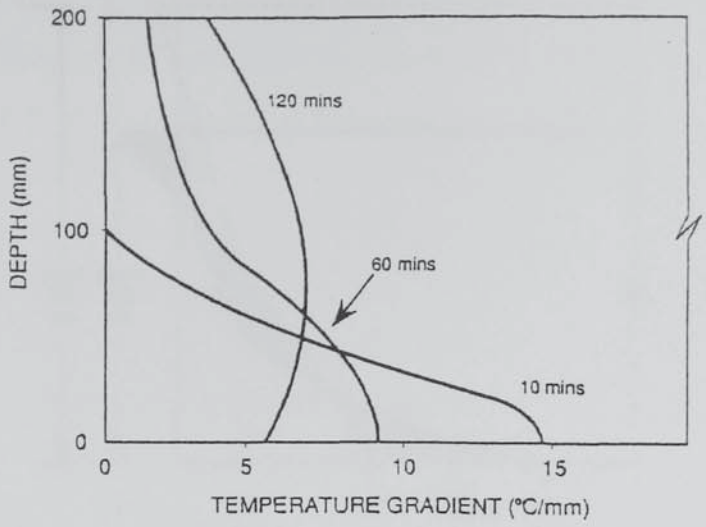

Fig. 2.3: Variation of temperature gradient with depth at different times during heating according to the BS 476:Part 20:1987 standard heating regime.

Stresses due to loading or pre-stress are super-imposed upon the thermal stresses; thus, according to Saito's hypothesis, the likelihood of spalling increases with the application of compressive load or pre-stress. The relationship between the application of compressive stresses and the increased likelihood of spalling has been confirmed in several different test programmes; this validates Saito's theory. Saito explained the increased susceptibility of concretes with high moisture contents to spalling by the occurrence of severe thermal gradients in concretes with high moisture contents due to the absorption of heat by the free water during evaporation. It has been demonstrated by Meyer-Ottens (1972) that spalling is less likely to occur in thick sections. Thus, a serious shortcoming of Saito's hypothesis is that it implies that spalling is more likely to occur in thick sections, since compressive stresses in thick sections are always greater than those in thinner ones (Fig. 2.4).

2.2.1.2 Dougill (1972)

Dougill (1972) suggested that heating a plane concrete panel is analogous to subjecting it to a BS 1881:Part 4:1970 tensile splitting test in a stiff testing machine, in which the tensile strength is assessed by subjecting the specimen to a compressive load, since the stress distribution is similar in both cases as shown in Fig. 2.5. According to Dougill, explosive spalling in concrete exposed to fire is similar to the mode of failure that occurs when a concrete specimen subjected to a load slightly greater than that which results in the maximum stress fails violently in a flexible testing machine.

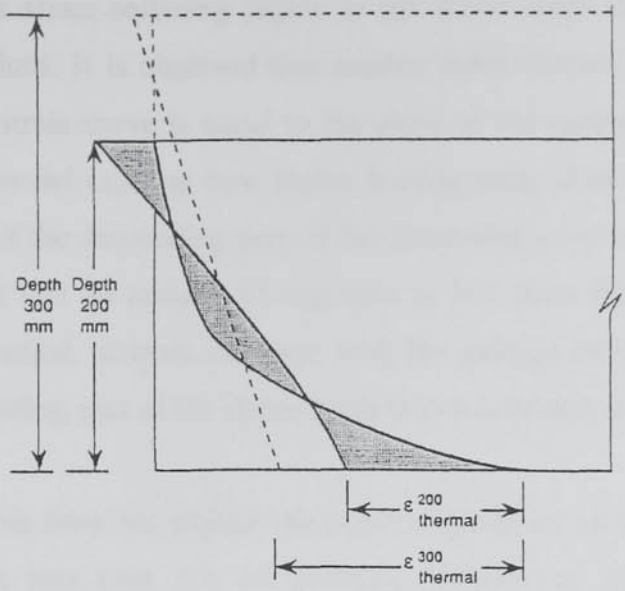

Fig. 2.4: Increased susceptibility of thicker concrete sections to spalling
(after Connolly, 1995)

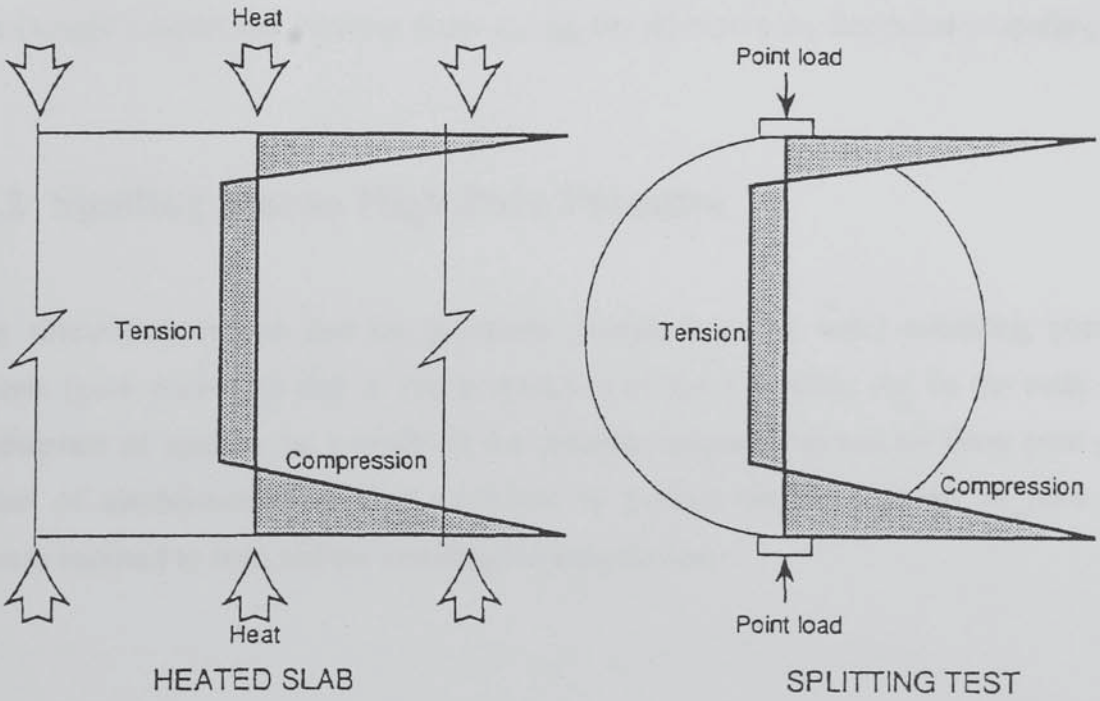

Fig. 2.5: Analogous stress fields generated by heating and splitting forces
(after Dougill, 1972)

Dougill explained that thick sections are less susceptible to spalling than thinner ones because the cool zone in thick sections occupies a greater proportion of the section, and thus provides a stiffer restraint to counterbalance the surface stiffness losses and preserves the overall stiffness of the concrete member. Thus, thick members act as stiff testing machines.

The presence of a strain softening region in the stress-strain curve is one of the reasons for the sudden violent failure. It is observed that sudden failure occurs when the slope of the descending part of the stress-strain curve is equal to the slope of the testing machine curve (Hognestad *et al.*, 1955). Dougill's model explains how higher heating rates promote spalling, since such rates result in steeper slopes of the descending part of the stress-strain curve. It also explains the occurrence of spalling within the first 30 minutes of exposure to fire, since the thermal gradients are the greatest during this time period, stresses decrease with the passage of time due to thermal creep, and the slope of the descending part of the stress-strain curve decreases as the temperature increases.

Dougill's hypothesis does not explain the effect of moisture on spalling and the absence of spalling in concretes with less than 3% of moisture contents as observed by Meyer-Ottens (1972). Furthermore, Akhtaruzzaman and Sullivan (1970) demonstrated that spalling occurs much more frequently in water-cured specimens than moist-cured ones, even though water-curing results in more complete hydration at the surface and thus in the ability to resist greater thermal stresses, while Dougill's model assumes that water-curing should reduce the likelihood of spalling.

2.2.2 Spalling Due to High Pore Pressure

Many researchers believe that the pressures developed in the water-containing pores of heated concrete (pore pressures) due to the evaporation of the free water can be the main cause of the phenomenon of spalling as a result of the bursting stresses imposed by these pore pressures. A number of mechanisms have been proposed to explain the development of pore pressures in concrete exposed to heat and the resulting bursting stresses.

2.2.2.1 Moisture Clog Spalling

Harmathy (1965) and Shorter and Harmathy (1965) proposed that spalling can occur as a result of two different mechanisms. The first is 'thermal' spalling, and is similar to that proposed by Saito (1965). The second is a completely different mechanism; they proposed that spalling may be the result of a phenomenon called **'moisture clog'** spalling. They explained this as follows: when a concrete section is subjected to fire, the water evaporates in a thin layer at the heated surface. The released water vapour travels to the cooler zone where it is cooled and condensed back to liquid. As

heating continues, the proportion of the dry zone increases, and, in time, a fully saturated layer called the 'moisture clog' develops at some distance from the fire-exposed surface. A well-defined front is formed between the dry and the saturated zones. The evaporation of the water at the interfacial plane causes the migration of the moisture clog into the concrete. Shorter and Harmathy's model is shown in Fig. 2.6.

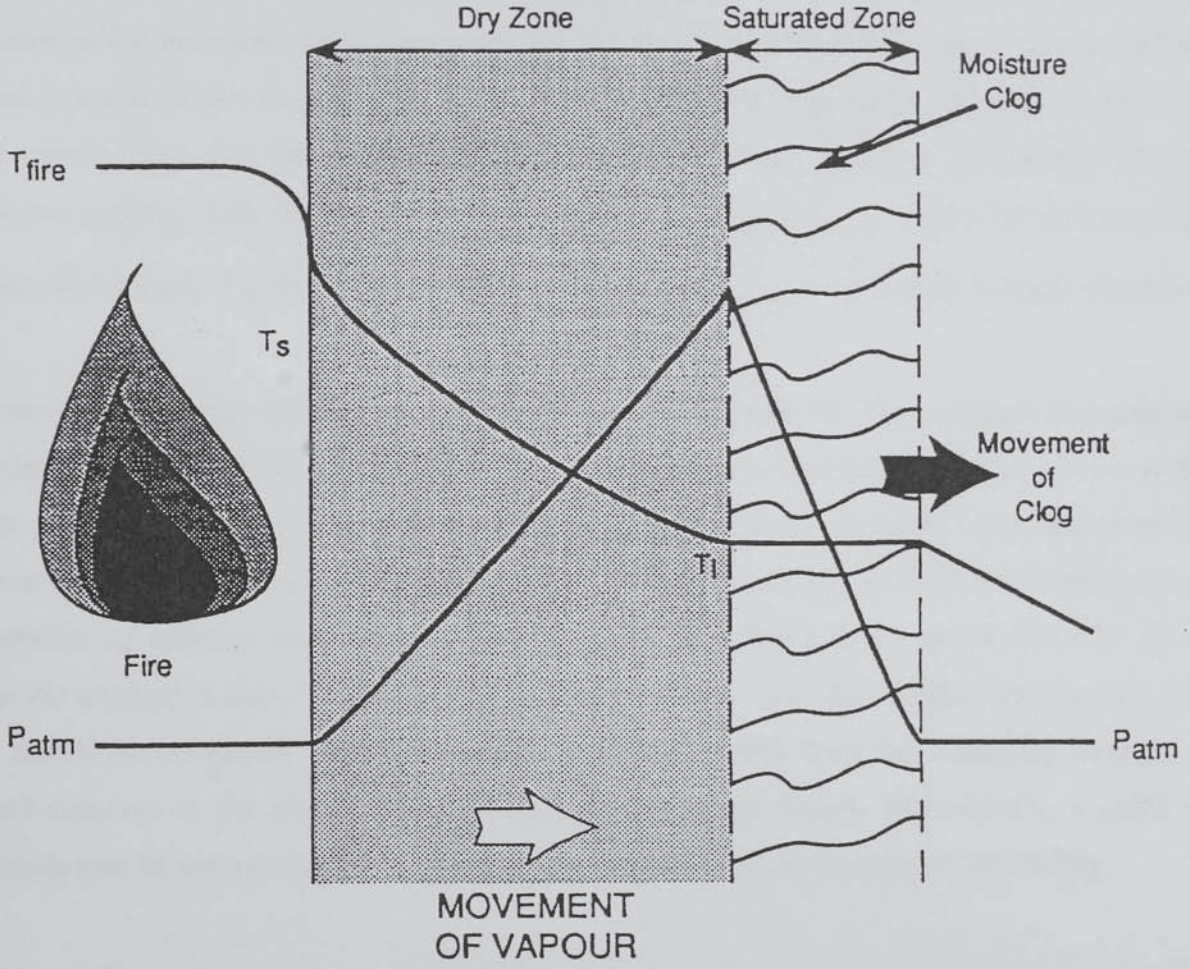

Fig. 2.6: Model for spalling of heated concrete (after Shorter and Harmathy, 1965)

Continued heating results in severe thermal gradients across the dry zone. When the temperature of the moisture clog reaches 100°C, the water evaporates, and the vapour attempts to travel into the cooler zone, but may be prevented from doing so due to the fact that the pores are saturated. Thus, the water vapour is acted upon by opposing forces of temperature and pressure gradients, and the direction of vapour movement depends on the magnitudes of these forces. Therefore, the rate of heating and the permeability are critical. As the heating continues, the rate of heat flow increases through the dry zone. If the saturation and permeability are such that the vapour cannot migrate

away from the heated surface, the vapour is forced against the thermal gradient across the dry zone, which results in the build-up of the pore pressure. The pore pressure continues to build up in the dry zone close to the moisture clog interface, and spalling is believed to occur when the pore pressure exceeds the tensile strength of the concrete.

Based on their model, Shorter and Harmathy derived an expression for the likelihood of spalling, and calculated the velocity at which the moisture clog travels into the heated concrete under the influence of the heat flux. Then, they predicted the velocity at which the drying front travels into the heated concrete under the influence of the pressure gradient. They proposed that when the drying front travels faster than the moisture clog, pore pressures are developed at the interface that lead to explosive spalling, with the failure condition being $(P_1 - P_{atm}) = \sigma_{stregth}$, where P_1 is the pressure at the interfacial layer, P_{atm} is the atmospheric pressure, and $\sigma_{stregth}$ is the tensile strength of concrete.

Shorter and Harmathy and others, e.g. Bažant and Thonguthai (1979), compare the measured, or calculated, pore pressures to the tensile strength in order to determine whether or not spalling is likely to occur. However, Connolly (1995) and Purkiss (2001, personal communication) rightly believe that comparing the pore pressure with the strength cannot determine the likelihood of the occurrence of spalling, since the stresses that result from the pressure are confined to the pores, while the strength is that of a unit area of concrete. It is the force that results from the pore pressure that should be compared with the resisting force that results from the remaining strength of the heated concrete at the plane where the maximum pressure occurs. Alternatively, a strain energy approach may be even better for determining the likelihood of the occurrence of spalling.

Based on the argument above, and realising that the surface porosity of the plane at which the maximum pressure occurs is equal to the initial porosity plus the porosity that results from the dehydration of the bound water between 105°C and the temperature at which the maximum pressure occurs, then the force that results from the pressure on a unit area of concrete normal to the direction of heating is equal to the pressure times the porosity at the evaporation front, while the resisting force is equal to the remaining tensile strength that corresponds to the temperature at the location where the maximum pressure occurs.

Shorter and Harmathy produced a spalling liability curve (Fig. 2.7) for a concrete with tensile strength of 1.7 MPa and porosity of 0.3 in terms of the fractional pore saturation ϕ / ε, where ϕ is the moisture content and ε is the porosity, and the permeability. From Fig. 2.7, no spalling will

occur if the permeability is sufficiently high even at full saturation, and explosive spalling is inevitable at very low permeabilities. They suggested a threshold permeability in the order of 10^{-9} m/s, but, according to Neville (1995), the permeability of most concretes is less than 10^{-9} m/s.

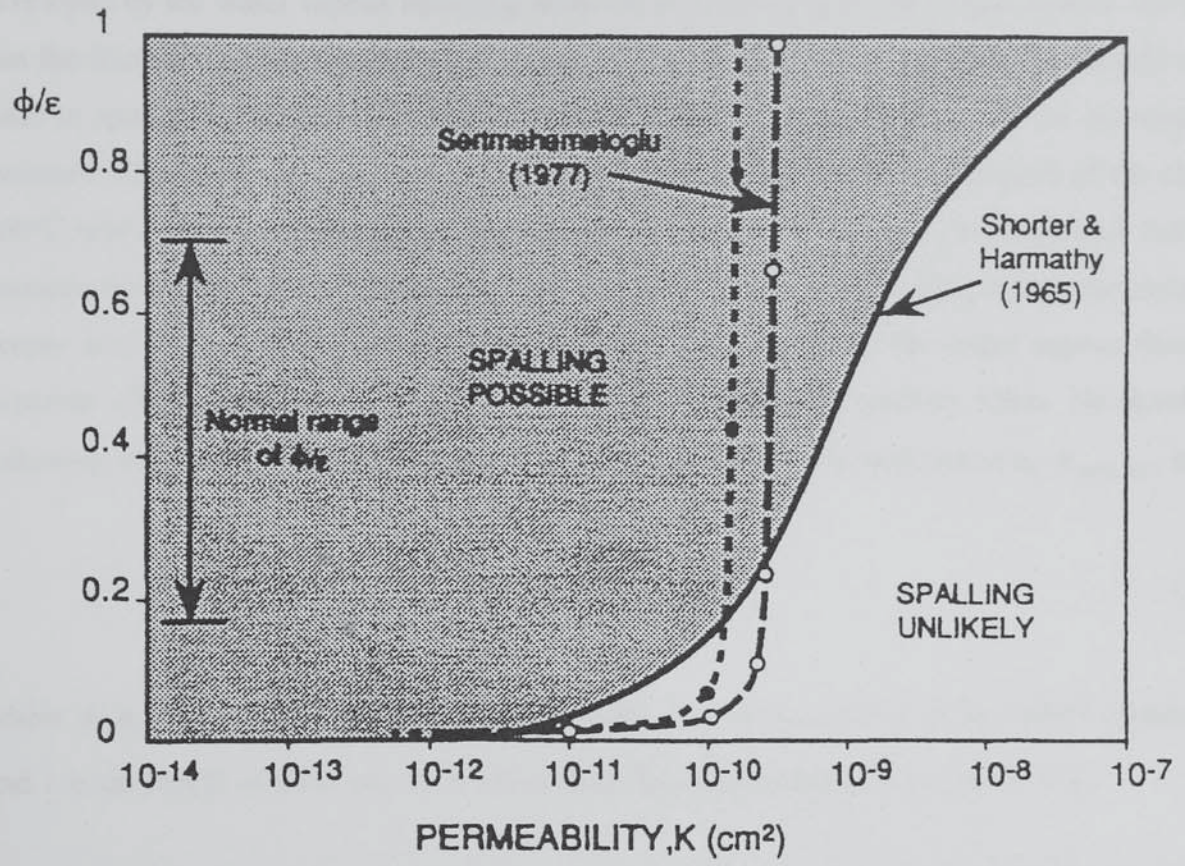

Fig. 2.7: Spalling liability based on the moisture clog model

Sertmehemetoglu (1977) modified the model of Shorter and Harmathy, and suggested that a significant proportion of the moisture may leave the clog across the dry zone before the building up of the pressures, and thus the decrease of the moisture content of the clog increases the rate at which the interfacial layer moves. Thus, he produced a modified spalling liability curves for concretes with tensile strengths of 1.73 MPa and 3.5 MPa that are also shown in Fig. 2.7. Sertmehemetoglu related the increased susceptibility of concretes with high moisture contents to spalling to the reduced permeability that result from the more complete hydration. The effect of load on spalling can also be explained in terms of the permeability. Compressive loads reduce the tension cracks that result from heating, and thus reduce the permeability. Conversely, as observed by England (1971), imposed loads that cause flexure may increase the cracks at the heated surface, as in the lower flange of a beam with a sagging moment, which reduces the pore pressure and thus reduces the likelihood of explosive spalling.

2.2.2.2 Spalling Due to Drag Forces

Meyer-Ottens (1972) proposed that the bursting stresses that cause spalling are due to drag forces developed by the water vapour travelling from the moisture clog to the heated surface. He suggested that the friction between the escaping vapour and the walls of the pores results in a tensile stress that leads to spalling if it exceeds the tensile strength. Meyer-Ottens assumed that the movement of the moisture clog is due to the evaporation of water, and thus related the location of the clog to the 100°C isotherm. He recognised the build up of pore pressure; however, he suggested that the pore pressure forces the vapour to travel towards the heated surface rather than driving the moisture clog deeper into the concrete. He produced a model by assuming that the water vapour flow through concrete can be represented by the flow through a bundle of capillary tubes. He developed the following equation for the bursting stress generated at 100°C in heated concrete, $\sigma_{burst,100}$, in MPa:

$$\sigma_{burst,100} = 7.16\phi V_{100} l \qquad (2.1)$$

where ϕ is the moisture content, in % by weight, V_{100} is the velocity of the 100°C contour, in m/s, and l is the length of flow, i.e. the distance from the clog to the heated surface, in m.

Meyer-Ottens proposed that the likelihood of spalling could be determined by comparing these bursting stresses with the tensile strength of concrete, and calculated the bursting stresses that could be developed in a range of different concretes. He observed that the stresses increased with depth to a maximum at 60 mm as shown in Fig. 2.8, and proposed that spalling is unlikely in heated sections with thicknesses in the order of 120 mm. He also provided in Fig. 2.9 the relationship between the velocity of the 100°C contour and the moisture contents.

It is important to note that, in addition to the shortcoming discussed earlier that many researchers compare the pore pressure to the tensile strength in order to determine the likelihood of the occurrence of spalling, another serious shortcoming is that, apart from Tenchev *et al.* (2001), different researchers assume that the evaporation front, or the moisture clog, and thus the maximum pressure, is located at the 100°C isotherm. However, the saturation temperature, i.e. the temperature at which a pure substance changes phase, is dependent on the pressure, called the saturation pressure (Abbot and Van Ness, 1976; Çengel and Boles, 1998). Water starts boiling at 100°C only when the pressure is equal to 1 atm (101325 Pa). It starts boiling at 200°C when the pressure is

1.554 MPa and at 250°C when the pressure is 3.973 MPa, as shown in Table 2.1. Thus, the temperature at which the evaporation front is located varies with the pressure. Also, as the water temperature increases, thermal expansion of the liquid phase occurs that increases the pore pressure.

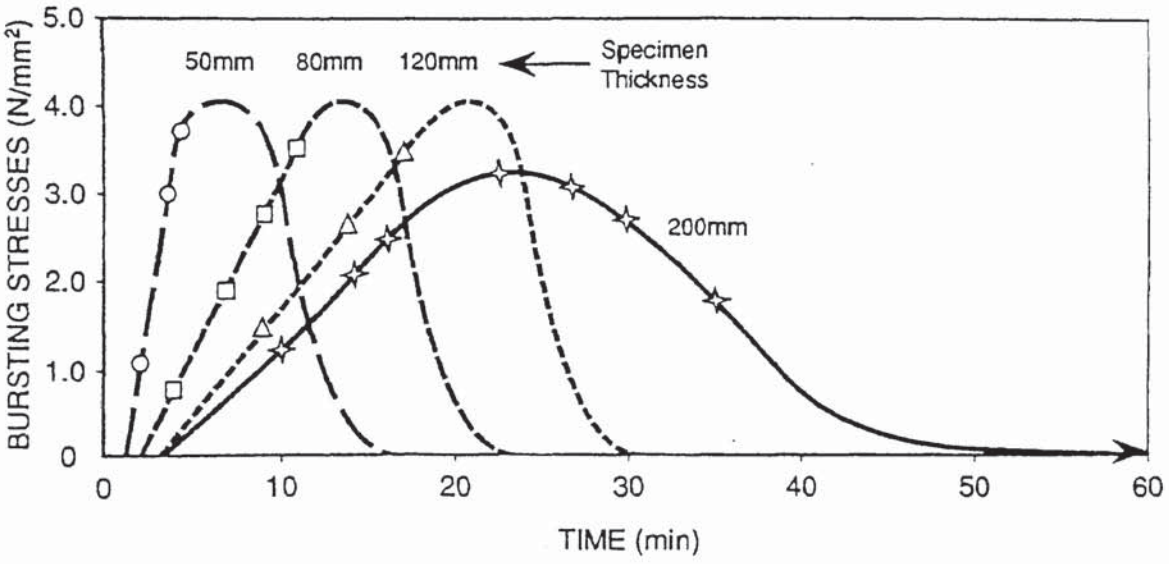

Fig. 2.8: Bursting stresses in heated concrete (after Meyer-Ottens (1972)

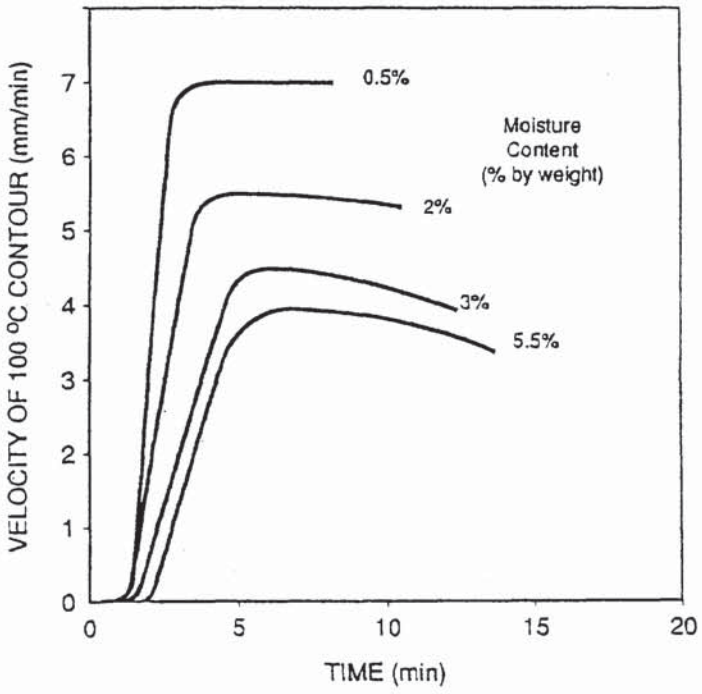

Fig. 2.9: Variation of velocity of 100°C contour and moisture content (after Meyer-Ottens (1972)

Temperature T, in °C	Saturation Pressure P_{sat}, in kPa
100	101.3 (1 atm)
150	475.8
200	1554
250	3973
300	8581

Table 2.1: Saturation (boiling) pressure of water at various temperatures (after Çengel and Boles, 1998)

This shortcoming has led to the comparison being made between the pressure, or the bursting stress (2.1) due to the movement of vapour at the velocity of the 100°C contour, generated at 100°C in heated concrete and the tensile strength at ambient temperature by assuming that the strength at 100°C may not be much smaller than that at ambient conditions. The temperature has a pronounced effect on the strength of concrete; at a temperature of 600°C, the strength is practically zero (Schneider, 1985). If the maximum pressure is, say, 4 MPa, and thus the temperature at the distance where the maximum pressure occurs is about 250°C, the tensile strength may be significantly smaller than that at the ambient temperature. Also, if spalling is due to drag forces, the vapour will not be travelling at the velocity of the 100°C contour; it will be travelling at a variable velocity that depends on the variable pressure, and thus on the variable temperature, at the evaporation front.

2.3 PORE PRESSURE MEASUREMENT

Nekrasov *et al.* (1967) attempted to measure the pore pressure in heated concrete by casting a number of 2-mm copper pipes into large blocks of refractory concrete, and used a manometer to record the pressure development during gradual heating to 800°C. They recorded a maximum pore pressure of 0.2 MPa after many hours of heating at a relatively slow rate, and did not encounter any spalling of the heated concrete.

Bremer (1967) used the measurement device illustrated in Fig. 2.10, and obtained the relationship between the temperature and pore pressure shown in Fig. 2.11. The pressures obtained by Bremer were rarely more than 40% of the saturated steam pressure.

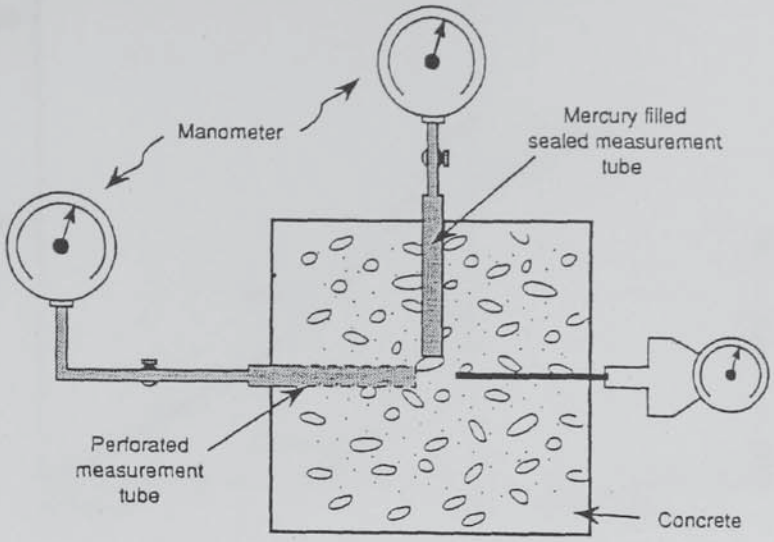

Fig. 2.10: Apparatus used by Bremer (1967)

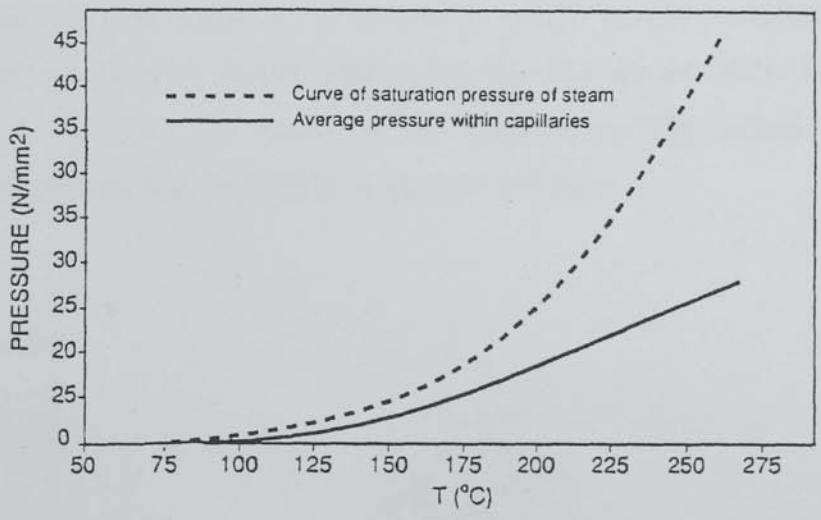

Fig. 2.11: Pore pressures measured by Bremer (1967)

Thelanderson (1974) studied 1500×150×150 mm rods of quartzite aggregate concrete with water/cement ratio of 0.55 and heating rates of 4 and 8°C, and recorded maximum pore pressures of 0.5 and 0.65 MPa, respectively; explosive spalling occurred. The rate of heating of 2°C/min did not cause spalling. The time history of the temperature and pore pressure recorded by Thelanderson is shown in Fig. 2.12.

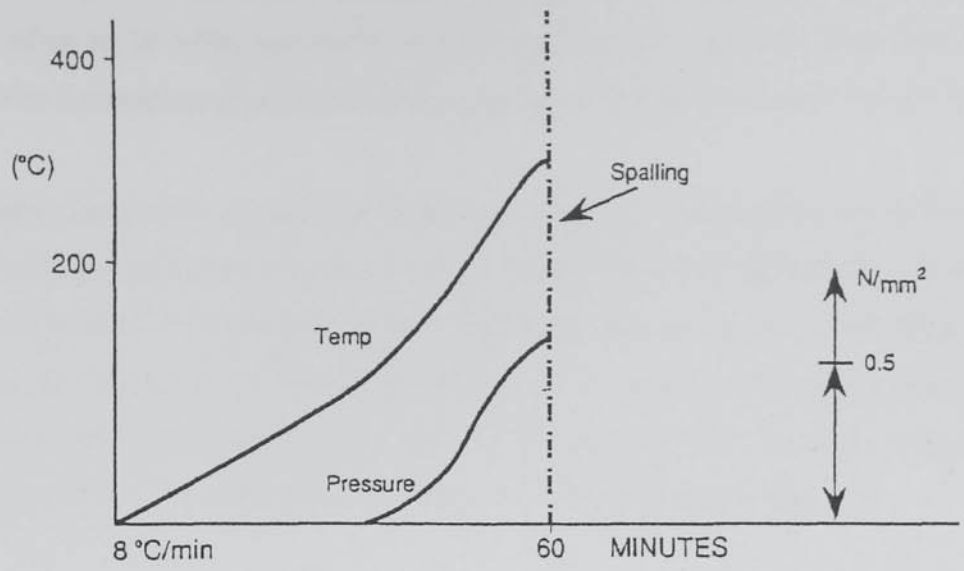

Fig. 2.12: Time history of temperature and pore pressure (after Thelanderson, 1974)

Chapman (1976) considered the use of concrete as a lining material in nuclear reactor vessels, and thus inspected the pore pressures developed in sealed concrete sections. He found that heating sealed concrete could result in pore pressures greater than the saturation vapour pressure of steam as can be seen in Fig. 2.13. He found that the initial ratio of the volume of liquid water to gas in concrete pores affected the magnitude of the pore pressure.

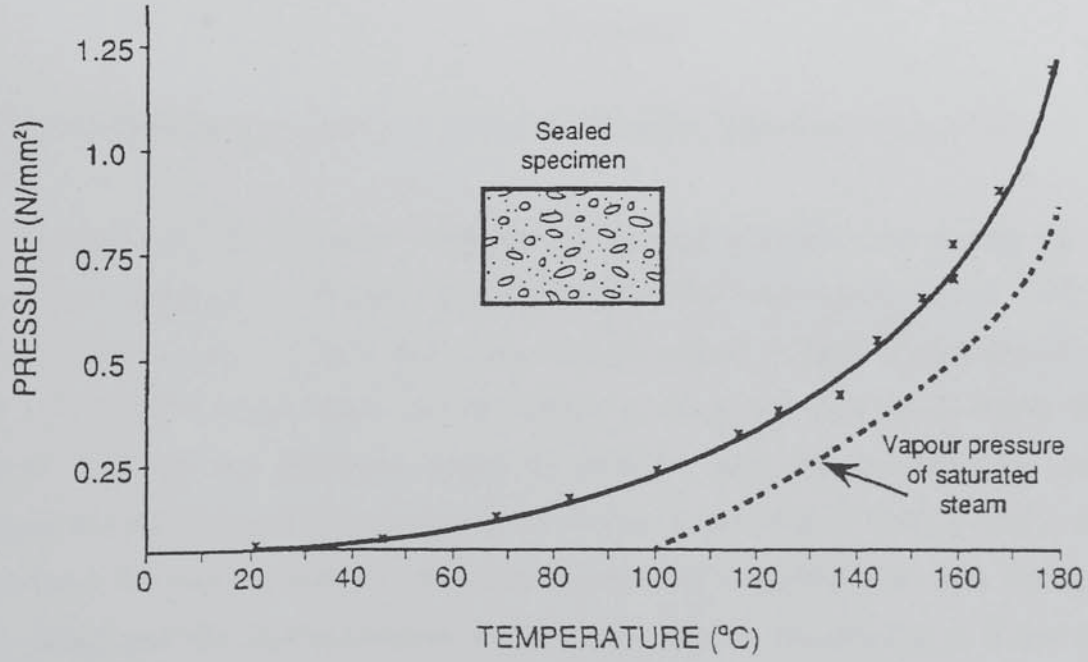

Fig. 2.13: Pore pressures measured by Chapman (1976)

England *et al.* (1991) confirmed Chapman's finding that heating sealed concrete can result in pore pressures of up to 10 MPa, and confirmed that the moisture migrates away from the heated surface and results in the maximum pore pressure occurring at remote distances from the heated surface.

Sertmehemetoglu (1977) investigated concrete specimens heated from one side only, and measured the pore pressure developed at the unexposed surface that was sealed with a diaphragm including a pressure transducer. He assumed that the diaphragm was equivalent to the moisture clog proposed by Shorter and Harmathy (1965). Sertmehemetoglu recorded the variation of the pore pressure with the thickness that was assumed to be equal to the depth of the moisture clog, and found that the pressure increased with thickness up to about 2.1 MPa as shown in Fig. 2.14.

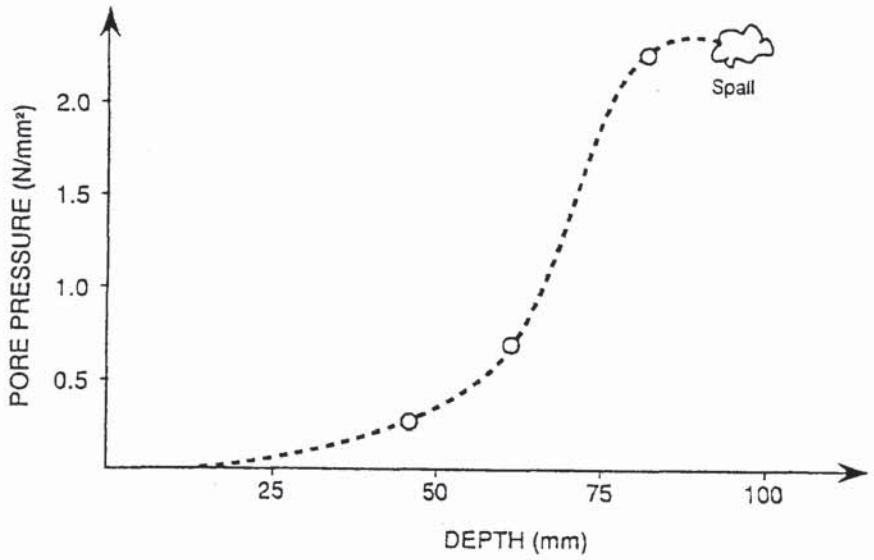

Fig. 2.14: Experimental pore pressure measurements (after Sertmehemetoglu, 1977)

The magnitudes of the pressure measured by Sertmehemetoglu cast doubts on the spalling mechanisms suggested by Shorter and Harmathy (1965) and Meyer-Ottens (1972), since the maximum pressure was 2.1 MPa that is less than the tensile strength of concrete of about 3 MPa even if the effect of temperature on the strength is taken into account. In order to explain the difference between the measured maximum pressure and that necessary to cause spalling, Sertmehemetoglu proposed a mechanism based on the earlier ideas of Dougill (1971) who observed the existence of cracks parallel to the heated surface. He suggested that these cracks fill with the water vapour, and the vapour pressure in the cracks subjects the concrete to forces normal to the direction of heating, which leads to the bursting stresses that cause spalling.

Sertmehemetoglu attempted to induce spalling artificially by generating artificial cracks parallel to the heated surface by casting discs at different depths within concrete specimens, and measuring the magnitudes of mechanically applied bursting stresses necessary to cause rupture of the surface. He found that the necessary bursting stresses depended on the crack size and depth, and that stresses of magnitudes of the measured pore pressures were sufficient as shown in Fig. 2.15. It is clear from Fig. 2.15 that, for unloaded concrete specimens, a bursting stress of about 2 MPa at a distance of up to 10 mm from the surface may cause rupture of the surface, and thus Sertmehemetoglu proposed a mechanism by which the maximum pore pressure of about 2 MPa can cause spalling.

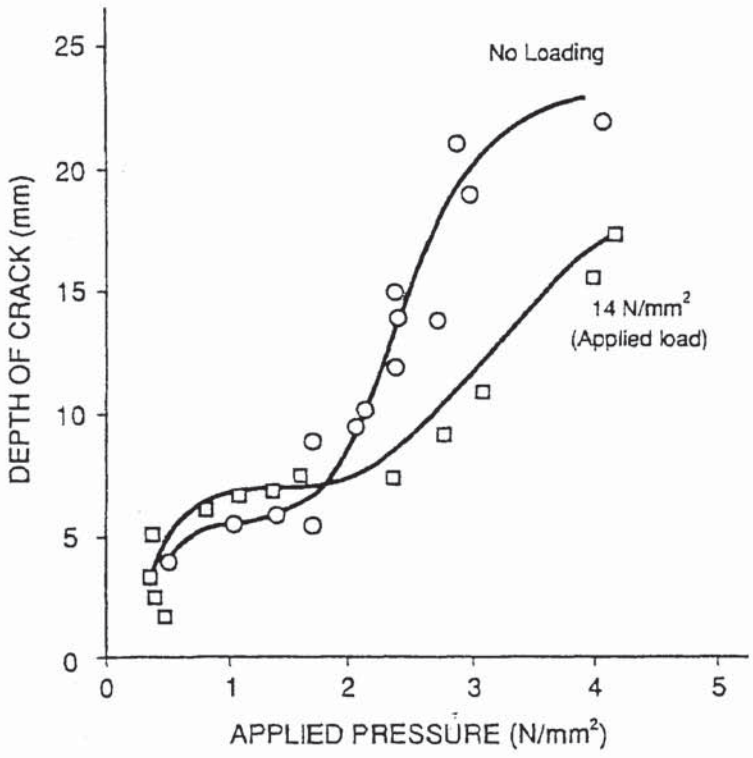

Fig. 2.15: Variation of rupture pressure imposed on a 50-mm-diameter crack with depth from the concrete surface (after Sertmehemetoglu, 1977)

Harada and Terai (1991) attempted to validate a mathematical model that they developed against experimental behaviour. They modelled the development of the pore pressure in heated concrete walls exposed to the standard ISO 834:1987 heating regime, and calculated a maximum pore pressure of 0.13 MPa, after 30 minutes of heating, that remained constant on further heating. Their attempts to validate the model failed due to practical difficulties in measuring the pore pressure. They used an embedded tube filled with silicone oil and connected to a transducer. Some pore pressure measurements were recorded in the early stages of the test, but evaporation of the oil and the release of the pressure due to cracking of the concrete prevented further measurements.

Consolazio *et al.* (1997) stated that when a partially saturated porous medium, e.g. concrete, is subjected to high temperatures, the developed internal pore pressures, in combination with differential thermal stresses, can cause explosive spalling of the material, and that the level to which these pressures ultimately rise depend on the saturation, the permeability, and the rate at which heat flows into the material. They recognised the moisture clog spalling proposed by Harmathy (1965) and Shorter and Harmathy (1965). Consolazio *et al.*'s experimental programme consisted of subjecting two nearly saturated, and identically prepared, cement mortar specimens with a porosity of 0.175 and a permeability of 8.324×10^{-17} m^2 to a high temperature radiant heating source, and measuring the transient temperatures and pore pressures with thermocouples and pore pressure transducers. The source of heating was an oven preheated to 925°C before placing it adjacent to the top of the specimens. They stated that this rapid heating was consistent with the type of thermal loading experienced by concrete runways subjected to jet exhaust. Two test runs were performed, and maximum pore pressures of about 3.1 MPa were recorded. In each test, spalling of the mortar surface was observed prior to removal of the oven after about 500 seconds.

It is clear that the rate of heating adopted by Consolazio *et al.* may be consistent with the type of thermal loading experienced by concrete runways subjected to jet exhaust, but is inappropriate for concrete structures exposed to fire. Nevertheless, the fact that the pore pressure is a major factor in the occurrence of spalling is confirmed.

2.4 PORE PRESSURE CALCULATIONS

Mathematical modelling of heat and mass transfer in heated concrete has been treated differently by many researchers. However, excluding the simple use of steam tables (Rogers and Mayhew, 1991), two approaches are commonly adopted: the first treats all phases of moisture, including water vapour, as one in one expression of mass conservation, and conservation of air is neglected. Thus, diffusion of vapour through air cannot be considered. This approach is adopted by, e.g. Bažant and Thonguthai (1978), Gong *et al.* (1991), Consolazio *et al.* (1997), and Majumdar and Marchertas (1997). In the second, mass conservation is divided into conservation of free water (including water released by dehydration), conservation of vapour, and conservation of air. Thus, diffusion of vapour and air through each other can be considered. This approach is adopted by, e.g. Luikov (1975), Dayan and Gluekler (1982), Ben-Nasrallah and Perre (1988), Šelih and Sousa (1996), Ahmed and Hurst (1997), Häupl *et al.* (1997), Künzel and Kiessl (1997), and Tenchev *et al.* (2001).

2.4.1 The First Approach Models

2.4.1.1 Bažant and Thonguthai (1978)

In 1978, Bažant and Thonguthai presented a mathematical model for concrete subjected to temperatures above 100°C in which the coupling of heat and mass (of moisture including water vapour, but not the mass of air) transfer is recognised. They stated that only the temperature range up to 100°C had been explored to any significant extent in mathematical modelling of heat and mass transfer in heated concrete, that no comprehensive and rationally based model for concrete exposed to temperatures above 100°C had been attempted, and thus this was the objective of their work.

Bažant and Thonguthai reported that the problem of coupled heat and mass transfer in a porous solid undergoing microstructural and chemical changes is extremely complex, and thus must be simplified. They stated that the moisture flux J should consist of the flux due to the gradient of moisture concentration w (Fick's law of diffusion) and the flux due to the gradient of temperature T (Soret flux), and the heat flux q should consist of the flux due to the gradient of moisture concentration (Dufour flux) and the flux due to the gradient of temperature (Fourier law); however, since the mass of all free evaporable water w at a given temperature is a function of the temperature T and the pore water pressure P, i.e. $w = w(P,T)$, and since the test data indicated that the thermal gradient contribution is rather small, the moisture flux can be expressed as

$$J = -\frac{a}{g}\nabla P \tag{2.2}$$

where a is the permeability, in m/s, and g is the acceleration of gravity included for reasons of dimensionality.

Thus, the mass flux is reduced to Darcy's law (2.2) that is limited to saturated porous media. However, as a result of data fitting, Bažant and Thonguthai found that (2.2) could be applied to both saturated and non-saturated concrete if the pressure in the pores of non-saturated concrete is interpreted as the water vapour pressure rather than the capillary water pressure.

It is important to note that, although the fact that the mass flux should include the flux due to the gradient of mass concentration (Fick's law of diffusion) is recognised, assuming that water vapour

is part of the moisture w and neglecting the mass of air result in the inability to consider mass transfer by diffusion (Fick's law) of vapour and air in the gaseous mixture, and thus in the mass flux being due to convection only (Darcy's law). Neglecting diffusion of vapour and air in concrete is not only to simplify the problem, but also the result of the belief of Bažant and Thonguthai that diffusion of vapour cannot occur in concrete as will be explained later in this section.

Depending on the fit of data, the coupled heat flux is neglected, and hence q is expressed as

$$q = -b\nabla T \tag{2.3}$$

where b is the heat conductivity.

Since w includes all free evaporable water, conservation of moisture is given as

$$\frac{\partial w}{\partial t} = -\nabla \cdot J + \frac{\partial w_d}{\partial t} \tag{2.4}$$

where w_d is the mass of free evaporable water released by dehydration, in kg/m^3.

Heat conservation is

$$\rho C \frac{\partial T}{\partial t} - C_a \frac{\partial w}{\partial t} - C_w J \cdot \nabla T = -\nabla \cdot q \tag{2.5}$$

where ρ is the mass density, C is the heat capacity of concrete (per kilogram of concrete) including the bound water, but excluding the free water, C_a is the heat of sorption of free water (per kilogram of free water), C_w is the mass density and heat capacity of bulk (liquid) water, and $C_w J \cdot \nabla T$ is the rate of heat supply due to heat convection by moving water.

The set of sorption isotherms from which the free water content for various temperatures can be determined is shown in Fig. 2.16a.

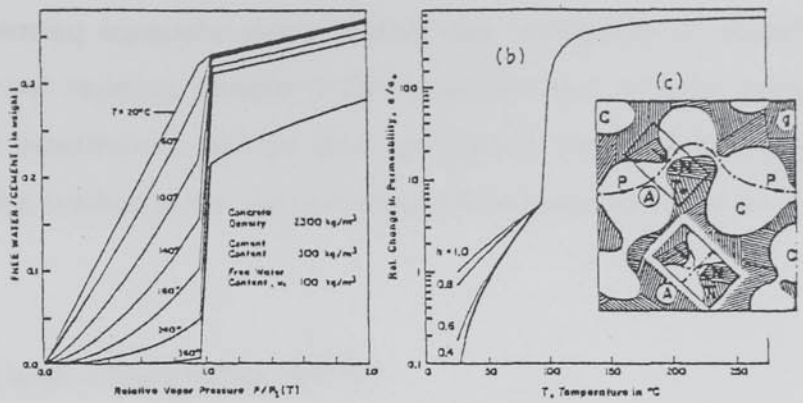

Fig. 2.16: (a) Sorption Isotherms; (b) Dependence of Permeability on Temperature; (c) Flow Passage in Cement Gel with Neck (after Bažant and Thonguthai, 1978)

As far as the permeability is concerned, Powers and Brownyard (1948) found that the major variable was the capillary porosity n_c of cement paste that depends on the water/cement ratio and the degree of hydration. Bažant and Thonguthai, however, argued that neither the capillary porosity n_c nor the total porosity n can be the basic factor, since moisture transfer below 100°C is not controlled by the flow of capillary liquid water, but is controlled by the 'necks' on the continuous flow passages (P in Fig. 2.16c). They argued that, in dense cement pastes, the necks are perhaps only about 50 Å wide, and thus can contain only adsorbed water, but no liquid water or vapour, since, even if the neck is not completely filled by water, hardly any vapour can pass because the mean free path, i.e. the average distance travelled by a molecule between two successive molecular collisions with other molecules, of water vapour molecules, is about 800 Å at 25°C and 1 atm and thus greatly exceeds the neck size. Therefore, they argued, the mechanism of moisture transfer at low temperature is controlled by the migration of molecules along the adsorbed water layers.

On the other hand, for temperatures exceeding 100°C, Bažant and Thonguthai found from the test data that the permeability increased by about two orders of magnitude. To explain this jump in permeability, they proposed the hypothesis that, due to smoothing of pore surfaces to reduce the surface energy, the width of the necks governing the flow increases many times when the temperature exceeds 100°C, and thus allows liquid water and vapour to pass while the volume of

the necks remains negligible. Thus, the effect of the large relative increase of the neck width on the measured pore size distribution at high temperature is insignificant, and cannot be detected.

Based on the governing equations above, Bažant and Thonguthai developed a 1D FE computer program for heat and moisture transfer in the radial direction of polar coordinates, and used the program to fit the experimental data for slow heating that are available in the literature. The most important conclusion reached is that the pore pressures in heated concrete do not exceed 1 MPa.

2.4.1.2 Bažant and Thonguthai (1979)

Using the computer program described above, Bažant and Thonguthai (1979) provided the distribution of temperature and pore pressure in a concrete wall rapidly heated at one surface such that the temperature of the surface rises linearly at the rate of 80°C/min. They considered two cases of boundary conditions: an unsealed heated surface, and thus the pressure at the boundary is the standard atmospheric pressure, and a sealed heated surface with a steel liner. The distributions of temperature and pore pressure for the two cases of boundary conditions are shown in Fig. 2.17. From these results, Bažant and Thonguthai concluded that the maximum values of the pore pressure in the unsealed wall are much higher (more than 2 MPa after 6 minutes of heating) than those obtained for slow heating in 1978, and are even higher in the sealed wall. They state that these values of the maximum pore pressure are quite significant compared with the tensile strength at high temperature, and that they can in fact cause tensile failure (spalling).

Considering that heating may be non-uniform along the wall surface in practical problems, a hot-spot problem is considered in which heating is applied to a circular hot spot on the unsealed surface of the wall at the same rate of 80°C/min. From the distribution of the pore pressure (Fig. 2.18), it is found that the maximum pore pressure of more than 3 MPa after 6 minutes of heating is about 50% higher than that obtained with uniform heating.

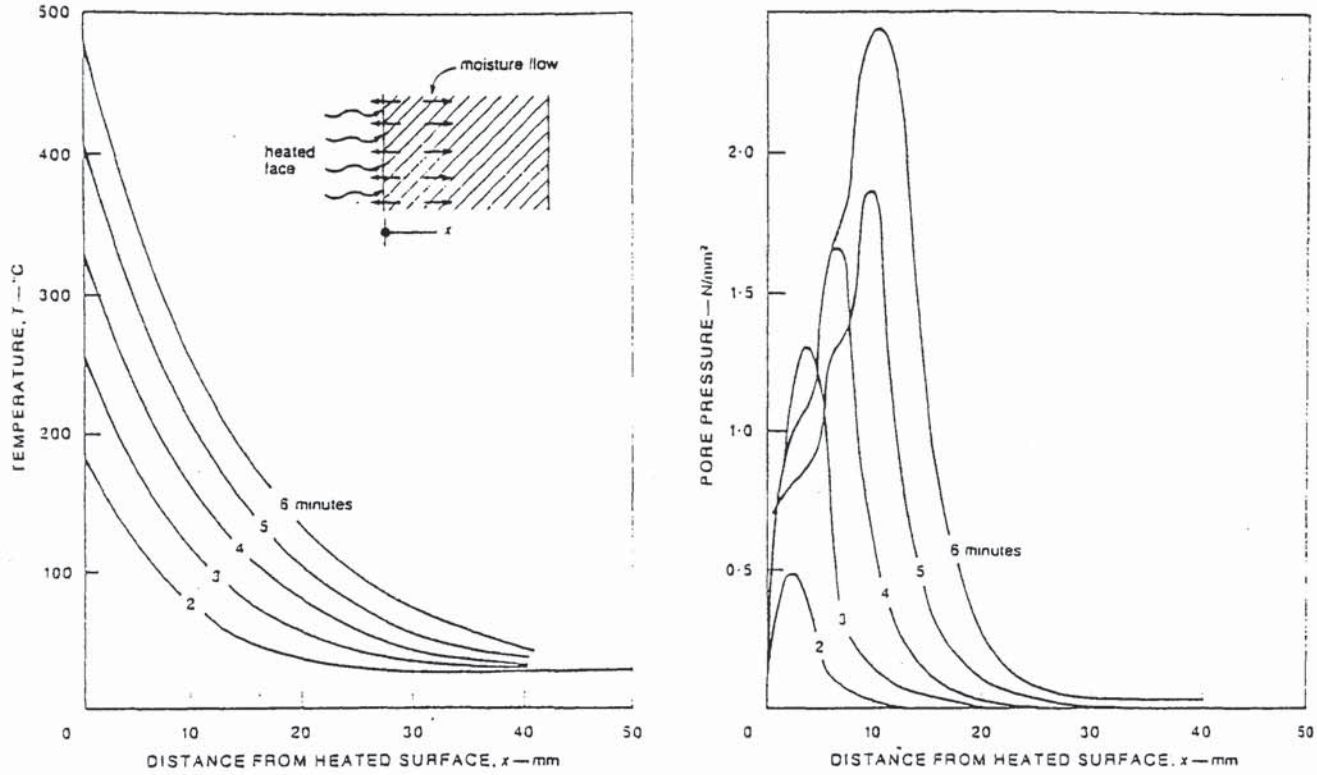

(a) *Unsealed surface*

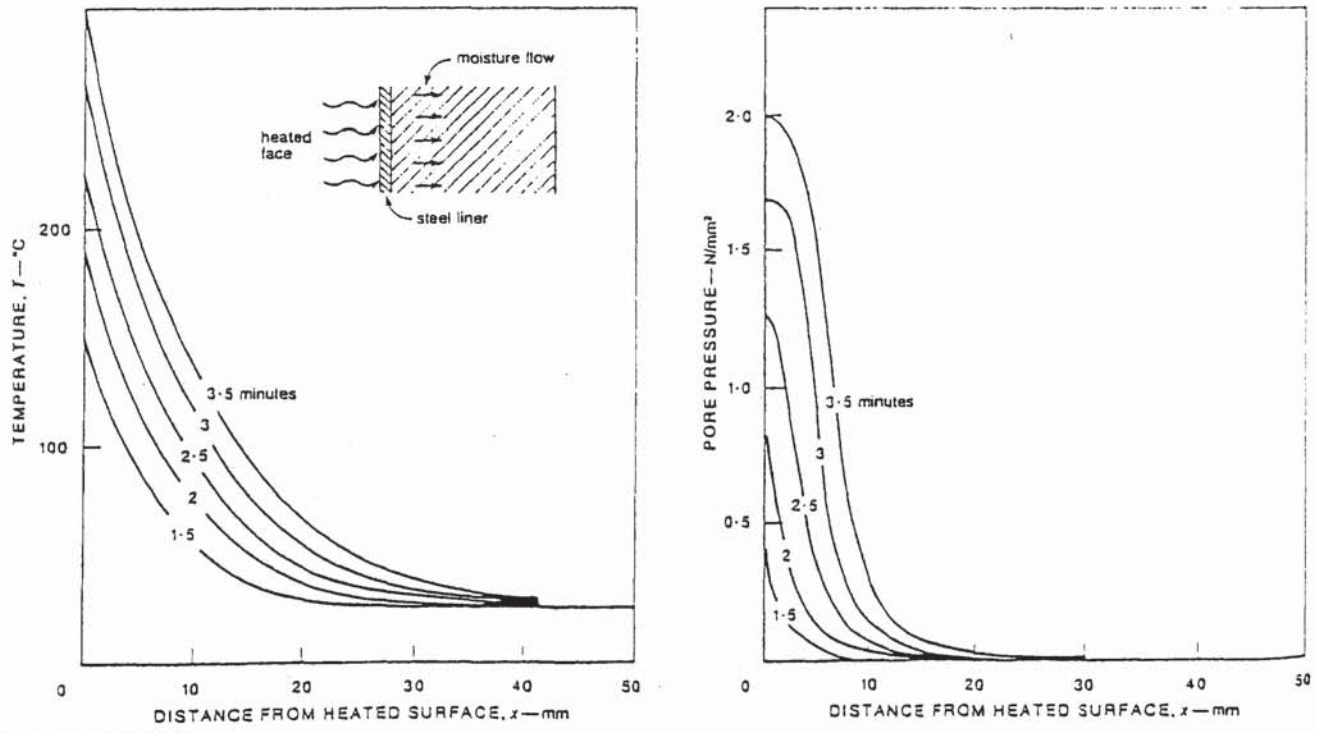

(b) *Sealed surface*

Fig. 2.17: Distribution of temperature and pore pressure (after Bažant and Thonguthai, 1979)

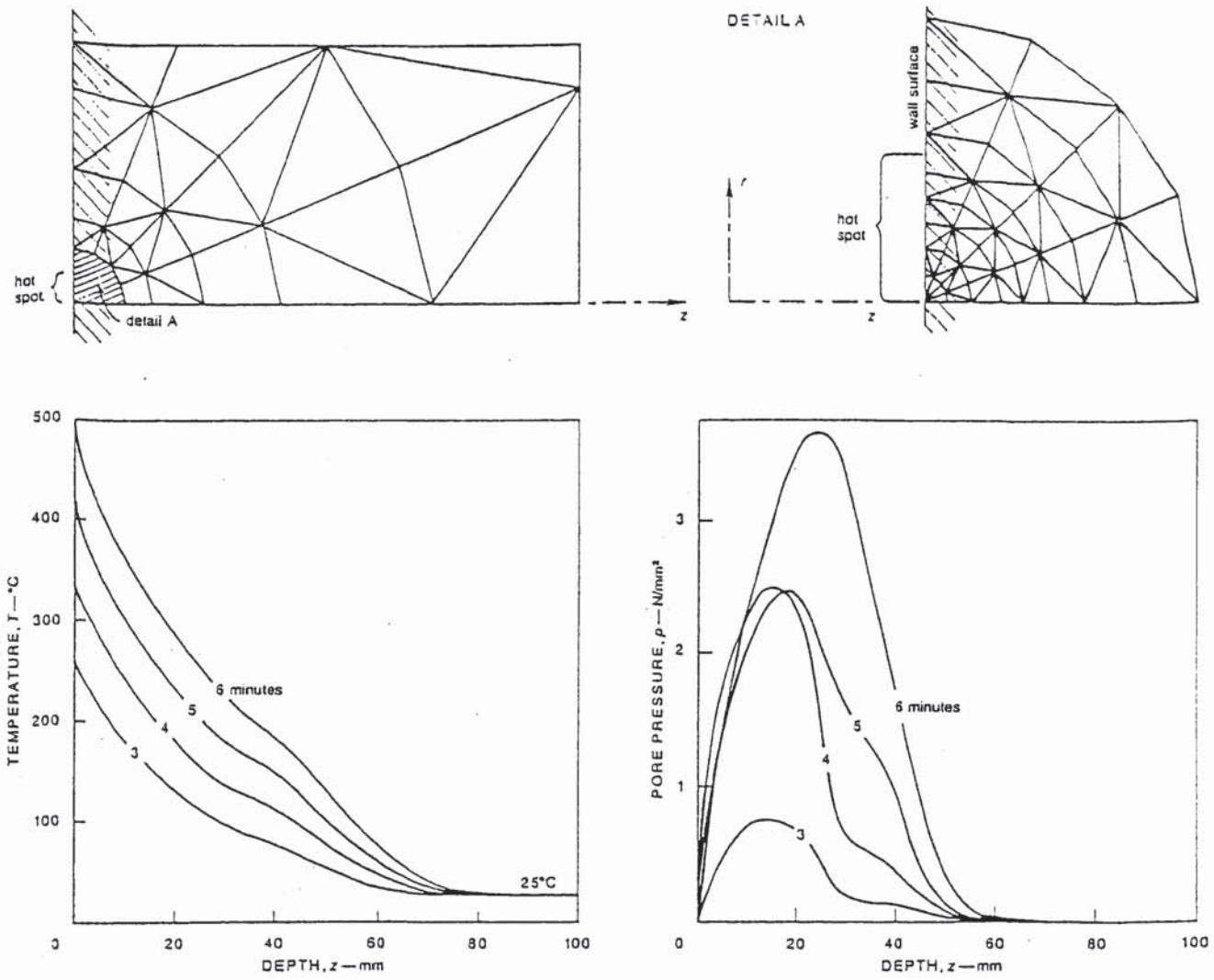

Fig. 2.18: Distribution of temperature and pore pressure (the hot-spot problem)
(after Bažant and Thonguthai, 1979)

2.4.1.3 Consolazio *et al.* (1997)

Consolazio *et al.* (1997) modified the TOUGH code (Pruess, 1987) developed primarily for use in geothermal problems, and used it to predict their experimental measurements of temperature and pore pressure build-up in heated moist mortar (Section 2.3). They found that the results from various simulations compared favourably with the experimentally measured data, especially with respect to predicting the peak pressures of about 3.1 MPa (Fig. 2.19). They concluded that pore pressure build-up is a major factor in the occurrence of spalling, but differential thermal stresses also have a significant influence, and that coupled pore pressure and differential thermal stress analyses are required to quantify the relative importance of pressure build-up and thermal stress.

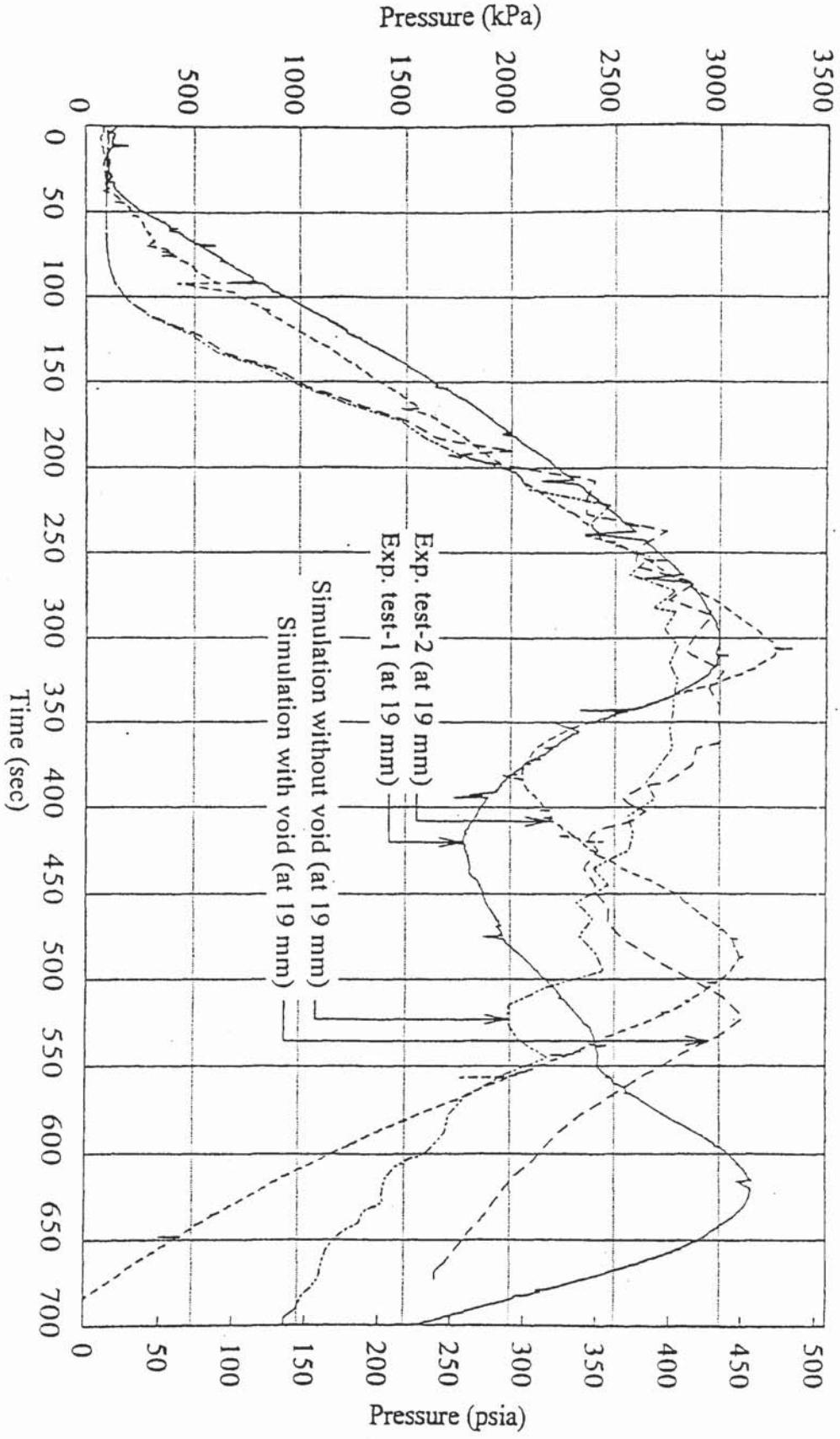

Fig. 2.19: Pore pressures measured experimentally and predicted using a 2-D simulation (after Consolazio *et al.*, 1997)

2.4.2 The Second Approach Models

2.4.2.1 Šelih and Sousa (1996)

Based on a mathematical model developed by Šelih *et al.* (1994) for heat and mass transfer in heated concrete in which diffusion of water vapour is considered, Šelih and Sousa (1996) presented the results of coupled heat and mass transfer due to non-uniform temperature distribution in a concrete wall exposed to two different fire curves as shown in Fig. 2.20.

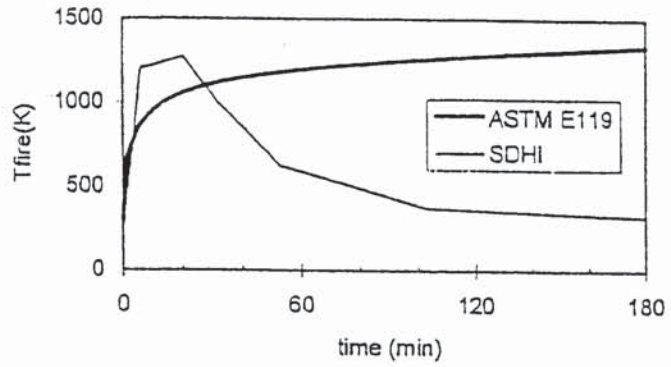

Fig. 2.20: Fire exposure curves according to ASTM E-119 standard and Ellingwood (SDHI=Short Duration High Intensity fire exposure curve) (after Šelih and Sousa, 1996)

The ASTM E-119 fire curve is similar to the BS 476:Part 20:1987 or the ISO 834:Part 1:1987 fire curves in that it is a conservative estimate of an actual fire during which the temperature increases with time implying an inexhaustible supply of fuel, while the fire curve proposed by Ellingwood (1991) is obtained by using an overall energy balance equation for the fire compartment, and shows that the temperature reaches an early maximum value and then decreases gradually.

The case considered is that of a 200-mm-thick lightweight concrete wall exposed to fire from one side that is unsealed, and thus the pressure at the fire-exposed surface is equal to the standard atmospheric pressure. Fig. 2.21 shows the distribution of temperature T, in K, saturation S, in %, and pore pressure P_{gg}, in MPa, in a wall exposed to fire according to both fire curves for 22 and 45 minutes. When the wall is exposed to ASTM E-119 fire curve, the maximum pore pressure is about 0.8 MPa at a distance of 20 mm from the fire-exposed surface after 22 minutes of exposure to fire. After 45 minutes of exposure to fire, the maximum pore pressure is 1.3 MPa at 40 mm from the fire-exposed surface.

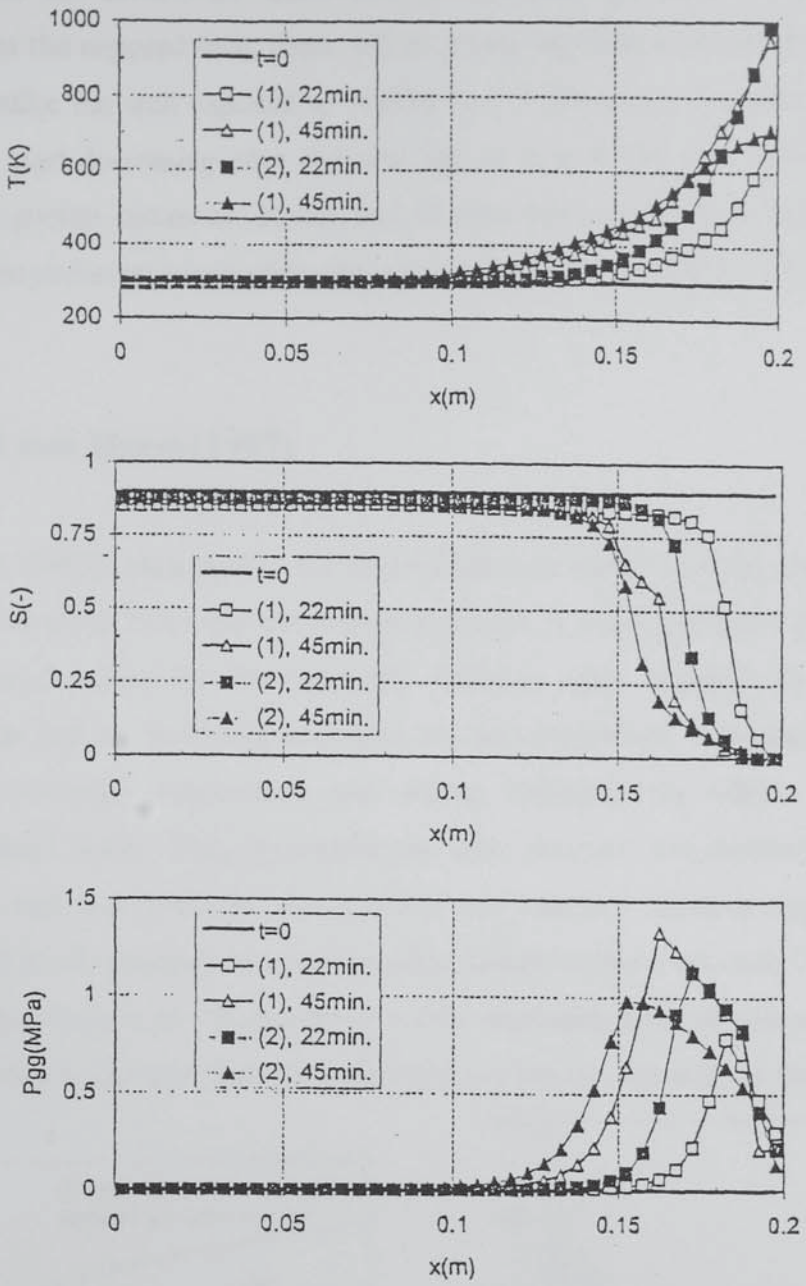

Fig. 2.21: Distribution of Temperature T, saturation S, and pore pressure P_{gg} in a concrete wall exposed to fire according to ASTM E-119 standard (1) and Ellingwood (2) after 22 and 45 minutes of exposure to fire (after Šelih and Sousa, 1996)

Šelih and Sousa stated that the continuous increase in the pore pressure with time is expected when the wall is exposed to ASTM E-119 fire curve. Surprisingly, however, they also stated that the same phenomenon is observed for the wall exposed to SDHI fire curve, even though it is clear from Fig. 2.21 that, when the wall is exposed to fire according to Ellingwood's fire curve, the maximum pore pressure of 1 MPa after 45 minutes of exposure to fire is smaller than that of 1.2 MPa after 22 minutes of exposure. It is true that, when the fire drops off, there will still be some increase in

temperatures within the section for some time (temperature gradient effects), and that although cooling will start at the exposed face, there will be a time lag before the section as a whole starts to cool. However, unlike the wall exposed to ASTM E-119 fire curve, it should be expected that the pore pressure will start decreasing after this time lag, as seen in Fig. 2.21. Also, the maximum pore pressures occur at greater distances (25 mm and 50 mm) from the fire-exposed surface than those at which the maximum pressures occur when the wall is exposed to ASTM E-119 fire.

2.4.2.2 Ahmed and Hurst (1997)

Ahmed and Hurst (1997) presented a 1D finite difference model for the coupled heat and mass transfer in heated concrete following the second approach in which the liquid phase and the gaseous phase are considered separately, and thus the diffusive mass transport by mass concentration gradients of vapour and air according to Fick's law are considered. The model takes into account the conservation of mass, momentum, and energy including the effects of evaporation and dehydration of bound water. They presented the time histories and distributions of temperature, moisture content, and pore pressure, for a 177.8 mm unsealed siliceous aggregate concrete slab exposed to ASTM E119 standard time-temperature condition from one side (Figs. 2.22-2.24). The most important observations are those related to the maximum pore pressures, their locations, and the time at which they occur, and thus the potential for explosive spalling, as shown in Fig. 2.24.

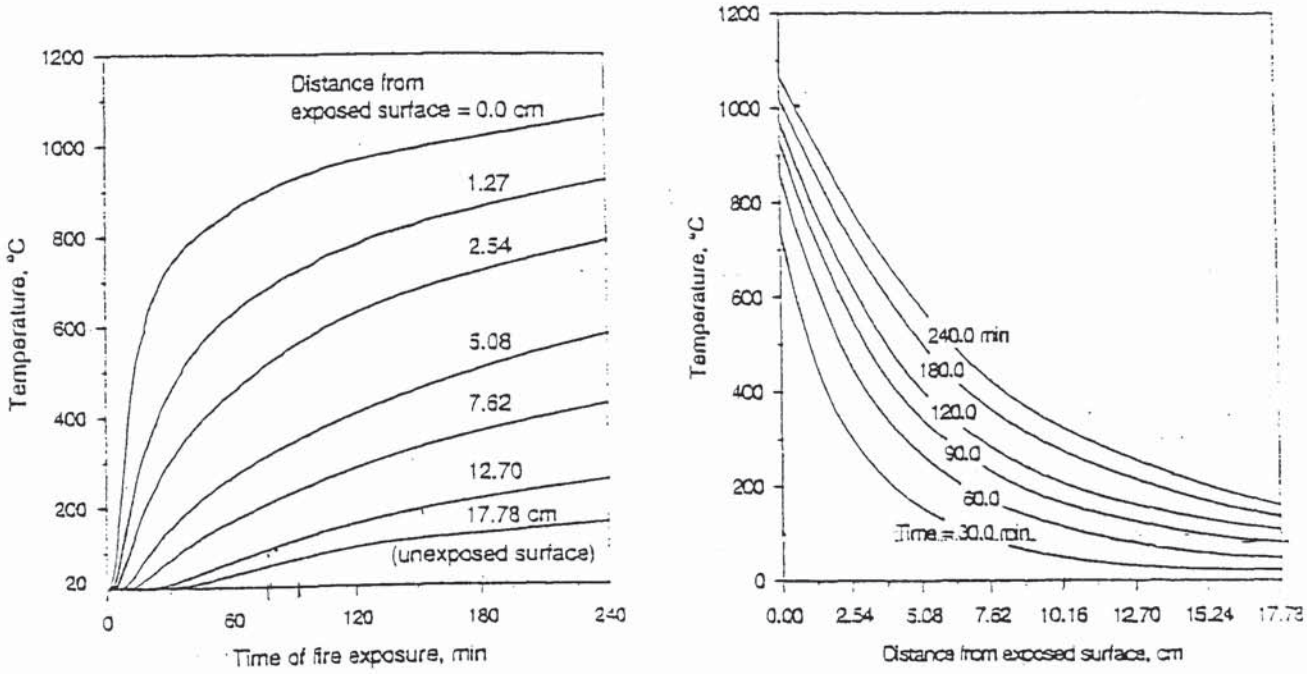

Fig. 2.22: Time history and distribution of temperature of a 177.8 mm concrete slab subjected to ASTM E119 temperature-time condition (after Ahmed and Hurst, 1997)

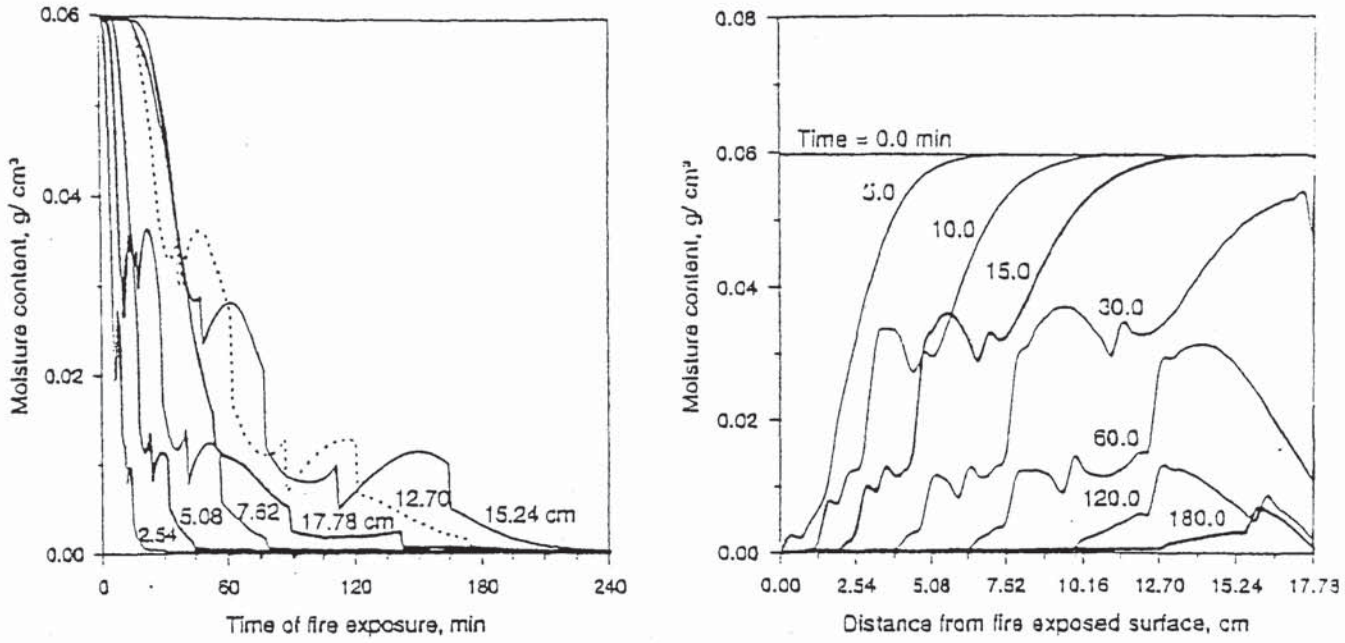

Fig. 2.23: Time history and distribution of moisture content of a 177.8 mm concrete slab subjected to ASTM E119 temperature-time condition (after Ahmed and Hurst, 1997)

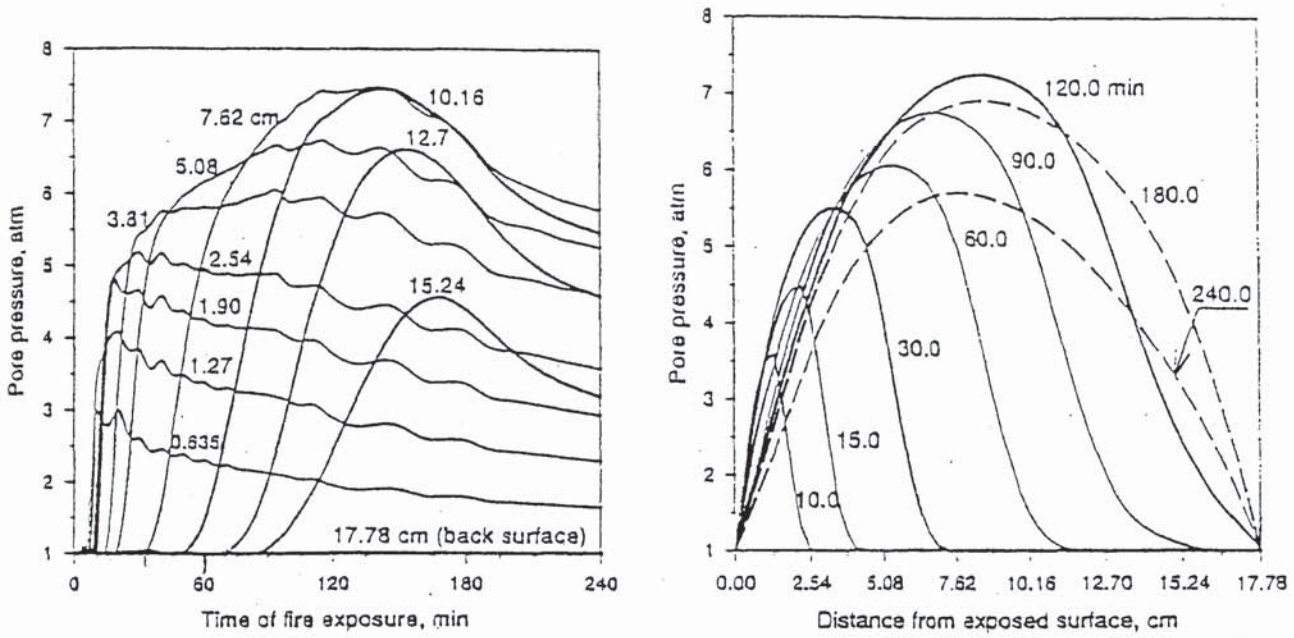

Fig. 2.24: Time history and distribution of pore pre pressure of a 177.8 mm concrete slab subjected to ASTM E119 temperature-time condition (after Ahmed and Hurst, 1997)

Ahmed and Hurst noted that the maximum pore pressure of about 0.75 MPa occurs at a distance of 76.2 mm from the exposed surface, and stated that cross-referencing this to Fig. 2.22 at the time of about 140 minutes at which the maximum pore pressure occurs shows that, although the pore pressure is relatively high, the temperature is relatively low at this depth. They concluded that the tendency for spalling at a depth that far from the exposed surface is almost nonexistent. They also

noted that the pore pressure is low at depths where the temperature is high (exposed surface and neighbouring zones). They stated that neither of these combinations is likely to cause spalling. They argued that the absence of spalling problems in Abrams and Gustaferro's (1968) test programme supports their premise, but one of the reasons for decreasing the occurrence of spalling in America is due to ASTM E-119 requiring specimen conditioning to low moisture contents (Malhotra, 1984).

2.4.2.3 Tenchev *et al.* (2001)

Tenchev *et al.* (2001a) developed a mathematical model for heat and mass transfer in heated concrete, and calculated maximum pore pressures of 2, 6.5, and 7.5 MPa after 10, 30, and 60 minutes, respectively, of exposure of a 400-mm-thick high-strength concrete wall to the ISO 834:Part 1:1987 standard fire regime from both sides as shown in Fig. 3 of Appendix C. Also, Tenchev *et al.* (2001b) calculated a maximum pore pressure of 2 MPa that occurs after 10 minutes of exposure of a normal-strength concrete wall of thickness over 200 mm to the same standard fire regime from both sides, after which the maximum pore pressure increases only slightly as shown in Fig. 1 of Appendix D. In a 400×400 mm concrete column exposed to fire on all four sides, maximum pore pressures of 2.5 and 3 MPa after 20 and 60 minutes of exposure to fire, respectively, were computed (Tenchev and Khalafallah, 2000) as shown in Fig. 2 of Appendix E.

2.5 PORE STRUCTURE OF CONCRETE

Neville (1995) reported that the median size of capillary pores is about 130 Å. On the other hand, at a water/cement ratio of about 0.38, the volume of the gel is sufficient to fill all the space available to it so that there will be no volume of capillary pores left after the process of hydration has been completed. Gel pores are much smaller than capillary pores. They are about 20-30 Å in nominal diameter, which is only one order of magnitude greater than the size of water molecules. Neville stressed that the importance of eliminating continuous capillaries is such that it is regarded a necessary condition for concrete to be classified as 'good'. The composition of cement paste at different stages of hydration is presented in Fig. 2.25, and a diagrammatic representation of the pore system in hydrated cement paste appears in Fig. 2.26. It can be seen from Fig. 2.25 that continuous capillary pores, with uniform cross sections, may not be present for w/c ratios of 0.38 or less. At such w/c ratios, capillary pores are segmented by gel pores that are only about 20 –30 Å.

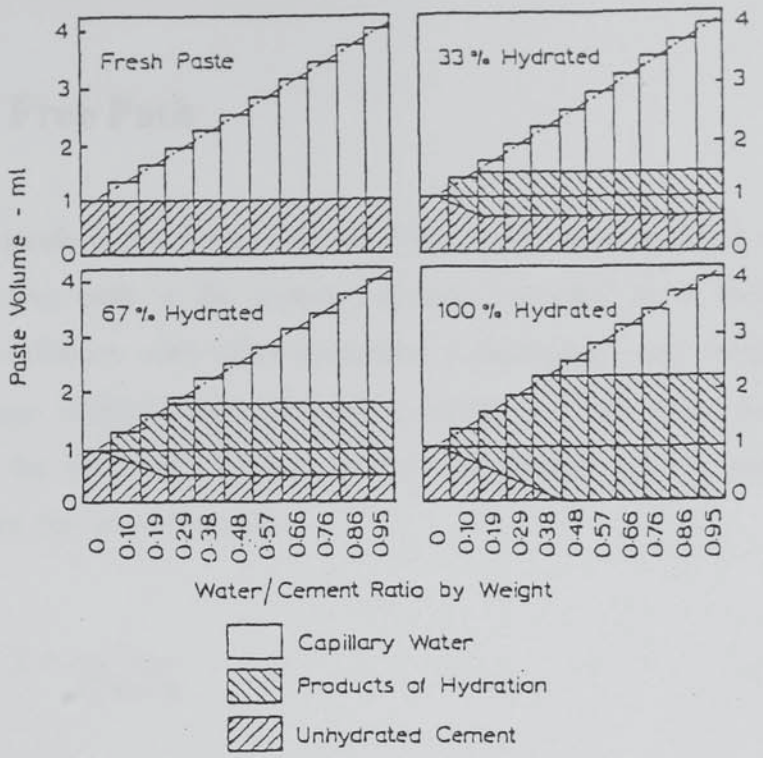

Fig. 2.25: Composition of Cement Paste at Different Stages of Hydration (after Neville, 1995)

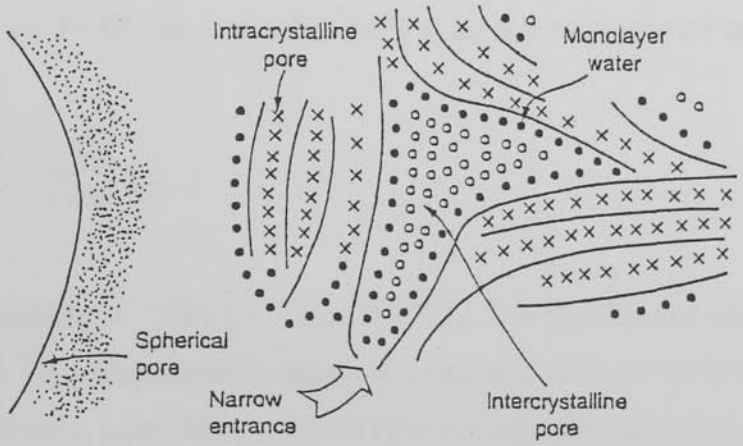

Fig. 2.26: Diagrammatic Representation of the Pore system in Hydrated Cement Paste (after Neville, 1995)

Skalny and Mindess (1991) discussed small-necked pores, and reported that only about 25% of the pore volume is composed of 'ink bottle' pores; the remaining 75% of the pore volume is composed of pores uniform in cross section.

2.6 DIFFUSION OF GASES

2.6.1 The Mean Free Path

The free path of a molecule is the distance travelled by the molecule before it collides with another molecule. The mean free path is the average distance travelled by a molecule between two successive molecular collisions with other molecules (Cunningham and Williams, 1980; Cussler, 1997). Cunningham and Williams used Maxwell's definition of the mean free path as the total distance travelled by the molecules divided by the total number of free paths to arrive at the following expression for the mean free path:

$$\lambda = \frac{1}{\sqrt{2}\pi\sigma^2 n} \tag{2.6}$$

where σ is the collision diameter (= 2.641×10^{-10} m for water), in m, and n is the molecular concentration.

Using the ideal gas law, $n = P/kT$, the mean free path, in m, can be expressed as

$$\lambda = \frac{kT}{\sqrt{2}\pi\sigma^2 P} \tag{2.7}$$

where k is Boltzmann constant (= 1.38×10^{-23} kg-m^2/s^2-°K), T is the absolute temperature, in K, and P is the pressure, in Pa. This characteristic length is compared with the pore diameter in order to determine the type of diffusion, other than surface diffusion, of gases in a porous medium.

2.6.2 Types of Diffusion

Cunningham and Williams discussed diffusion of gases, in general, and diffusion of gases in porous media, in particular, in detail. They classified the systems in which diffusion of gases occurs into systems with and without walls.

2.6.2.1 Systems without Walls (Molecular Diffusion)

If the gas occupies a large volume and can be considered unconfined by walls, the molecules collide only with each other. In this case, the resistance to the diffusive flux is due to molecule-molecule collisions, and the molecules do not lose momentum. This type of diffusion is known as molecular diffusion.

2.6.2.2 Systems with Walls (Porous Media)

The presence of walls results in another type of collisions, that is, molecule-wall collisions, and thus in another type of resistance to the diffusive flux. Depending on the ratio of the mean free path, λ, to the distance between the walls (or the diameter of the pore), d, diffusion is classified into two main types: viscous flux and Knudsen diffusion.

(a) Viscous Flux

If λ is much smaller than d, some of the molecules collide with other molecules while other molecules collide with the wall. Thus, resistance to the diffusive flux is due to both molecule-molecule and molecule-wall collisions. Some researchers, e.g. Cussler (1997), do not differentiate between molecular diffusion in systems without walls and the viscous flux, since molecule-molecule collisions are dominant when λ is much smaller than d, and the diffusive flux can be considered independent of the pore diameter. Also, the viscous flux is often called bulk diffusion.

(b) Knudsen Diffusion

When λ is much greater than d, the probability of a molecule colliding with another molecule is extremely small, and the molecules collide only with the wall. Molecules lose momentum in molecule-wall collisions, and thus resistance to the diffusive flux is greater than that due to molecule-molecule collisions. Diffusion of gases in such porous media where the pore diameter is much smaller than the mean free path is known as Knudsen diffusion.

The ratio of the mean free path to the pore diameter λ/d upon which the type of diffusion depends is known as Knudsen number *Kn*. Thus, bulk diffusion is dominant when *Kn* is much smaller than unity whereas Knudsen diffusion prevails when *Kn* is much greater than unity.

Other types of diffusion that do not depend on Knudsen number include surface and configurational diffusion.

(c) Surface Diffusion

Surface diffusion occurs due to the movement of the molecules that are adsorbed by the walls of the pores due to surface energy. It increases rapidly with temperature. However, as the temperature increases, the concentration of the adsorbed molecules decreases. Consequently, at a certain temperature, the surface concentration of adsorbed molecules as well as the surface flux will be practically zero. Therefore, the cross sectional area of the pores available for bulk diffusion or Knudsen diffusion, and thus the diffusive flux, increases when the temperature increases.

(d) Configurational Diffusion

When the pore diameter is decreased such that the molecular size is no longer negligible compared with the pore diameter, another resistance appears and another type of diffusion prevails known as configurational diffusion. Configurational diffusion appears in pores smaller than 20 Å in diameter (Fig. 2.27). In such pores, the shape (configuration) of a molecule affects the molecule-wall interaction potential (Cunningham and Williams, 1980).

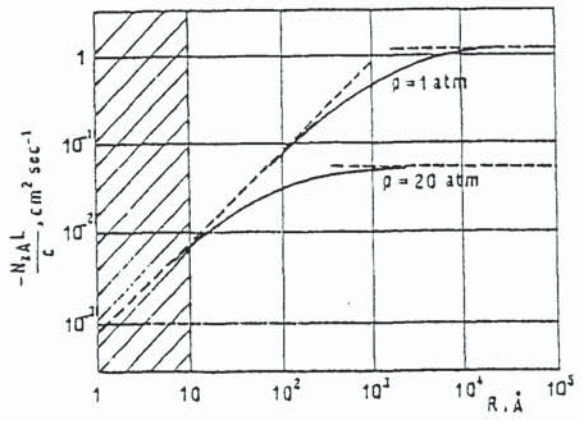

Fig. 2.27: Diffusive Flux in a Capillary as a Function of its Radius
(after Cunningham and Williams, 1980)

Figs. 2.28 and 2.29 demonstrate the types of diffusion as a function of the pore diameter.

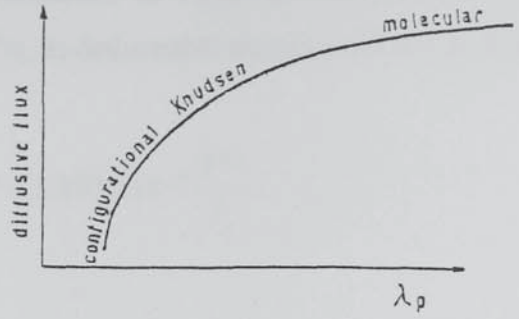

Fig. 2.28: Type of Diffusion Regime as a Function of the Pore Diameter
(after Cunningham and Williams, 1980)

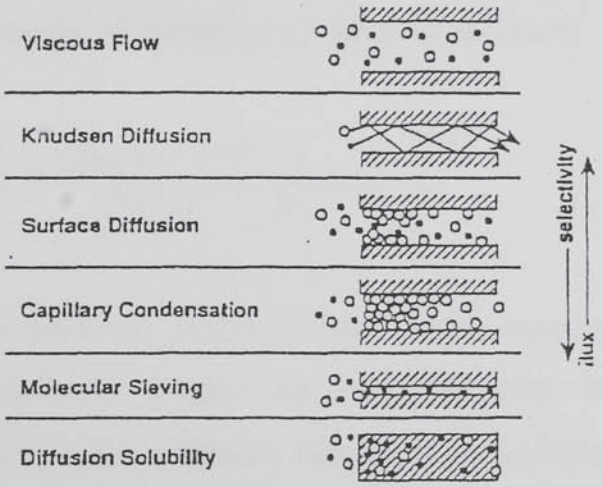

Fig. 2.29: Pore Diffusion Effects (The flux drops from top to bottom of the figure)
(after Cussler, 1997)

2.6.3 Molecular Diffusivity

Due to the lack of a diffusivity equation that is specific for concrete under transient heating conditions, researchers who adopt the second approach in mathematical modelling of heat and mass transfer in heated concrete have had to either assume that the diffusivities of water vapour and air are constant or rely on molecular diffusivity equations that are related to molecular (or bulk) diffusion. As discussed in the preceding section, molecular diffusion prevails only when the mean free path of gas molecules is much smaller than the pore diameter.

Thomas and He (1997), Zou *et al.* (1998), and Thomas and Missoum (1999) used an expression given by Krischer and Rohnalter in 1940 for the molecular diffusivity of water vapour and air through each other, in m^2/s, in deformable unsaturated soil as follows:

$$D = 5.893 \times 10^{-6} \frac{T^{2.3}}{P_g} \tag{2.8}$$

Tenchev *et al.* (2001b) (see Appendix D) depended on (2.8), but, realising that it is too great to be appropriate for concrete, they divided it by 10.

Bird *et al.* (1960) and Cussler (1997) provided the following expression, based on Chapman-Enskog theory, for the theoretical estimation of molecular diffusivity:

$$D = \frac{1.86 \times 10^{-7} T^{3/2}}{P \sigma_{12}^2 \Omega} \left(\frac{1}{M_1} + \frac{1}{M_2} \right)^{1/2} \tag{2.9}$$

where D is the diffusion coefficient, in m^2/s, T is the absolute temperature, in K, P is the pressure, in atm, and M_i are the molecular weights (also called the molar masses), in kg/kmol. σ_{12} is the collision diameter, in Å; it is the arithmetic average of the collision diameters of the two species present:

$$\sigma_{12} = \frac{1}{2}(\sigma_1 + \sigma_2) \tag{2.10}$$

Values of σ_1 and σ_2 for different species are listed by Cussler (1997).

The collision integral Ω is a dimensionless molecular property characteristic of the detailed theory usually of order 1. Its detailed calculation depends on an integration of the interaction between the two species. The integral depends on the temperature and the energy of interaction ε_{12} that is a geometric average of contributions from the two species:

$$\varepsilon_{12} = \sqrt{\varepsilon_1 \varepsilon_2} \tag{2.11}$$

Values of ε_i and Ω as a function of $\varepsilon_{12} / k\,T$ are listed by Cussler (1997).

From (2.9), molecular diffusion of water vapour through air, in m^2/s, according to Chapman-Enskog theory, is

$$D_{VA} = 5.6 \times 10^{-4} T^{1.5} / P_g \tag{2.12}$$

This expression leads to smaller values of diffusivity at high temperatures, due to its weaker dependence on temperature, than Krischer and Rohnalter's (2.8) even though (2.8) is cited for soil that is a porous medium while (2.12) is for systems devoid of walls. Thus, the reasonableness of (2.8) for mathematical modelling of heat and mass transfer in heated concrete is even more questionable. Ahmed and Hurst (1997) adopted (2.12).

De Vries (1958) provided the following expression for the molecular diffusion coefficient of water vapour through air, in m^2/s, in simultaneous heat and moisture transfer in soil:

$$D = 4.42 \times 10^{-8} T^{2.3} / P \tag{2.13}$$

This expression has a similar dependence on temperature as (2.8), but is two orders of magnitude smaller.

Çengel (1998) stated that the molecular diffusion coefficient is independent of the mixture composition and increases with temperature while decreasing with pressure:

$$D_{AB} \propto T^{1.5} / P \tag{2.14}$$

Marrero and Mason (1972) proposed the following expression for the molecular diffusivity of water vapour through air, in m^2/s, for $280°K < T < 450°K$:

$$D_{H_2O-Air} = 1.87 \times 10^{-10} T^{2.072} / P \tag{2.15}$$

where P is pressure, in atm, and T is the temperature, in K. Tenchev *et al.* (2001a) used (2.15).

Molecular diffusivity equations are inversely proportional to the pressure since, when the concentration, and thus the pressure, increases, the number of molecule-molecule collisions, and thus the resistance to diffusion, increases.

2.6.4 Knudsen Diffusivity

When the mean free path is greater than the pore diameter, Knudsen diffusivity is estimated from the kinetic theory as (Cunningham and Williams, 1980; Cussler, 1997):

$$D_{Kn} = \frac{1}{3} dv \tag{2.16}$$

where d is the diameter of the pore and v is the molecular velocity. This is the same as that used to predict molecular diffusivity (2.9) but with the mean free path λ replaced by the pore diameter d. The molecular velocity is given as:

$$v = \sqrt{\frac{2kT}{m}} \tag{2.17}$$

where m is the molecular mass. Thus, Knudsen diffusivity is given by:

$$D_{Kn} = \frac{d}{3}\left(\frac{2kT}{m}\right)^{0.5} \tag{2.18}$$

Cussler also provided a slightly larger value based on a more exact kinetic theory for Knudsen diffusivity, in m^2/s:

$$D_{Kn} = 48.5d\sqrt{T/M} \tag{2.19}$$

where d is the pore diameter, in m, T is the absolute temperature, in K, and M is the molecular weight, in kg/kmol. Unlike the molecular diffusion coefficient, Knudsen diffusion coefficient is independent of the pressure and of the molecular weight of the second species, because the molecules do not collide with each other; they only collide with the wall.

The general form of (2.19) is expected, since, in Knudsen diffusion, the resistance to the diffusive flux in pores smaller than the mean free path of the gas molecules is due to molecule-wall collisions. This fact implies that Knudsen diffusivity is proportional to the pore diameter, since the number of molecule-wall collisions, and thus the resistance to diffusion, is inversely proportional to the diameter of the pore; the larger the pore, the smaller the number of collisions, and thus the

smaller the resistance to diffusion, i.e. the greater the diffusivity. The effects of the temperature and the molecular weight are also expected, since the velocity of the molecules, and thus the diffusivity, increases with the temperature, and the resistance to diffusion increases with the molecular weight, i.e. the diffusivity decreases.

It should be noted that the definition given in the literature by different researchers, e.g. Cunningham and Williams (1980) and Cussler (1997), for d in Knudsen diffusivity (2.16) and (2.19) is that it is the pore diameter. It is extremely important to realise that this definition is a special case that is valid only in dry porous media. In moist concrete, Knudsen diffusion does not take place through the entire cross section of the pore. Due to the presence of free water, diffusion occurs only in the remaining cross section of the pore that is occupied by the gaseous mixture volume fraction. Thus, in moist concrete, Knudsen diffusivity must be a function of the diameter of the remaining cross section of the pore, i.e. the diameter of the pore minus the thickness of the film of free water, say w, that covers the wall of the pore. Thus, the general forms of Knudsen diffusivity (2.16) and (2.19) are

$$D_{Kn} = \frac{1}{3}(d - w)v \tag{2.20}$$

and

$$D_{Kn} = 48.5(d - w)\sqrt{\frac{T}{M}} \tag{2.21}$$

2.6.5 Effective Diffusivity

2.6.5.1 Effective Diffusivity in Porous Media

The diffusion coefficients discussed in Sections 2.6.3 and 2.6.4 define the diffusivity in the gaseous phase, and thus are valid when the pores are straight and the medium does not contain impermeable solids. However, in a porous medium such as concrete, the pores are not straight, and the medium contains impermeable solids through which diffusion does not take place. Thus, diffusion takes place over a longer distance and over a smaller cross-sectional area (Fig. 2.30). Cunningham and Williams (1980) took into account the effects of longer pores and smaller cross-sectional area by an obstruction factor of the form:

$$Q = \varepsilon_s / \tau \tag{2.22}$$

where ε_s is the surface porosity of the porous medium and τ is a tortuosity factor. Thus,

$$D_e = QD \tag{2.23}$$

where D_e is the (totally) effective diffusivity that accounts for both effects of longer pores and smaller area, and D is the diffusivity in the gaseous phase.

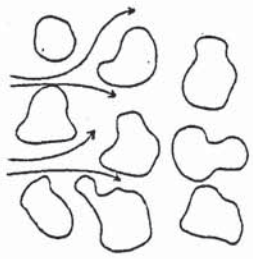

Fig. 2.30: Tortuous Diffusion in a Porous Solid (after Cussler, 1997)

They stated that the tortuosity ranges between 3 and 7, and that, in most cases, it ranges between 3 and 5. For isotropic pore systems, $\tau = 3$ is found accurate by several researchers, e.g. Johnson and Stewart (1965), Brown *et al.* (1969), and Feng and Stewart (1973). Thus, the value of 3 for the tortuosity in concrete at ambient temperature appears to be appropriate.

The effects of longer pores and smaller cross-sectional areas were also included in the definition of the effective diffusion coefficient by Cussler (1997):

$$D_e = \varepsilon_g D / \tau \tag{2.24}$$

where D_e is the totally effective diffusivity and ε_g is the volume fraction of the gas. He reported that τ ranges between 2 and 6 with an average of 3.

An approach in which the effect of the smaller cross-sectional area is not included in the definition of the effective diffusivity, but included in the diffusive flux, is adopted by several researchers, e.g. Johnson and Stewart (1964), Feng and Stewart (1973), Ahmed and Hurst (1997), and Tenchev *et al.*

(2001). (Some researchers, e.g. Ahmed and Hurst, neglect the tortuosity, and thus assume that the pores are straight; $\varepsilon_g D$ is *not* totally effective diffusivity.) In this approach, the effective diffusivity is expressed as

$$D_e' = D/\tau \tag{2.25}$$

where D_e' is the (partially) effective diffusivity that takes account of the effect of longer pores, but not of the effect of the smaller area.

The distinction between the totally effective diffusivity (or simply the effective diffusivity) and the partially effective diffusivity is very important to the discussion in Chapter 3. These descriptions of the effective diffusivity are introduced in this investigation to aid in the development of a new diffusivity equation for concrete at various temperatures.

From (2.24) and (2.25), the relation between the effective diffusivity, D_e, and the partially effective diffusivity, D_e', is

$$D_e = \varepsilon_g D_e' \tag{2.26}$$

The effective diffusivity of gases in porous media can be found theoretically. Theoretical models require a geometrical model in order to determine the tortuosity. They also require such properties as the porosity and the pore size distribution. Then, molecular diffusivity is used for macropores where the mean free path is smaller than the pore diameter, whereas Knudsen diffusivity is used for micropores where the mean free path is greater than the pore diameter, to evaluate the overall effective diffusivity of the gas in the porous medium (Wakao and Smith, 1962; Johnson and Stewart, 1965; Feng and Stewart, 1973; Carniglia, 1986).

At ambient temperature, the effective diffusivity can also be determined experimentally. In fact, advantage will be taken of experimental diffusivity investigations on different concretes with different porosities at ambient temperature in order to develop an effective diffusivity equation for one and the same concrete at any temperature, because the effective diffusivity in concrete under transient heating conditions cannot be directly determined neither theoretically nor experimentally. Determination of the effective diffusivity in concrete at ambient temperature will be discussed in greater detail in the following section.

2.6.5.2 Effective Diffusivity in Concrete at Ambient Temperature

The theoretical approach for determining the effective diffusivity has been applied to dry porous media, other than concrete, at normal temperature. In concrete, however, the vast majority of the pores are much smaller than the mean free paths of the molecules of different gases, and thus Knudsen diffusion is the dominant type of diffusion that takes place. This is particularly true in concrete with w/c ratios of 0.38 or less since, according to Neville (1995), at this w/c ratio, capillary pores become segmented by gel pores, and thus cease to have uniform cross sections.

In theory, it appears that, for moist concretes with w/c ratios higher than 0.38 where continuous capillary pores with uniform cross sections can exist, both types of diffusion can be considered to determine the overall effective diffusivity at ambient temperature using the theoretical approach. Due to the presence of moisture, it would be necessary to determine an *effective* pore size distribution that describes only the space occupied by the gaseous mixture volume fraction through which diffusion can take place, by eliminating the pores that are completely filled with water and subtracting the film of water from other pores. However, it appears that only the experimental approach has been applied to determine the effective diffusivity of gases such as CO_2 and O_2 in different concretes with different porosities at ambient temperature.

Papadakis *et al.* (1991) determined experimentally the effective diffusivity of N_2, and thus of CO_2, at ambient temperature in terms of the porosity of the paste and the relative humidity. They found the following expression for the effective diffusivity, in m^2/s, of CO_2 in concrete at normal temperature:

$$D_{e,CO_2} = 1.64 \times 10^{-6} \varepsilon_p^{\,1.8} (1 - RH/100)^{2.2} \qquad (2.27)$$

where ε_p is the porosity of the paste and RH is the ambient relative humidity. They adopted the approach in which the effective diffusivity refers to the total cross section of the porous medium, and thus the gaseous mixture volume fraction ε_g through which diffusion takes place is included in D_e, i.e. D_{e,CO_2} is the totally effective diffusivity of CO_2 in concrete at ambient temperature. Fig. 2.31 demonstrates the dependence of cement paste porosity on the water/cement ratio and age, and illustrates the comparison with measurements at 100 days of age obtained by Papadakis *et al.* Fig. 2.32 shows Papadakis *et al.*'s results for the dependence of the effective diffusivity of CO_2 in concrete on the relative humidity, w/c ratio, presence of aggregates, and carbonation. Papadakis *et al.* also stated that Knudsen diffusion is the dominant type of diffusion of gases in concrete.

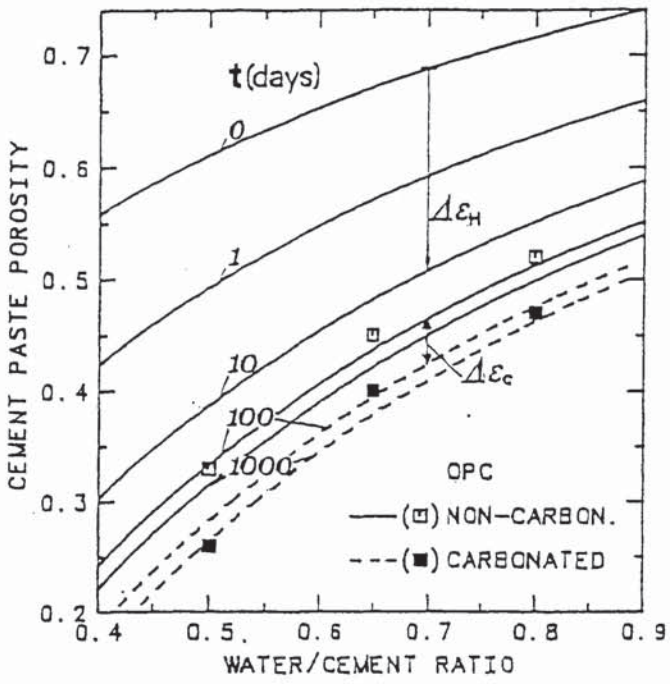

Fig. 2.31: Dependence of Cement Paste Porosity on Age and W/C Ratio (after Papadakis *et al.*, 1991)

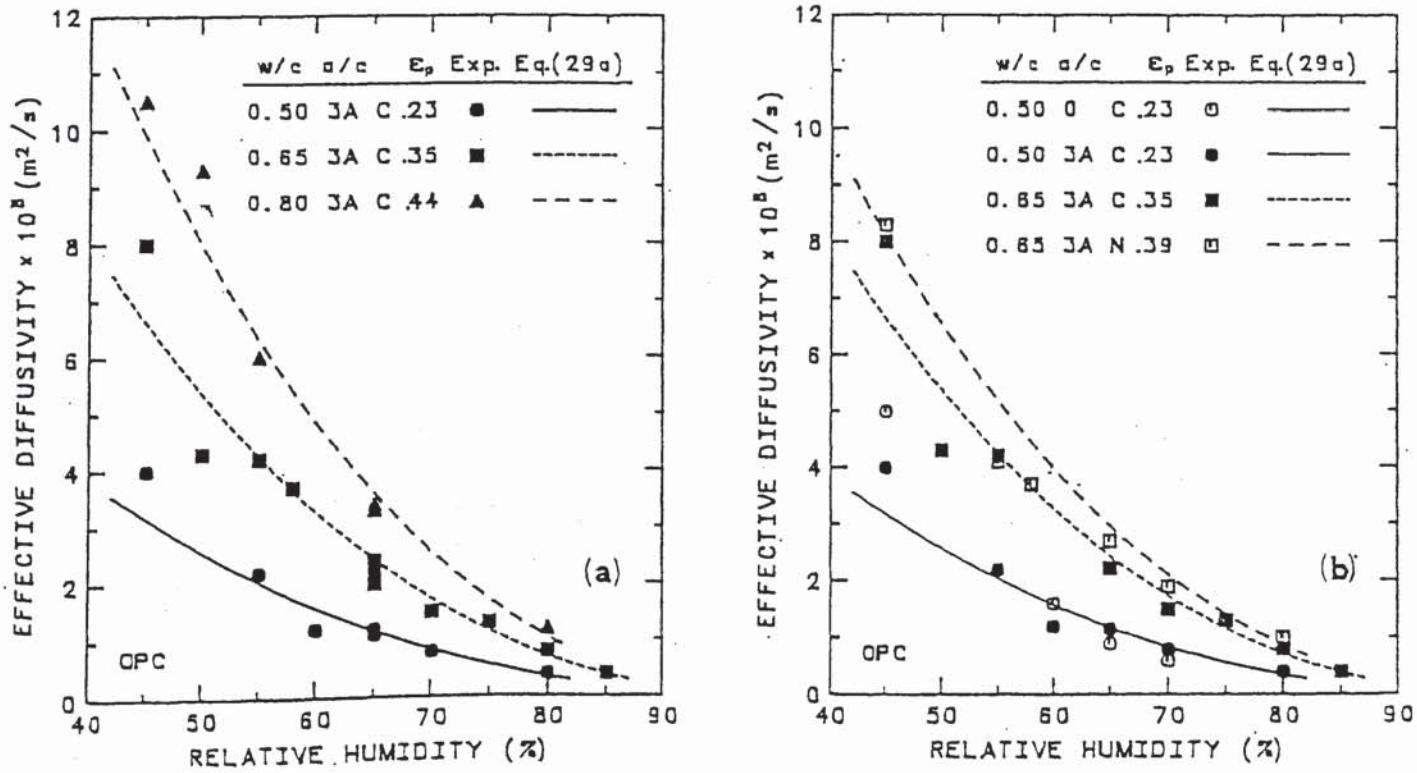

Fig. 2.32: Dependence of Effective Diffusivity of CO_2 on Relative Humidity, W/C Ratio, Presence of Aggregates, and Carbonation (after Papadakis *et al.*, 1991)

In order to determine the fraction of the pore volume ε_g available for diffusion of gases such as CO_2, O_2, or water vapour, it is necessary to determine the degree of saturation of the pores with water. The degree of saturation is determined from the pore size distribution and the solid surface chemistry. Pores with diameters less than the Kelvin diameter d_k are completely filled with water. whereas the walls of pores with diameters greater than d_k will be covered by a continuous film of water of thickness w. Papadakis *et al.* provided the following expressions for w, in μm, and d_k, in μm, in terms of the absolute temperature, in °K, and the relative humidity RH:

$$w = \frac{Cxd_w}{[1+(C-1)x](1-x)}\left(1 - x^{d/2d_w}\right) \tag{2.28}$$

$$d_k = 2w + \frac{A}{T\ln(1/x)} \tag{2.29}$$

where $x = RH/100$, A is a constant equals to 0.6323 (noncarbonated material) and 0.2968 (carbonated material), C is the BET-constant for the particular temperature and water vapour-solid surface system, d is the pore diameter, in μm, and d_w is the molecular diameter of water ($= 3\times10^{-4}$ μm). They found that the BET-constant C is approximately equal to 100 for non-carbonated cements and is equal to 1 for carbonated cements. They reported that this large difference is due to fact that the pore surface of non-carbonated cement is hydrophilic due to the presence of $Ca(OH)_2$, while that of carbonated concrete is not due to the absence of $Ca(OH)_2$.

2.7 CONCLUSIONS

- So far, the mechanisms proposed to explain explosive spalling in heated concrete suggest that it is due to thermal stresses, high pore pressures, or both. As far as thermal stresses are concerned, estimates have been made using elastic theory. Also, constitutive models for heated concrete have been investigated, and models for predicting the thermal stresses have been developed. However, the theory does not agree with the experimental observations regarding the susceptibility of water-cured, low moisture, high strength, and thick concrete sections to spalling.

- The magnitudes of the pore pressure in heated concrete are difficult to predict. Consequently, the measured as well as the calculated magnitudes of the pressure vary enormously.

Experimentally, they range from as low as 0.2 MPa to 0.65 MPa in unsealed heated concrete, and up to 10 MPa in sealed concrete. Pore pressure calculations with mathematical models predict pore pressures from as low as 0.13 MPa to more than 3 MPa in heated normal-strength concrete, and up to 7.5 MPa in heated high-strength concrete.

- In mathematical modelling, two approaches are adopted; diffusion of water vapour is neglected in the first approach, but is considered in the second one. Obviously, only one of the two approaches is correct; diffusion either occurs or does not, and thus only the results of one approach can be reliable. Furthermore, researchers who consider diffusion either assume that the diffusivity is constant or depend on molecular diffusivity equations intended for systems devoid of walls.

In order to determine whether the results of a certain mathematical model are correct, it is necessary to determine the validity of the assumptions adopted. Also, if a certain assumption is found invalid, it is necessary to find the solution to the problem. These issues will be investigated in Chapter3.

CHAPTER 3

THE FIRST DIFFUSIVITY EQUATION FOR HEATED CONCRETE

3.1 INTRODUCTION

It is clear from the discussion in Section 2.4 that whether or not diffusion of water vapour through air occurs in concrete is quietly debateable. Furthermore, researchers who adopt the second approach to mathematical modelling of heat and mass transfer in heated concrete in which diffusion is considered have had to either assume constant values for the diffusivities of vapour and air or rely on molecular diffusivity equations due to the lack of a diffusivity expression that is specific for concrete at any temperature. Evidently, such assumptions that affect the formulation of the governing equations have very significant effect on the magnitudes of the pressure in particular, since the unreliability of the results of different models is very clear from the spread in the results.

This unreliability has led to researchers who are concerned with spalling of heated concrete insisting on the need for experimental work to verify the accuracy of different models. For example, Connolly (1995) stated that the maximum pressures predicted by different researchers vary enormously despite the fact that they were all modelling essentially similar situations, and thus recommended dependence on experimental work. Nevertheless, the development of mathematical models for heat and mass transfer in heated concrete has been continuing to be carried out using both approaches since 1978, while no attempt has been made to investigate whether or not diffusion of water vapour occurs in concrete nor that diffusion of gases in concrete is molecular is reasonable.

The lack of research regarding whether diffusion of vapour occurs in concrete may seem surprising. On the other hand, the fact that no attempt has been made to investigate whether the assumption of molecular diffusion holds is less surprising although the effect on the realism of the results might be significant since, should this assumption be unreasonable, then it will be necessary to develop a diffusivity equation that is specific for concrete at any temperature. That no attempt has been made to develop a diffusivity equation specifically for concrete is because such an equation cannot be directly developed. However, it will be demonstrated that, by combining theory with experiment, it is possible to develop an effective diffusivity equation for any gas in concrete at any temperature.

3.2 FLUX EQUATIONS

The governing equations and various assumptions upon which the second approach to mathematical modelling is based are described in detail in Appendix C. For convenience, however, the equations of the total mass flux of water vapour and air only are written below, since these equations will be referred to later in this chapter. Equally, it should be noted that the partially effective diffusivities of water vapour and air are expressed differently in these equations; they are assumed to be same $(= D_{AV})$ in (5) and (6) in Appendix C, since Tenchev *at al.* (2001a) depended on molecular diffusivity in systems devoid of walls in which the diffusivity of water vapour through air is the same as that of air through water vapour.

The total mass flux of water vapour per unit area of concrete, in kg/m^{2}s, is:

$$J_v = -\varepsilon_g \rho_v \frac{KK_g}{\mu_g} \nabla P_g - \rho_g \varepsilon_g D'_{e,v} \nabla \left(\frac{\rho_v}{\rho_g} \right) \tag{3.1}$$

where ε_g is the volume fraction of the gaseous mixture of water vapour and air, ρ_v is the mass of water vapour per unit volume of the gaseous mixture, in kg/m^3, K is the intrinsic permeability of concrete, in m^2, K_g is the relative permeability of the gaseous mixture through concrete, μ_g is the dynamic viscosity of the gaseous mixture, in kg/ms, P_g is the pore pressure of the gaseous mixture, in Pa, ρ_g is the mass of the gaseous mixture per unit volume of the gaseous mixture, in kg/m^3, and $D'_{e,v}$ is the partially effective diffusivity (Section 2.6.5) of water vapour in concrete, in m^2/s.

The total mass flux of air per unit area of concrete, in kg/m^{2}s, is:

$$J_a = -\varepsilon_g \rho_a \frac{KK_g}{\mu_g} \nabla P_g - \rho_g \varepsilon_g D'_{e,a} \nabla \left(\frac{\rho_a}{\rho_g} \right) \tag{3.2}$$

where ρ_a is the mass of air per unit volume of the gaseous mixture, in kg/m^3, and $D'_{e,a}$ is the partially effective diffusivity of air in concrete, in m^2/s.

3.3 MATHEMATICAL MODELLING OF HEAT AND MASS TRANSFER IN HEATED CONCRETE

3.3.1 The First Approach to Mathematical Modelling

3.3.1.1 The Basic Assumption

Bažant (1997) argued that the more complicated approach in which the free water phase and the water vapour phase are treated separately is unnecessary and, more importantly, unreasonable because it implies that liquid water molecules and water vapour molecules can travel freely and independently of each other over finite distances macroscopically through concrete. He stated that this implication is unreasonable particularly because water vapour molecules cannot pass through the pores of subcapillary dimensions that block the passages through concrete. Bažant argued that the reason is that the mean free path of water vapour molecules is about 800 Å at room temperature, and *much more* at high temperature, compared with the width of the necks through concrete of about 10 Å (about 50 Å in dense cement pastes according to Bažant and Thonguthai (1978) and Bažant and Kaplan (1996); this difference is extremely significant as far as diffusion is concerned, as discussed in Section 2.6.2.2). He stated: *'When the mean free path of water vapour molecules is larger than the opening, the passage of a molecule through such opening is virtually impossible.'*

This argument has been cited since 1972 when Bažant and Najjar (1972) considered that, at room temperature, the transfer of moisture takes place only within the adsorbed water layers. Bažant and Thonguthai (1978) depended on this argument, and reported that Powers and Brownyard (1948) found that the major variable in permeability of cement paste and concrete was the capillary porosity but this finding cannot be true because moisture transfer below 100°C is not controlled by the flow of capillary water. They stated that flow is controlled by the necks on the continuous flow passages through the cement paste (P in Fig. 2.16(c)). A similar argument was also cited by Bažant and Kaplan (1996).

This argument has very serious consequences:

(1) The first is the conclusion reached by Bažant and Najjar (1972) that liquid water transfer at normal temperature is only due to surface diffusion.

(2) The second, and most important, is the basic assumption that diffusion of water vapour through air does not take place in concrete at any temperature. This is the basic assumption upon which the first approach to mathematical modelling of heat and mass transfer in heated concrete was founded by Bažant and Thonguthai (1978) when they developed their mathematical model in which diffusion of water vapour through air is neglected at all temperatures (Section 2.4.1.1).

(3) The third is the hypothesis proposed by Bažant and Thonguthai (1978) to explain the jump in permeability by two orders of magnitude when the temperature exceeds 100°C. This hypothesis will be presented in the following section.

3.3.1.2 The Hypothesis

Chapman and England (1977) tested concrete cylinders subjected to a sustained temperature difference between their ends, with maximum temperatures between 105°C and 200°C. They found that samples taken from the hot side of the drying front showed an increase in the values of the coefficient of permeability in the order of 100 times greater than those of the wet regions where the total water content per unit weight of mix water was greater than unity. They reported that the permeability appears to be significantly affected by three interdependent factors: the elevated temperature to which the concrete is subjected, the time for which the concrete is subjected to high temperature, and the evaporable water content of the concrete.

Likewise, Bažant and Thonguthai (1978) independently found from their test data that the permeability increases by about two orders of magnitude for temperatures exceeding 100°C. In order to explain this jump in permeability, they proposed the following hypothesis: due to smoothing of pore surfaces to reduce the surface energy, the width of the necks governing the flow (N in Fig. 2.16(c)) increases many times as the temperature exceeds 100°C, allowing liquid water and water vapour to pass through the necks whilst at the same time the volume of the necks is negligible, so that no significant effect of the large relative increase of the necks width on the measured pore size distribution at high temperature can be detected.

3.3.1.3 Diffusion of Water Vapour in Concrete at High Temperature

Bažant (1997) stressed that water vapour cannot pass through pores in concrete at any temperature, because the mean free path is much more than 800 Å at high temperature, and thus, based on this concept, it is assumed that diffusion of water vapour through air does not occur on a macroscopic scale in concrete at any temperature. Consequently, diffusion of water vapour through air in Bažant and Thonguthai's (1978) mathematical model was neglected at all temperatures.

However, in contrast to the argument, the hypothesis presented in the previous Section confirms that, at temperatures greater than 100°C, water vapour does pass through concrete pores, and hence travels macroscopically through concrete. Thus, at high temperature, diffusion of water vapour through air does occur on a macroscopic scale in concrete. Therefore, it is not only reasonable, but also necessary to separate the water phase and the vapour phase, and to consider the mass flux of air, in order to be able to include diffusion of water vapour and air through each other in the treatment, unless the effect of diffusion on the results in general and on the pore pressure in particular is proven negligible.

3.3.1.4 Diffusion of Water Vapour in Concrete at Ambient Temperature

The pore structure of concrete was discussed in Section 2.5. Bažant and Thonguthai's (1978) representation of the pore system in concrete is completely different as shown in Fig. 2.16(c). They represented the cement gel such that it consists of flow passages of large capillary pores (larger than the mean free path of water vapour molecules) connected with very small necks that can be widened from 10-50 Å to 800 Å, rather than segmented by gel pores that cannot be widened 16 times. In fact, the mean free path of water vapour molecules at 100°C and 1 atm is about 1600 Å. Thus, if water vapour molecules cannot pass through openings smaller than the mean free path, and if water vapour does pass through the necks at 100°C, then the necks need to be widened from about 10-50 Å to 1600 Å, and the pores must be at least 1600 Å in size.

Bažant and Thonguthai's hypothesis does not convincingly explain how water vapour can pass at a temperature of 100°C in good concrete with dense cement paste that may not contain capillary pores as large as 1600 Å. Even if such pores are present, they will be segmented by gel pores that cannot be widened 32 times. The fact that vapour can, at least when the temperature exceeds 100°C, travel

macroscopically through 'good' concrete implies that the basic assumption that a water vapour molecule cannot pass through an opening smaller than the mean free path in a porous medium in which the gas is confined is questionable.

It would appear that there is not a single independent evidence that this assumption is valid in a porous medium. On the contrary, the literature supplies much evidence on the diffusion of gases in porous media where the pore diameter is much smaller than the mean free path. For example, diffusion of helium (mean free path of about 1400 Å) through nitrogen (mean free path of more than 600 Å) in micropores as small as 23 Å at 24°C and 1 atm was considered by Wakao and Smith (1962). Diffusion of hydrogen (mean free path of about 1150 Å) through nitrogen in micropores as small as 20 Å at 25°C was considered by Johnson and Stewart (1965). Diffusion of gases such as oxygen, carbon dioxide, and water vapour in concrete at normal temperature is recognized by, e.g. Lawrence (1984), The Concrete Society (1987), the CEB Model Code (1990), Papadakis *et al.* (1991), and Neville (1995).

As discussed in Section 2.6.2.2, this type of diffusion is known as Knudsen diffusion (see, e.g., Bird *et al.*, 1960; Wakao and Smith, 1962; Johnson and Stewart, 1965; Feng and stewart, 1973; Cunningham and Williams, 1980; Burganos and Sotirchos, 1987; Lawrence, 1984; Papadakis *et al.*, 1991; Cussler, 1997; Çengel, 1998). Diffusion which occurs in pores that are smaller than 20 Å is known as configurational diffusion (Section 2.6.2.2).

It is clear that the basic assumption upon which the first approach to mathematical modelling of heat and mass transfer in heated concrete is founded can be valid in a system devoid of walls where the gas molecules do not have to pass through an orifice in a plane through the system that is smaller than the mean free path. In such system, since the motion of each molecule is chaotic at the molecular level, the probability of a molecule passing through such opening is small, because there is nothing that forces the molecule to pass through the opening; a molecule is free to travel in any direction without being forced to change direction until it collides with another molecule. The smaller the opening compared with the mean free path, the smaller the probability of a molecule passing through the opening.

However, in a porous medium, gas molecules are trapped between the walls of the pores. The molecule keeps colliding with the opposite sides of the wall, and thus changes direction. The collision of a molecule with the wall is not specular, and thus, on the molecular level, a molecule

may or may not advance through the pore. However, if a concentration gradient exists, the molecules simply have to pass through the only available orifice, unless it is completely filled with water. Some of the molecules will be adsorbed by the walls due to the surface energy, and surface diffusion within the adsorbed water layers occurs. However, if the remaining cross section is larger than the molecular diameter, there is nothing that prevents the remaining molecules from passing.

The fact that the distance that needs to be travelled by a molecule before it can collide with another molecule is greater than an opening in a porous medium in which the molecule is trapped has nothing to do with the ability of the 3 Å molecule to pass through the only available opening that is, say, 20 Å wide, although the smaller the opening, the greater the number of molecule-wall collisions, and thus the greater the resistance to diffusion, i.e. the smaller the diffusivity.

Thus, it can be stated: **The basic assumption upon which the first approach to mathematical modelling of heat and mass transfer in heated concrete is founded, i.e. diffusion of water vapour through air does not occur in concrete, is invalid, and thus the results of mathematical models in which the first approach is adopted are questionable.**

Furthermore, the hypothesis proposed to explain the jump in permeability is unreasonable, since it implies that the microstructure of concrete instantly changes very significantly in that gel pores can be widened 32 times as the temperature exceeds 100°C.

3.3.2 The Second Approach to Mathematical Modelling

3.3.2.1 The First Major Shortcoming of Present Models

Researchers who adopt the second approach in mathematical modelling of heat and mass transfer in heated concrete have had to either assume that the diffusivities of water vapour and air are constant or rely on molecular diffusivity equations such as that presented by Krischer and Rohnalter in 1940 (2.8), that based on Chapman-Enskog theory (2.12), or that proposed by Marrero and Mason (1972) (2.15) due to the lack of a diffusivity equation that is specific for concrete at different temperatures. Ahmed and Hurst (1997) relied on (2.12), Tenchev *et al.* (2001a) depended on (2.15), and Tenchev *et al.* (2001b) used (2.8).

Thomas and He (1997), Zou *et al.* (1998), and Thomas and Missoum (1999) depended on (2.8) for heat and mass transfer in soil. As discussed in Section 2.6, molecular diffusion is the type of diffusion that occurs in systems without walls in which diffusion is the very maximum that can occur, since the molecules do not lose momentum during molecule-molecule collisions. Thus, molecular diffusivity equations provide the maximum diffusivity of gases. They may be appropriate for soil where the effect of the walls of the pores may be neglected. However, no investigation to determine whether the assumption that the type of diffusion of gases in concrete is molecular, and thus the use of molecular diffusivity equations in mathematical modelling of heat and mass transfer in heated concrete, is reasonable. Nor has any determination of the significance of this assumption on different parameters in general and on the pore pressure in particular been attempted so far.

Although Bažant and Thonguthai (1978) (Section 2.4.1.1) and Neville (1995) (Section 2.5) described the microstructure of concrete differently, they independently confirmed that continuous capillary pores with uniform cross sections much larger than the mean free path of water vapour molecules do not exist in good concrete. Also, Papadakis *et al.* (1991) stated that the type of diffusion of gases in concrete is Knudsen diffusion in their study of diffusion of gases in concrete. Thus, Knudsen diffusion would appear to be the dominant type of diffusion in concrete.

Assuming that the diffusivities of water vapour and air in heated concrete are constant must be questioned, since the real effective diffusivity in heated concrete, i.e. the effective Knudsen diffusivity (Sections 2.6.4 and 2.6.5), in addition to being proportional to the gaseous mixture volume fraction, varies with temperature, with the mean pore diameter that itself varies with the pore size distribution that is a function of the porosity, and with the tortuosity that is also a function of the pore size distribution.

Also, assuming that the type of diffusion in concrete is molecular is equivalent to Bažant and Thonguthai's (1978) invalid assumption that diffusion does not occur in pores smaller than the mean free path of water vapour molecules. More importantly, by multiplying the *entire* gaseous mixture volume fraction by the molecular diffusivity in the diffusive flux terms in (3.1) and (3.2), researchers who consider diffusion not only assume that diffusion does not occur in pores smaller than the mean free path, but also assume that *all* pores in concrete are much larger than the mean free path, since a proportion of the gaseous mixture exists in every pore that is not completely filled by water and in every single pore in the dry zone. Clearly, assuming that all pores in concrete are much larger than the mean free path of water vapour, or any other gas, molecules is incorrect.

Realising that diffusion of gases cannot be molecular in every pore in concrete, Lawrence (1984) proposed that, in general, diffusion can be considered to be molecular in 50% of the gas, or the gaseous mixture, volume fraction, and Knudsen in the remaining 50% of the gas volume fraction. However, as Bažant, Neville, and Papadakis *et al.* suggest, capillary pores with uniform cross sections much larger than the mean free path of water vapour molecules do not exist in good concrete; concrete structures are expected to be constructed with good concrete in which Knudsen diffusion is the dominant type of diffusion.

Li (1999, personal communication) recognised that molecular diffusivity is too great to be appropriate for concrete. Consequently, Tenchev *et al.* (2001b) (Appendix D) divided Krischer and Rohnalter's molecular diffusivity (2.8) by 10. Also, Tenchev *et al.* (2001a) (Appendix C) used Marrero and Mason's (1972) molecular diffusivity (2.15), but they took advantage of the ionic diffusion concept of using the square of the tortuosity factor τ (τ^2) and a constrictivity factor δ in the equations to determine the effective diffusivity (see, e.g., Atkison and Nickerson, 1984; Li and Page, 2000; and Wang *et al.*, 2000), and thus multiplied (2.15) by a constrictivity factor of 0.5 and divided it by the square of a tortuosity factor of 3. This is equivalent to $\tau = 18$ in (2.25), compared with the gas diffusion concept adopted by researchers who study gas diffusion (Section 2.6.5.1) of using the same average of 3 for τ but dividing the diffusivity in the gaseous phase by τ in (2.25).

Wakao and Smith (1962), Johnson and Stewart (1964), Feng and stewart (1973), Cunningham and Williams (1980), Carniglia (1986), and Burganos and Sotirchos (1987), for example, do not use molecular diffusivity for pores smaller than the mean free path of the gas molecules, simply because the real diffusivity in such pores (Knudsen diffusivity) in which the molecules collide only with the walls does not vary with the pressure, i.e. does not vary with the number of molecule-molecule collisions that do not occur in such pores. Variation with the pressure means variation with the number of molecule-molecule collisions; the higher the pressure, the greater the number of molecule-molecule collisions, and thus the smaller the molecular diffusivity. They use molecular diffusivity only in pores larger than the mean free path where the molecules do collide with each other, and thus the diffusivity is inversely proportional to the pressure.

Thus, they do not have to reduce the diffusivity in the gaseous phase by one or two orders of magnitude. But, they only deal with gas diffusion in dry porous media at ambient temperature when the pore size distribution is constant. Thus, they can determine the diameters of different pores, and use the corresponding, and appropriate, diffusivity for each group of pores. On the other hand, in

mathematical modelling of heat and mass transfer in heated concrete, there has been no choice other than depending on molecular diffusivity or assuming that the diffusivity is constant.

These artificial attempts to reduce the unreasonableness of using molecular diffusivity for all pores in concrete in mathematical modelling by dividing the diffusivity by a relatively large factor do *not* make the resulting equation equivalent to Knudsen diffusivity, and thus do *not* make it any more reasonable for concrete for three reasons:

(a) As can be seen from Section 2.6.3, there are different molecular diffusivity equations, and thus reducing any of them by a factor of 10, 20, or any other number only results in yet another molecular diffusivity equation that is still a function of the pore pressure, i.e. a function of the number of molecule-molecule collisions that do not occur in concrete pores, while the real diffusivity in concrete (Knudsen diffusivity) does not vary with the pressure, since the molecules collide only with the walls of the pores.

(b) Molecular diffusivity equations have a stronger dependence on the temperature than Knudsen diffusivity.

(c) Knudsen diffusivity increases when the mean pore diameter increases, since it is a function of the number of molecule-wall collisions, while molecular diffusivity does not.

Even if these artificial attempts lead to seemingly realistic results for a given set of initial data, e.g. porosity, water content, and permeability, they are not guaranteed to lead to reliable results under all circumstances. More importantly, unless there is no other alternative, the apparent realism of the results does not justify the adoption of an unreasonable assumption that is not guaranteed to lead to real results; after all, an invalid assumption, if it affects the results, *cannot* lead to real results.

Thus, it can be concluded that:

The assumption that the diffusivity in heated concrete is constant is incorrect. Also, the assumption that the type of diffusion of gases in concrete is molecular, and thus the use of molecular diffusivity equations in mathematical modelling of heat and mass transfer in heated concrete, appears to be unreasonable. Thus, the results from mathematical models in which the diffusivities of water vapour and air have had to be assumed either constant or molecular are questionable.

3.3.2.2 The Second Major Shortcoming of Most Models

The effective diffusivity in porous media is discussed in Section 2.6.5.1. The effect of the smaller cross-sectional area through which diffusion takes place is considered in present mathematical models that consider diffusion by including ε_g that appears in the diffusive flux term in (3.1) and (3.2). However, apart from Tenchev *et al.* (2001), different researchers incorrectly neglect the effect of the tortuous path in their models.

At first, it may appear that this shortcoming is not particularly serious, and that it can be easily eliminated by simply using a suitable value, say 3, for the tortuosity. However, the tortuosity cannot remain constant when the porosity increases due to dehydration of the bound water and thus the pore size distribution changes, since the tortuosity varies with pore size distribution (Carniglia, 1986). The determination of variable tortuosity in heated concrete is far from straightforward, since the tortuosity has been determined in porous media at ambient temperature only, i.e. when the pore size distribution is constant. Nevertheless, the use of a constant value for the tortuosity in heated concrete reduces, albeit does not eliminate, the unrealism of the results. The combined effects of neglecting the tortuosity and of using molecular diffusivity on the results may be very significant.

Based on the discussion related to the effective diffusivity (Section 2.6.5.1), the effective diffusivity of water vapour through air when diffusion in the gaseous phase is molecular according to (2.8) is:

$$D_{e,VA} = 5.893 \times 10^{-6} \frac{\varepsilon_g}{\tau} \frac{T^{2.3}}{P_g} \tag{3.3}$$

The effective diffusivity of water vapour through air when diffusion in the gaseous phase is molecular according to (2.12) is:

$$D_{e,VA} = 5.6 \times 10^{-4} \frac{\varepsilon_g}{\tau} \frac{T^{1.5}}{P_g} \tag{3.4}$$

3.4 CONCRETE DIFFUSIVITY

It is clear from the two detailed criticisms outlined in this chapter that, to obtain consistent results and potentially realistic values of pore pressures in heated concrete, it is necessary to develop a diffusivity equation specifically for concrete that provides the true effective diffusivity of different gases in different concretes at any temperature. This task, however, is far from straightforward.

3.4.1 The Problem

Evidently, the invalidity of the assumption that diffusion of water vapour does not occur in concrete has been recognised, since several researchers have developed mathematical models in which diffusion of water vapour is considered. Also, the use of molecular diffusivity may not imply that the unreasonableness of the assumption that diffusion in concrete is molecular has not been recognised. The unreasonableness of using molecular diffusivity in mathematical modelling of heat and mass transfer in heated concrete might have been recognised, since the fact that the pores in concrete are much smaller than the mean free path of water vapour molecules is independently confirmed by other researchers, e.g. Papadakis *et al.* (1991) and Neville (1995).

Nevertheless, no attempt has been made to develop a diffusivity equation specifically for concrete at variable temperature, because such equation cannot be directly developed. To date, only the constant effective diffusivity of different gases has been determined theoretically as well as experimentally in porous media, including concrete, at ambient temperature when the pressure, the porosity, the pore size distribution, the mean pore diameter, the tortuosity, and the gaseous mixture volume fraction are constant (Papadakis *et al.*, 1991).

The effective diffusivity (Section 2.6.5) takes into account the actual area through which diffusion takes place, i.e. the gaseous mixture volume fraction, the longer distance a gas needs to travel due to the tortuosity, and the diffusivity, molecular or Knudsen, in the gaseous phase. Thus, the effective diffusivity varies with any of these three parameters. In concrete under transient heating conditions, the effective diffusivity cannot be directly determined, because

(1) There are three regions that exist in heated concrete, each with a different effective cross-sectional area (gaseous mixture volume fraction) available for diffusion:

(a) normal (cool) zone with constant gaseous mixture volume fraction,

(b) over-saturated zone with less effective cross-sectional area, and

(c) dry zone with maximum cross section available for diffusion.

Thus, there is a different effective diffusivity for each zone.

(2) The proportion of each zone changes with temperature. When the temperature increases, the proportion of the dry zone increases, the proportion of the over-saturated zone increases for a certain time and then decreases, and the proportion of the cool zone decreases. Thus, the regions in which the three different effective diffusivities exist vary.

(3) The porosity of the dry zone increases when the temperature increases, due to dehydration of the bound water, and thus the gaseous volume fraction increases. Therefore, the effective diffusivity in the dry zone increases, and thus is variable.

(4) In the over-saturated zone, the amount of free water varies due to condensation of water vapour and then evaporation of the free water, and thus the gaseous volume fraction varies. Therefore, the effective diffusivity in the over-saturated zone is variable.

(5) The effective diffusivity also varies because the diffusivity in the gaseous phase varies with temperature and mean pore diameter that varies with pore size distribution when the porosity increases due to dehydration of the chemically bound water.

(6) The tortuosity, and thus the effective diffusivity, varies in the dry zone, since the microstructure of the dry zone changes when the porosity increases.

Mathematical models determine the variable gaseous mixture volume fraction. They also determine the variable parameters upon which molecular diffusivity in the gaseous phase depends, i.e. temperature and pore pressure. Thus, if it is assumed that the tortuosity remains constant, the variable effective molecular diffusivity can be determined. However, Knudsen diffusivity (Section 2.6.4) is proportional to the pore diameter. Thus, the resistance to diffusion is proportional to the number of molecule-wall collisions that is inversely proportional to the pore diameter; when the pore diameter increases, the number of molecule-wall collisions, and thus the resistance to diffusion, decreases and Knudsen diffusivity increases.

In heated concrete, the porosity increases in the dry zone due to dehydration of the chemically bound water. Thus, the pore size distribution, and hence the mean pore diameter and thus Knudsen diffusivity in the gaseous phase, is variable. Mathematical models determine the variable porosity in the dry zone. However, there is no expression that determines the variable mean pore diameter as a function of the porosity. Thus, mathematical models cannot determine the variable effective Knudsen diffusivity in the dry zone directly.

Furthermore, as discussed in Section 2.6.4, the definition given in the literature by different researchers for Knudsen diffusivity as a function of the pore diameter is a special case that is valid only in dry porous media. In moist concrete, Knudsen diffusivity must be a function of the diameter of the remaining cross section of the pore according to (2.20) or (2.21). Therefore, even in the over-saturated zone, where the porosity and the mean pore diameter remain constant, Knudsen diffusivity in the gaseous phase is variable, because the free water content varies due to condensation of water vapour and evaporation of the free water. Thus, the diameter of the remaining cross section through which diffusion occurs is variable.

Mathematical models determine the variable free water content. However, even if the mean pore diameter in the over-saturated zone is known, there is no expression that determines the thickness of the film of free water that must be a function of the pore diameter. Therefore, the diameter of the remaining cross section of the pore cannot be determined, and thus the effective Knudsen diffusivity cannot be determined directly in the over-saturated zone. Papadakis *et al.* (1991) provided an expression (2.28) that determines the thickness of the film of free water as a function of the pore diameter and the relative humidity at ambient temperature. However, the relative humidity at ambient temperature does not determine the free water content in concrete at high temperature.

Therefore, at first, it may appear that a diffusivity equation that is specific for concrete and that determines the real effective diffusivity of any gas in concrete under transient heating conditions cannot be developed. However, a general effective diffusivity equation for any gas in concrete with any initial porosity under transient heating conditions *can* be developed from actual diffusivity tests on different concretes with different porosities at ambient temperature. This effective diffusivity equation provides the effective diffusivity in concrete, since it is based on diffusivity tests on concrete and on the real diffusivity in concrete, i.e. Knudsen diffusivity. One of the most important characteristics of the new diffusivity equation is that the exact tortuosity, although it is variable and cannot be precisely determined, is implicitly included in the equation.

3.4.2 Development of the New Diffusivity Equation

This requires the following:

- Knudsen diffusivity. As this study is concerned with fire exposed concrete structures cast from good quality concrete in which continuous capillary pores with uniform cross sections much greater than the mean free path of water vapour molecules do not exist, Knudsen diffusivity must be one of the key elements in this development.

- Effective diffusivity in concrete at ambient temperature. The fact that the porosity varies in heated concrete leads to the conclusion that the second, and most important, key to the development of this equation must be in investigating the effective diffusivity of gases in different concretes with different porosities at ambient temperature.

- Dehydration of chemically bound water. This begins to occur at 105°C together with an increase in the porosity. Thus, the cross sectional area, and hence the mean pore diameter, through which diffusion takes place increases. This fact represents the most difficult obstacle in developing a diffusivity equation for concrete at variable temperature. At the same time, however, it, along with the second requirement above, provides the crucial key to the development of such equation.

The key to the development of an effective diffusivity equation for heated concrete is:

The porosity changes in one and the same concrete when the temperature exceeds 105°C due to dehydration of the chemically bound water as it does in different concretes with different water/cement ratios at ambient temperature.

Thus, the crucial, and most important, basic concept upon which the development of a diffusivity equation specifically for concrete at variable temperature can be based is the following analogy:

As far as the change in the porosity is concerned, a certain concrete at high temperature is equivalent to an unlimited number of different concretes with different porosities at ambient temperature.

Based on this concept, there are two approaches that can be adopted to develop an equation determining variable effective diffusivity of gases in heated concrete. Both approaches depend on actual tests on different concretes with different, but constant, porosities at ambient temperature:

(1) The first approach is to carry out, or to take advantage of, experimental tests of diffusivity of any gas in different concretes with different porosities at ambient temperature. In order to determine the effective diffusivity of a certain gas in a certain concrete at normal temperature, the porosity and the gaseous mixture volume fraction must remain constant during an experiment (Lawrence, 1984; Papadakis *et al.*, 1991). However, by repeating the experiment for different concretes with different w/c ratios, and thus with different porosities, and possibly with different moisture contents, it is possible to use regression analysis to develop a diffusivity equation for a certain gas in different concretes with different porosities. Thus, the resulting equation for the diffusivity of the gas in concrete at normal temperature will be a function of the porosity and, possibly, of the moisture content.

The determination of Knudsen diffusivity of a gas at a certain temperature from that of another gas at a different temperature can be achieved with the derivation of a general relation that can be derived from the Knudsen diffusivities of two different gases, say, A and B with different molecular weights at different temperatures.

Thus, a diffusivity equation can be developed for the effective diffusivity of water vapour, air, or any other gas in concrete with any porosity at any temperature from that of a certain gas at ambient temperature. Such equation determines the actual effective diffusivity in concrete under transient heating conditions, since it is based on diffusivity tests on concrete and on Knudsen diffusivity. One of the most important advantages of this approach is that the exact tortuosity, although it is variable, will be implicitly included in the equation.

(2) The second approach is to develop an equation for the mean pore diameter as a function of the porosity from the pore size distributions of different specimens of dry concrete with different porosities at normal temperature, to develop an equation that determines the variable tortuosity as a function of the porosity, and to develop an equation that determines the thickness of the film of water w that exists in the over-saturated zone and in the cool zone because, in these two zones, the effective Knudsen diffusivity is a function of the diameter of the remaining cross section of the pore, i.e. the diameter of the pore minus w.

The equation for w must be in terms of the free water content, rather than the relative humidity as in (2.28), since, although the relative humidity determines the free water content at normal temperature, it does not determine the water content when the temperature increases. The thickness w must also be a function of the mean pore diameter for which an equation is needed as mentioned above. Then, the required effective diffusivity equations for water vapour and air in heated concrete can be determined from (2.24) in which D is Knudsen diffusivity (2.21). Thus, the effective diffusivity of a gas i at temperature T in concrete is

$$D_{e,i} = 48.5\frac{\varepsilon_g}{\tau}(d_m - w)\sqrt{\frac{T}{M_i}} \tag{3.5}$$

The first approach will be adopted in this study, since the experimental investigation of Papadakis *et al.* (1991) provides the totally effective diffusivity of CO_2 at ambient temperature (2.27).

A general relation can be derived from which the effective Knudsen diffusivity of a gas at any temperature can be determined from that of another gas at a certain temperature as follows:

From (2.19), Knudsen diffusivity of a gas A at a temperature T_1 is

$$D_{Kn,A,T_1} = 48.5d\left(\frac{T_1}{M_A}\right)^{0.5} \tag{3.6}$$

Knudsen diffusivity of a gas B at a temperature T_2 is

$$D_{Kn,B,T_2} = 48.5d\left(\frac{T_2}{M_B}\right)^{0.5} \tag{3.7}$$

or

$$\frac{D_{Kn,A,T_1}}{D_{Kn,B,T_2}} = \left(\frac{T_1/M_A}{T_2/M_B}\right)^{0.5} \tag{3.8}$$

Thus, the required general relation between the two values of the effective Knudsen diffusivity is

$$D_{Kn,B,T_2} = D_{Kn,A,T_1}\left(\frac{T_2 M_A}{T_1 M_B}\right)^{0.5} \tag{3.9}$$

or

$$D_{e,B,T_2} = D_{e,A,T_1}\left(\frac{T_2 M_A}{T_1 M_B}\right)^{0.5} \tag{3.10}$$

The totally effective diffusivity of CO_2 at ambient temperature (2.27) is rewritten here for convenience:

$$D_{e,CO_2} = 1.64\times10^{-6}\varepsilon_p^{\,1.8}(1-RH/100)^{2.2} \tag{3.11}$$

Thus, using (3.10) and (3.11), the new equation for the effective diffusivity of a gas i, $D_{Conc,i}$, in concrete at temperature T can be developed as follows:

$$\varepsilon_g D'_{e,i} = 1.64\times10^{-6}\varepsilon_p^{\,1.8}(1-RH/100)^{2.2}\left(\frac{T\times44.01}{293\times M_i}\right)^{0.5} \tag{3.12}$$

or

$$\varepsilon_g D'_{e,i} = 6.356\times10^{-7}\varepsilon_p^{\,1.8}(1-RH/100)^{2.2}\left(\frac{T}{M_i}\right)^{0.5} \tag{3.13}$$

The relative humidity RH determines the gaseous mixture volume fraction ε_g at normal temperature. However, it does not determine ε_g when the temperature increases. Thus, it is necessary to eliminate RH from (3.13). Also, since (3.11) is derived from experimental work, ε_g on the right hand sides of (3.11) and (3.13) is in terms of the porosity as well as RH, $\varepsilon_g = f(\varepsilon_p, RH)$. Thus, it is necessary to eliminate the gaseous mixture volume fraction from both sides of (3.13), and then re-introduce it as ε_g that is determined by the mathematical model in any zone at any temperature. This is the same as determining the diffusivity in a tortuous gaseous phase in which no impermeable solids are present, i.e. determining the partially effective diffusivity (Section 2.6.5), and then determining the effective diffusivity by re-introducing ε_g at any free water content, and at any temperature, as determined by the mathematical model.

From (3.13), it is possible to eliminate ε_g, and thus determine the partially effective diffusivity, only when $RH = 0$, because any other value of RH results in the presence of a continuous film of water of

thickness w that cannot be determined, since w is a function of the pore diameter that is unknown. and thus the gaseous mixture volume fraction ε_g on the right hand side of (3.13) cannot be determined. When $RH = 0$, $w = 0$, and thus ε_g is equal to the porosity ε_p.

Thus, from (3.13), the new equation for the partially effective diffusivity of gas i in concrete at temperature T is

$$D'_{Conc,i} = 6.356 \times 10^{-7} \varepsilon_p^{0.8} \left(\frac{T}{M_i} \right)^{0.5} \tag{3.14}$$

In general, and using the notations adopted in this study, (3.14) can be expressed as

$$D'_{Conc} = 6.356 \times 10^{-7} P_{or}^{0.8} \left(\frac{T}{M} \right)^{0.5} \tag{3.15}$$

Thus, the very first equation for the effective diffusivity of any gas, $D_{Conc} (= \varepsilon_g D'_{Conc})$, in concrete with porosity P_{or} at temperature T (or simply concrete diffusivity) is

$$D_{Conc} = 6.356 \times 10^{-7} \varepsilon_g P_{or}^{0.8} \left(\frac{T}{M} \right)^{0.5} \tag{3.16}$$

An appropriate description for the new diffusivity equation (3.16) is **"concrete diffusivity".** Compared with "molecular diffusivity" and "Knudsen diffusivity" that determine different types of diffusivity in the gaseous phase, "concrete diffusivity" implies that (3.16) determines the *effective* diffusivity in concrete. The exact tortuosity of concrete, although it is unknown and variable and thus, similar to (3.16), cannot be directly determined, is implicitly included in (3.15) and (3.16), since these equations are based on actual diffusivity tests on concrete and on the real diffusivity in concrete (Knudsen diffusivity).

Comparing (3.13) and (3.14) leads to

$$\varepsilon_g = \varepsilon_p (1 - RH/100)^{2.2} \tag{3.17}$$

(3.17) is valid only at ambient temperature, since the right hand side accounts for the change in ε_g due to the variation in the free water at normal temperature. When the temperature reaches 100°C, the right hand side cannot predict ε_g because, for the same ambient relative humidity, w decreases, and thus ε_g increases. Thus, when the temperature increases, ε_g is no longer given by (3.17). The determination of ε_g at any temperature will be discussed later in this section.

Now that ε_g at normal temperature is known, the partially effective diffusivity of CO_2 at ambient temperature is

$$D'_{e,CO_2} = 1.64 \times 10^{-6} \varepsilon_p^{0.8} \tag{3.18}$$

The fact that the partially effective diffusivity in concrete at normal temperature is dependent on the porosity is crucial to the development of the new equation that determines the effective diffusivity in concrete at high temperatures. An equation such as (3.18), determines the partially effective diffusivity in different concretes with different porosities at normal temperature. For a certain concrete, the porosity is a constant that is equal to the initial porosity ${}^0P_{or}$, and thus the equation results in a constant value for the partially effective diffusivity.

At normal temperature, when the w/c ratio changes, the porosity changes, a different concrete results, and a different partially effective diffusivity is obtained. But this is exactly what happens in one and the same concrete with a certain w/c ratio when the temperature exceeds 105°C: the porosity changes due to dehydration of the bound water. Thus, the determination of the partially effective diffusivity, and hence of the effective diffusivity, of a certain gas in a certain concrete with a variable porosity using (3.14) at high temperature is similar to the determination of the partially effective diffusivities, and hence of the effective diffusivities, of the gas in an unlimited number of different concretes with different, but constant, porosities at ambient temperature.

Thus, while ε_p in (3.18), is the initial porosity ${}^0P_{or}$, P_{or} in (3.15) is

$$P_{or} = {}^0P_{or} + \varepsilon_d \tag{3.19}$$

where ε_d is volume fraction of the dehydrated water.

Thus, the partial concrete diffusivity (3.15) can be expressed as

$$D'_{Conc} = 6.356\times10^{-7}\left({}^{0}P_{or} + \varepsilon_d\right)^{0.8}\left(\frac{T}{M}\right)^{0.5} \tag{3.20}$$

and concrete diffusivity (3.16) can be expressed as

$$D_{Conc} = 6.356\times10^{-7}\varepsilon_g\left({}^{0}P_{or} + \varepsilon_d\right)^{0.8}\left(\frac{T}{M}\right)^{0.5} \tag{3.21}$$

The dehydrated water volume fraction is

$$\varepsilon_d = \frac{\rho_d}{\rho_l} \tag{3.22}$$

where ρ_d is the dehydrated water content, in kg/m^3, and ρ_l is the density of water (=1000 kg/m^3).

Fig. 3.1 shows the coefficient $\bar{T}$ giving the dehydrated water content at various temperatures, for mature concretes, as (Bažant and Kaplan, 1996):

$$\rho_d = 0.24\rho_{cem}(1-\bar{T}) \tag{3.23}$$

where ρ_{cem} is the anhydrous cement content, in kg/m^3.

A tri-linear fit results in the following expression for $\bar{T}$:

$$\bar{T} = \begin{cases} 1 & T \le 105°C \\ (700-T)/595 & 105°C < T \le 700°C \\ 0 & T > 700°C \end{cases} \tag{3.24}$$

The variation of $\bar{T}$ according to (3.24) is also shown in Fig. 3.1.

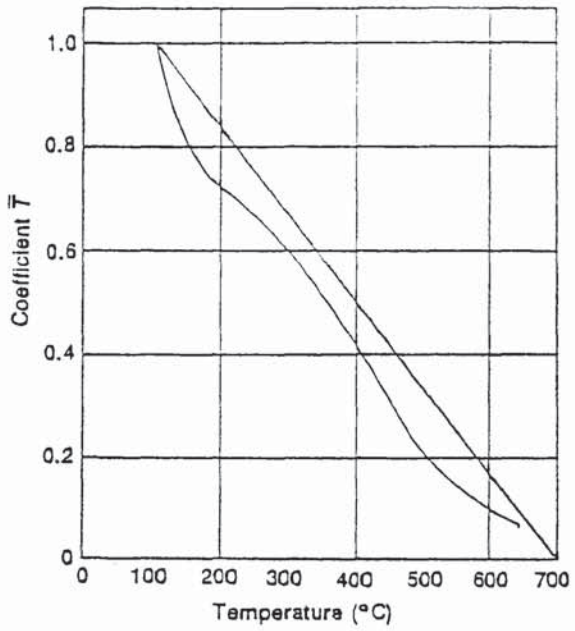

Fig. 3.1: Coefficient $\bar{T}$ Giving the Dehydrated Water Content at Various Temperatures (after Bažant and Kaplan, 1996, excluding the tri-linear fit)

The gaseous mixture volume fraction ε_g at any temperature in (3.16) or (3.21) is

$$\varepsilon_g = P_{or} - \varepsilon_l = {}^0P_{or} + \varepsilon_d - \varepsilon_l \tag{3.25}$$

where ε_l is the volume fraction of the free water. The free water content $\varepsilon_l \rho_l$ is determined from the sorption isotherms (Section 2.4.1.1). The details of determining the free water content, and thus its volume fraction, are presented in Appendix C.

3.4.3 Concrete Diffusivity of Water Vapour

Unlike molecular diffusivity, a very important characteristic of Knudsen diffusivity, and thus of concrete diffusivity (3.16), or (3.21), is its independence of the other gas molecular weight, because the molecules do not collide with the molecules of the other gas. Therefore, each gas in the gaseous mixture has a different diffusivity depending on its own molecular weight. Thus, the diffusivities in the diffusive mass fluxes of water vapour and air in (3.1) and (3.2) may not be assumed equal to each other as in the models of, e.g., Ahmed and Hurst (1997) and Tenchev *et al.* (2001). Also, it is no longer appropriate to use the subscripts VA and AV to describe the diffusivities of water vapour and air in concrete, since they are independent of each other. Thus,

$$D_{e,V} \neq D_{e,A} \tag{3.26}$$

Equation (3.1) can be rewritten as

$$J_v = -\varepsilon_g \rho_v \frac{KK_g}{\mu_g} \nabla P_g - \rho_g D_{Conc,V} \nabla \left(\frac{\rho_v}{\rho_g} \right) \tag{3.27}$$

where $D_{Conc,V} (= \varepsilon_g D'_{Conc,V})$ is concrete diffusivity of water vapour, in m^2/s.

The partial concrete diffusivity of water vapour at any temperature, in m^2/s, is determined from (3.15) as:

$$D'_{Conc,V} = 1.5 \times 10^{-7} P_{or}^{0.8} T^{0.5} \tag{3.28}$$

Concrete diffusivity of water vapour at any temperature, in m^2/s, is determined from (3.16) as

$$D_{Conc,V} = 1.5 \times 10^{-7} \varepsilon_g P_{or}^{0.8} T^{0.5} \tag{3.29}$$

3.4.4 Concrete Diffusivity of Air

Equation (3.2) can be rewritten as

$$J_a = -\varepsilon_g \rho_a \frac{KK_g}{\mu_g} \nabla P_g - \rho_g D_{Conc,A} \nabla \left(\frac{\rho_a}{\rho_g} \right) \tag{3.30}$$

where $D_{Conc,A} (= \varepsilon_g D'_{Conc,A})$ is concrete diffusivity of air, in m^2/s.

The partial concrete diffusivity of air at temperature T is determined from (3.15) as

$$D'_{Conc,A} = 1.18 \times 10^{-7} P_{or}^{0.8} T^{0.5} \tag{3.31}$$

Concrete diffusivity of air is determined from (3.16) as

$$D_{Conc,A} = 1.18 \times 10^{-7} \varepsilon_g P_{or}^{0.8} T^{0.5} \tag{3.32}$$

3.4.5 Implication of the Dependence of Diffusivity on Porosity

By far, the most important characteristic of concrete diffusivity (3.16), or (3.21), is that it is a function of the porosity. The development of this equation is based on the strong belief that Knudsen diffusion is the dominant type of diffusion in concrete, because the vast majority of the pores in concrete are smaller than the mean free paths of the molecules of gases, in general, and the mean free path of water vapour molecules, in particular. The strong dependence of the experimental results of Papadakis *et al.* (1991) for the effective diffusivity of CO_2 in concrete at normal temperature (3.11) on the porosity supports this belief, and very clearly implies that Knudsen diffusion is indeed the dominant type of diffusion that takes place in concrete, even though the w/c ratios upon which the experimental results of Papadakis *et al.* are based are 0.5, 0.65 and 0.80.

According to Neville (1995), at w/c ratios greater than 0.38, continuous capillary pores with uniform cross sections are present in concrete, and thus molecular diffusion appears if the size of some of these pores is much greater than the mean free path. However, the strong dependence of the diffusivity on the porosity even at w/c ratios of 0.5, 0.65, and 0.8 clearly indicates that Knudsen diffusion remains dominant since, although continuous capillary pores appear when the porosity increases, the number and proportion of small pores with diameters smaller than the mean free path also increase. Furthermore, the mean free path of water vapour molecules at normal temperature and 1 atm is more than 1300 Å, and is more than 1600 Å at 100°C and 1 atm. In pores that are about the same size as the mean free path, molecular diffusion only *begins* to appear, and the majority of the molecules still collide with the wall. Thus, Knudsen diffusion dominates even in capillary pores as large as 1600 Å, when the temperature approaches 100°C, while, according to Neville, the mean diameter of capillary pores is about 130 Å.

Molecular diffusion does not dominate unless the pore diameter is much greater than the mean free path. This study is concerned with concrete structures exposed to fire; continuous capillary pores much larger than the mean free path of water vapour molecules are not expected to be present in good concrete structures. Even if such pores are present, their proportion will be negligible. In fact, Neville stresses that the importance of eliminating continuous capillaries is such that it is regarded a necessary condition for concrete to be classified as good.

Mathematically, this implication can be clarified by noting that molecular diffusivity is not a function of the porosity. If molecular diffusion were dominant, the effect of the porosity would be

limited to the gaseous mixture volume fraction (3.17); thus the experimental effective diffusivity of CO_2 (3.11) would be a function of ε_p rather than $\varepsilon_p^{1.8}$. In other words, if molecular diffusion were dominant, the partially effective diffusivity (3.18) would *not* be a function of the porosity. On the other hand, Knudsen diffusivity is proportional to the mean pore diameter that is a function of the porosity. Thus, in the effective Knudsen diffusivity, not only the gaseous mixture volume fraction is a function of the porosity, but also the diffusivity in the gaseous phase is a function of the porosity. Therefore, the fact that the effective diffusivity of CO_2 at normal temperature is a function of $\varepsilon_p^{1.8}$ rather than ε_p confirms that the type of diffusion in concrete is Knudsen diffusion at all w/c ratios.

3.4.6 The Crucial Criterion

The discussion on the types of diffusivity (Section 2.6) leads to early expectations regarding the quantitative analysis of this study that will be carried out in Chapters 5 and 6. It is strongly believed that the effect of the type of diffusivity, and thus of the variation of the diffusive flux, on the pore pressure can be predicted from (3.1) and (3.2), and certain trends can be determined that must appear in the results of the pore pressure when they are analysed quantitatively in those chapters. Thus, the following hypothesis is proposed:

The smaller the pore size, the greater the number of molecule-wall collisions, and thus the greater the resistance to the diffusive flux and the smaller the diffusive flux. When the diffusive fluxes decrease, the total, i.e. convective plus diffusive, fluxes in (3.1) and (3.2) decrease. Thus, provided that the air content remains insignificant (as it is supposed to be) compared with the maximum vapour content and thus does not significantly contribute to the increase of the pore pressure, the smaller the diffusivity of vapour, the smaller the vapour diffusive flux, the smaller the vapour content, and thus the smaller the pore pressure. Nevertheless, whether or not the air contributes to the increase of the pore pressure, the smaller the diffusivities of vapour and air, the smaller the gaseous mixture content, and thus, again, the smaller the pore pressure. Assuming that diffusion does not occur in concrete is an extreme case that is equivalent to the presence of an infinite resistance to diffusion. This assumption results in the diffusive fluxes being zero and thus in the greatest underestimation of the pore pressure. Similarly, assuming that the type of diffusion in concrete is molecular is the other extreme case in which the resistance to the diffusive flux is

minimum. This assumption results in the maximum diffusive fluxes and thus in the maximum total fluxes in (3.1) and (3.2), and hence leads to the greatest overestimation of the pore pressure.

The fact that is beyond doubt is that the real pore pressure in heated concrete *must* be between the pore pressures that result from the two extreme assumptions that diffusion does not occur in concrete and that diffusion in concrete is molecular, since the real diffusivity in concrete is between the two extreme assumptions; Knudsen diffusivity is much smaller than molecular diffusivity, since the molecules lose momentum during molecule-wall collisions (Section 2.6). Thus,

The crucial, and most important, criterion in determining the validity and realism of concrete diffusivity is that it *must* result in pore pressures that are between the two extreme pore pressures resulting from the assumptions that diffusion does not occur in concrete and that diffusion in concrete is molecular, when the same mathematical model is used to ensure that all other assumptions that may affect the pore pressure are exactly the same.

3.4.7 Further Discussion

Clearly, an equation that determines the effective diffusivity of a certain gas in different concretes with different porosities at ambient temperature can be developed from any experimental diffusivity study on different concretes with different porosities. Thus, this investigation paves the way to the development of other diffusivity equations for heated concrete. Different diffusivity studies at ambient temperature may lead to different diffusivity equations for concrete at high temperatures. Thus, other diffusivity equations that may be developed using this methodology may be different. However, such equations are expected to lead to similar results, since they will be based on actual diffusivity tests and on the real diffusivity in concrete (Knudsen diffusivity). Furthermore, more sophisticated equations may be developed that take into account the possibility of molecular diffusion occurring in pores, if any, that are much greater than the mean free path of certain gases, particularly in concretes with w/c ratios greater than 0.38. However, concrete structures are constructed with good concrete in which Knudsen diffusion is the dominant type of diffusion, and thus the diffusivity equation developed in this investigation, and similar equations based on Knudsen diffusivity that may be developed, are the most reasonable for concrete structures exposed to fire. Moreover, as confirmed in the previous section, Knudsen diffusion remains dominant even in concretes with w/c ratios greater than 0.38.

It may be argued that the basic concept that, regarding the change in porosity, a certain concrete at high temperature is equivalent to an unlimited number of different concretes at normal temperature may be unreasonable, because the pore size distribution and the mean pore diameter of a concrete with a certain porosity at high temperature may or may not be the same as that of a concrete with the same porosity at normal temperature, and thus the effective diffusivity may or may not be exactly the same in both concretes. However, to this author's knowledge, no comparison has been made so far to determine whether the pore size distribution in a concrete with a certain porosity at high temperature is the same as that in a concrete with the same porosity at normal temperature.

Furthermore, experimental diffusivity tests relate the effective diffusivity to the porosity regardless of the pore size distribution and the mean pore diameter, and the results are assumed valid for all concretes with the same porosity. Moreover, the use of a diffusivity equation based on this concept in mathematical modelling is more reasonable, and leads to more reliable results, than invalidly neglecting diffusion, invalidly assuming that the diffusivities in heated concrete are constant, or invalidly using molecular diffusivity. After all, the equation developed using this concept determines, at every instant, the actual effective diffusivity in a concrete with the same porosity.

More importantly, the tenability of the new effective diffusivity equation may only be determined from the realism and reasonableness of the results of different parameters such as the temperature, pore pressure, water vapour content and pressure, air content and pressure, gaseous mixture, and free water content, at variable temperature. In particular, as discussed in Section 3.4.6, the crucial criterion in determining the tenability of concrete diffusivity is the fact that the real pore pressure in concrete must be between the pore pressures that result from the extreme assumptions that diffusion does not occur in concrete and that diffusion in concrete is molecular.

3.5 THE FIRST 'MEAN PORE DIAMETER' EQUATION

It is argued (Section 3.4.1) that, although present mathematical models determine the variable porosity in heated concrete, they cannot determine the variable effective Knudsen diffusivity, because there is no expression that relates the mean pore diameter to the porosity, and that it appears extremely difficult to develop such expression, because the mean pore diameter is determined from the pore size distribution that cannot be predicted when the porosity varies with temperature. However, now that concrete diffusivity has been developed, it is possible to develop

an equation that determines the variable mean pore diameter as a function of the tortuosity and the porosity as follows:

Knudsen diffusivity of a gas A, in m^2/s, in dry porous media is

$$D_{Kn,A} = 4.85 \times 10^{-9} d_m \left(\frac{T}{M_A} \right)^{0.5} \tag{3.33}$$

where d_m is the mean pore diameter, in Å.

Thus, in dry concrete where the thickness of the film of water $w = 0$, the partially effective Knudsen diffusivity is

$$D_{e,Kn,A}^{'} = 4.85 \times 10^{-9} \frac{d_m}{\tau} \left(\frac{T}{M_A} \right)^{0.5} \tag{3.34}$$

From (3.15) and (3.34), the first mean pore diameter equation is

$$d_m = 130 \tau P_{or}^{0.8} \tag{3.35}$$

where d_m is the mean pore diameter, in Å, τ is the tortuosity, and P_{or} is the porosity.

In Section 2.6.5, it has been concluded that a value of 3 for the tortuosity in concrete at ambient temperature seems to be appropriate. Thus, the mean pore diameter, in Å, in concrete can be determined as

$$d_m = 390 P_{or}^{0.8} \tag{3.36}$$

The value adopted for the initial porosity is 0.18. Thus, the initial mean pore diameter, in Å, of this concrete is

$$^0 d_m \approx 100 \tag{3.37}$$

Wang *et al.* (2000) adopt a value of 2 for the tortuosity of concrete. Using this value in (3.35) yields

$$d_m = 260 P_{or}^{0.8} \tag{3.38}$$

From (3.38), for $P_{or} = 0.18$, the initial mean pore diameter, in Å, of this concrete is

$$^{0}d_{m} \approx 66 \tag{3.39}$$

It is interesting to note that these values for the mean diameter of all pores are smaller than the mean diameter of capillary pores (= 130 Å) reported by Neville (1995). This implies that a value between 2 and 3 for the tortuosity is appropriate for concrete, and that the values obtained for $^{0}d_{m}$ are reasonable. Of course, the mean diameter of capillary pores varies with the porosity, but the porosity for which this diameter is cited is unclear. However, these values appear to be reasonable for *good* concrete.

The values obtained for the initial mean pore diameter provide the conclusive evidence that the type of diffusion in concrete is Knudsen diffusion indeed, since these values are smaller than the mean free paths, at normal temperature and 1 atm, of the molecules of different gases such as CO_2 ($\lambda \approx 600$ Å), O_2 ($\lambda \approx 760$ Å), and air ($\lambda \approx 660$ Å), in general, and water vapour ($\lambda \approx 1300$ Å), in particular, for all practical values of the porosity. For example, from (3.36), a value of 0.25 for the porosity leads to an initial mean pore diameter of only about 130 Å.

3.6 CONCLUSIONS

- The basic assumption, i.e. diffusion of water vapour does not occur in concrete, upon which the first approach to mathematical modelling of heat and mass transfer in heated concrete is founded is invalid, since it is confirmed by many researchers that diffusion, known as Knudsen diffusion, of different gases does occur through micropores in porous media, and thus the results of mathematical models in which this approach is adopted are questionable. It is believed that neglecting diffusion leads to underestimating the pore pressure in heated concrete.

- In the second, and reasonable, approach in which diffusion is considered, assuming that the diffusivities of water vapour and air are constant is incorrect, since the diffusivity in heated concrete, i.e. Knudsen diffusivity, varies with temperature, mean pore diameter, and tortuosity. Also, assuming that the diffusivities of water vapour and air in concrete are molecular is unreasonable since, unlike Knudsen diffusivity, molecular diffusivity has a stronger dependence on

the temperature, varies with the pressure, and does not vary with the mean pore diameter. Thus, the results of present models in which diffusion is considered are questionable. It is believed that the use molecular diffusivity leads to overestimating the pore pressure. Another major shortcoming of most models in which diffusion is considered is that the tortuosity in concrete is neglected.

- Consequently, one of the most important findings of the study is the development of the first effective diffusivity equation for heated concrete, named concrete diffusivity, that determines the effective diffusivity, in m^2/s, of any gas in concrete at any temperature, that is,

$$D_{Conc} = 6.356 \times 10^{-7} \varepsilon_g P_{or}^{0.8} \left(\frac{T}{M} \right)^{0.5} \tag{3.16}$$

where ε_g is the gaseous mixture volume fraction, P_{or} is the porosity, T is the absolute temperature, in K, and M is the molecular weight, in kg/kmol. On of the most important advantages of concrete diffusivity is that the actual, and variable, tortuosity is implicitly included in the equation.

- A by-product of concrete diffusivity is the development of a new equation that determines the mean pore diameter, in Å, in heated concrete, that is,

$$d_m = 130 \tau P_{or}^{0.8} \tag{3.35}$$

where τ is the tortuosity.

The effect and significance of neglecting diffusion will be investigated quantitatively in Chapter 5. In Chapter 6, the effects and significance of using molecular diffusivity and of the tortuosity will be studied. Also, the performance of concrete diffusivity will be demonstrated and compared with that of molecular diffusivity in Chapter 6. The crucial criterion for determining the validity of concrete diffusivity is that it must lead to pore pressures between the pressures that result from the extreme assumptions that diffusion does not occur in concrete and that diffusion in concrete is molecular, since the real diffusivity in concrete is between the two extremes. Before these objectives are carried out, however, the mathematical model used (Appendix C) will be discussed and the necessary modifications will be described in Chapter 4.

CHAPTER 4

FINITE ELEMENT MODEL

4.1 INTRODUCTION

The mathematical model used in this study is one of the most recent models developed for coupled heat and mass transfer in heated concrete. Developed by Tenchev *et al.* (2001a), the model is two-dimensional in which the system of differential equations governing heat and mass transfer in concrete subjected to intensive heating is solved using finite element methods. The primary unknowns are temperature, water vapour content, and pore pressure.

The most important feature of the model is that the liquid phase and the gaseous phase are considered separately in the mass transfer formulation. Thus, the convective mass transfer of free water and gaseous mixture of water vapour and air as well as the diffusive mass transfer of water vapour and air through each other are considered. Full details of the mathematical model including the solution of the governing equations are provided in Appendix C.

In this chapter, an overview of the model will be provided including such aspects as boundary conditions, element type, and solution method. Also, in order to check the correctness of the methodology and thus ensure the reliability of the results, a different arbitrary set of primary unknowns, i.e. temperature, pore pressure, and water vapour pressure, is selected. Thus, the equations related to this set will be derived in this chapter, the necessary modifications that must be made to the model will be described, and the results of different parameters from the original set and this one will be compared.

Since a diffusivity equation specifically for heated concrete did not exist when the model was developed, Tenchev *et al.* had to depend on molecular diffusivity equations, and thus the original model was designed such that the diffusivity of water vapour through air is the same as that of air through vapour. Thus, the necessary modifications for implementing concrete diffusivity will be described. Furthermore, the necessary modifications for implementing molecular diffusivity according to Chapman-Enskog theory (2.12) and tortuosity (2.24) will be described. Moreover, since the intrinsic permeability is assumed to remain constant at all temperatures in the first version

of the model used in this study, the necessary modifications to implement an expression given by Zou *et al.* (1998) that determines the variable intrinsic permeability that is a function of the porosity will be described.

Evaluation of mesh density and time step will be included.

4.2 OVERVIEW

4.2.1 General Overview

In an attempt to overcome some of the shortcomings of the mathematical models developed so far, Tenchev *et al.* (2001a) developed a comprehensive model for heat and mass transfer in heated concrete. The corresponding two-dimensional finite element formulation is found in Appendix C. The most important feature of the model is that the second approach to modelling was adopted in which the liquid water, water vapour, and dry air are treated separately, and thus mass transfer by diffusion, in addition to convection, could be considered. The basic laws of mass (of water, water vapour, and air) and energy conservation, given in (1)-(4) of Appendix C, were used to derive the coupled system of three differential equations presented in (17) of Appendix C.

The solution method adopted is the backward difference algorithm, and thus the numerical analysis is unconditionally stable (Zienkiewicz and Taylor, 1991 and 1994; Bathe, 1996). Four noded quadrilateral elements are used, and thus, from the general finite element method recommendations, square elements are selected, as the geometry of the problem considered is rectangular.

In an earlier version of model (Tenchev and Khalafallah, 2000; Tenchev *et al.* 2001b), the intrinsic permeability is assumed constant at all temperatures. In the latest version, however, Tenchev *et al.* (2001a) used the expression (A8) (Appendix C) to account for the increase of the intrinsic permeability when the porosity increases due to dehydration of bound water.

The original arbitrary set of three unknown variables selected is temperature, water vapour content, and pore pressure. For a small-size problem, an analytical solution for a certain set of unknowns may be relatively easily obtained by hand, and thus checked independently for correctness. Nevertheless, even for small-size problems where analytical solutions can be obtained by hand, the

best way to check whether the solution obtained with a certain set is correct is to obtain solutions with other sets and compare the results that must be identical. However, analytical solutions for large-scale problems are extremely difficult to obtain, and thus a numerical method, e.g. finite element method, and programming are used. Consequently, unless one develops his/her own program simply to check someone else's, the *only* way to check that a computer program is flawless and leads to the correct solution with a certain set of unknowns is to repeat the analysis with one or more different sets and compare the results. Since the finite element method is a numerical one, the results are not expected to be identical but, if the program leads to the correct solution, they should be virtually identical.

From the system of differential equations (17) (Appendix C), the problem of heat and mass transfer in heated concrete is a function of many variables, e.g. temperature T, water vapour content ρ_V, water vapour pressure P_V, air content ρ_A, air pressure P_A, gaseous mixture content ρ_G, and pore pressure P_G. Since (17) is a system of three differential equations, and since there are enough auxiliary equations, e.g. ideal gas law, to determine the remaining variables, it can be solved when *any* three unknowns are arbitrarily chosen as the primary unknowns. This is a large-scale problem the solution of which required the use of the finite element method and programming, and thus the only way to check that the program leads to the correct solution is to repeat the analysis with different sets of unknowns and compare the results to ensure that they are virtually identical.

Consequently, in order to check that the model leads to the correct solution of (17), Tenchev *et al.* (2001a) repeated all analyses for two other sets of unknown variables, i.e. temperature, air content, and water vapour content (T, ρ_A, ρ_V) and temperature, air pressure, and water vapour pressure (T, P_A, P_V), and obtained results that are virtually identical to those obtained with the original set of temperature, pore pressure, and water vapour content (T, P_G, ρ_V).

Nevertheless, Li (2001, personal communication) believes that a researcher, particularly in a PhD study, should *not* depend on the statements of the developer(s) of a software package, and should *independently* confirm that the software used in the study leads to correct results. Thus, in this study, in order to confirm that the model used is flawless and leads to the correct solution, a different arbitrary set of unknowns, i.e. temperature, pore pressure, and water vapour pressure (T, P_G, P_V), is chosen, the corresponding system of differential equations is derived, the necessary

modifications that must be made to the model are undertaken, and the results of various parameters from this set and the original one are compared.

The system of differential equations derived for the set T, P_G, P_V is given in Section 4.3.

4.2.2 Boundary Conditions

The model is designed for *unsealed* concrete sections exposed to high temperatures, as can be seen from (21)-(26) of Appendix C. Thus, the boundary conditions are determined as follows:

4.2.2.1 Surfaces Exposed to the Environment

For this study, the temperature, in °C, of the environment at a heated boundary is given by the standard fire curve (ISO 834, 1987), i.e. $T_\infty = {}^0T + 345\log_{10}(8t+1)$ where ${}^0T = 20°C$ and t is time, in min. The temperature of the environment at an unheated boundary is $T_\infty = 20°C$. As discussed by Tenchev *et al.* (2001a) (Appendix C), assuming that the liquid flux J_L at an exposed surface can be omitted, the energy balance at such a boundary is given by (23) of Appendix C. If the same assumption holds for an unexposed surface, which is likely during the service life of a structure, the same expression is valid for such a surface; otherwise, (22) of Appendix C should be used.

The water vapour pressure of the environment at a fire-exposed (and an unexposed) surface can be assumed equal to the saturation pressure at ambient temperature given by Çengel (1998), or $P_{V,\infty} = {}^0P_{sat}\left({}^0T\right) = 2339$ Pa. Thus, from the ideal gas law $P_V = R_V \rho_V T$ (Çengel, 1998), the water vapour content of the environment at a fire-exposed (and an unexposed) surface is given as $\rho_{V,\infty} = 0.017$ kg/m^3. Since the vapour contents in concrete at a boundary surface ρ_V and in the environment $\rho_{V,\infty}$ (and thus the vapour pressures P_V and $P_{V,\infty}$) may *not* be equal, the vapour balance at a boundary surface is given by (24) of Appendix C.

The pore pressure on a fire-exposed (and an unexposed) surface is equal to the standard atmospheric pressure, i.e. $P_G = P_{G,\infty} = 101325$ Pa. Thus, $\partial P_G / \partial n = 0$ where n is the normal to the

surface. This can be assumed to be true, even though P_V may be greater than $P_{V,\infty}$, since water vapour displaces some of the air (Bird *et al.*, 1960), and thus the air pressure P_A would be smaller than $P_{A,\infty}$, as will be discussed in Chapter 6, and hence $P_G (= P_V + P_A)$ can be assumed to remain equal to the standard atmospheric pressure on both sides of the surface.

4.2.2.2 Surfaces of Symmetry

Where a surface of symmetry, e.g. the centre-plane of a wall exposed to fire from both sides and the x- and y-axes of a column exposed to fire from two opposite or all four sides, of which advantage can be taken exists, the magnitudes of various parameters immediately adjacent to such a surface are equal, and thus the gradients (or fluxes) of these variables across, i.e. normal to, the surface, are zero. Thus, normal to the surface of symmetry,

$$\frac{\partial \phi}{\partial n} = 0 \tag{4.1}$$

where ϕ is the unknown variable considered and n is the normal to the surface of symmetry. Thus, for the set T, P_G, ρ_V, $\phi = T$, P_G, or ρ_V, and, for the set T, P_G, P_V, $\phi = T$, P_G, or P_V.

4.2.2.3 Implementation

The problems that will be analysed in this study are walls exposed to fire on both sides (Chapters 5, 6, and 7) and columns exposed to fire on all four sides (Chapter 8). Cross sections of these problems along with the parts analysed and the corresponding boundary conditions are shown in Figs. 4.1 and 4.2. A wall can be considered as a 1D problem, since the width of, say, 4000 mm is much greater than the thickness of, say, 400 mm. Thus, the magnitude of a parameter is the same at a certain distance along the width, i.e. along lines parallel to the centreline. Thus, lines normal to the centreline are equivalent to lines of symmetry. For columns exposed to fire on all four sides, only one eighth of the cross section needs to be analysed. However, the version of the model used in this study is the very first one that is designed to deal with rectangular elements only. Thus, one fourth of the cross section is used.

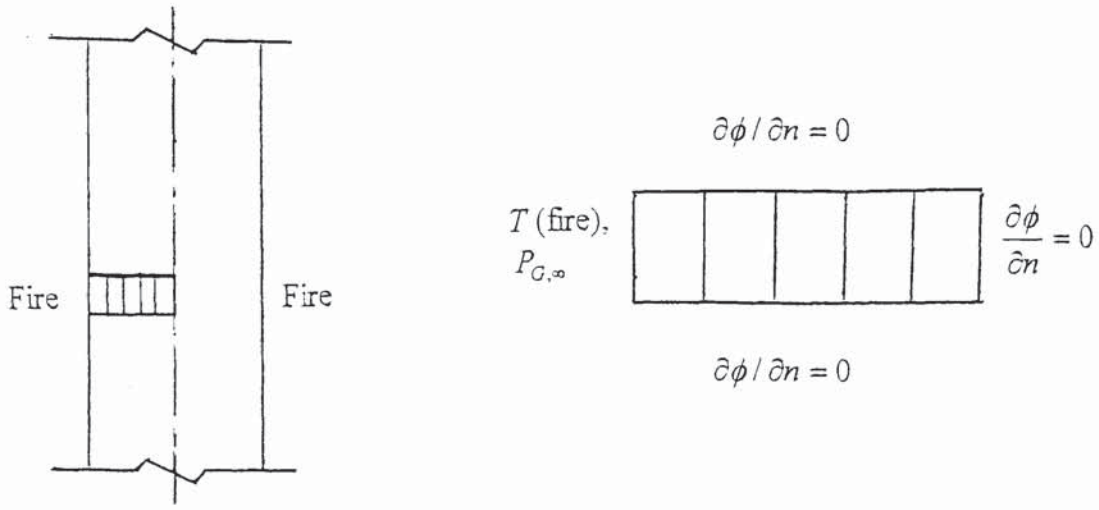

Fig. 4.1: Cross section of a wall exposed to fire on both sides and part meshed and analysed with the corresponding boundary conditions.

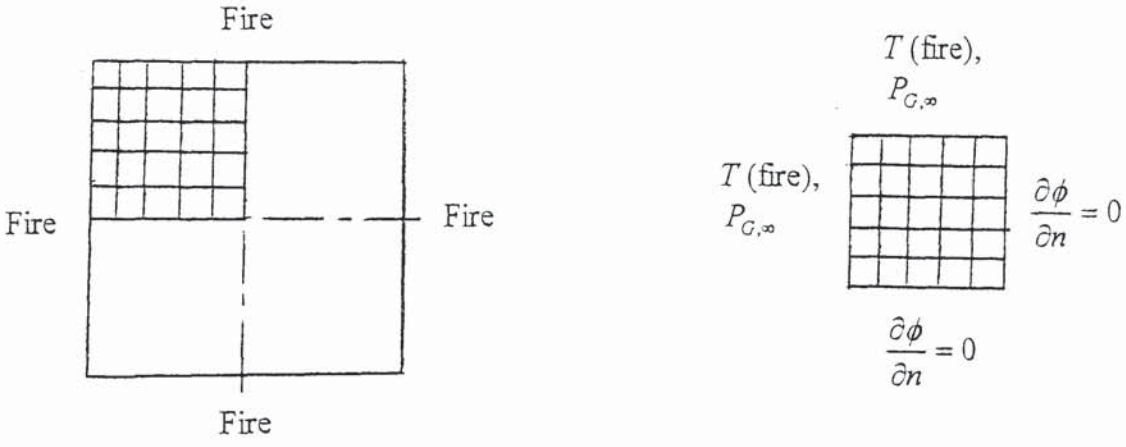

Fig. 4.2: Cross section of a column exposed to fire on all four sides and part meshed and analysed with the corresponding boundary conditions.

4.3 SYSTEM OF DIFFERENTIAL EQUATIONS FOR SET T, P_G, P_V

For the set of unknown variables T, P_G, P_V, the system of differential equations that is suitable for a finite element solution is:

$$C_{AT}\frac{\partial T}{\partial t}+C_{AP}\frac{\partial P_G}{\partial t}+C_{AV}\frac{\partial P_V}{\partial t}=\nabla\cdot\left(K_{AT}\nabla T+K_{AP}\nabla P_G+K_{AV}\nabla P_V\right) \tag{4.2a}$$

$$C_{MT}\frac{\partial T}{\partial t}+C_{MP}\frac{\partial P_G}{\partial t}+C_{MV}\frac{\partial P_V}{\partial t}=\nabla\cdot\left(K_{MT}\nabla T+K_{MP}\nabla P_G+K_{MV}\nabla P_V\right) \tag{4.2b}$$

$$C_{TT}\frac{\partial T}{\partial t}+C_{TP}\frac{\partial P_G}{\partial t}+C_{TV}\frac{\partial P_V}{\partial t}=\nabla\cdot\left(K_{TT}\nabla T+K_{TP}\nabla P_G+K_{TV}\nabla P_V\right) \tag{4.2c}$$

where

$$C_{AT}=\frac{\varepsilon_G}{R_A T^2}\left(P_V-P_G\right)+\rho_A\frac{\partial P_{or}}{\partial T}-\frac{\rho_A}{\rho_L}\frac{\partial\bar{\rho}_L}{\partial T},\quad C_{AP}=\frac{\varepsilon_G}{R_A T},$$

$$C_{AV}=-\frac{\varepsilon_G}{R_A T}-\frac{\rho_A}{\rho_L}\frac{\partial\bar{\rho}_L}{\partial P_V} \tag{4.3a}$$

$$C_{MT}=\rho_V\left(-\frac{\varepsilon_G}{T}+\frac{\partial P_{or}}{\partial T}-\frac{1}{\rho_L}\frac{\partial\bar{\rho}_L}{\partial T}\right)+\frac{\partial\bar{\rho}_L}{\partial T}-\frac{\partial\bar{\rho}_D}{\partial T},\quad C_{MP}=0,$$

$$C_{MV}=\frac{\varepsilon_G}{R_V T}+\left(1-\frac{\rho_V}{\rho_L}\right)\frac{\partial\bar{\rho}_L}{\partial P_V} \tag{4.3b}$$

$$C_{TT}=\left(\overline{\rho C}\right)-\lambda_E\frac{\partial\bar{\rho}_L}{\partial T}+\left(\lambda_D+\lambda_E\right)\frac{\partial\bar{\rho}_D}{\partial T},\quad C_{TP}=0,\quad C_{TV}=-\lambda_E\frac{\partial\bar{\rho}_L}{\partial P_V} \tag{4.3c}$$

$$K_{AT}=\frac{\varepsilon_G\rho_V}{\rho_G T}D_{AV}\left(\rho_A+\frac{R_V}{R_A}\rho_V-\frac{P_G}{R_A T}\right),\quad K_{AP}=\varepsilon_G\left(\rho_A\frac{KK_G}{\mu_G}+\frac{\rho_V}{\rho_G R_A T}D_{AV}\right),$$

$$K_{AV}=-\frac{\varepsilon_G}{\rho_G T}D_{AV}\left(\frac{\rho_A}{R_V}+\frac{\rho_V}{R_A}\right) \tag{4.4a}$$

$$K_{MT} = \frac{\varepsilon_G \rho_V}{\rho_G T} D_{VA}\left(\frac{P_G}{R_A T} - \rho_A - \frac{R_V}{R_A}\rho_V\right),\ K_{MP} = \varepsilon_G \rho_V\left(\frac{KK_G}{\mu_G} - \frac{1}{\rho_G R_A T} D_{VA}\right) + \bar{\rho}_L \frac{KK_L}{\mu_L},$$

$$K_{MV} = \frac{\varepsilon_G}{\rho_G T} D_{VA}\left(\frac{\rho_A}{R_V} + \frac{\rho_V}{R_A}\right) \tag{4.4b}$$

$$K_{TT} = k_{eff},\ K_{TP} = -\lambda_E \bar{\rho}_L \frac{KK_L}{\mu_L},\ K_{TV} = 0 \tag{4.4c}$$

By comparing (4.2)-(4.4) with (18)-(20) of Appendix C, it can be seen that, since the two systems of differential equations (4.2) and (18) are different, 9 of the 18 coefficients are different. These are C_{TV}, C_{AT}, C_{AV}, C_{MT}, C_{MV}, K_{AT}, K_{AV}, K_{MT}, and K_{MV}.

Details of the derivation of these equations are given in Appendix A.

4.4 MODIFICATIONS

In this section, an overview of the modifications made to the mathematical model is presented. Details of these modifications are given in Appendix B. Modifications are required for implementing concrete diffusivity (Section B.1), for implementing the set T, P_G, P_V to check if the model leads to the correct solution of (17) of Appendix C and thus ensure that the results computed and discussed in Chapters 5-8 are correct (Section B.2), for implementing molecular diffusivity according to Chapman-Enskog theory (2.12) and tortuosity (2.24) (Section B.3), and for implementing variable intrinsic permeability (Section B.4).

Since a diffusivity equation specifically for heated concrete did not exist when the model was developed, Tenchev *et al.* had to rely on molecular diffusivity equations. Marrero and Mason's molecular diffusivity (2.15) was used by Tenchev *et al.* (2001a) (Appendix C) and Krischer and Rohnalter's molecular diffusivity (2.8) was adopted by Tenchev *et al.* (2001b) (Appendix D) and Tenchev and Khalafallah (2000) (Appendix E). As discussed in Chapter 2, unlike Knudsen diffusivities, molecular diffusivities of different gases in a gaseous mixture are the same. Thus, advantage was taken of this fact, and hence the original model was designed such that the diffusivity of water vapour through air D_{VA} is the same as that of air through water vapour D_{AV}. As

can be seen from (B2c) (Appendix C), the actual coefficients K_{AT}, K_{AP}, and K_{AV} in the air flux (B2d) are in terms of D_{AV}:

$$K_{AT} = -\frac{D_{AV}\varepsilon_G \rho_V}{\rho_G R_A T}\frac{P_G}{T},\ K_{AP} = \frac{KK_G}{\mu_G}\varepsilon_G \rho_A + \frac{D_{AV}\varepsilon_G \rho_V}{\rho_G R_A T},\ K_{AV} = -\left(\rho_A + \frac{R_V}{R_A}\rho_V\right)\frac{D_{AV}\varepsilon_G}{\rho_G}$$

However, since molecular diffusivity was used and thus $D_{AV} = D_{VA}$, K_{AT}, K_{AP}, and K_{AV} are expressed in terms of D_{VA} in the program as can be seen in (20b) (Appendix C).

Thus, as described in Section B.1, the modifications related to the implementation of concrete diffusivity had to be made to the Fortran statements that define, and thus determine, D_{AV} and D_{VA}, and to the Fortran statements that define the coefficients K_{AT}, K_{AP}, and K_{AV} in which D_{VA}, rather than D_{AV}, appears.

Notwithstanding the simplicity of the modifications required for implementing concrete diffusivity, some of these modifications, i.e. those made to the Fortran statements that define the coefficients K_{AT}, K_{AP}, and K_{AV}, are permanent, and made the model workable with any type of diffusivity. All that needed to adopt different diffusivities is to modify the statements related to defining the diffusivities D_{AV} and D_{VA}.

The modifications required for implementing the set of unknowns T, P_G, P_V were more extensive than those discussed above. In addition to the modifications discussed above, modifications were required to the 9 coefficients, i.e. C_{TV}, C_{AT}, C_{AV}, C_{MT}, C_{MV}, K_{AT}, K_{AV}, K_{MT}, and K_{MV} outlined in Section 4.3. Furthermore, since the system of differential equations (4.2), or (A.6) (Appendix A), to be solved is different than (18) of Appendix C, other modifications were required to several subroutines. Moreover, modifications were required to subroutines related to the output in order to list the results of water vapour pressure rather than water vapour content; these were minor and related to post-processing, and thus may not be of interest to the reader.

The systems of differential equations along with the associated coefficients, i.e. (18)-(20) of Appendix C and (4.2)-(4.4), are provided, and thus the modifications related to these coefficients

are described in Section B.2. On the other hand, description of other modifications related to the solution of the set T, P_G, P_V will not be provided, as they are not an integral part of the research.

Results of eight variables, i.e. temperature, pore pressure, water vapour content and pressure, air content and pressure, gaseous mixture content, and free water content, for problems in four application areas (Chapters 5-8) were computed using both the original set of unknowns T, P_G, ρ_V and the set T, P_G, P_V used to check the methodology. The results were virtually identical for both sets. This confirms that the model is flawless and leads to the correct solution of (A.5) (Appendix A), or (17) (Appendix C). Thus, the results presented and investigated in this study are correct and reliable.

In order to demonstrate that the results are virtually identical for both sets of unknowns, the time history and distribution of various parameters in a 100-mm-thick wall exposed to fire for 60 minutes are shown in Figs. 4.3-4.6. As will be discussed in Section 4.5.3, the combination of a 500 elements mesh and a 1 second time step is adopted for this wall. These results among others will be discussed in Chapter7. Here, it is only necessary to note that the results, particularly those of the pore pressure that is the most important parameter as far as spalling due to pore pressure is concerned, are virtually identical for both sets of unknowns. Very minor differences may be observed only in the results of the air contents and thus air pressures that have no effect at all on the maximum pore pressures.

As mentioned in Chapter 3, a major shortcoming of most mathematical models for heat and mass transfer in heated concrete is assuming that the pores are straight by neglecting the tortuosity. It was also argued that the tortuosity cannot remain constant when the microstructure of concrete changes due to dehydration of bound water, but, since there is no expression for determining the variable tortuosity, the use of a constant value, such as the well-known average of 3 cited for porous media at ambient temperature, reduces the unreasonableness of neglecting the tortuosity. Thus, all that required is to divide a molecular diffusivity equation by, say, 3. Therefore, in order to implement Krischer and Rohnalter's molecular diffusivity with the tortuosity considered (3.3), it was only necessary to modify one statement and the value of 3 was adopted for the tortuosity factor τ (Section B.3). Similarly, in order to implement molecular diffusivity according to Chapman-Enskog theory (2.12), it was only necessary to modify one Fortran statement that defines, and thus determines, the diffusivity of water vapour through air. Again, the same statement is the only one modified in order to consider the tortuosity (Section B.3).

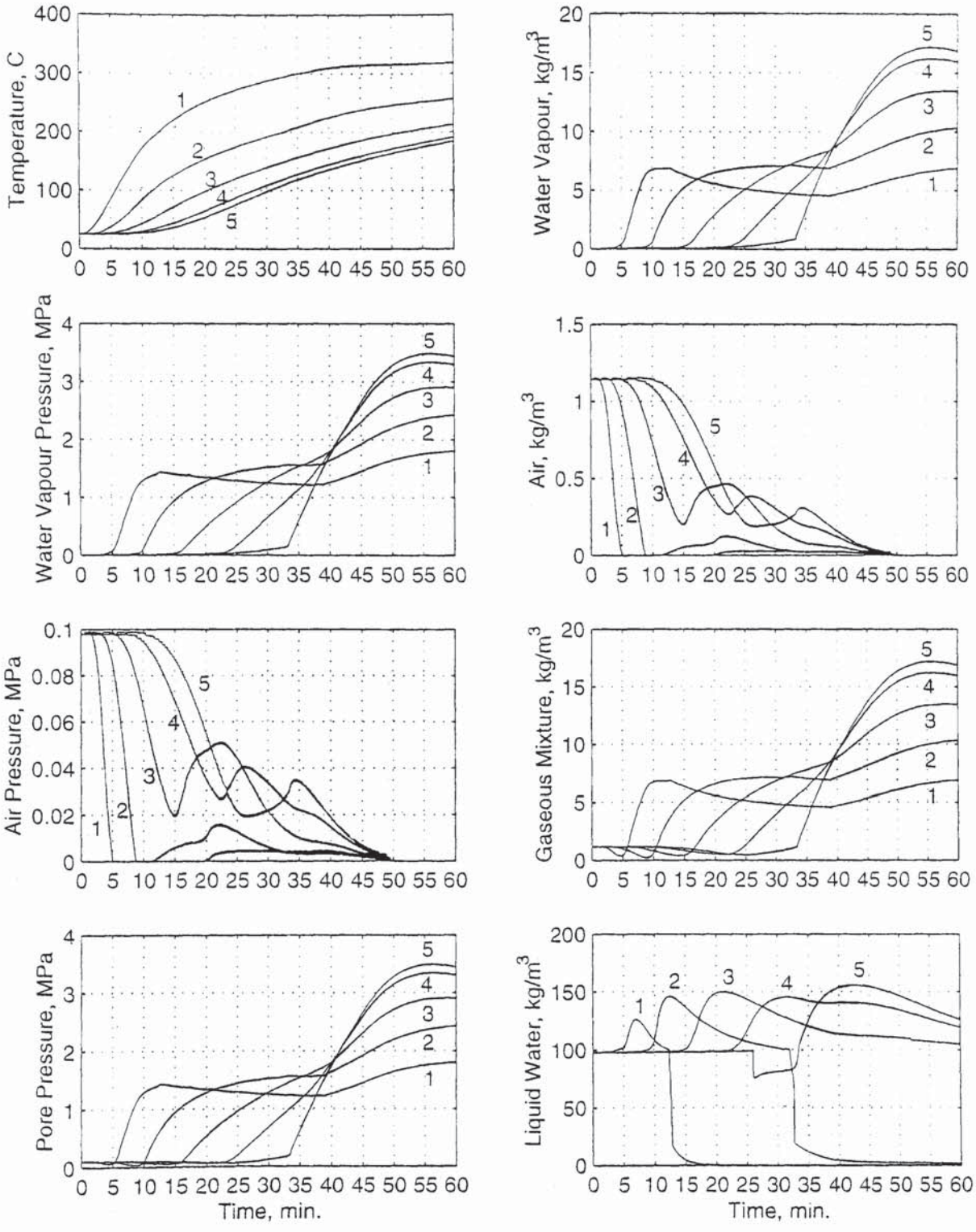

Fig. 4.3: Time history of T, in °C, ρ_v, in kg/m^3, P_v, in MPa, ρ_a, in kg/m^3, P_a, in MPa, ρ_g, in kg/m^3, P_g, in MPa, and $\varepsilon_l \rho_l$, in kg/m^3, at (1) 10, (2) 20, (3) 30, (4) 40, and (5) 50 mm from any of the fire-exposed surfaces of a 100-mm-thick concrete wall exposed to fire from both sides for 60 minutes. (Set T, P_G, ρ_V).

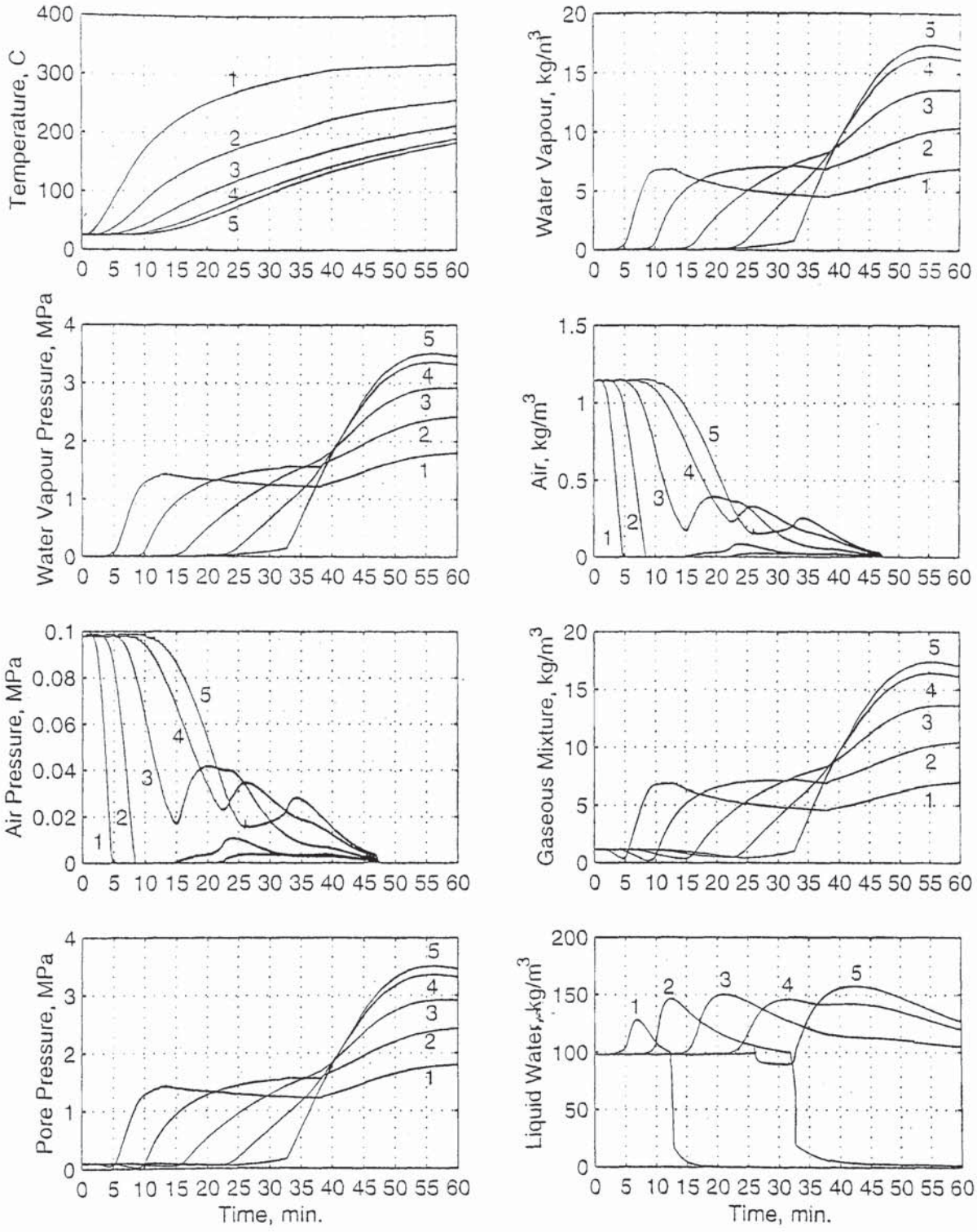

Fig. 4.4: Time history of T, in °C, ρ_v, in kg/m^3, P_v, in MPa, ρ_a, in kg/m^3, P_a, in MPa, ρ_g, in kg/m^3, P_g, in MPa, and $\varepsilon_l \rho_l$, in kg/m^3, at (1) 10, (2) 20, (3) 30, (4) 40, and (5) 50 mm from any of the fire-exposed surfaces of a 100-mm-thick concrete wall exposed to fire from both sides for 60 minutes. (Set T, P_G, P_V).

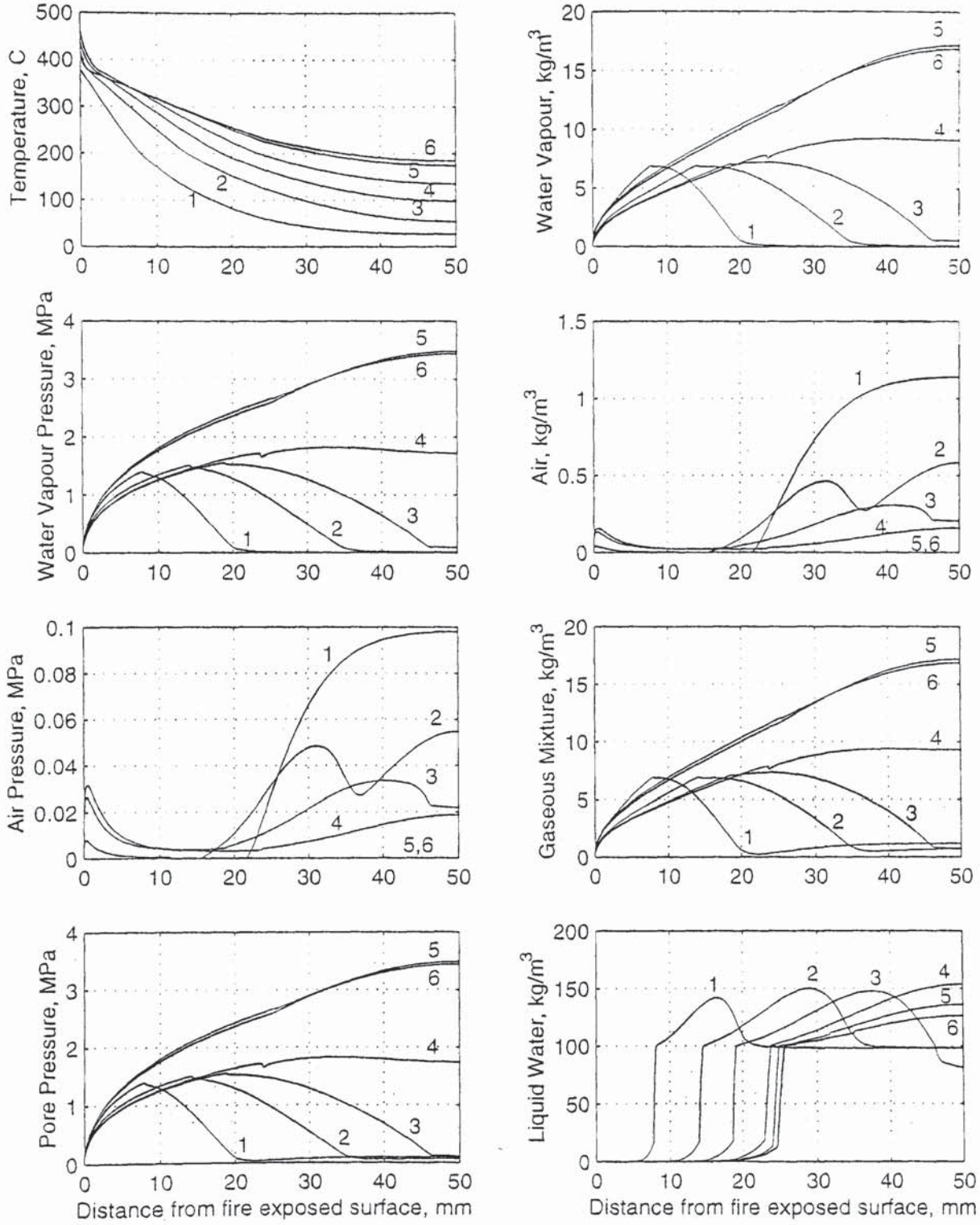

Fig. 4.5: Distribution of T, in °C, ρ_v, in kg/m^3, P_v, in MPa, ρ_a, in kg/m^3, P_a, in MPa, ρ_g, in kg/m^3, P_g, in MPa, and $\varepsilon_l \rho_l$, in kg/m^3, after (1) 10, (2) 20, (3) 30, (4) 40, (5) 55, and (6) 60 minutes of exposure to fire in a 100-mm-thick concrete wall exposed to fire from both sides for 60 minutes. (Set T, P_G, ρ_V).

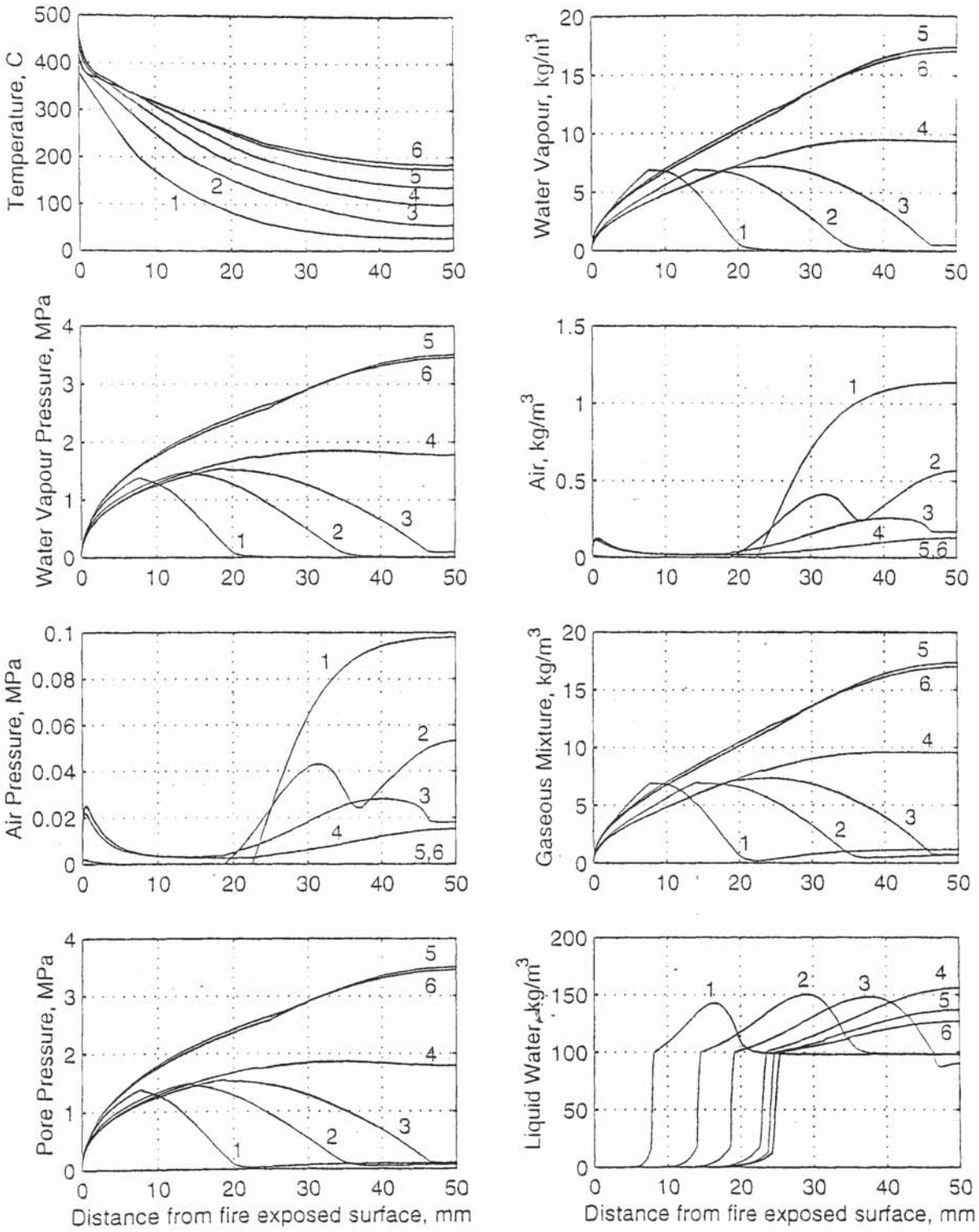

Fig. 4.6: Distribution of T, in °C, ρ_v, in kg/m^3, P_v, in MPa, ρ_a, in kg/m^3, P_a, in MPa, ρ_g, in kg/m^3, P_g, in MPa, and $\varepsilon_l \rho_l$, in kg/m^3, after (1) 10, (2) 20, (3) 30, (4) 40, (5) 55, and (6) 60 minutes of exposure to fire in a 100-mm-thick concrete wall exposed to fire from both sides for 60 minutes. (Set T, P_G, P_V).

In addition to the two major shortcomings discussed in Chapter 3, it appears that, apart from Tenchev *et al.* (2001a), a third major shortcoming is that, in all mathematical models for heat and mass transfer in heated concrete in which diffusion is considered, it has been assumed that the intrinsic permeability is constant at all temperatures. The permeability cannot remain constant when the porosity increases due to dehydration of bound water; it has to increase. This assumption leads to an overestimation of the pore pressure, since the smaller the permeability, the greater the water vapour content that cannot escape. The results obtained using constant permeability will not be presented in this study, since they cannot be reliable and will not be depended on. Tenchev *et al.* (2001a) paid attention to this shortcoming, and used the expression (A8) (Appendix C) for the intrinsic permeability. Throughout this study, the following expression (Zhou *et al.*, 1998) is adopted for K, in m^2:

$$K = {}^0K\left(\frac{P_{or}}{{}^0P_{or}}\right)^3\left(\frac{1-{}^0P_{or}}{1-P_{or}}\right)^2 \tag{4.5}$$

To implement (4.5), it was only necessary to add one Fortran statement in its proper location in the program (Section B.4).

4.5 MESH AND TIME STEP EVALUATION

Following the work described in Chapter 3 and in this chapter, four application areas are investigated. Unlike the vast majority of investigations in this field that concentrate on the results of temperature and pore pressure only, eight variables, i.e. temperature, pore pressure, water vapour content and pressure, air content and pressure, gaseous mixture content, and free water content, are investigated. The four application areas are:

(1) Neglecting diffusion. The effect and significance of neglecting diffusion of water vapour and air on the results, in general, and on the pore pressure, in particular, in heated concrete are investigated by considering a 400-mm-thick wall exposed to fire.

(2) Concrete diffusivity, molecular diffusivity, and tortuosity. The performance of concrete diffusivity, the reasonableness, or unreasonableness, of the results obtained when diffusion in concrete is assumed to be molecular, and the effect and significance of the tortuosity of

the pores of concrete on the pore pressure are investigated by considering a 400-mm-thick wall exposed to fire.

(3) Concrete walls in fire. Concrete walls of different thicknesses exposed to fire for different periods of time are investigated. Concentration is on the pore pressure.

(4) Concrete columns in fire. Square columns of different sizes subjected to fire from all four sides for 60 minutes are investigated. The time of exposure to fire is limited to 60 minutes, since spalling due to pore pressures usually occurs within the first 30 minutes of exposure.

The results computed for the four application areas will be investigated in detail in the following Chapters 5-8. Thus, in this section, the discussion is limited to the numerical aspects of mesh and time step evaluation. The results shown and discussed in Chapters 5-8 are those obtained when the results become virtually identical (stable) as the number of elements increases and the time step decreases. The unstable results, i.e. before they become virtually identical, obtained with coarser meshes and greater time steps will not be provided, as they are not relevant.

4.5.1 Neglecting Diffusion

To investigate the effect and significance of neglecting diffusion of water vapour and air in mathematical modelling of heat and mass transfer in heated concrete, a 400-mm-thick wall exposed to fire from both sides for 60 minutes was investigated. From Appendix C and Section 4.4, it is evident that diffusion is an integral part of the governing equations, and thus it cannot be entirely eliminated; assuming that the diffusivities of water vapour and air are zero invalidates the model. Thus, it was only possible to consider cases in which the diffusivities approach zero. Therefore, results were obtained when concrete diffusivity (3.16) and Krischer and Rohnalter's molecular diffusivity (2.8) are used and when these diffusivities are reduced by one and two orders of magnitude, and the results were compared.

As discussed in Section 4.2, the solution method adopted in the model is the backward difference algorithm, and thus the numerical analysis is unconditionally stable (Zienkiewicz and Taylor, 1991, 1994; Bathe, 1996). The problem is to obtain results of various parameters along the wall thickness,

and thus could be considered one-dimensional, since the width of the wall of, say, 4000 mm is much greater than the thickness of 400 mm.

Meshes of 100, 200, 400, 500, 800, and 1000 elements and time steps of 10, 5, 2, 1, 0.5, and 0.1 seconds were used. Since four-noded quadrilateral elements are used, square elements are chosen according to the general finite element method recommendations (Zienkiewicz and Taylor, 1991; Logan, 1993; Bathe, 1996).

When concrete diffusivity is adopted, virtually identical results were obtained for the mesh of 500 elements and finer meshes with time steps of 1 sec and smaller. The same behaviour was observed when concrete diffusivity is reduced by one order of magnitude. However, when concrete diffusivity was reduced by two orders of magnitude, it was not possible to get results with meshes coarser than 800 elements with any of the time steps used. Virtually identical results were obtained with the mesh of 800 elements and finer meshes with time steps of 1 sec and smaller. Of course, since the reduced concrete diffusivity cannot be the real diffusivity in concrete, it was not expected to get realistic results with any mesh and any time step. The reason for the necessity to use finer meshes to obtain results when concrete diffusivity is reduced by two orders of magnitude is unclear.

When molecular diffusivity is adopted, virtually identical results were obtained when a mesh of 400 elements, and finer meshes, with time steps of 1 sec and smaller are used. Also, it was possible to obtain results with the same mesh and time step when molecular diffusivity was reduced by one and two orders of magnitude. It appears that reducing molecular diffusivity by three or four orders of magnitude might have required a finer mesh and/or a smaller time step, since molecular diffusivity is greater than concrete diffusivity, and thus, a greater reduction may be required to affect the performance of the model. However, the objective is to investigate the effect and significance of neglecting diffusion, and the required results were obtained when concrete diffusivity was reduced by two orders of magnitude. Thus, it was not necessary to reduce molecular diffusivity any more.

The reason for the need to use finer meshes when the diffusivity approaches zero is unclear. Nevertheless, it is found that assuming that the diffusivity is zero invalidates the model. Li (2001, personal communication) believes that the reason is that somewhere in the program the diffusivity appears in the denominator, and thus when the diffusivity is zero, the program fails. Thus, it appears that, when the diffusivity is almost zero, there is an effect on the performance of the model.

One of the most important observations is the effect of the type of diffusivity, i.e. concrete (or Knudsen) or molecular, on the mesh density. As discussed above, meshes of 500 elements and greater are required to obtain stable results with concrete diffusivity, compared with 400 elements for molecular diffusivity. Evidently, this is *not* because concrete diffusivity is smaller than molecular diffusivity, since reducing molecular diffusivity even by two orders of magnitude did not require a mesh finer than 400 elements. (Reducing molecular diffusivity by about 20 leads to almost the same maximum pore pressure computed with concrete diffusivity for a certain set of initial data, which means that, as far as the magnitude, not the location or time, of pore pressure is concerned, concrete diffusivity is around 20 times smaller than molecular diffusivity.)

It appears that this effect of the type of diffusivity on the mesh density is due to the fact that concrete diffusivity is a function of the porosity and thus, like Knudsen diffusivity, is a function of the mean pore diameter, while molecular diffusivity is a function of the pressure. This reasoning is confirmed by the fact that Tenchev *et al.* (2001a) (Appendix C) computed stable results with a mesh of 200 elements and a time step of 2 sec for a 200 mm wall when molecular diffusivity is reduced by a factor of 18, while concrete diffusivity requires 500 elements and 1 sec for walls of different thicknesses from 400 to 75 mm as will be discussed in the following section. The reason for this effect of the type of diffusivity on the mesh density is unclear.

4.5.2 Concrete Diffusivity, Molecular Diffusivity, and Tortuosity

As discussed in Section 4.5.1, results were obtained with concrete diffusivity and Krischer and Rohnalter's molecular diffusivity before these diffusivities were reduced. Meshes of 500 and 400 elements, respectively, and a time step of 1 sec were the appropriate combinations that led to virtually identical results to those obtained when finer meshes and smaller time steps were used. These results are part of the investigation carried out in Chapters 5 and 6.

However, while Chapter 5 concentrates on comparing the computed pore pressures with those obtained when the diffusivities are reduced, the investigation in Chapter 6 includes considering and comparing all parameters. Additionally, the results of another molecular diffusivity (2.12) that was derived in Chapter 2 according to Chapman-Enskog theory, are computed and discussed. Furthermore, the effect and significance of the tortuosity is investigated, and thus the molecular diffusivities (2.8) and (2.12) are divided by the tortuosity factor τ according to (2.25). The well-

known average of 3 for τ at ambient temperature is used, since there is no expression to determine the variable tortuosity when the porosity increases due to dehydration of bound water.

Even though molecular diffusivity according to Chapman-Enskog theory (2.12) is smaller than Krischer and Rohnalter's molecular diffusivity (2.8), it is found that a mesh of 400 elements and a time step of 1 sec is, again, the appropriate combination the results of which are virtually identical to those computed with finer meshes and smaller time steps. Furthermore, reducing (2.8) and (2.12) by a factor of 3 to account for the tortuosity does not require a finer mesh or a smaller time step to obtain stable results. This is expected, since this combination was found appropriate when (2.8) was reduced by one order of magnitude in Section 4.5.1. Thus, the combination of 400 elements and 1 sec is used with all four molecular diffusivity equations.

4.5.3 Concrete Walls in Fire

One of the most important objectives of this study is to investigate the effect of thickness of concrete sections exposed to fire since, as discussed by Purkiss (1996), spalling is exacerbated in thin heated sections, and many researchers believe that this is due to the build-up of pore pressure (Chapter 2). Thus, walls with different thicknesses of 400, 150, 100, 75, 50, and 25 mm exposed to fire for 240, 120, 60, 60, 60, and 60 minutes, respectively, were investigated in order to determine the overall behaviour pattern whilst recognising the impracticality of the smaller sizes. Only concrete diffusivity was adopted since, as discussed in Chapter 3, the type of diffusion in concrete can never be totally molecular in every single pore, and thus the results of molecular diffusivity cannot be correct. Detailed results and discussion of walls in fire will be provided in Chapter 7.

The same combination of 500 elements and 1 sec led to results that are virtually identical to those obtained with finer meshes and smaller time steps for the 400, 150, 100, and 75-mm-thick walls. However, when the 50 and 25-mm-thick wall was analysed, meshes finer than 200 elements with different time steps led to unrealistic results. Realistic results were computed only with the mesh of 200 elements and time steps of 1 sec and smaller. A coarser mesh of 100 elements and time steps of 1 sec and smaller led to virtually identical results to those obtained with the 200 elements mesh. Coarser meshes did not lead to stable results with any of the time steps used.

4.5.4 Concrete Columns in Fire

The effect of thickness of concrete sections in fire was also investigated by considering square columns of different sizes, i.e. 400×400, 300×300, 200×200, 100×100, 50×50, and 25×25 mm, exposed to fire from all four sides for 60 minutes. Meshes of 40×40, 25×25, 20×20, and 10×10 elements and time steps of 10, 5, 4, 2, 1, 0.5, and 0.25 sec were used. For the 400×400 mm column, dependence was on a previous work (Tenchev and Khalafallah, 2000) (Appendix E) in which molecular diffusivity was adopted. The problem required a mesh of 40×40 elements and a time step of 5 sec. This combination led to oscillations in the time history of pore pressure that can be reduced by using a finer mesh, and may be avoided if a 100×100 is used. However, 2-D analysis is computationally expensive; the solution of a 40×40 elements mesh with a time step of 5 sec for 60 minutes of exposure to fire required about 60 h on a SUN Ultra10 computer, and it is found that the solution time increases with the cube of the ratio of numbers of elements, i.e. the solution time for a mesh of 100×100 elements with the same time step would be about $(100/40)^3 \approx 16$ times.

For the remaining columns, i.e. 300×300, 200×200, 100×100, 50×50, and 25×25 mm columns, concrete diffusivity was adopted. Consequently, for the 300×300 mm column, realistic results could not be obtained until a mesh of 40×40 elements and a time step of 0.25 sec were used; coarser meshes and greater time steps did not lead to realistic results. Thus, the solution required about two months on the Sun Ultra10 computer. It is interesting to note that, even with this combination, the realism of the results was limited to the first 30 minutes of exposure to fire for this column; it will be discussed in Chapter 8 that the results after 60 minutes of exposure were not realistic, and thus the 300×300 column requires a denser mesh of, say, 60×60 elements the analysis of which is computationally expensive and impractical. This confirms the effect of the type of diffusivity on the mesh density and/or time step that was observed and discussed in Section 4.5.1.

For the 200×200 mm column, realistic results could be obtained with a mesh of 40×40 elements and a time step of 0.5 sec; coarser meshes and greater time steps did not lead to realistic results. For the 100×100 mm column, virtually identical results were computed with meshes of 25×25 and 40×40 elements and time steps of 1, 0.5, and 0.25 sec; the results that will be presented in Chapter 8 for this column are those computed with a mesh of 40×40 elements and a time step of 0.5 sec. For the 50×50 mm column, virtually identical results were obtained with meshes of 20×20, 25×25 and 40×40 elements and time steps of 1 sec and smaller; the results that will be presented

in Chapter 8 for this column are those computed with a mesh of 25×25 elements and a time step of 0.25 sec. Finally, for the 25×25 mm column, virtually identical results were computed with meshes of 20×20 and 25×25 elements and time steps of 1 sec and smaller; the results that will be presented in Chapter 8 for this column are those computed with a mesh of 25×25 elements and a time step of 0.5 sec.

4.6 CONCLUSIONS

- In order to confirm the correctness of methodology, i.e. confirm that the model is flawless and leads to the correct numerical solution, and thus ensure the correctness of the results investigated in this study within the reasonableness of various assumptions adopted, an arbitrary set of unknown variables, i.e. temperature, pore pressure, and water vapour pressure, was chosen that is different from the original set of temperature, pore pressure, and water vapour content, the equations corresponding to this set were derived, the model was modified, and results for different problems were computed. The results were found virtually identical to those obtained with the original set, which ensures the reliability of the results.

- One of the major shortcomings of most mathematical models of heat and mass transfer in heated concrete in which diffusion is considered is the assumption that the intrinsic permeability remains constant at all temperatures. The permeability increases when the porosity increases due to dehydration of bound water. This assumption leads to an overestimation of the pore pressure, since the smaller the permeability, the greater the water vapour content that cannot escape.

- Some of the modifications made to implement concrete diffusivity are permanent, since they made the model workable with any type of diffusivity; all that needed to adopt different diffusivities is to modify the statements that define the diffusivities.

- As the diffusivity approaches zero, finer meshes are required to compute any results, albeit unreasonable since the reduced diffusivities are not the real ones. The reason for this effect is unclear. However, assuming that the diffusivities of water vapour and air are zero invalidates the model. This is believed to be due to the diffusivities being in the denominator somewhere in the program. The effect of very small diffusivities on the performance of the model may be due to this fact.

- One of the most important observations is that the type of diffusivity, i.e. concrete (or Knudsen) or molecular, has an effect on the mesh density and/or time step. Concrete diffusivity, and thus Knudsen diffusivity, requires a finer mesh and/or a smaller time step than those required by molecular diffusivity. This is not due to the fact that concrete diffusivity is smaller than molecular diffusivity, since reducing molecular diffusivity even by two orders of magnitude does not require a finer mesh or a smaller time step. Evidently, this is due to the fact that concrete diffusivity is a function of the porosity and thus, like Knudsen diffusivity, is a function of the mean pore diameter, while molecular diffusivity is a function of the pore pressure. The reason for this effect of the type of diffusivity on the mesh density and time step is unclear.

- The thicker the section to be analysed, the greater the number of elements required to obtain stable, and thus realistic, results. This is expected since, when the same number of elements is used for a thicker section as that used for a thin one, the size of an element increases, and thus such a coarse mesh becomes less representative of the continuum, while, depending on the size of the element, the same number of elements may be representative of a smaller continuum.

In the following Chapters 5-8, the results of various parameters for the four application areas outlined in Section 4.5 will be presented and investigated in detail.

CHAPTER 5

NEGLECTING DIFFUSION

5.1 INTRODUCTION

In Section 3.3.1, it was demonstrated qualitatively that the assumption that diffusion does not occur in concrete is invalid. The qualitative treatment, however, is not enough, and it is one of the major objectives of this study to carry out quantitative analyses in order to determine the effect, and significance, of neglecting diffusion on the pore pressure, compared with the pore pressure obtained when concrete diffusivity (3.16) is adopted. Also, in Section 3.4.6, it was argued that neglecting diffusion in mathematical modelling results in the maximum possible underestimation of the pore pressure, and the use of molecular diffusivity results in the maximum possible overestimation of the pore pressure. Thus, the first part of this argument will be confirmed, or refuted, in this chapter. Furthermore, the results of this chapter are particularly important in that they can provide a clear indication of the realism of the results obtained when concrete diffusivity is used.

Since the mathematical model used in this study is based on the second approach in which diffusion is an integral part of the governing equations, it is not possible to eliminate diffusion completely. Thus, it is only possible to reduce concrete diffusivity by one and two orders of magnitude, and hence analyse problems in which the diffusivity approaches zero. Of course, the smaller diffusivities obtained by reducing concrete diffusivity are unrealistic, and thus it is not expected to obtain realistic results of different parameters. Nevertheless, the effect of neglecting diffusion on the pore pressure can be confirmed, and the significance can be estimated.

It is also interesting to check if the performance of molecular diffusivity can approach that of concrete diffusivity when molecular diffusivity is reduced. Thus, Krischer and Rohnalter's molecular diffusivity (2.8) (Section 2.6.3) is reduced by one and two orders of magnitude, and the effect on the pore pressure is analysed in this chapter.

The results of this chapter also demonstrate the unreasonableness of neglecting diffusion. Obviously, if the results of the temperature and pore pressure are the only ones presented as has been done so far by different researchers, the unreasonableness of neglecting diffusion can only be

proved qualitatively. However, when the variation of other variables, i.e. the water vapour content, vapour pressure, air content, and air pressure, is considered, the unreasonableness of the first approach to mathematical modelling becomes clear. Of course, researchers who use models in which diffusion is neglected cannot consider these other variables in the first place, since some of these variables (vapour content and vapour pressure) are implicitly included with those of the free water while the others (air content and air pressure) are neglected, and thus cannot be determined.

5.2 INITIAL DATA

An ideal gas is defined as a gas that obeys the relation (Çengel, 1998):

$$P = \rho RT \tag{5.1}$$

where P is the pressure, ρ is the density, R is the gas constant, and T is the absolute temperature.

Thus, for water vapour:

$$P_v = \rho_v R_v T \tag{5.2}$$

For air:

$$P_a = \rho_a R_a T \tag{5.3}$$

For the gaseous mixture of water vapour and air, Dalton's law of additive pressures is (Çengel, 1998):

$$P_g = P_v + P_a \tag{5.4}$$

Also,

$$\rho_g = \rho_v + \rho_a \tag{5.5}$$

The initial pore pressure ${}^0P_g$ at ambient temperature is equal to the standard atmospheric pressure, i.e. ${}^0P_g = 101325$ Pa.

The water vapour pressure at ambient temperature ${}^0P_v$ can be assumed equal to the saturation pressure at ambient temperature given by Çengel, that is, ${}^0P_v = {}^0P_{sat} = 2339$ Pa. Thus, from (5.4), the initial air pressure at ambient temperature ${}^0P_a$ is ${}^0P_a = 98986$ Pa.

From (5.2), the initial water vapour content per unit volume of the gaseous mixture can be determined as ${}^0\rho_v = 0.017$ kg/m^3.

From (5.3), the initial air content per unit volume of the gaseous mixture is ${}^0\rho_a = 1.18$ kg/m^3. Thus, from (5.5), the initial gaseous mixture content per unit volume of the gaseous mixture is ${}^0\rho_g = 1.2$ kg/m^3.

The initial free water content per unit volume of concrete ${}^0(\varepsilon_l \rho_l) = 100$ kg/m^3 where ε_l is the free water volume fraction and ρ_l is the density of water, the initial porosity ${}^0P_{or} = 0.18$, and the intrinsic permeability $K = 8 \times 10^{-17}$ m^2.

5.3 DIFFUSIVITY EQUATIONS

5.3.1 Reduced Concrete Diffusivity

Concrete diffusivities of water vapour (3.29) and air (3.32) are rewritten as follows:

Concrete diffusivity of water vapour:

$$D_{Conc,V} = 1.5 \times 10^{-7} \varepsilon_g P_{or}^{0.8} T^{0.5} \tag{5.6a}$$

Concrete diffusivity of air:

$$D_{Conc,A} = 1.18 \times 10^{-7} \varepsilon_g P_{or}^{0.8} T^{0.5} \tag{5.6b}$$

Then, the case in which the diffusivities of water vapour and air are reduced by one order of magnitude is considered:

Diffusivity of vapour:

$$D_{e,V} = 1.5 \times 10^{-8} \varepsilon_g P_{or}^{0.8} T^{0.5} \tag{5.7a}$$

Diffusivity of air:

$$D_{e,A} = 1.18 \times 10^{-8} \varepsilon_g P_{or}^{0.8} T^{0.5} \tag{5.7b}$$

Finally, the case in which the diffusivities of water vapour and air are reduced by two orders of magnitude is considered:

Diffusivity of water vapour:

$$D_{e,V} = 1.5 \times 10^{-9} \varepsilon_g P_{or}^{0.8} T^{0.5} \tag{5.8a}$$

Diffusivity of air:

$$D_{e,A} = 1.18 \times 10^{-9} \varepsilon_g P_{or}^{0.8} T^{0.5} \tag{5.8b}$$

5.3.2 Reduced Molecular Diffusivity

In order to analyse the performance of reducing molecular diffusivity, Krischer and Rohnalter's molecular diffusivity (2.8) is reduced by one and two orders of magnitude. The original molecular diffusivity (2.8) is

$$D_{AV} = D_{VA} = 5.893 \times 10^{-6} \frac{T^{2.3}}{P_g} \tag{5.9}$$

Reducing (5.9) by one and two orders of magnitude yields, respectively,

$$D_{AV} = D_{VA} = 5.893 \times 10^{-7} \frac{T^{2.3}}{P_g} \tag{5.10}$$

$$D_{AV} = D_{VA} = 5.893 \times 10^{-8} \frac{T^{2.3}}{P_g} \tag{5.11}$$

5.4 RESULTS OF REDUCED CONCRETE DIFFUSIVITY

The distribution and time history of the temperature T, in °C, water vapour content ρ_v per unit volume of the gaseous mixture, in kg/m^3, water vapour pressure P_v, in MPa, air content ρ_a per unit volume of the gaseous mixture, in kg/m^3, air pressure P_a, in MPa, gaseous mixture content ρ_g per unit volume of the gaseous mixture, in kg/m^3, pore pressure P_g, in MPa, and free water content $\varepsilon_l \rho_l$ per unit volume of concrete, in kg/m^3, in an unsealed 400-mm-thick normal-concrete wall exposed to fire from both sides for 60 minutes according to (5.6)-(5.8) are presented.

Figs. 5.1 and 5.2 show that the maximum pore pressure obtained when concrete diffusivity (5.6) is adopted is about 1.5 MPa at 30 mm from any of the fire-exposed surfaces after 60 minutes of exposure to fire.

The distribution and time history of the same parameters when concrete diffusivities of water vapour and air are reduced by one order of magnitude, i.e. according to (5.7), are demonstrated in Figs. 5.3 and 5.4. It can be seen that reducing the diffusivities of vapour and air by one order of magnitude results in a maximum pore pressure of about 1.2 MPa at the same distance of 30 mm from the fire-exposed surface after the same period of exposure of 60 minutes.

It is interesting to note that the maximum pore pressures are entirely due to water vapour pressure. However, the variation of the water vapour pressure is totally inconsistent with the variation of the water vapour content. The water vapour content remains almost constant at about 7 kg/m^3 everywhere from the beginning until after 60 minutes of exposure to fire, while the water vapour pressure and the pore pressure vary from about 0.4 MPa after 5 minutes of exposure to fire to 1.2 MPa after 60 minutes of exposure. The air, and thus air pressure, is totally displaced by the water vapour from the regions where the water vapour content is greater than the initial value, and appears only where the water vapour is at its initial value, as shown in Fig. 5.3. Then, the air content and air pressure recur and reach greater values than their initial ones before they start decreasing. The same observations can be seen in Fig. 5.4.

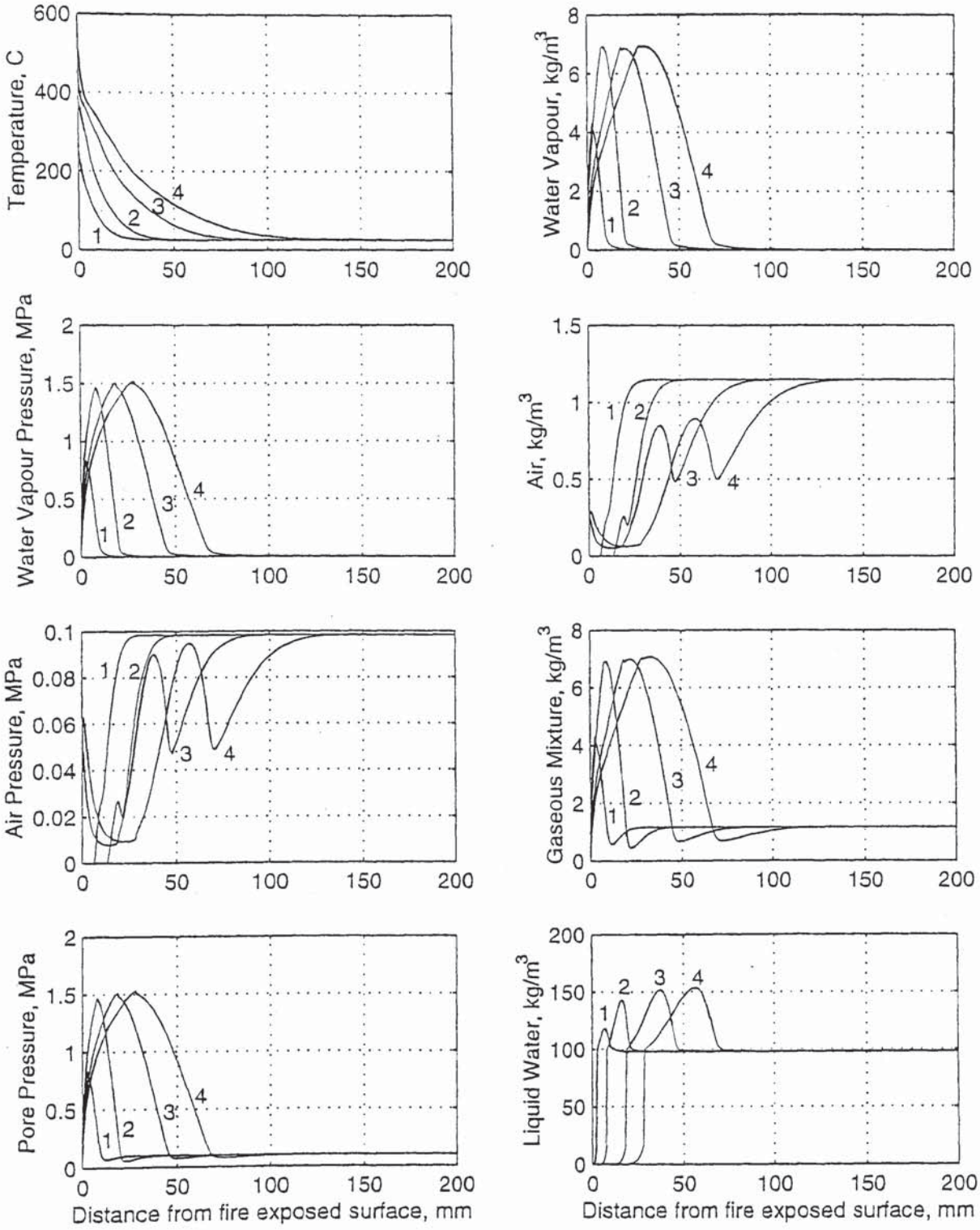

Fig. 5.1: Distribution of T, in °C, ρ_v, in kg/m^3, P_v, in MPa, ρ_a, in kg/m^3, P_a, in MPa, ρ_g, in kg/m^3, P_g, in MPa, and $\varepsilon_l \rho_l$, in kg/m^3, after (1) 5, (2) 10, (3) 30, and (4) 60 minutes of exposure to fire according to concrete diffusivity (5.6).

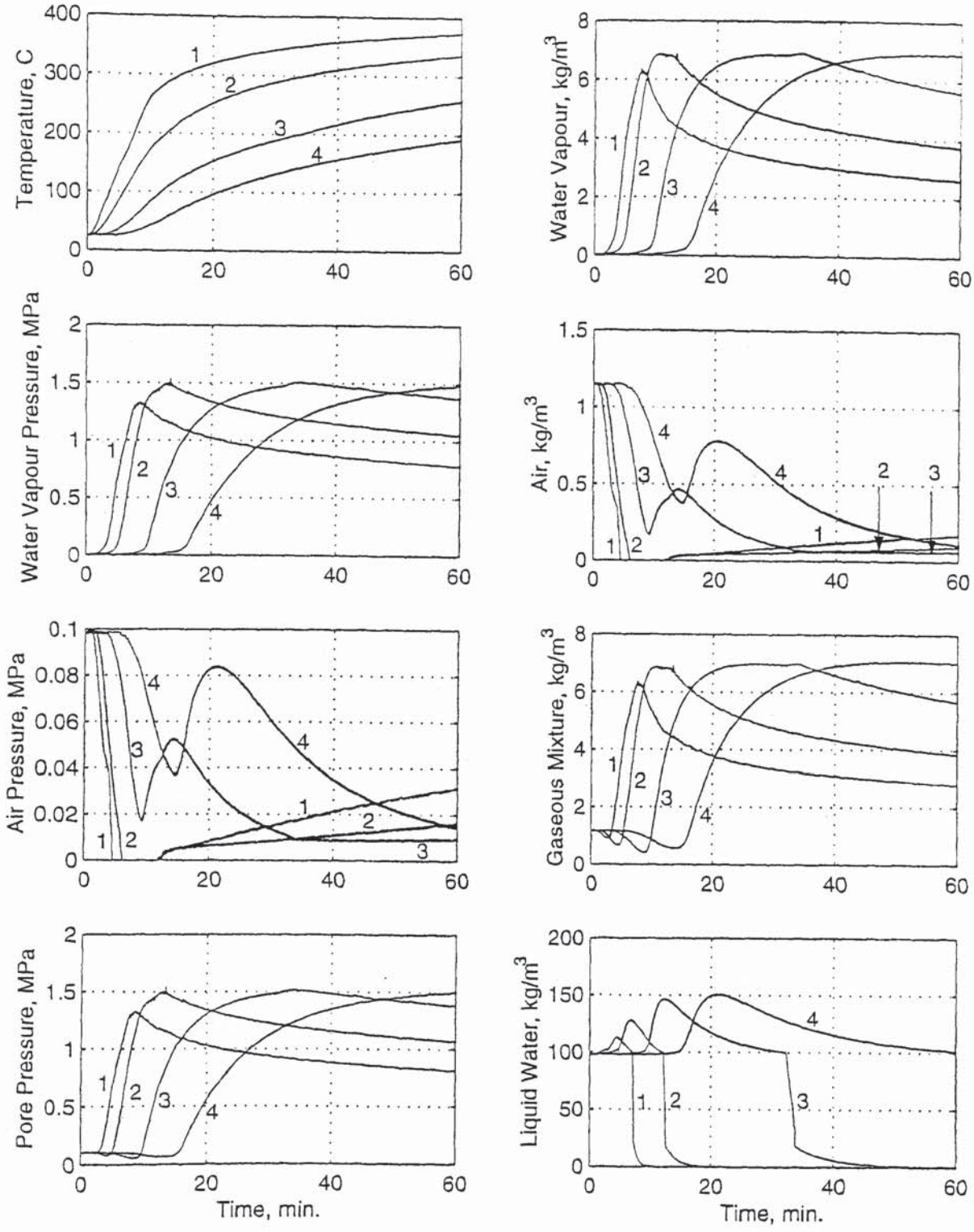

Fig. 5.2: Time history of T, in °C, ρ_v, in kg/m^3, P_v, in MPa, ρ_a, in kg/m^3, P_a, in MPa, ρ_g, in kg/m^3, P_g, in MPa, and $\varepsilon_l \rho_l$, in kg/m^3, at (1) 5, (2) 10, (3) 20, and (4) 30 mm from the fire-exposed surface according to concrete diffusivity (5.6).

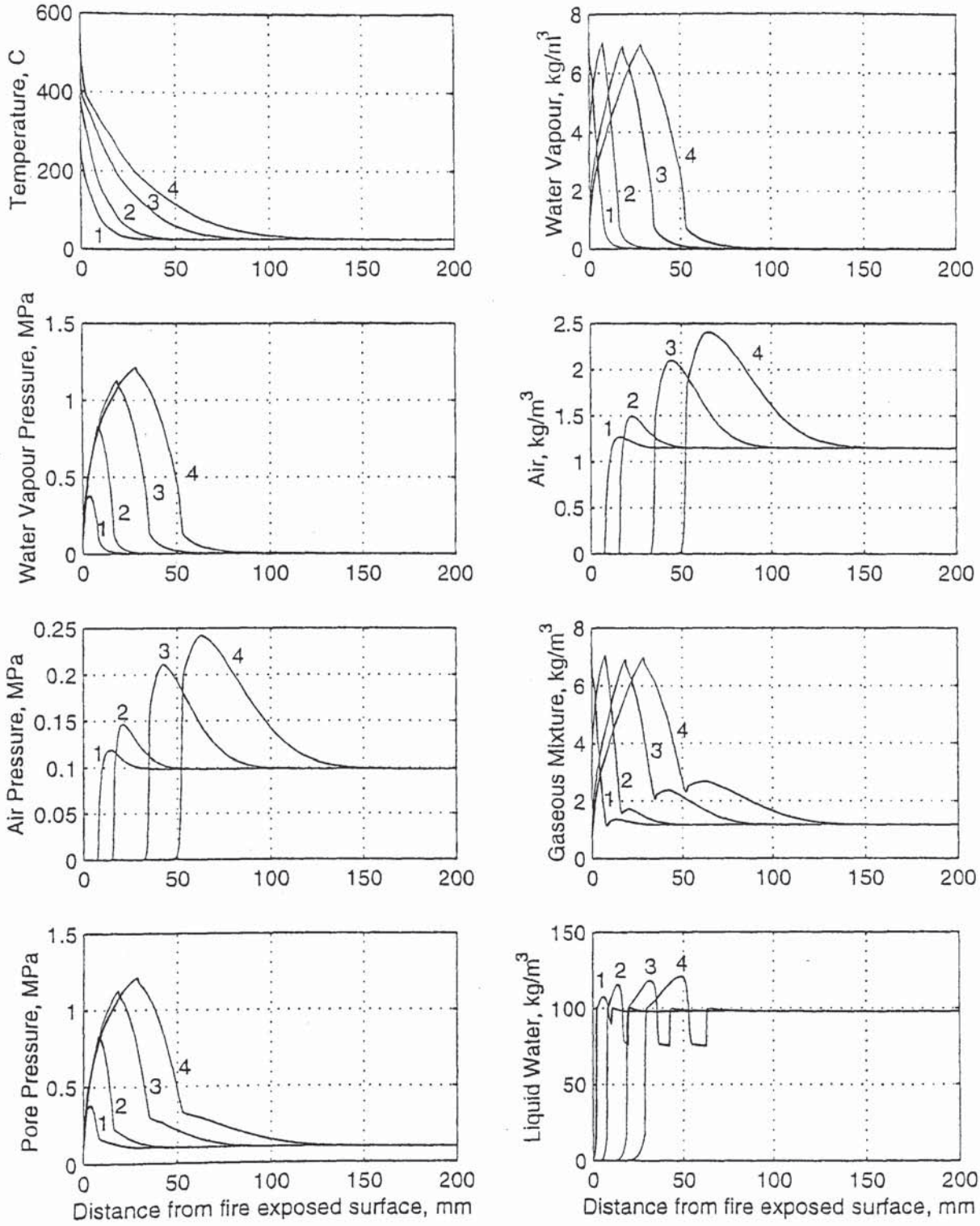

Fig. 5.3: Distribution of T, in °C, ρ_v, in kg/m^3, P_v, in MPa, ρ_a, in kg/m^3, P_a, in MPa, ρ_g, in kg/m^3, P_g, in MPa, and $\varepsilon_l \rho_l$, in kg/m^3, after (1) 5, (2) 10, (3) 30, and (4) 60 minutes of exposure to fire according to (5.7).

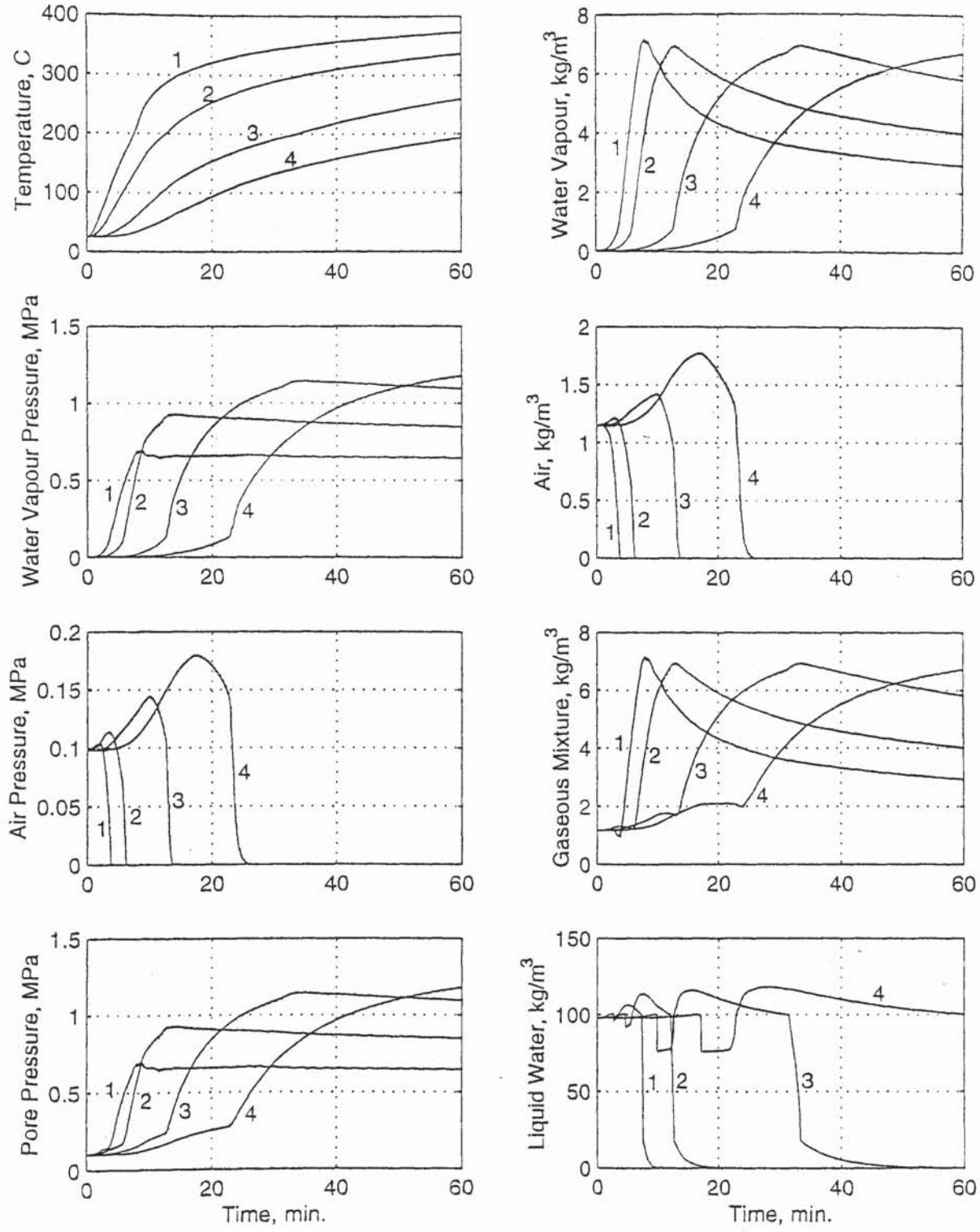

Fig. 5.4: Time history of T, in °C, ρ_v, in kg/m^3, P_v, in MPa, ρ_a, in kg/m^3, P_a, in MPa, ρ_g, in kg/m^3, P_g, in MPa, and $\varepsilon_l \rho_l$, in kg/m^3, at (1) 5, (2) 10, (3) 20, and (4) 30 mm from the surface exposed to fire according to (5.7).

Figs. 5.5 and 5.6 show the distribution and time history, respectively, of different parameters according to (5.8) in which the diffusivities of vapour and air are reduced by two orders of magnitude. Fig. 5.5 shows that, after 10 minutes of exposure to fire, the maximum pore pressure is 0.85 MPa at a distance of 10 mm from the exposed surface, compared with the maximum pore pressure of almost 1.5 MPa obtained from concrete diffusivity at the same distance after the same period of exposure. This pore pressure is only 57% of the maximum pore pressure that results from concrete diffusivity at the same distance after the same period of exposure. A maximum pore pressure of 1 MPa is reached only after 60 minutes of exposure to fire at 30 mm from the fire-exposed surface. The time history (Fig. 5.6) shows that, at a distance of 5 mm from the exposed surface, the maximum pore pressure is only 0.7 MPa after about 5 minutes of exposure to fire, compared with the maximum pressure of 1.3 MPa obtained from concrete diffusivity.

It is clear from the results above that neglecting diffusion underestimates the pore pressure significantly. The maximum pore pressure of about 1.5 MPa obtained with concrete diffusivity is *at least* 50% greater than that obtained with mathematical models that are based on the first approach to mathematical modelling in which diffusion of water vapour and air is neglected.

Furthermore, these results are particularly important in that they provide a clear indication of the realism of the results obtained when concrete diffusivity is used. This is explained as follows: Bažant (1997), who believes that diffusion does not occur in concrete, stated that the calculated pressures were considerably smaller than initially expected, and never exceeded about 1 MPa. Thus, the fact that the maximum pore pressure obtained when diffusion approaches zero does not exceed 1 MPa implies that different assumptions, other than diffusion, that affect the pore pressure and that are adopted in the mathematical model used in this study are equivalent to those of researchers who neglect diffusion.

It is unlikely that any of these other assumptions is unreasonable. Also, concrete diffusivity is based on actual diffusivity tests on concrete and on the real type of diffusion in concrete, i.e. Knudsen diffusion; thus, it appears that concrete diffusivity provides the real effective diffusivity in concrete under transient heating conditions, and, provided that all other assumptions are reasonable, leads to tenable results. Therefore, assuming that all assumptions are now reasonable, it can be concluded that the results obtained when concrete diffusivity is used are correct and reliable, and thus the maximum pore pressure of 1.5 MPa appears to be the real maximum pore pressure than can occur in unsealed thick normal-concrete sections exposed to fire.

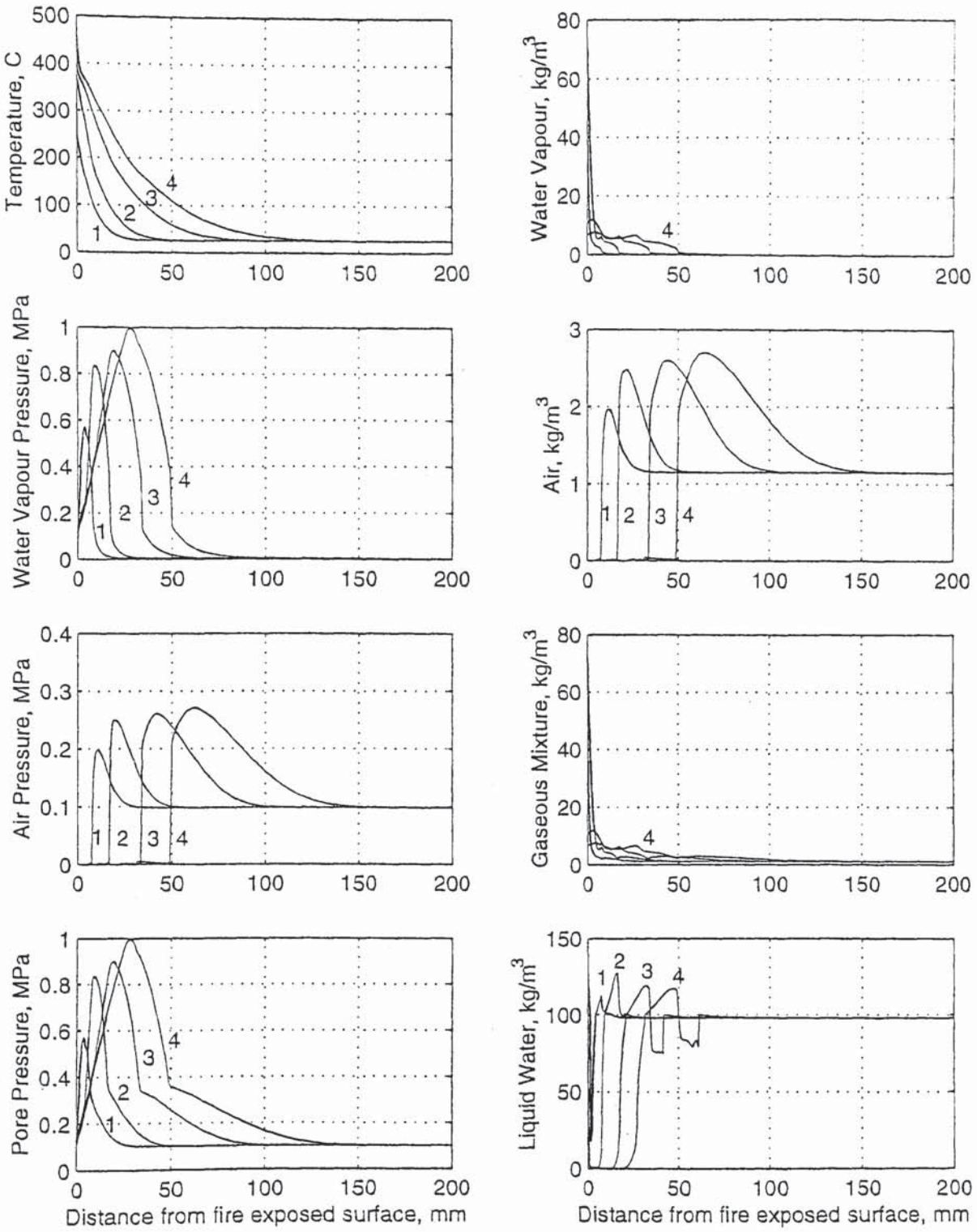

Fig. 5.5: Distribution of T, in °C, ρ_v, in kg/m^3, P_v, in MPa, ρ_a, in kg/m^3, P_a, in MPa, ρ_g, in kg/m^3, P_g, in MPa, and $\varepsilon_l \rho_l$, in kg/m^3, after (1) 5, (2) 10, (3) 30, and (4) 60 minutes of exposure to fire according to (5.8).

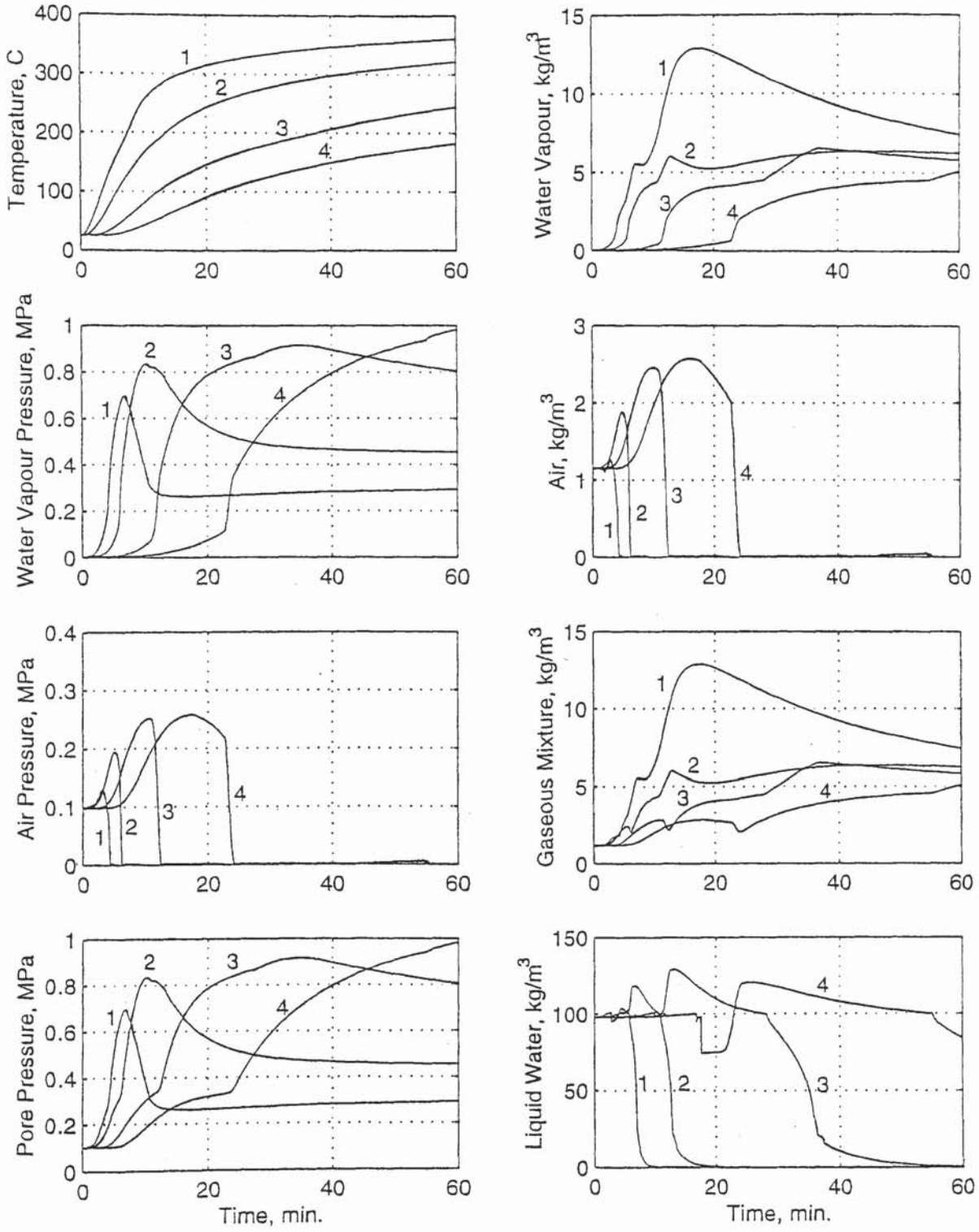

Fig. 5.6: Time history of T, in °C, ρ_v, in kg/m^3, P_v, in MPa, ρ_a, in kg/m^3, P_a, in MPa, ρ_g, in kg/m^3, P_g, in MPa, and $\varepsilon_l \rho_l$, in kg/m^3, at (1) 5, (2) 10, (3) 20, and (4) 30 mm from the surface exposed to fire according to (5.8).

5.5 RESULTS OF REDUCED MOLECULAR DIFFUSIVITY

The distribution and time history of various parameters according to (5.9) are illustrated in Figs. 5.7 and 5.8. The anomalies in the results of different parameters when molecular diffusivity is adopted for heated concrete will be discussed in Chapter 6. Thus, only the results of the maximum pore pressure are of concern here. From Figs. 5.7 and 5.8, the maximum pore pressure after 60 minutes of exposure to fire is 2.7 MPa at a distance of about 30 mm from any of the fire-exposed surfaces.

The distribution and time history of the same parameters according to (5.10) are shown in Figs. 5.9 and 5.10. A significant difference in the performance results when Krischer and Rohnalter's molecular diffusivity is reduced by one order of magnitude. Generally, the same performance can be observed from Fig. 1 of Tenchev *et al.* (2001b) (Appendix D). The maximum pore pressure after 60 minutes of exposure to fire is 2.1 MPa. One of the most important observations is that, like concrete diffusivity, (5.10) leads to maximum pore pressures that are almost entirely due to vapour pressure. Also, the time history (Fig. 5.10) shows the natural behaviour in which the air content and air pressure start increasing after reaching a minimum as soon as the vapour content and vapour pressure start decreasing after reaching a maximum.

However, the air content and air pressure reach values significantly higher than their initial values at other locations where the vapour content, vapour pressure, and pore pressure are smaller than their maximum values. Fig. 5.9 shows that the air content is 3 kg/m^3 at 60 mm from the exposed surface after 60 minutes of exposure to fire, and the air pressure is 0.6 MPa near the exposed surface. Although these values do not contribute to the maximum pore pressure, they are unreasonable.

After 10 minutes of exposure, the maximum vapour content of 7 kg/m^3 and maximum vapour and pore pressures of 1.5 MPa are equal to the maximum vapour content, vapour pressure, and pore pressure that remain almost constant when concrete diffusivity is adopted. However, these maximum values do not remain almost constant. The vapour content increases to 8.5 kg/m^3 after 30 minutes of exposure, and thus the vapour and pore pressures increase to about 2 MPa, and then remain almost constant. Due to the differences in the vapour contents, the values of the free water content in the over-saturated zone according to (5.10) are smaller than those obtained with concrete diffusivity within about 40 mm from the exposed surface, and are greater at other distances.

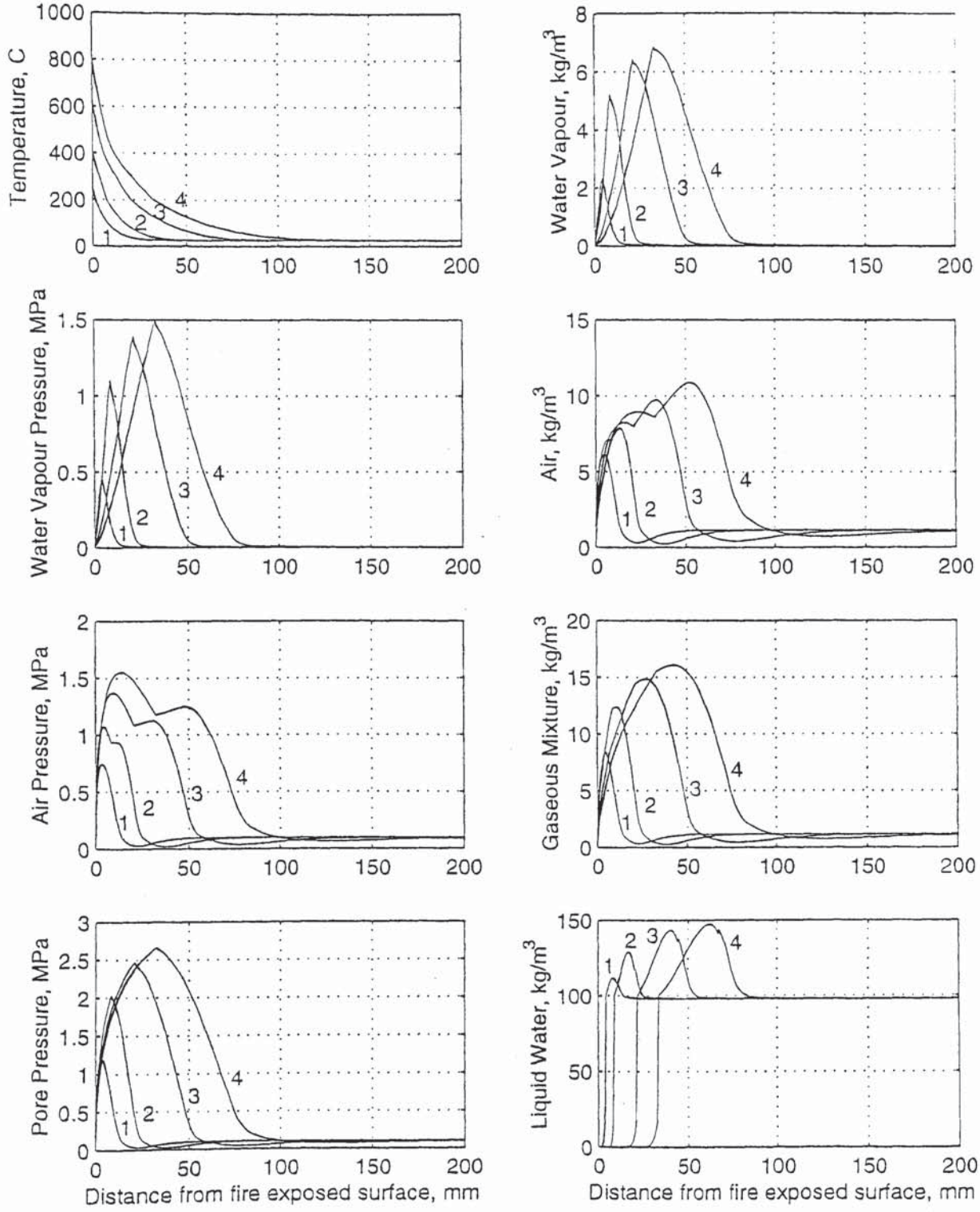

Fig. 5.7: Distribution of T, in °C, ρ_v, in kg/m^3, P_v, in MPa, ρ_a, in kg/m^3, P_a, in MPa, ρ_g, in kg/m^3, P_g, in MPa, and $\varepsilon_l \rho_l$, in kg/m^3, after (1) 5, (2) 10, (3) 30, and (4) 60 minutes of exposure to fire according to (5.9).

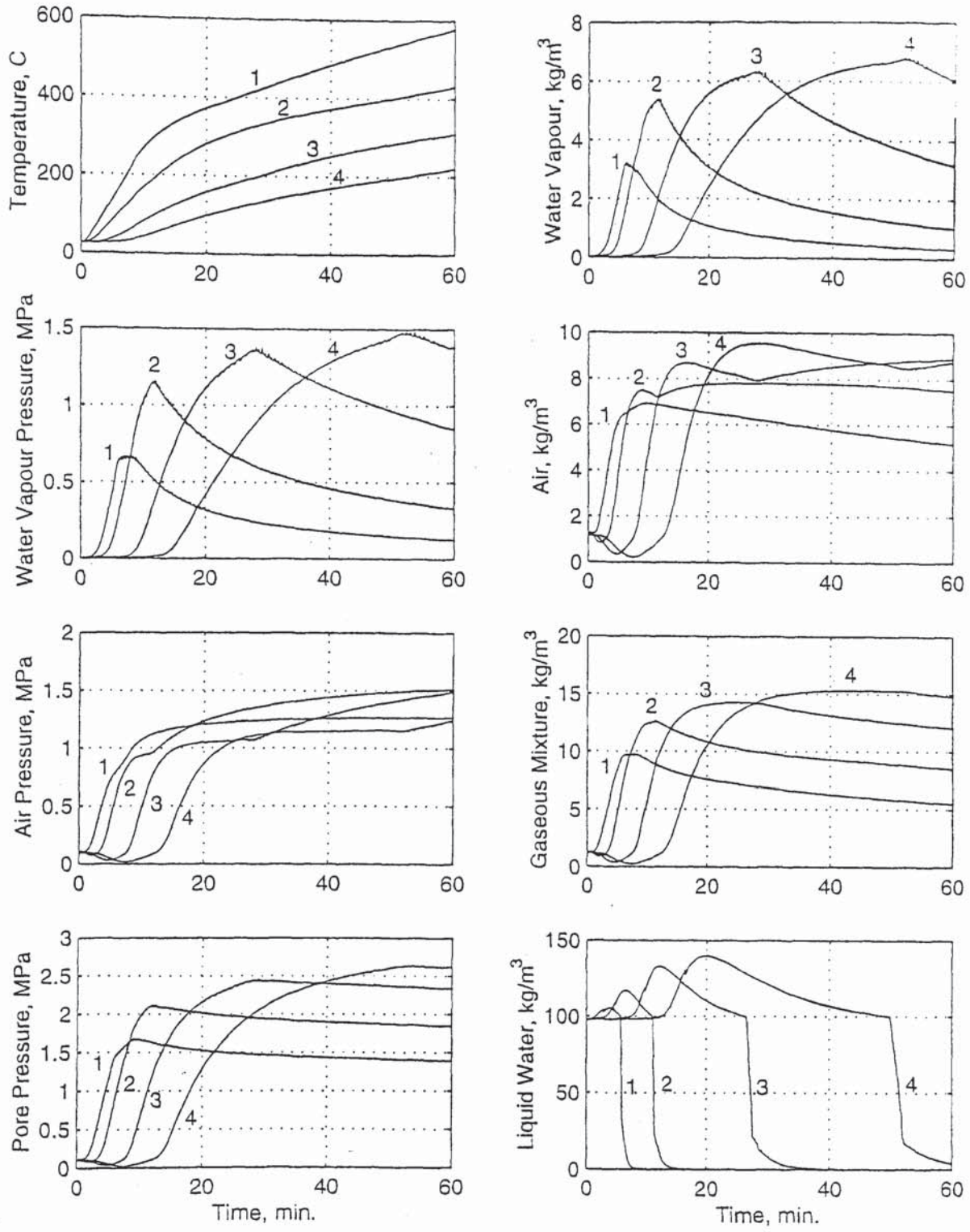

Fig. 5.8: Time history of T, in °C, ρ_v, in kg/m^3, P_v, in MPa, ρ_a, in kg/m^3, P_a, in MPa, ρ_g, in kg/m^3, P_g, in MPa, and $\varepsilon_l \rho_l$, in kg/m^3, at (1) 5, (2) 10, (3) 20, and (4) 30 mm from the surface exposed to fire according to (5.9).

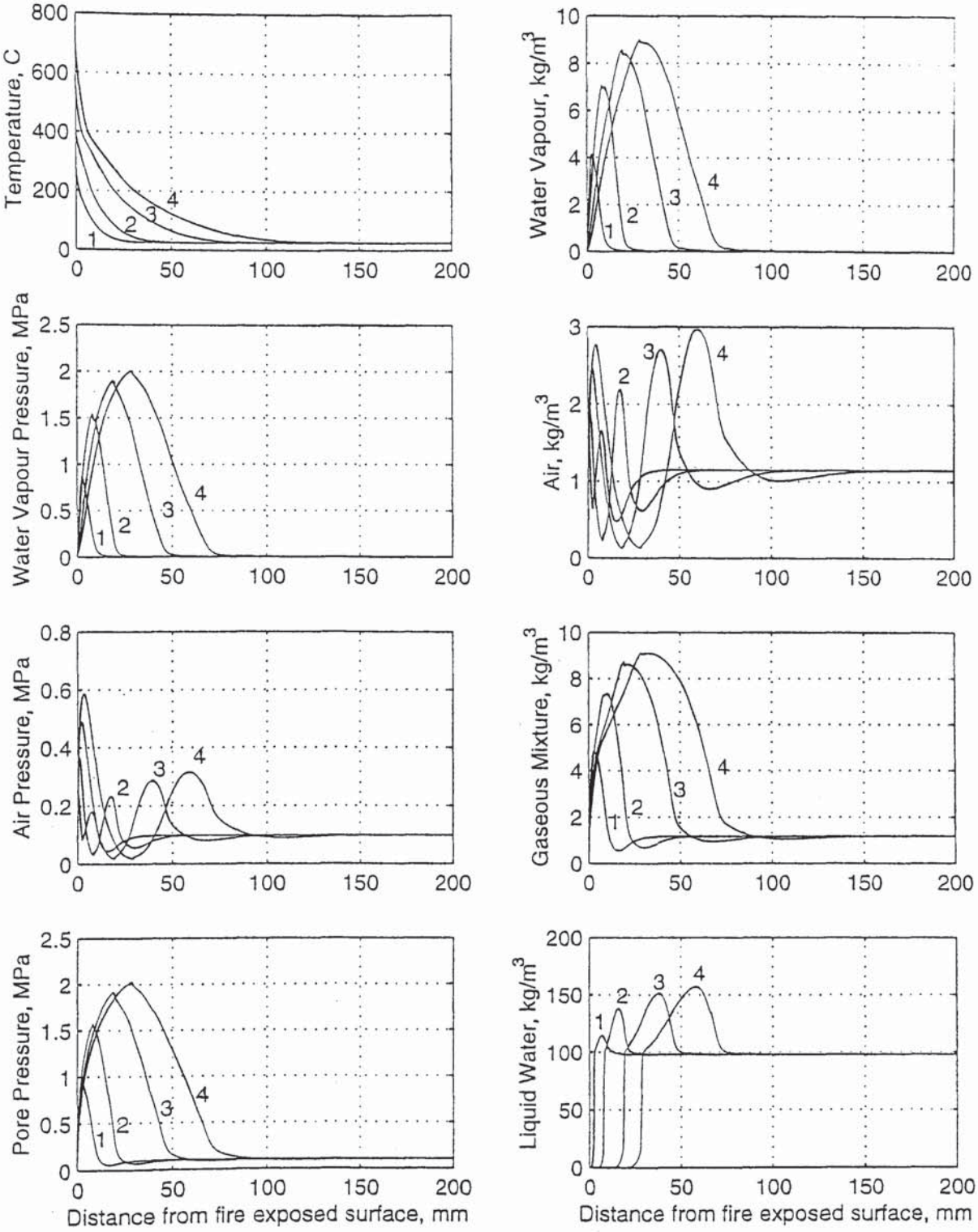

Fig. 5.9: Distribution of T, in °C, ρ_v, in kg/m^3, P_v, in MPa, ρ_a, in kg/m^3, P_a, in MPa, ρ_g, in kg/m^3, P_g, in MPa, and $\varepsilon_l \rho_l$, in kg/m^3, after (1) 5, (2) 10, (3) 30, and (4) 60 minutes of exposure to fire according to (5.10).

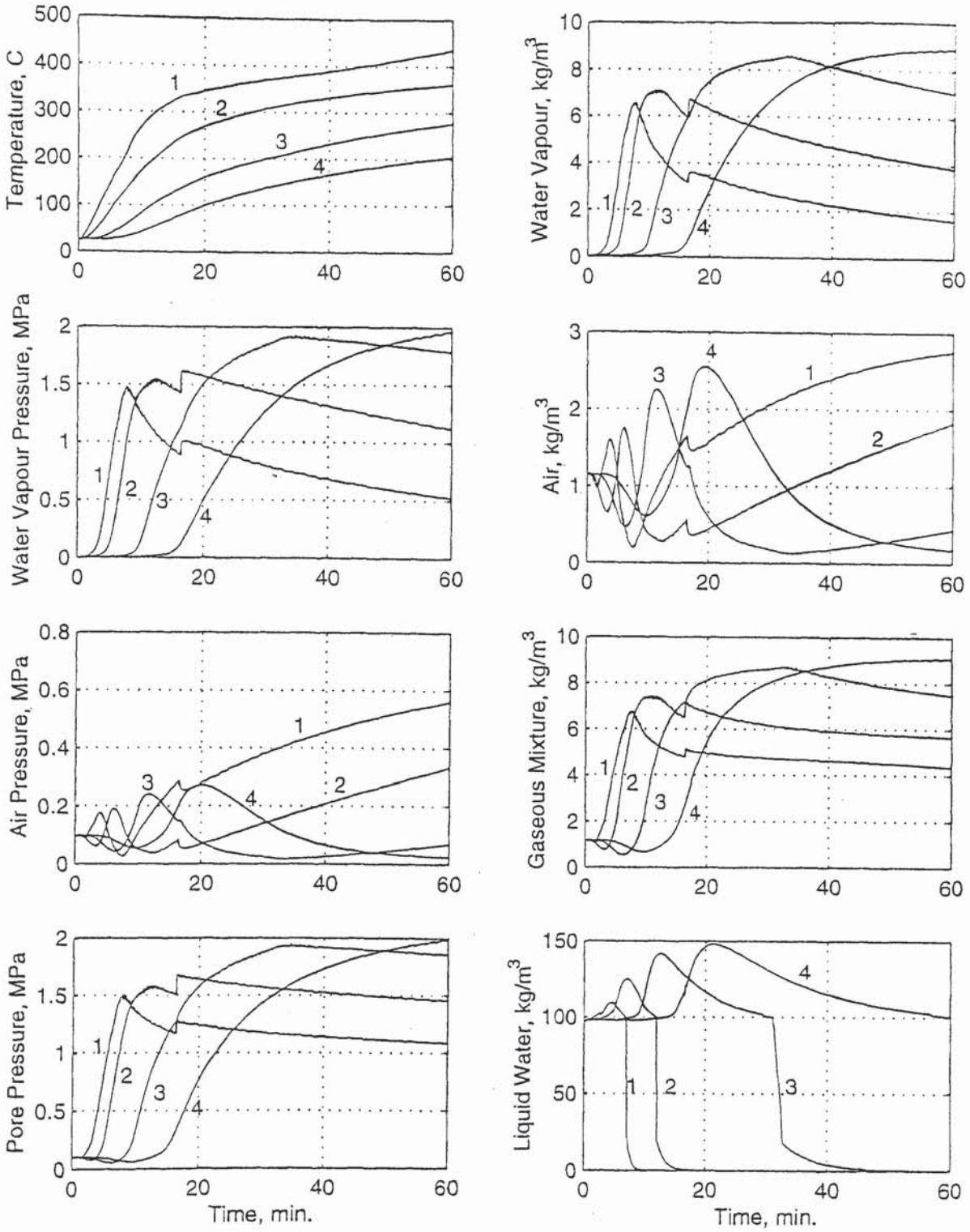

Fig. 5.10: Time history of T, in °C, ρ_v, in kg/m^3, P_v, in MPa, ρ_a, in kg/m^3, P_a, in MPa, ρ_g, in kg/m^3, P_g, in MPa, and $\varepsilon_l \rho_l$, in kg/m^3, at (1) 5, (2) 10, (3) 20, and (4) 30 mm from the surface exposed to fire according to (5.10).

The distribution and time history of various parameters according to (5.11) are shown in Figs. 5.11 and 5.12. Reducing the molecular diffusivity by two orders of magnitude leads to maximum pore pressures that are slightly smaller than those resulting from concrete diffusivity (5.6) during the first 30 minutes of exposure to fire. After 60 minutes of exposure to fire, however, the water vapour content increases to 8 kg/m^3, and the vapour pressure and pore pressure increase to 1.7 MPa. Although the maximum pore pressures are entirely due to vapour pressure, the variation of the air content and air pressure is as unreasonable as that obtained with (5.7) in which concrete diffusivity is reduced by one order of magnitude. The performance of (5.11) is not as good as that of (5.10). However, as expected, the maximum pore pressures obtained with (5.11) are smaller than those resulting from (5.10).

At first, it may appear that reducing molecular diffusivity by, say, 20 may lead to results that approach those obtained with concrete diffusivity. As discussed in Chapter 3, however, reducing molecular diffusivity is unreasonable, and thus cannot lead to reliable results under all circumstances, and is pointless. Reducing a molecular diffusivity equation is unreasonable, since it simply results in yet another molecular diffusivity equation that, unlike the real diffusivity in concrete, is still a function of the pore pressure, i.e. a function of the number of molecule-molecule collisions that do not occur in concrete, has a stronger dependence on temperature, and does not vary with the mean pore diameter; thus it may not lead to actual results if a different set of initial data, e.g. a different concrete with a different porosity or a different permeability, is adopted.

It cannot be rational to use an equation based on molecular diffusion whilst there is now an effective diffusivity equation (concrete diffusivity) that is specific for concrete since it is based on actual diffusivity tests on concrete and on Knudsen diffusivity, that determines the effective diffusivity of any gas in concrete at any temperature, and that takes into account the type of concrete due to its dependence on the porosity.

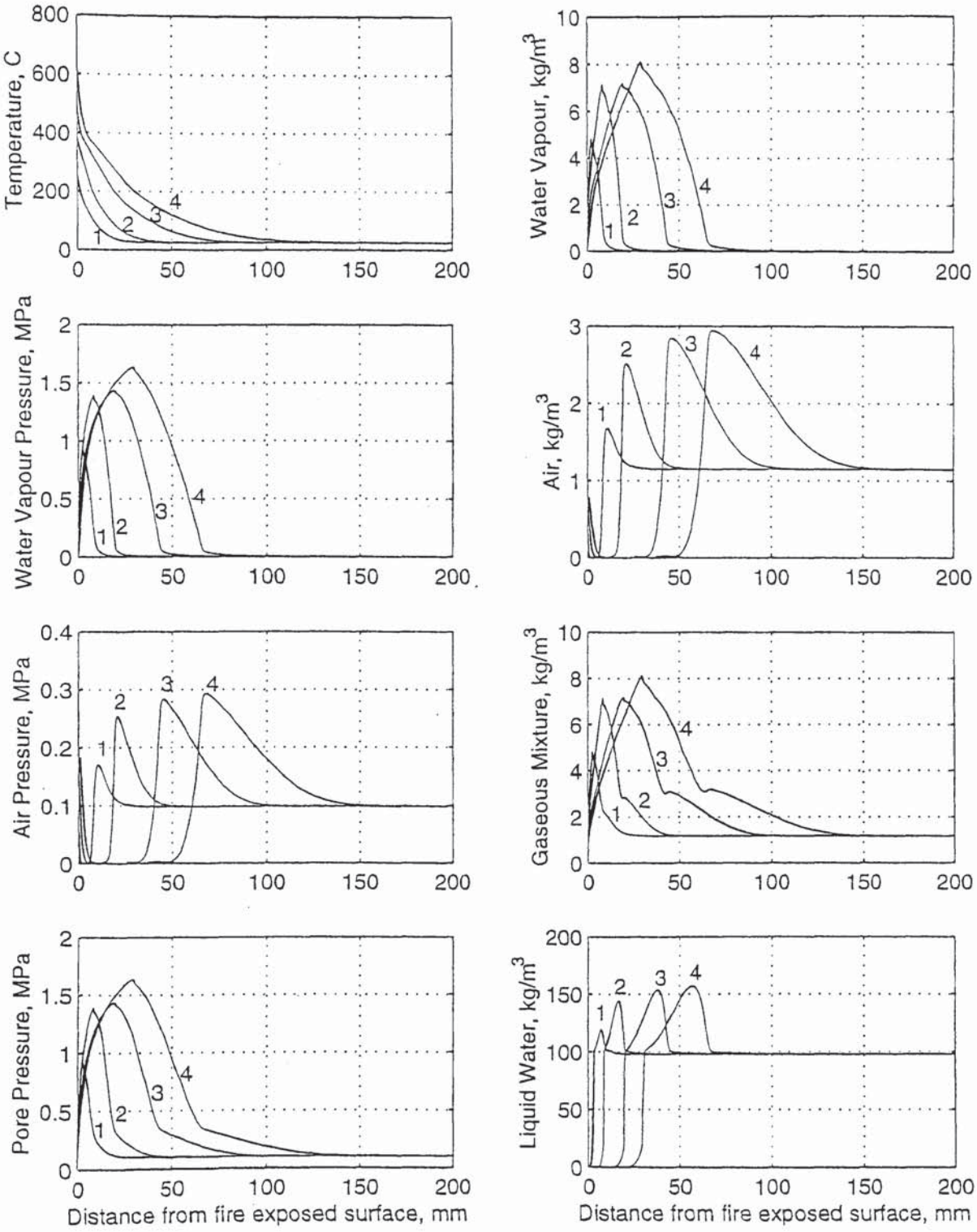

Fig. 5.11: Distribution of T, in °C, ρ_v, in kg/m^3, P_v, in MPa, ρ_a, in kg/m^3, P_a, in MPa, ρ_g, in kg/m^3, P_g, in MPa, and $\varepsilon_l \rho_l$, in kg/m^3, after (1) 5, (2) 10, (3) 30, and (4) 60 minutes of exposure to fire according to (5.11).

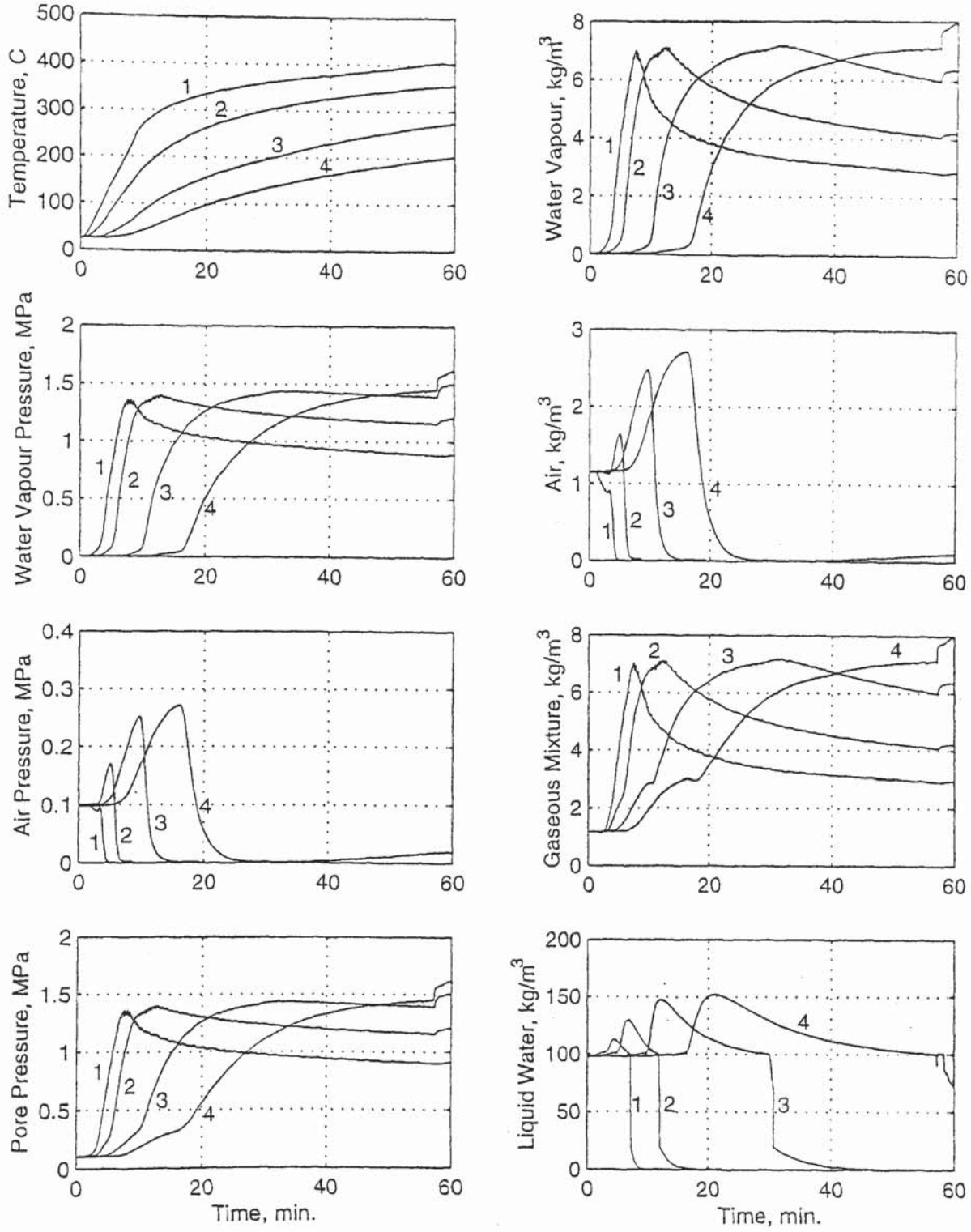

Fig. 5.12: Time history of T, in °C, ρ_v, in kg/m^3, P_v, in MPa, ρ_a, in kg/m^3, P_a, in MPa, ρ_g, in kg/m^3, P_g, in MPa, and $\varepsilon_l \rho_l$, in kg/m^3, at (1) 5, (2) 10, (3) 20, and (4) 30 mm from the surface exposed to fire according to (5.11).

5.6 FURTHER DISCUSSION

It is believed that the validity and realism of concrete diffusivity does not require to be ensured, since it is based on diffusivity tests on concrete and on Knudsen diffusivity. Nevertheless, the results of this chapter demonstrate the validity of the new equation, because the crucial criterion is that it *must* lead to pore pressures between those resulting from the extreme case of neglecting diffusion and from the other extreme case of using molecular diffusivity since the real diffusivity in concrete is between the two extremes (Section 3.4.6).

Furthermore, the hypothesis proposed in Section 3.4.6 is confirmed; neglecting diffusion leads to the greatest underestimation of the pore pressure, and using molecular diffusivity results in the greatest overestimation of the pore pressure. Moreover, the reasons for the underestimation and for the overestimation of the pore pressure are also confirmed; as can be seen from Figs. 5.9 and 5.11 (or Figs. 5.9 and 5.1), provided that the air does not significantly contribute to the increase of the pore pressure, the smaller the diffusivity, the smaller the diffusive flux, the smaller the total flux, the smaller the water vapour content, and thus the smaller the pore pressure; conversely, the greater the diffusivity, the greater the pore pressure.

The reason for the water vapour content of 7 kg/m^3 in Fig. 5.7 being smaller than that of 9 kg/m^3 in Fig. 5.9, even though (5.9) is greater than (5.10), is that the vapour content of 7 kg/m^3 is *not* the real vapour content that corresponds to the maximum pore pressure of 2.7 MPa; this maximum pore pressure is *not* mainly due to water vapour. As can be seen from Fig. 5.7, at the location where the maximum pore pressure of 2.7 MPa occurs, the air content is 9 kg/m^3 and the air pressure is very significant (1.2 MPa). From (5.3), if the air content remained equal to or smaller than its initial value of 1.18 kg/m^3, as it is supposed to be according to Bird *et al.* (1960), and realising that the temperature at which the maximum pore pressure occurs is about 200°C, the very maximum contribution of the air to the pore pressure cannot exceed 0.16 MPa. Thus, from (5.2), the remaining pore pressure of 2.54 MPa should have been due to 11.6 kg/m^3 of water vapour, compared with 9 kg/m^3 of water vapour when molecular diffusivity is reduced by one order of magnitude. Therefore, if the pore pressure of 2.7 MPa were mainly due to water vapour, then, again, the smaller the diffusivity, the smaller the water vapour content, and thus the smaller the pore pressure.

The hypothesis is also confirmed from Figs. 5.7, 5.9, and 5.11 (or Figs. 5.7, 5.9, and 5.1); whether or not the air significantly contributes to the increase of the pore pressure, the smaller the

diffusivities of vapour and air, the smaller the gaseous mixture content, and thus the smaller the pore pressure. Thus, again, neglecting diffusion always results in the maximum underestimation of the pore pressure, while the use of molecular diffusivity always leads to the maximum overestimation of the pore pressure.

It is also clear from Figs. 5.9, 5.11, and 5.1 that, since molecular diffusivity results in an unrealistic air generation, the effect of decreasing the molecular diffusivity, within limits, is to improve the results by increasing the water vapour content, and thus increasing the vapour pressure, and decreasing the air content at a higher rate, and thus decreasing the air pressure, towards more realistic values with respect to the new decreased pore pressure, but, nevertheless, decreasing the molecular diffusivity cannot lead to correct results.

5.7 CONCLUSIONS

- Neglecting diffusion in mathematical modelling of heat and mass transfer in heated concrete results in underestimating the pore pressure significantly. It leads to a maximum pore pressure of less than 1 MPa in thick unsealed normal-concrete sections exposed to fire, compared with the maximum pore pressure of 1.5 MPa that results when concrete diffusivity is adopted.

- The validity of concrete diffusivity is ensured, since it leads to maximum pressures between those obtained from the extreme assumptions that diffusion does not occur in concrete and that diffusion in concrete is molecular. Also, the fact that the maximum pore pressure of 1 MPa obtained when the diffusivity approaches zero is about the same as that cited by researchers who neglect diffusion implies that different assumptions, other than diffusion, adopted in the model used in this study are equivalent to those adopted by researchers who neglect diffusion. It is unlikely that any of these other assumptions is unreasonable. Thus, assuming that all assumptions are now reasonable, it can be concluded that the maximum pore pressure of 1.5 MPa obtained with concrete diffusivity is the real pore pressure that can occur in unsealed thick normal-concrete sections exposed to fire.

The unrealism and unreasonableness of the results of different parameters, in general, and of the pore pressure, in particular, when molecular diffusivity is used, the effect and significance of the tortuosity, and the realism and reasonableness of the results when concrete diffusivity is adopted will be investigated in detail in Chapter 6.

CHAPTER 6

CONCRETE DIFFUSIVITY, MOLECULAR DIFFUSIVITY, AND TORTUOSITY

6.1 INTRODUCTION

In this chapter, the unreasonableness of the assumption that diffusion in concrete is molecular, the effect and significance of neglecting the tortuosity when molecular diffusivity is used, and the tenability of concrete diffusivity will be quantitatively demonstrated from the realism, or unrealism, and reasonableness, or unreasonableness, of the results of various parameters.

So far, researchers who are concerned with mathematical modelling of heat and mass transfer in heated concrete have concentrated on determining the temperature and pore pressure only, since it is widely believed that the pore pressure is one of the two main causes of spalling. They also rightly believe that the increase in the pore pressure must be due to water vapour pressure that results from the evaporation of free water. Thus, in order to determine the appropriateness of a diffusivity equation for heated concrete, it is necessary to determine whether the increase of the pore pressure is mainly due to the increase of the water vapour pressure rather than an increase of the air pressure.

The mathematical model used in this study determines the water vapour content and pore pressure. Thus, it is possible to determine the water vapour pressure and the air pressure without the need to determine the air content; in fact, the air content can only be determined after the determination of the air pressure. Thus, it is possible to determine whether the pore pressure is mainly due to vapour pressure. The air pressure, however, may be slightly greater than its initial value, since it is a function of the temperature as well as the air content. On the other hand, determination of the air content can provide the conclusive evidence regarding the reasonableness, or unreasonableness, of any diffusivity equation, since the air content must *not* be greater than the initial air content anywhere within concrete at any time. Any increase in the air content above its initial value cannot be justified. On the contrary, the air content must be smaller than its initial value whenever and wherever the vapour content is greater than its initial value, because the water vapour displaces some, or all, of the air. This natural behaviour is discussed by Bird *et al.* (1960).

One-dimensional analysis is sufficient to demonstrate the reasonableness, or unreasonableness, of a diffusivity equation, and enables comparison with other studies in the field, since most investigations rely on 1-D analysis. Thus, walls exposed to fire will be investigated. The necessary modifications will be made to the model, and six types of diffusion will be investigated:

(A) Molecular diffusion according to Krischer and Rohnalter with the tortuosity neglected (2.8). This is the type of diffusion adopted in the original model (Tenchev and Khalafallah, 2000; Tenchev *et al.*, 2001b).

(B) Molecular diffusion according to Krischer and Rohnalter with the tortuosity τ (= 3) considered (3.3).

(C) Molecular diffusion according to Chapman-Enskog theory with the tortuosity neglected (2.12). This is the type of diffusion adopted by Ahmed and Hurst (1997).

(D) Molecular diffusion according to Chapman-Enskog theory with the tortuosity τ (= 3) considered (3.4).

(E) Diffusion in concrete according to concrete diffusivity (3.16) where $D_{Conc,A} \neq D_{Conc,V}$, i.e. concrete diffusivity of water vapour (3.29) and concrete diffusivity of air (3.32). The exact tortuosity of concrete is implicitly included in these equations.

(F) Noting that concrete diffusivity of air (3.32) does not differ significantly from that of water vapour (3.29), a sixth case is considered where $D_{e,A} = D_{Conc,V}$, i.e. according to (3.29) only for both vapour and air, in order to determine the significance of this assumption.

It should be emphasised that (2.8) is equal to (2.12) at ambient temperature, and is smaller than (2.12) at lower temperatures, since the constant in (2.8) is two orders of magnitude smaller than that in (2.12). However, when the temperature increases, (2.8) leads to greater values of diffusivity than (2.12) due to its stronger dependence on temperature.

For each one of the six types of diffusion listed above, distribution and time history of the same parameters, i.e. temperature T, in °C, water vapour content ρ_v per unit volume of the gaseous mixture, in kg/m^3, water vapour pressure P_v, in MPa, air content ρ_a per unit volume of the gaseous mixture, in kg/m^3, air pressure P_a, in MPa, gaseous mixture content ρ_g per unit volume of the gaseous mixture, in kg/m^3, pore pressure P_g, in MPa, and free water content $\varepsilon_l \rho_l$ per unit volume of concrete, in kg/m^3, in the same unsealed 400-mm-thick normal-concrete wall considered in Chapter 5, with the same initial data, will be determined.

6.2 TEMPERATURE

The distribution of various parameters for each of the six types of diffusion considered is illustrated in Figs. 6.1-6.6. The distribution of temperature, in °C, for the six cases is shown in Fig. 6.7. At the beginning of the fire (after 5 minutes of exposure) there is no significant difference between the six values of the surface temperature of slightly over 200°C obtained by all six cases of diffusion. However, when the time of exposure increases, very significant differences appear in the temperatures of the exposed surface obtained from the six assumptions. After 60 minutes of exposure, molecular diffusivity according to (2.8) leads to a temperature of about 800°C at the exposed surface. The effect of considering the tortuosity on the temperature of the exposed surface when diffusion is assumed to be molecular according to Krischer and Rohnalter (3.3) is clear from Fig. 6.2 or Fig. 6.7(B). After 60 minutes of exposure, the surface temperature is about 750°C, and thus is lower than that obtained when the tortuosity is neglected after the same period of exposure.

Molecular diffusivity according to Chapman-Enskog theory when the tortuosity is neglected (2.12) leads to a temperature of about 775°C at the exposed surface after 60 minutes of exposure to fire. The effect of the tortuosity on the surface temperature when diffusion is assumed to be molecular according to Chapman-Enskog theory (3.4) is clear from Fig. 6.4 or Fig. 6.7(D). The temperature at the fire-exposed surface is about 700°C after 60 minutes of exposure to fire. This is the smallest value for the surface temperature obtained with the molecular diffusivity equations used.

The performance of concrete diffusivity (3.16) is shown in Fig. 6.5, and, as far as the temperature is concerned, in Fig. 6.7(E). Concrete diffusivity of water vapour (3.29) and concrete diffusivity of air (3.32) lead to a temperature of about 500°C at the fire-exposed surface after 60 minutes of exposure to fire. Also, the sixth case, shown in Fig. 6.6 or Fig. 6.7(F), in which concrete diffusivity of water vapour (3.29) is used for both water vapour and air, and thus the effective diffusivity of air is slightly higher than the real one (3.32), leads to a temperature of about 500°C.

It is clear that the use of molecular diffusivity equations leads to a very significant overestimation of the temperature. In particular, (2.8) results in the temperature of the fire-exposed surface (800°C) being about 60% higher than that (500°C) obtained with concrete diffusivity after 60 minutes of exposure to fire. By noting the differences in the temperatures after 5, 10, 30, and 60 minutes of exposure to fire, it can be seen that the significance increases with the time of exposure.

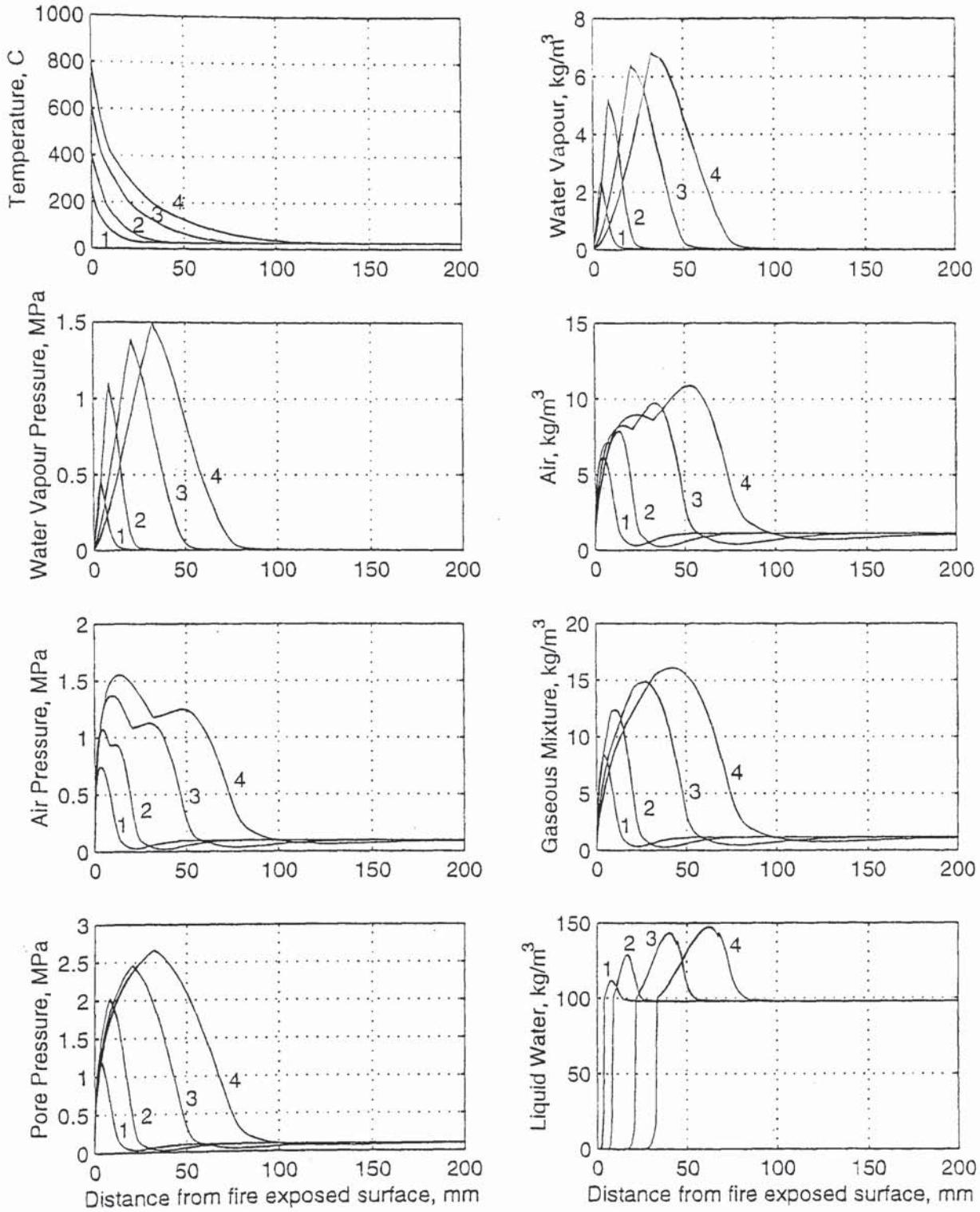

Fig. 6.1: Distribution of T, in °C, ρ_v, in kg/m^3, P_v, in MPa, ρ_a, in kg/m^3, P_a, in MPa, ρ_g, in kg/m^3, P_g, in MPa, and $\varepsilon_l \rho_l$, in kg/m^3, after (1) 5, (2) 10, (3) 30, and (4) 60 minutes of exposure to fire, according to Krischer and Rohnalter's molecular diffusivity with the tortuosity neglected (2.8).

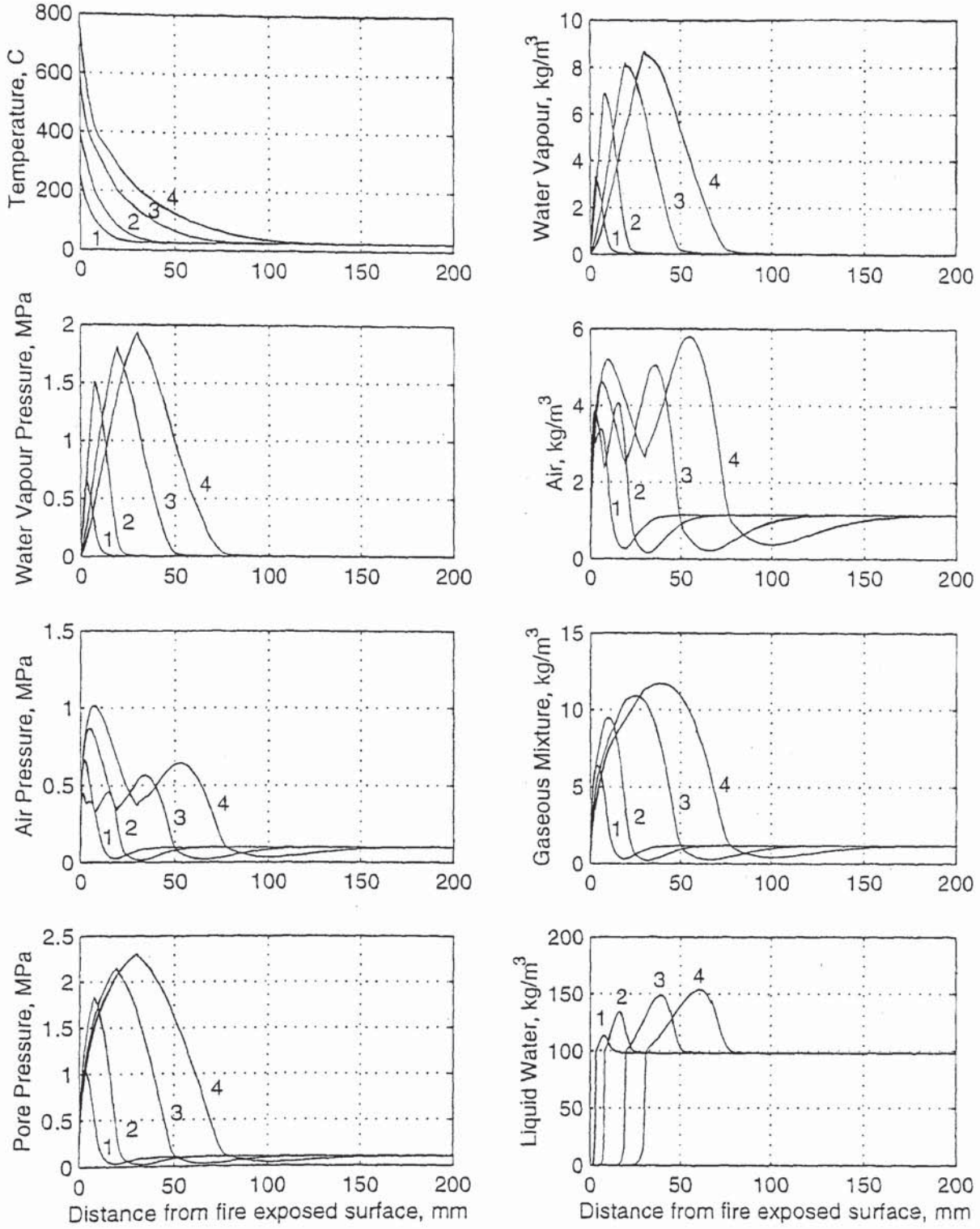

Fig. 6.2: Distribution of T, in °C, ρ_v, in kg/m^3, P_v, in MPa, ρ_a, in kg/m^3, P_a, in MPa, ρ_g, in kg/m^3, P_g, in MPa, and $\varepsilon_l \rho_l$, in kg/m^3, after (1) 5, (2) 10, (3) 30, and (4) 60 minutes of exposure to fire according to Krischer and Rohnalter's molecular diffusivity with the tortuosity considered (3.3).

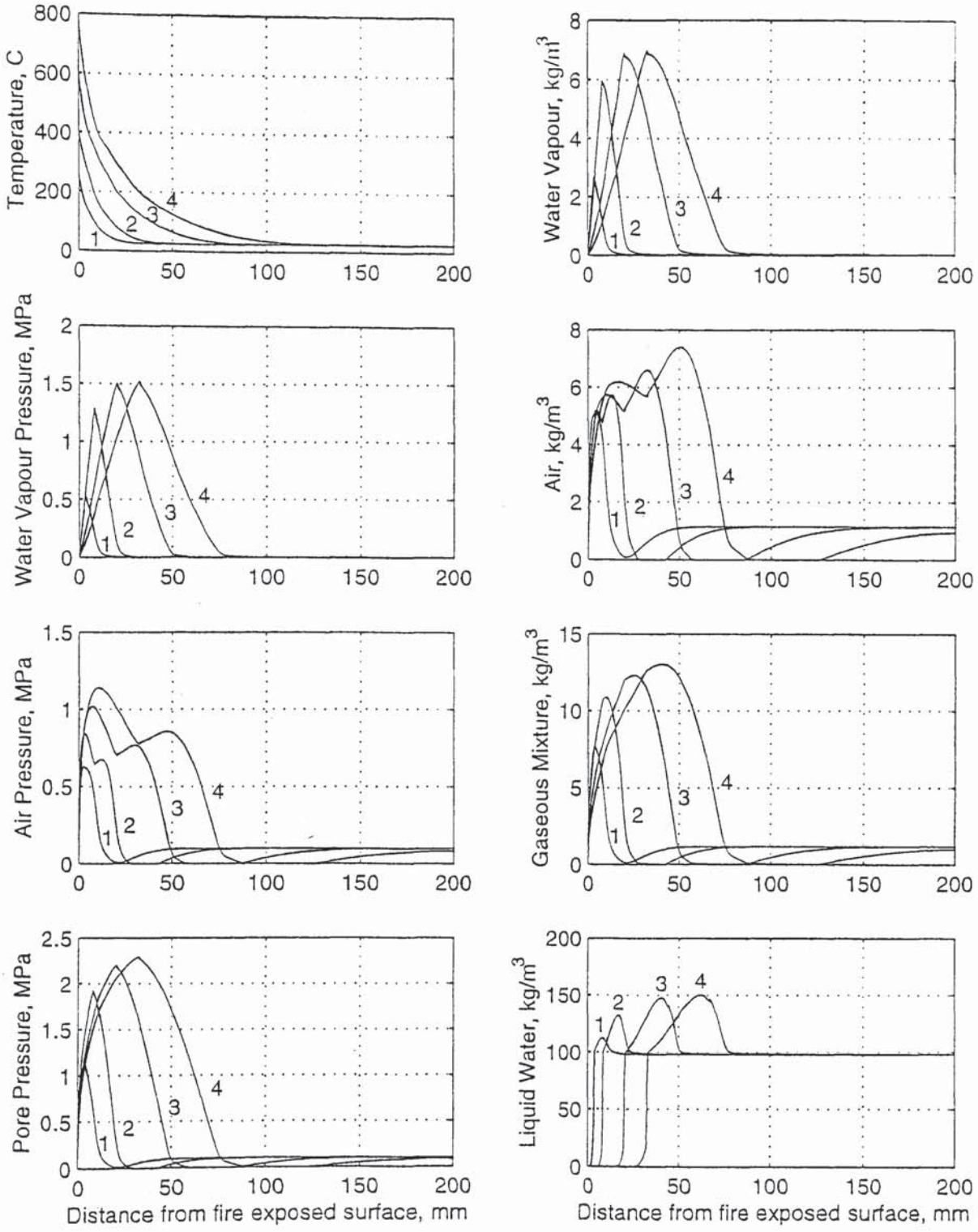

Fig. 6.3: Distribution of T, in °C, ρ_v, in kg/m^3, P_v, in MPa, ρ_a, in kg/m^3, P_a, in MPa, ρ_g, in kg/m^3, P_g, in MPa, and $\varepsilon_l \rho_l$, in kg/m^3, after (1) 5, (2) 10, (3) 30, and (4) 60 minutes of exposure to fire; molecular diffusivity according to Chapman-Enskog theory with the tortuosity neglected (2.12).

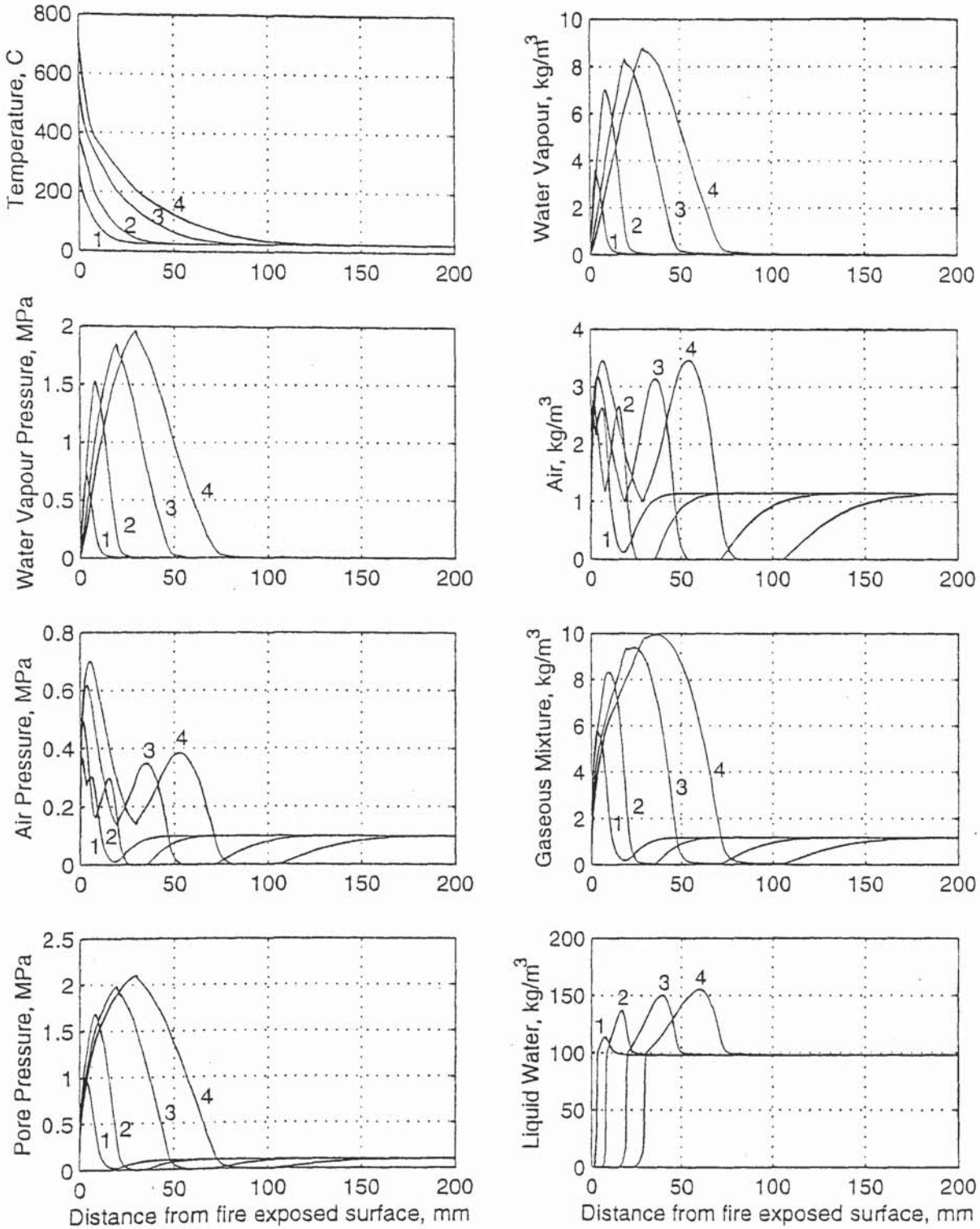

Fig. 6.4: Distribution of T, in °C, ρ_v, in kg/m^3, P_v, in MPa, ρ_a, in kg/m^3, P_a, in MPa, ρ_g, in kg/m^3, P_g, in MPa, and $\varepsilon_l \rho_l$, in kg/m^3, after (1) 5, (2) 10, (3) 30, and (4) 60 minutes of exposure to fire; molecular diffusivity according to Chapman-Enskog theory with the tortuosity considered (3.4).

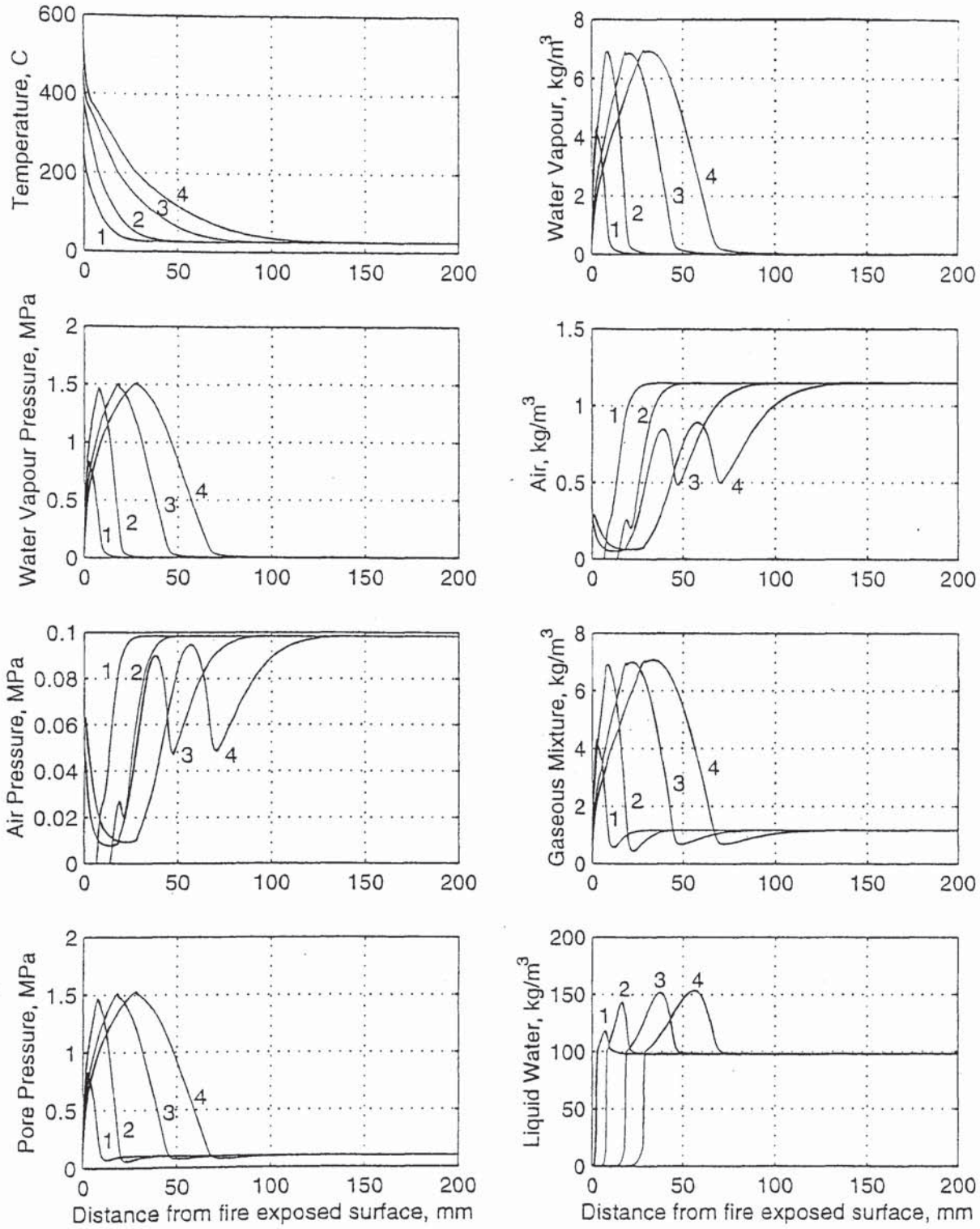

Fig. 6.5: Distribution of T, in °C, ρ_v, in kg/m^3, P_v, in MPa, ρ_a, in kg/m^3, P_a, in MPa, ρ_g, in kg/m^3, P_g, in MPa, and $\varepsilon_l \rho_l$, in kg/m^3, after (1) 5, (2) 10, (3) 30, and (4) 60 minutes of exposure to fire according to concrete diffusivity (3.16) with (3.29) for water vapour and (3.32) for air.

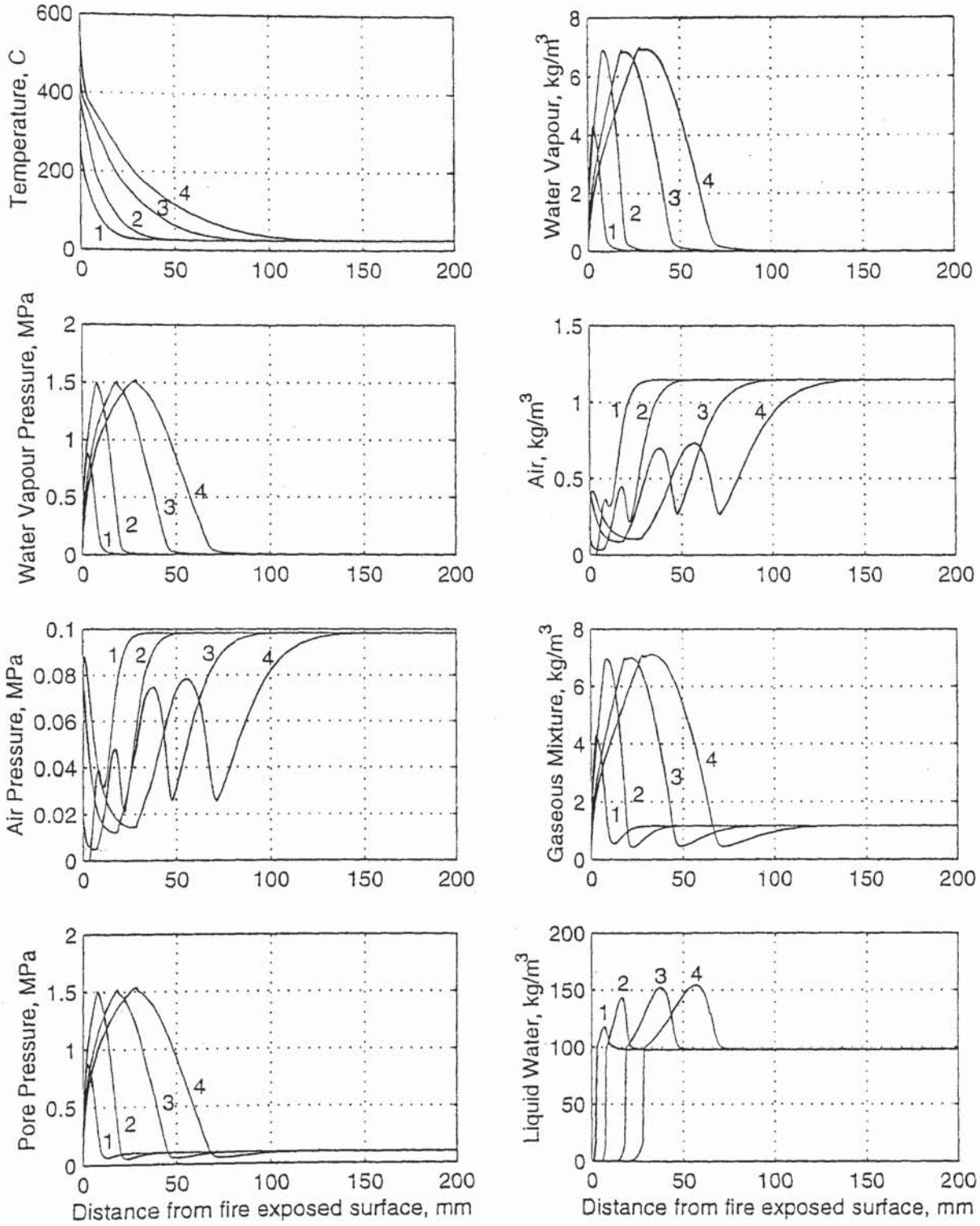

Fig. 6.6: Distribution of T, in °C, ρ_v, in kg/m^3, P_v, in MPa, ρ_a, in kg/m^3, P_a, in MPa, ρ_g, in kg/m^3, P_g, in MPa, and $\varepsilon_l \rho_l$, in kg/m^3, after (1) 5, (2) 10, (3) 30, and (4) 60 minutes of exposure to fire according to concrete diffusivity of water vapour (3.29) for both water vapour and air.

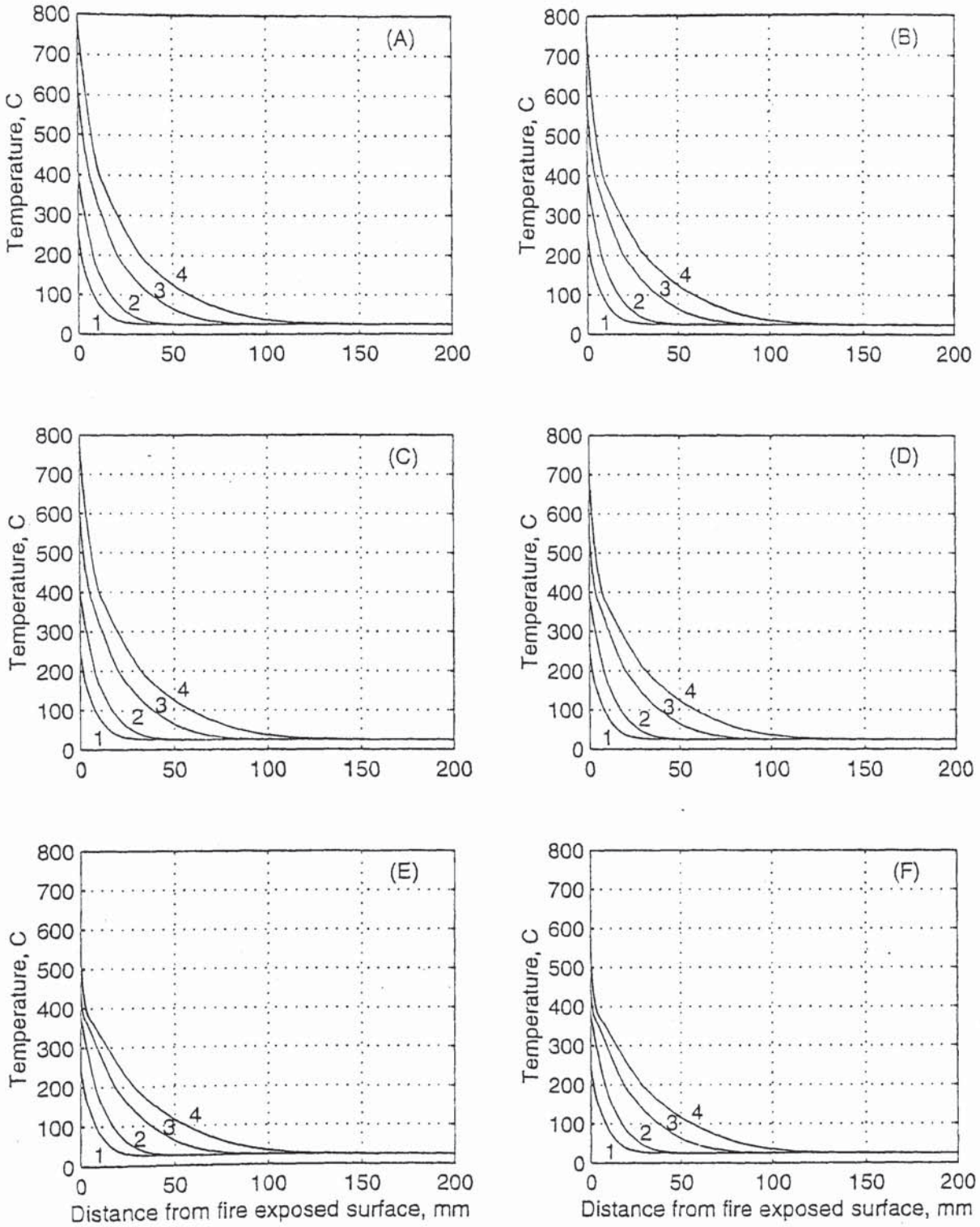

Fig. 6.7: Distribution of temperature T, in °C, after (1) 5, (2) 10, (3) 30, and (4) 60 minutes of exposure to fire according to: (A) (2.8), (B) (3.3), (C) (2.12), (D) (3.4), (E) (3.29) for water vapour and (3.32) for air, and (F) (3.29) for both water vapour and air.

The time history of various parameters for each of the six cases of diffusion is shown in Figs. 6.8-6.13. The time history of temperature that results from the six types of diffusion is demonstrated in Fig. 6.14; similar observations can be made. The most important observation when the results of temperature with the tortuosity neglected are compared with those when the tortuosity is considered is that the smaller the diffusivity, the lower the temperature. Thus, from the second major finding of Chapter 3 that the actual diffusivity in concrete is Knudsen diffusivity that is smaller than molecular diffusivity, and noting that the temperature obtained from concrete diffusivity is smaller than those obtained from different molecular equations, the first demonstration of the reasonableness of concrete diffusivity is provided. Also, it is clear that neglecting heat and mass transfer by diffusion leads to an underestimation of temperature (400°C in Fig. 5.5 of Section 5.4), while assuming that diffusion in concrete is molecular results in an overestimation of temperature (800°C in Fig. 6.1).

6.3 WATER VAPOUR CONTENT

The distribution of the water vapour content ρ_v, in kg/m^3 for the six types of diffusion is shown in Figs. 6.1-6.6 and 6.15, and the time history is presented in Figs. 6.8-6.13 and 6.16. After 60 minutes of exposure to fire, (2.8) leads to increasing amounts of water vapour up to about 7 kg/m^3 at a distance of 30 mm from the exposed surface. When the tortuosity is considered, (3.3) results in 8.5 kg/m^3 of water vapour after the same time of exposure. Molecular diffusivity according to Chapman-Enskog theory (2.12) leads to slightly greater amounts of water vapour (up to 7 kg/m^3 after 30 minutes of exposure to fire) than the amounts obtained from (2.8); the increase takes place during the first 30 minutes after which the water vapour content remains almost the same. When the tortuosity is considered, (3.4) results in greater amounts of water vapour up to about 9 kg/m^3.

When the results of molecular diffusivity with the tortuosity neglected are compared with those when the tortuosity is considered, the effect of the variation of the diffusivity on the vapour content is such that the smaller the diffusivity, the greater the vapour content. The effect of reducing molecular diffusivity is to correct the results by increasing the vapour content and decreasing the air content at a higher rate towards more realistic values (Section 5.6). These unreasonable results are because molecular diffusivity leads to unrealistic air generation that significantly contributes to the pore pressure; the very maximum air pressure should not have exceeded 0.16 MPa.

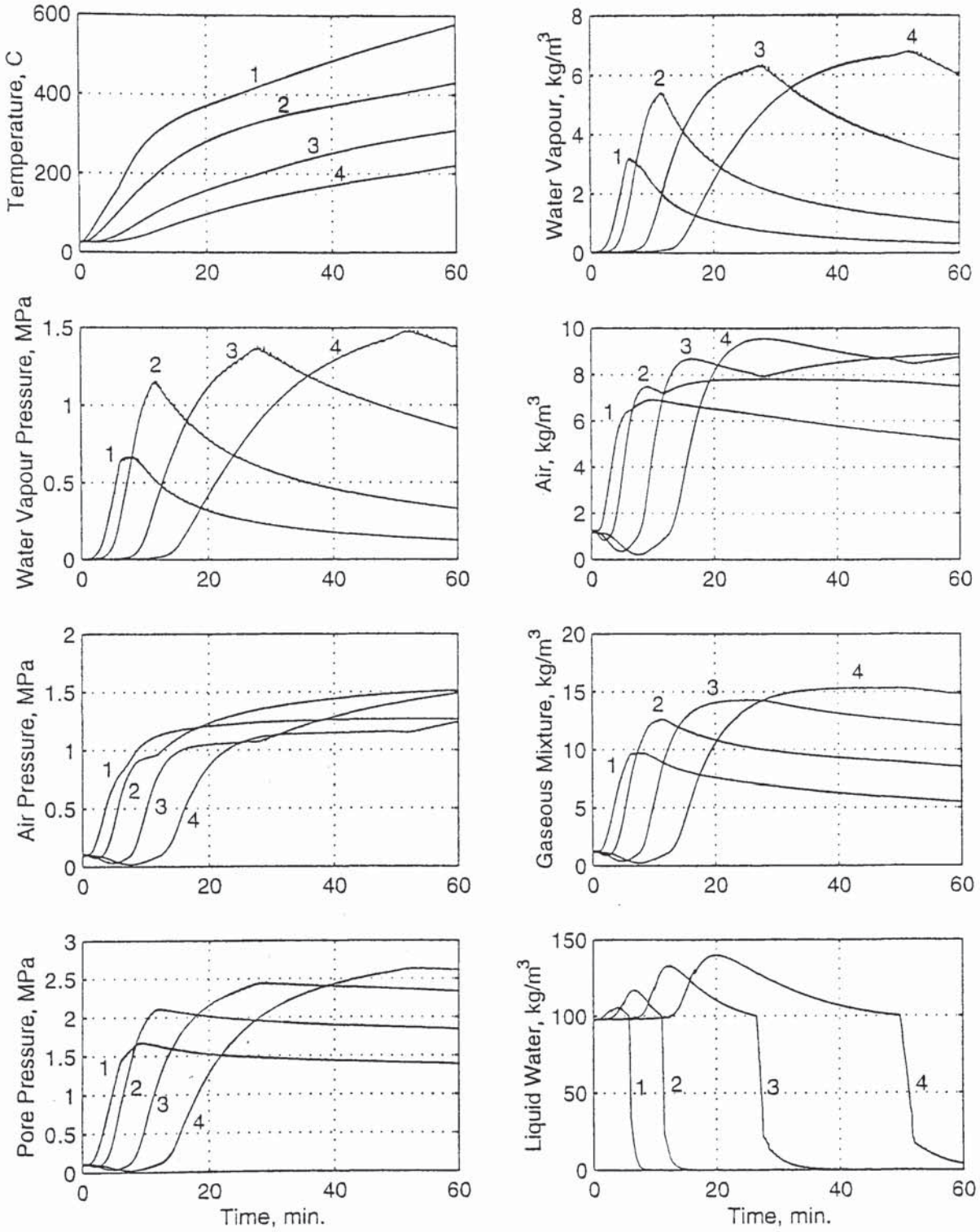

Fig. 6.8: Time history of T, in °C, ρ_v, in kg/m^3, P_v, in MPa, ρ_a, in kg/m^3, P_a, in MPa, ρ_g, in kg/m^3, P_g, in MPa, and $\varepsilon_l \rho_l$, in kg/m^3, at (1) 5, (2) 10, (3) 20, and (4) 30 mm from the fire-exposed surface according to Krischer and Rohnalter's molecular diffusivity with the tortuosity neglected (2.8).

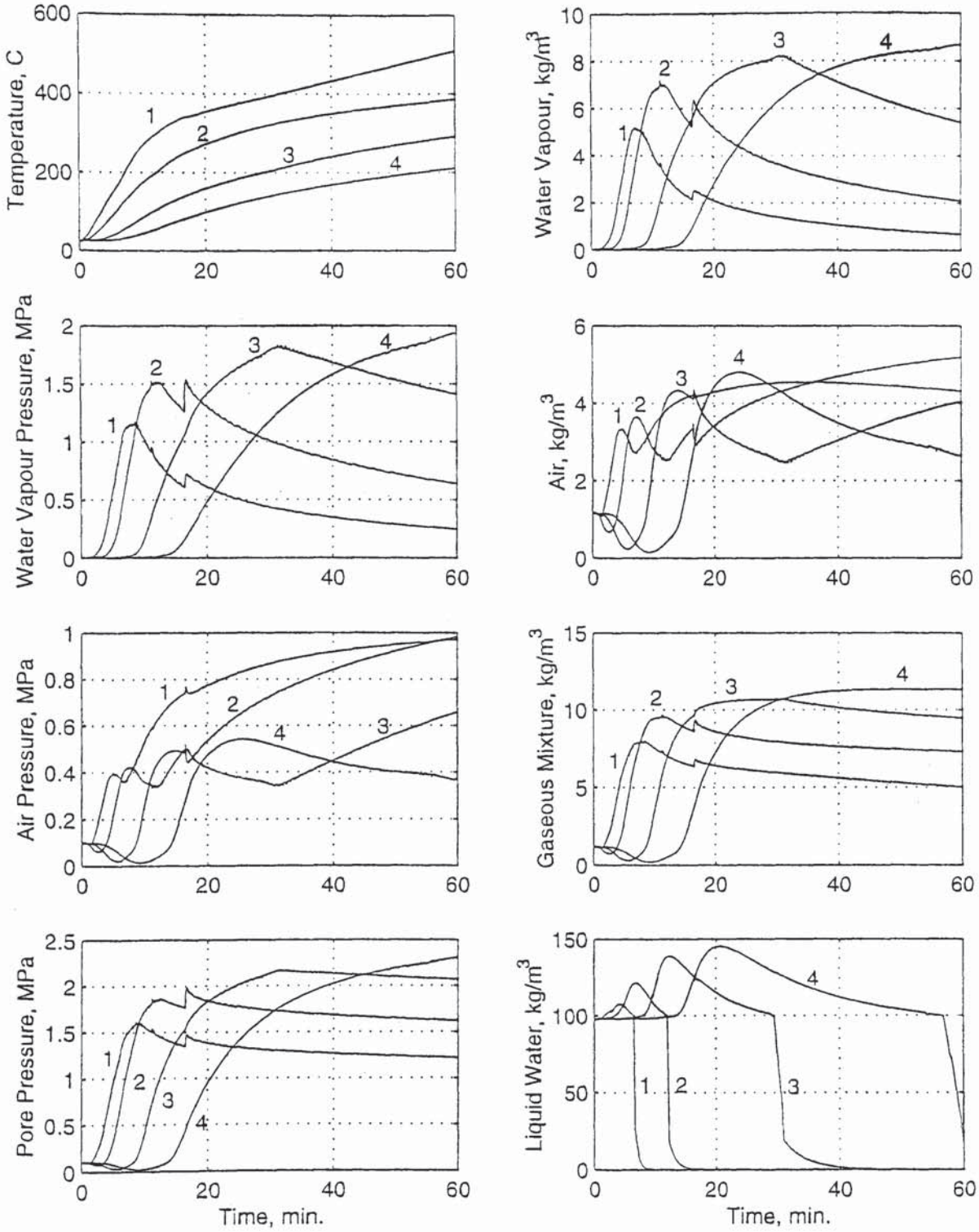

Fig. 6.9: Time history of T, in °C, ρ_v, in kg/m^3, P_v, in MPa, ρ_a, in kg/m^3, P_a, in MPa, ρ_g, in kg/m^3, P_g, in MPa, and $\varepsilon_l \rho_l$, in kg/m^3, at (1) 5, (2) 10, (3) 20, and (4) 30 mm from the fire-exposed surface fire according to Krischer and Rohnalter's molecular diffusivity with the tortuosity considered (3.3).

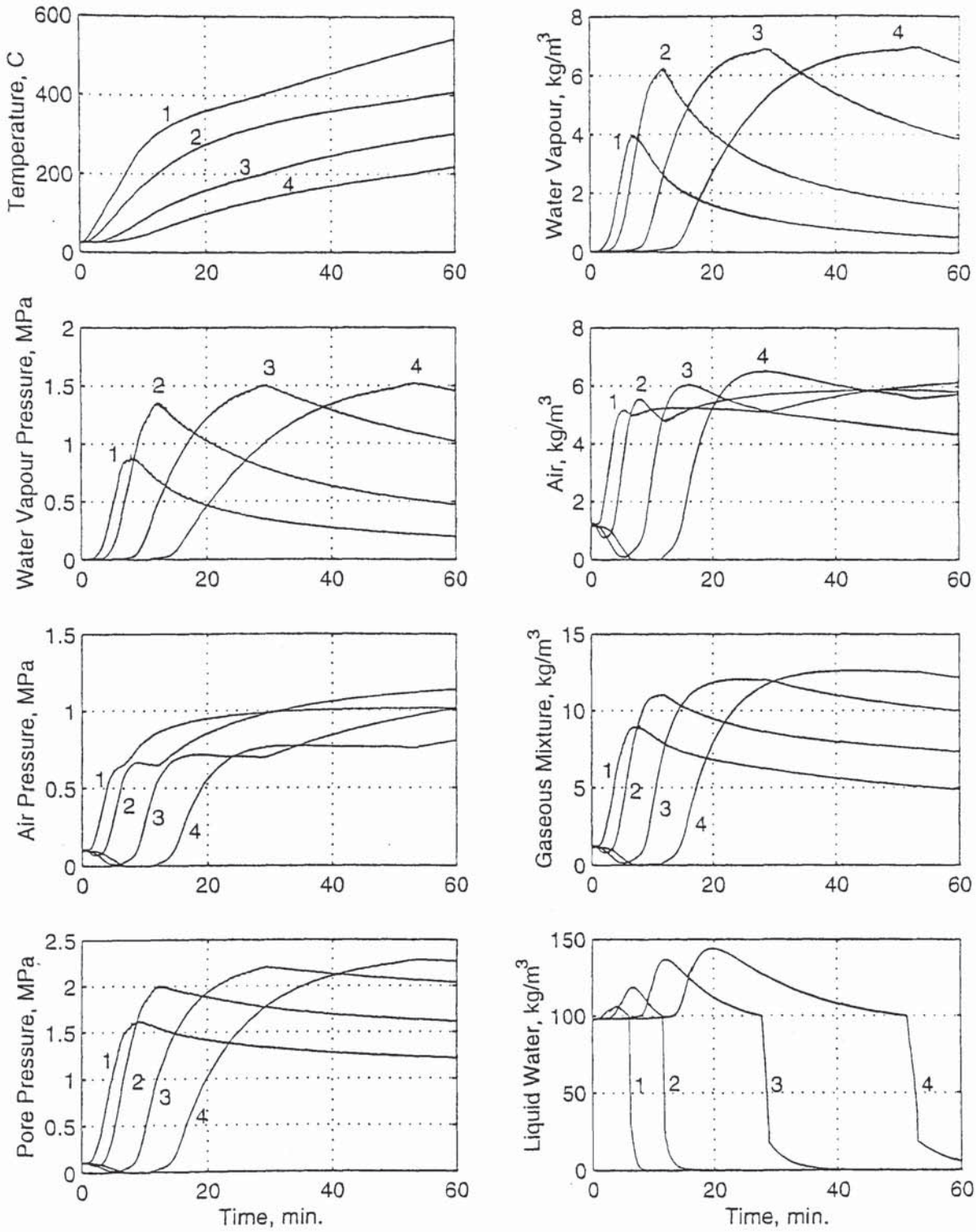

Fig. 6.10: Time history of T, in °C, ρ_v, in kg/m^3, P_v, in MPa, ρ_a, in kg/m^3, P_a, in MPa, ρ_g, in kg/m^3, P_g, in MPa, and $\varepsilon_l \rho_l$, in kg/m^3, at (1) 5, (2) 10, (3) 20, and (4) 30 mm from the fire-exposed surface; molecular diffusivity according to Chapman-Enskog theory with the tortuosity neglected (2.12).

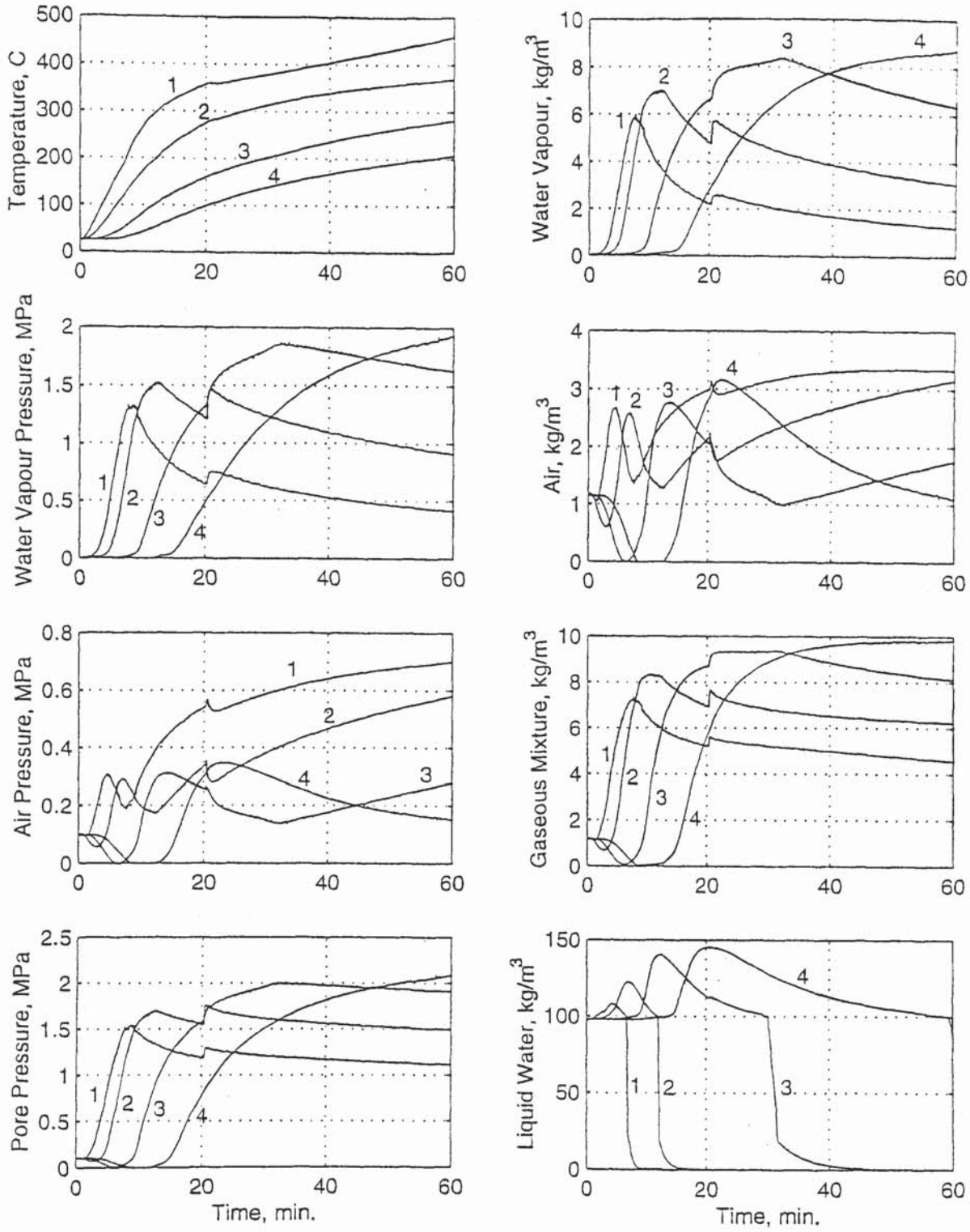

Fig. 6.11: Time history of T, in °C, ρ_v, in kg/m^3, P_v, in MPa, ρ_a, in kg/m^3, P_a, in MPa, ρ_g, in kg/m^3. P_g, in MPa, and $\varepsilon_l \rho_l$, in kg/m^3, at (1) 5, (2) 10, (3) 20, and (4) 30 mm from the fire-exposed surface; molecular diffusivity according to Chapman-Enskog theory with the tortuosity considered (3.4).

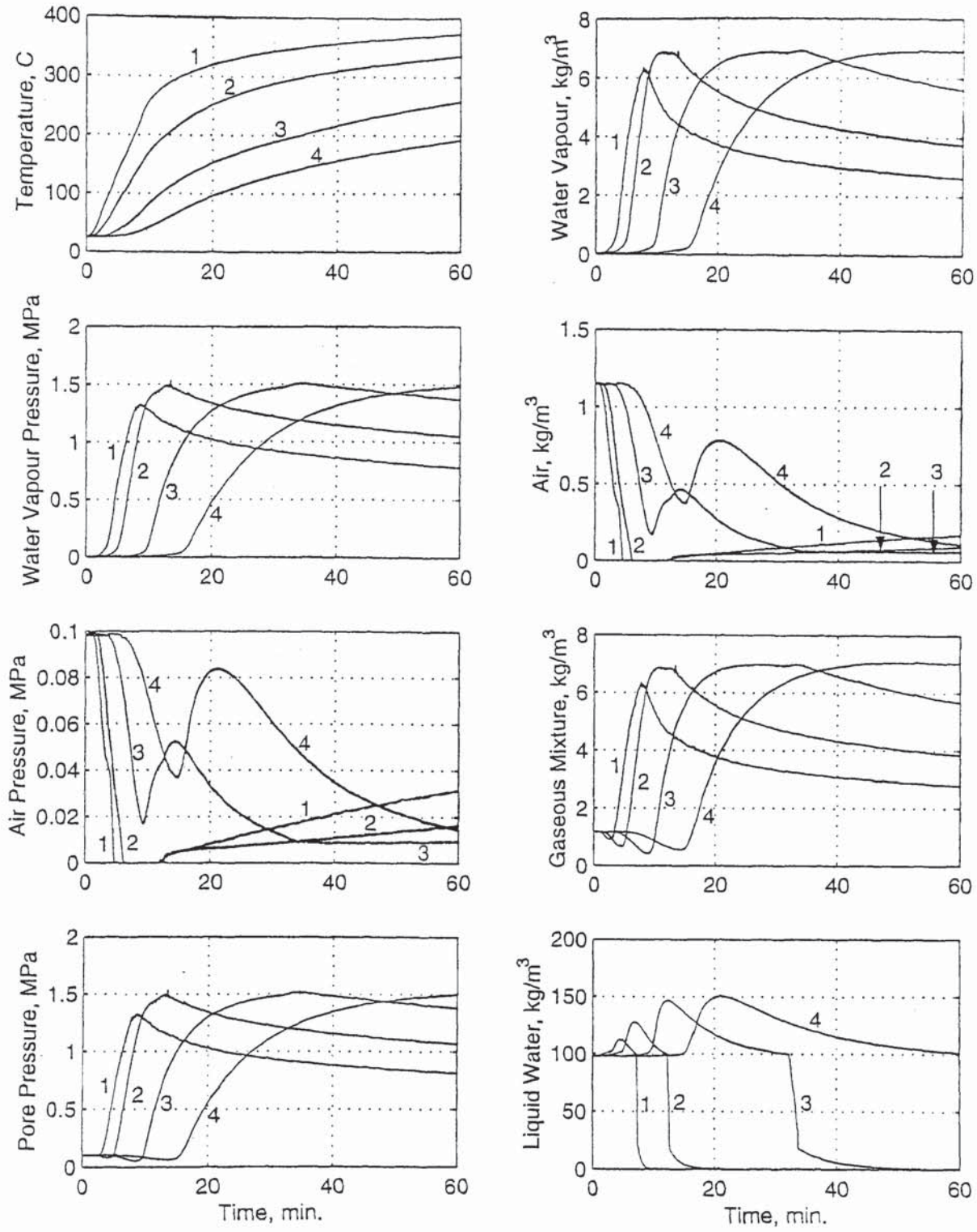

Fig. 6.12: Time history of T, in °C, ρ_v, in kg/m^3, P_v, in MPa, ρ_a, in kg/m^3, P_a, in MPa, ρ_g, in kg/m^3, P_g, in MPa, and $\varepsilon_l \rho_l$, in kg/m^3, at (1) 5, (2) 10, (3) 20, and (4) 30 mm from the fire-exposed surface according to concrete diffusivity (3.16) with (3.29) for water vapour and (3.32) for air.

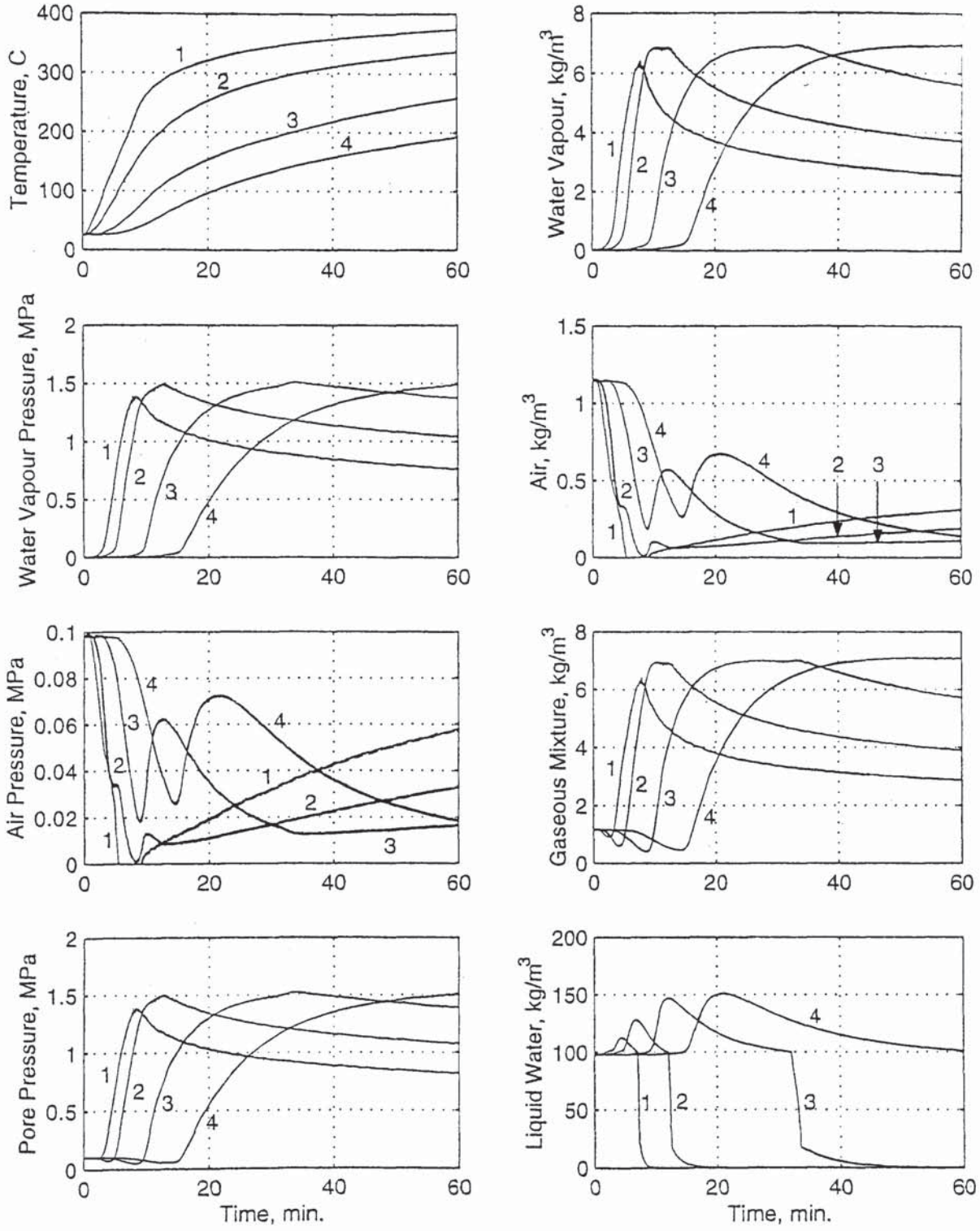

Fig. 6.13: Time history of T, in °C, ρ_v, in kg/m^3, P_v, in MPa, ρ_a, in kg/m^3, P_a, in MPa, ρ_g, in kg/m^3, P_g, in MPa, and $\varepsilon_l \rho_l$, in kg/m^3, at (1) 5, (2) 10, (3) 20, and (4) 30 mm from the fire-exposed surface according to concrete diffusivity of water vapour (3.29) for both water vapour and air.

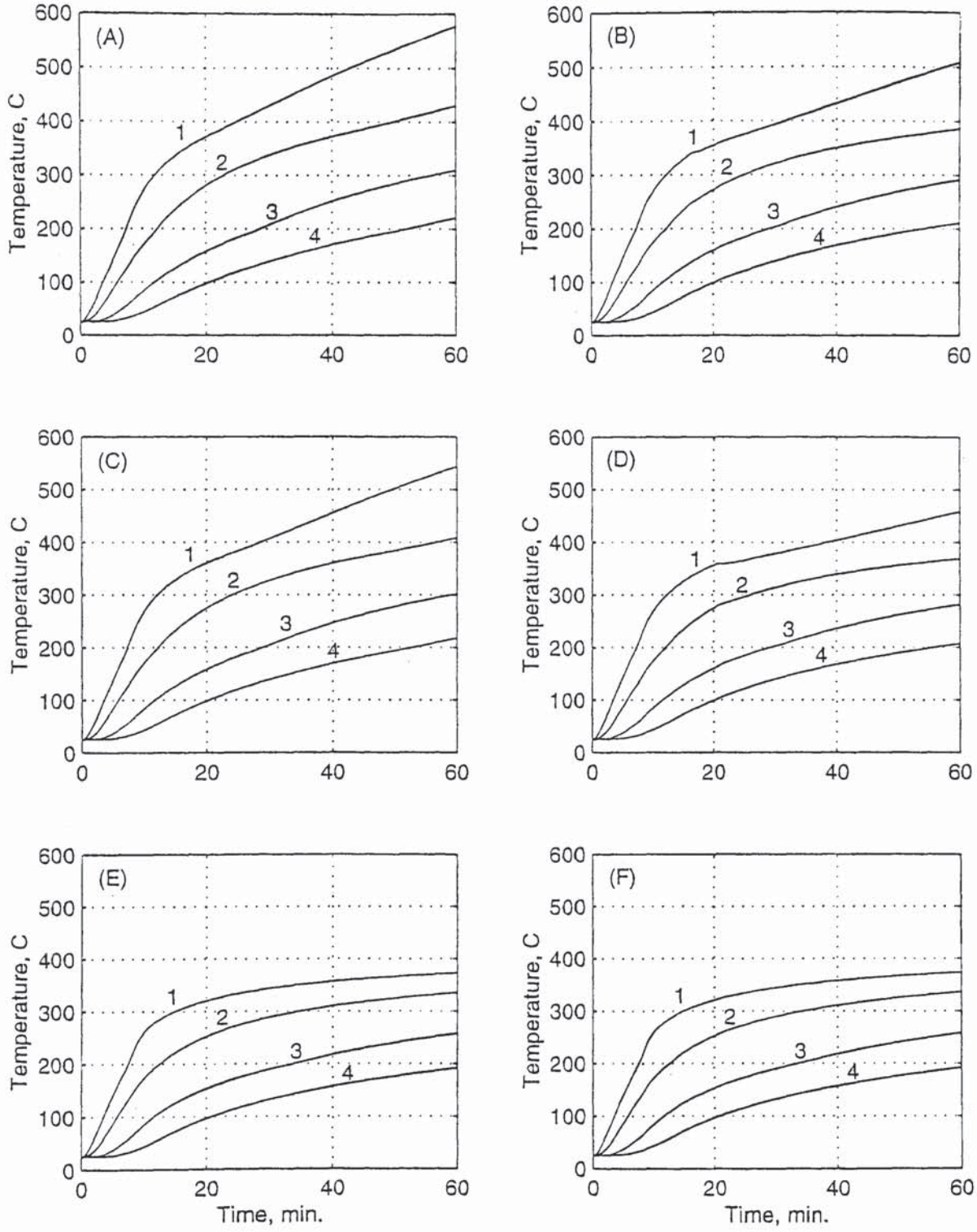

Fig. 6.14: Time history of temperature T, in °C, at (1) 5, (2) 10, (3) 20, and (4) 30 mm from the fire-exposed surface according to: (A) (2.8), (B) (3.3), (C) (2.12), (D) (3.4), (E) (3.29) for water vapour and (3.32) for air, and (F) (3.29) for both water vapour and air.

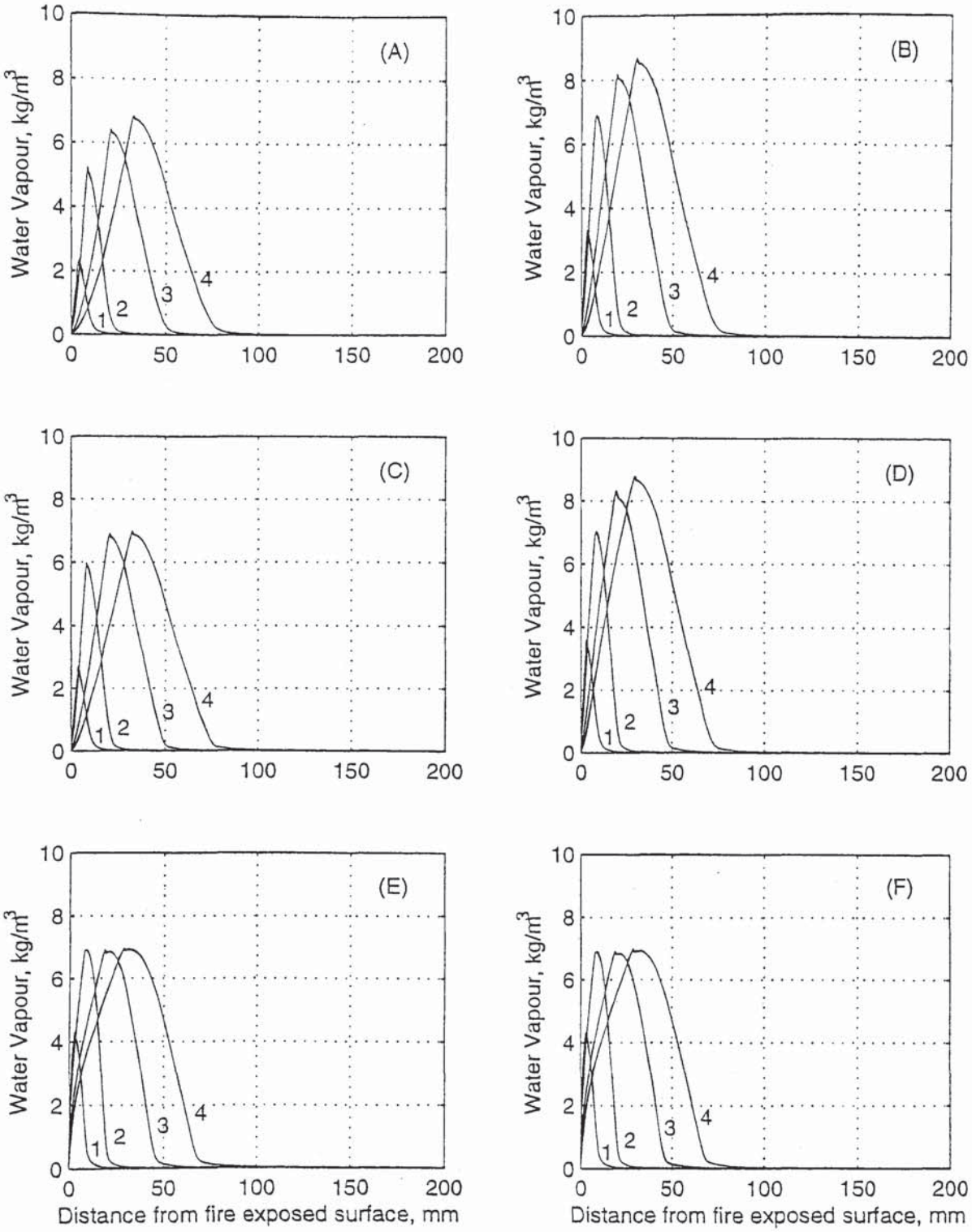

Fig. 6.15: Distribution of water vapour content ρ_v, in kg/m^3, after (1) 5, (2) 10, (3) 30, and (4) 60 minutes of exposure to fire according to: (A) (2.8), (B) (3.3), (C) (2.12), (D) (3.4), (E) (3.29) for water vapour and (3.32) for air, and (F) (3.29) for both water vapour and air.

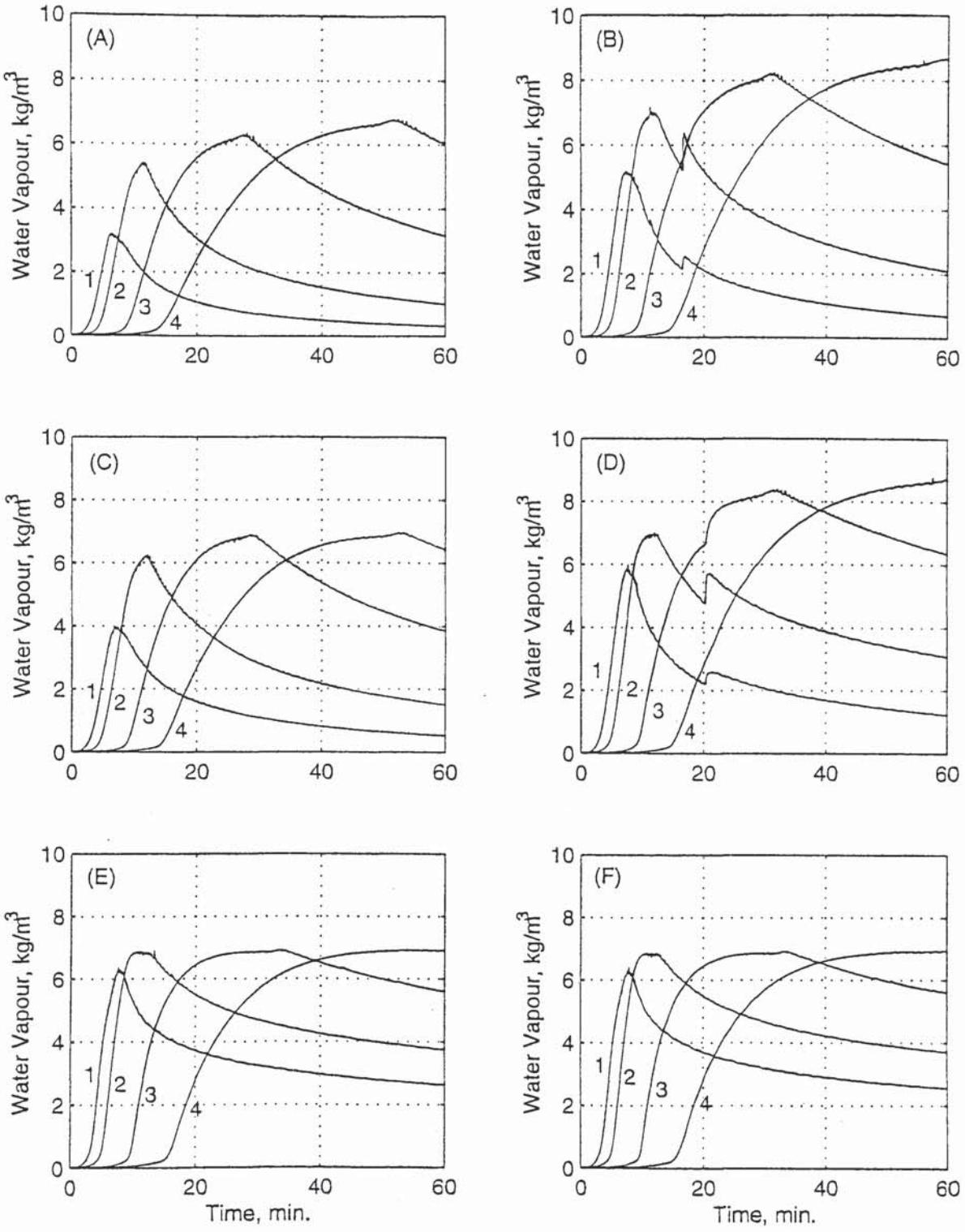

Fig. 6.16: Time history of water vapour content ρ_v, in kg/m^3, at (1) 5, (2) 10, (3) 20, and (4) 30 mm from the fire-exposed surface according to: (A) (2.8), (B) (3.3), (C) (2.12), (D) (3.4), (E) (3.29) for water vapour and (3.32) for air, and (F) (3.29) for both water vapour and air.

Thus, from (5.2), the realistic vapour contents that correspond to the maximum pore pressures of 2.7, 2.3, 2.3, and 2.1 MPa should have been, at least, 11.7, 9.85, 9.85, and 8.9 kg/m^3 when (2.8). (3.3), (2.12), and (3.4) are used, respectively. This confirms the hypothesis proposed in Section 3.4.6 that, provided that the air does not significantly contribute to the increase of the pore pressure, the smaller the diffusivity, the smaller the vapour content and thus the smaller the pore pressure.

Concrete diffusivity (3.16) results in increasing amounts of water vapour up to 7 kg/m^3 at about 30 mm from the exposed surface after 60 minutes of exposure. This amount is about the same as that obtained with molecular diffusivity (2.12) at the same distance and after the same period of exposure. However, unlike molecular diffusivity, the increase in the vapour content takes place during the first 10 minutes when the amount reaches 7 kg/m^3 at a distance of 10 mm from the surface. Then, the vapour content remains almost constant at 7 kg/m^3, while the evaporation front moves away from the exposed surface to a distance of 30 mm after 60 minutes. The sixth case results in vapour contents that are the same as the real values in Figs. 6.5 and 6.15(E), since the diffusivity of water vapour is the same in both cases; it is the diffusivity of air that is different.

6.4 WATER VAPOUR PRESSURE

The distribution of the water vapour pressure for the six types of diffusion is shown in Figs. 6.1-6.6 and Fig. 6.17. The time history is presented in Fig. 6.18. (2.8) leads to increasing values of the vapour pressure up to 1.5 MPa at about 30 mm from the exposed surface after 60 minutes of exposure to fire. On the other hand, (3.3) results in a vapour pressure that is close to 2 MPa. (2.12) leads to slightly higher values of vapour pressure than those obtained from the corresponding (2.8); after 30 minutes of exposure, the maximum vapour pressure is 1.5 MPa at a distance of about 20 mm from the exposed surface. Like the water vapour content, the vapour pressure remains almost constant as the evaporation front advances. (3.3) results in a maximum vapour pressure of about 2 MPa at a distance of about 30 mm from the surface after 60 minutes of exposure to fire. Again, the greater the diffusivity, the smaller the water vapour pressure, since the vapour pressure is proportional to the vapour content. Concrete diffusivity (3.16) and the sixth case lead to a maximum vapour pressure of about 1.5 MPa at a distance of 10 mm from the exposed surface after 10 minutes of exposure. Like the vapour content, the vapour pressure increases only slightly afterwards, and remains at about 1.5 MPa.

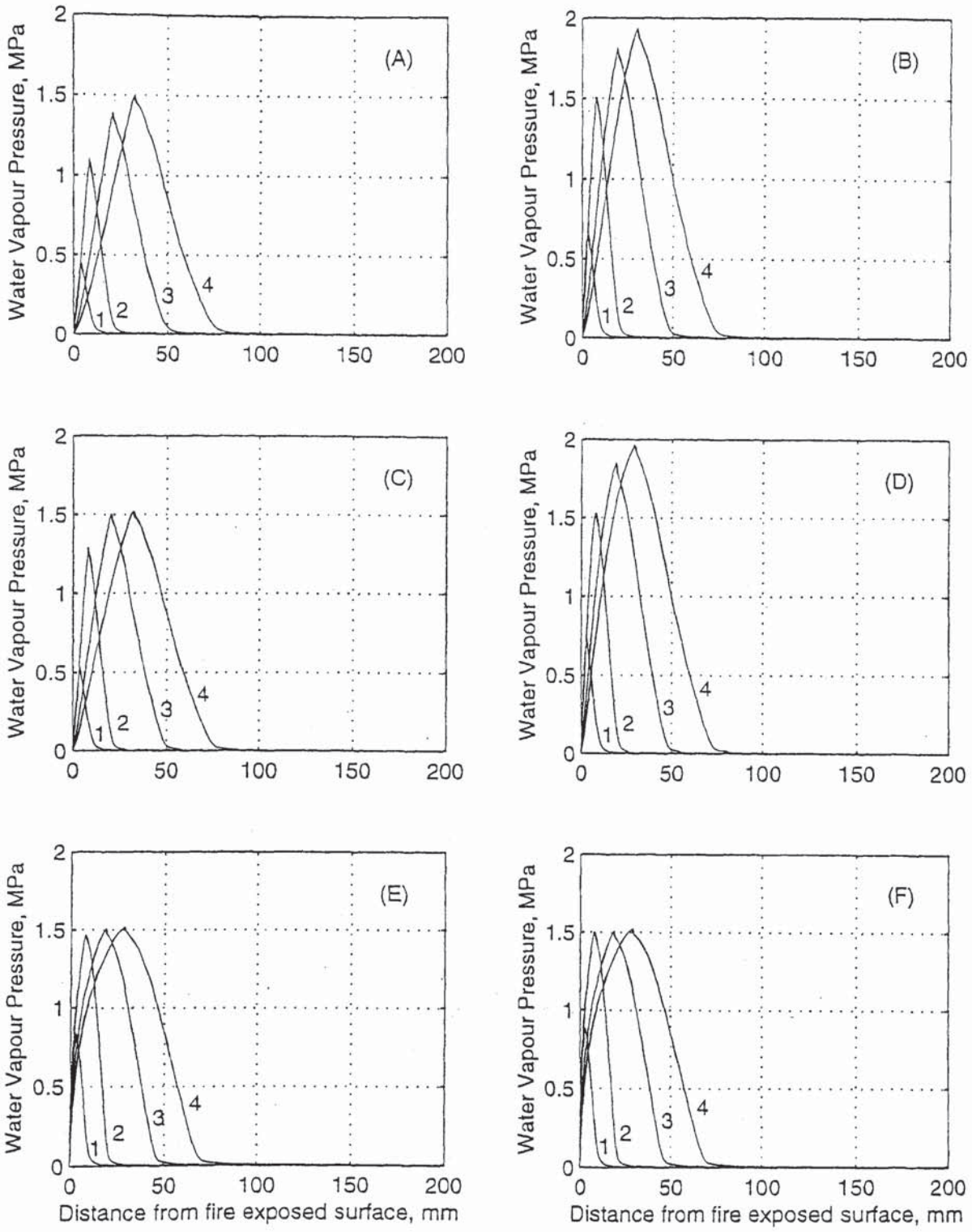

Fig. 6.17: Distribution of water vapour pressure P_v, in MPa, after (1) 5, (2) 10, (3) 30, and (4) 60 minutes of exposure to fire according to: (A) (2.8), (B) (3.3), (C) (2.12), (D) (3.4), (E) (3.29) for water vapour and (3.32) for air, and (F) (3.29) for both water vapour and air.

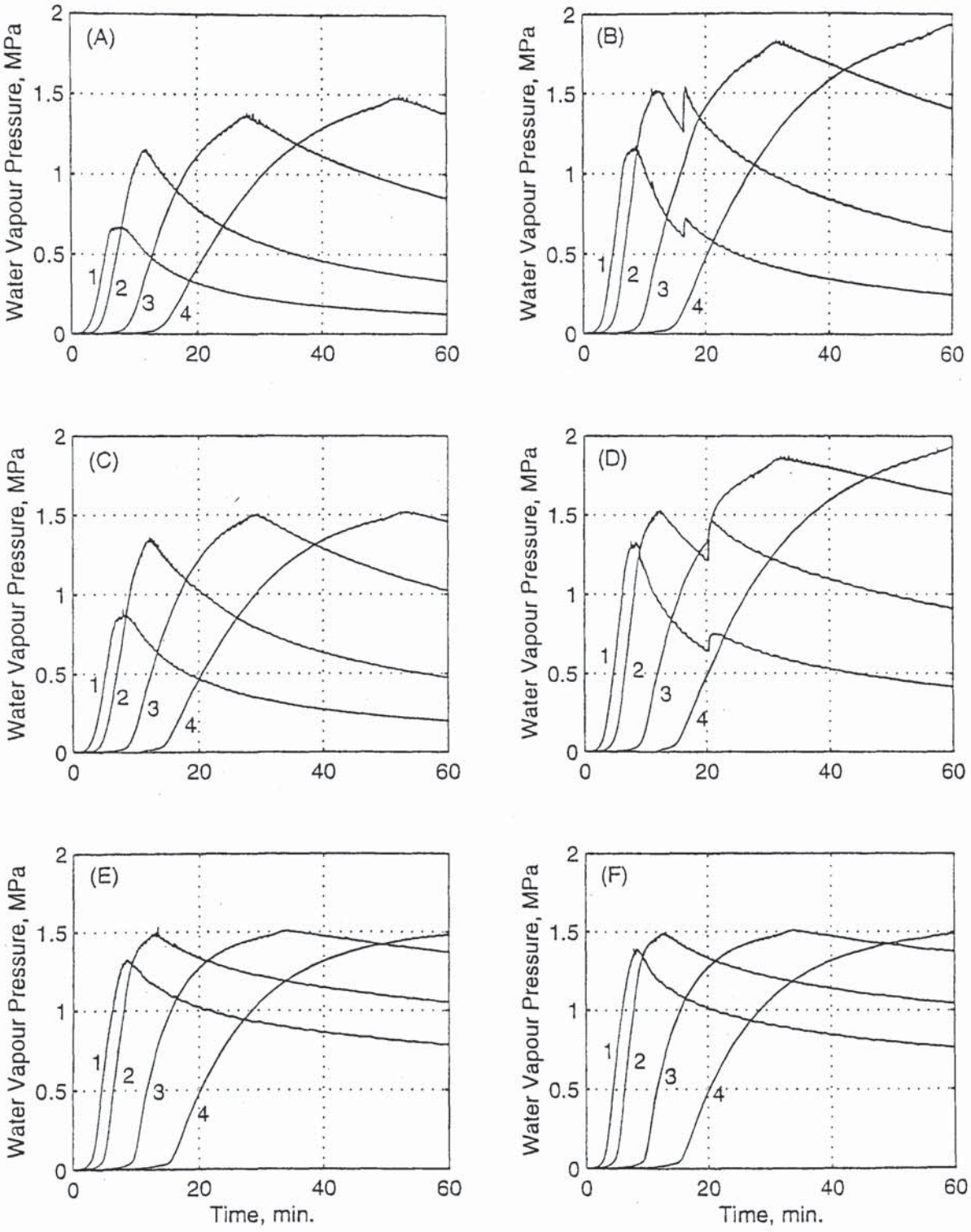

Fig. 6.18: Time history of water vapour pressure P_v, in MPa, at (1) 5, (2) 10, (3) 20, and (4) 30 mm from the fire-exposed surface according to: (A) (2.8), (B) (3.3), (C) (2.12), (D) (3.4), (E) (3.29) for water vapour and (3.32) for air, and (F) (3.29) for both water vapour and air.

6.5 AIR CONTENT

Determination of the air content can provide the conclusive evidence regarding the unreasonableness of using molecular diffusivity equations in mathematical modelling of heat and mass transfer in heated concrete, and regarding the validity and realism of concrete diffusivity, since the air content must *not* be greater than the initial air content anywhere within concrete at any time. Any increase in the air content above its initial value cannot be physically acceptable. On the contrary, the air content must be smaller than its initial value whenever and wherever the water vapour content is greater than its initial value, because the additional water vapour displaces some, or all, of the air. This natural behaviour is recognised by, e.g. Bird *et al.* (1960).

The distribution of the air content as determined by the six types of diffusion is shown in Figs. 6.1-6.6 and in Fig. 6.19. The time history is presented in Figs. 6.8-6.13 and 6.20. (The vertical scale in Figs. 6.19 (E) and (F) and 6.20 (E) and (F) is different for clarity.) When (2.8) is used, the air content increases as the water vapour content increases; the air content is even greater than the vapour content. Also, the air content is even greater at locations where the vapour content is smaller than the maximum. For example, after 60 minutes of exposure to fire, the air content is 9 kg/m^3 at 20 mm from the surface where the vapour content is only 2 kg/m^3. The same behaviour is observed even when the tortuosity is considered (3.3). The air contents obtained from (3.3) are smaller than those computed with (2.8), but remain greater than the initial air content wherever the vapour content is greater than its initial value.

A similar behaviour occurs when (2.12) is adopted, but the values of the air content are smaller than those obtained from (2.8). When (3.4) is used, the air content increases above the initial value, and reaches maximum values on both sides of the evaporation front. However, the maximum values are the smallest obtained with molecular diffusivity equations. Also, a significant improvement in the values of the air content appears at locations where the maximum water vapour contents occur.

The results of the air content above provide the conclusive evidence that molecular diffusivity equations are inappropriate for concrete even when the tortuosity is taken into account, because there is no justification for the air content to be greater than the initial value of 1.18 kg/m^3 anywhere in concrete at any time. They quantitatively confirm that the assumption that diffusion in concrete is molecular is unreasonable indeed.

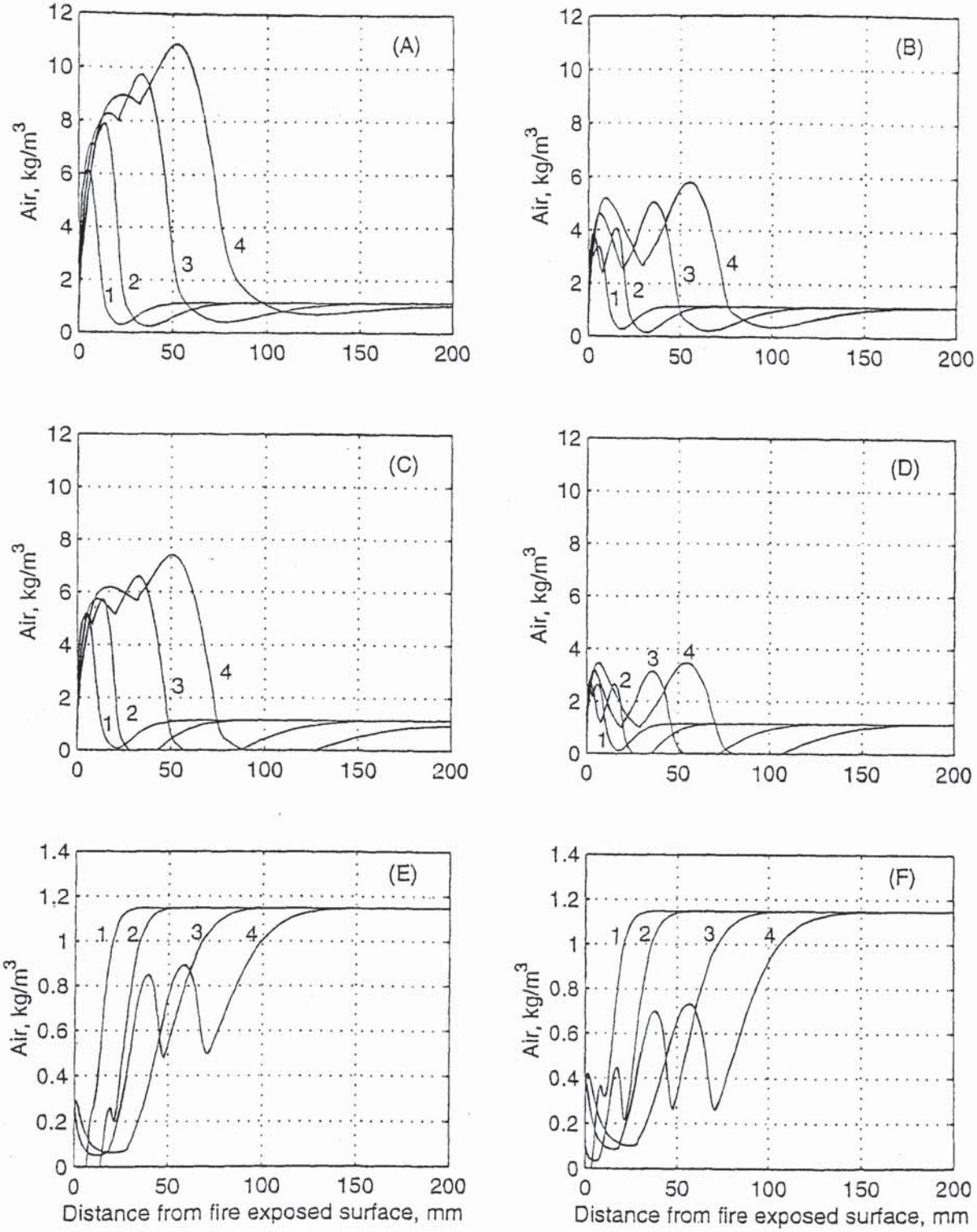

Fig. 6.19: Distribution of air content ρ_a, in kg/m^3, after (1) 5, (2) 10, (3) 30, and (4) 60 minutes of exposure to fire according to: (A) (2.8), (B) (3.3), (C) (2.12), (D) (3.4), (E) (3.29) for water vapour and (3.32) for air, and (F) (3.29) for both water vapour and air.

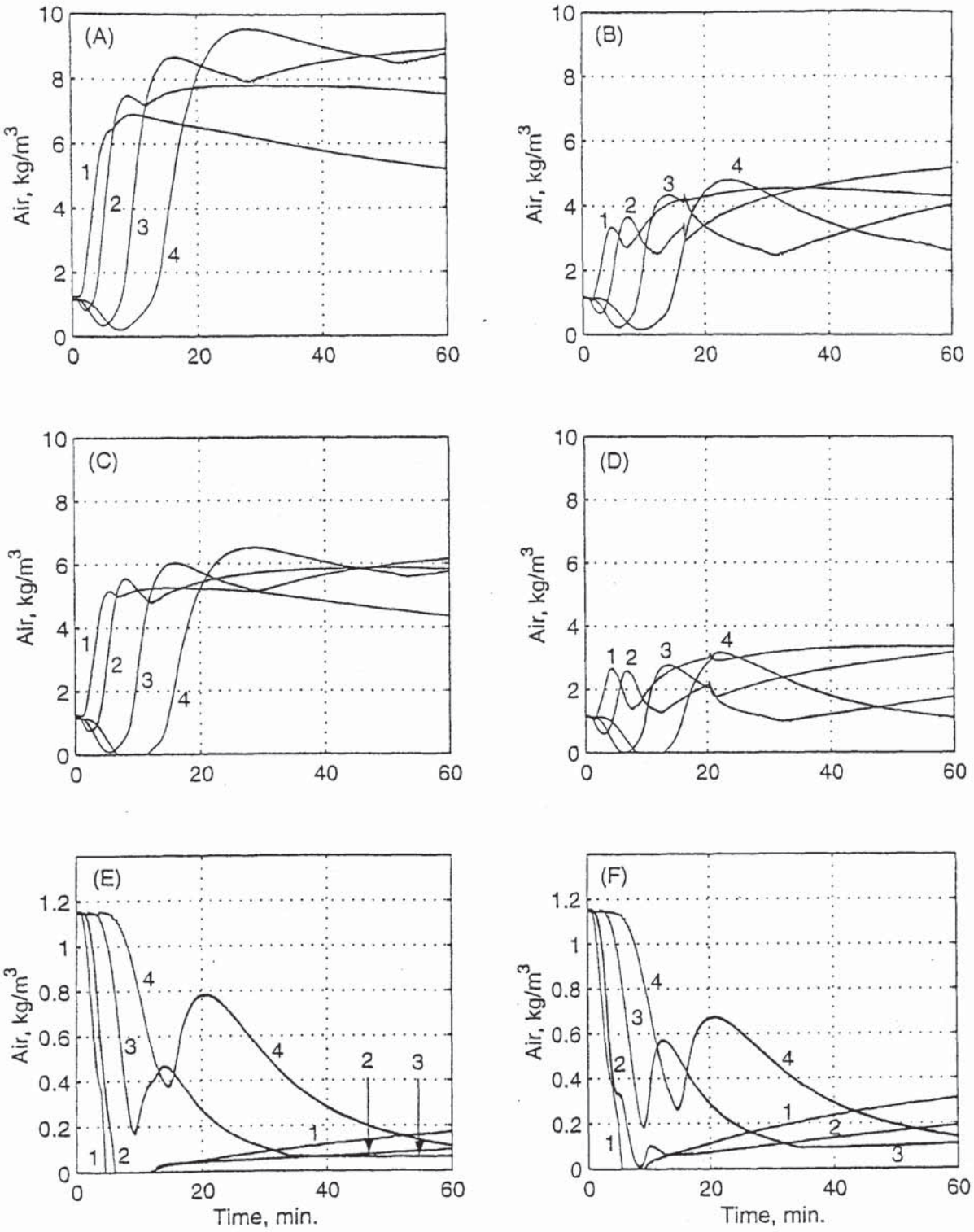

Fig. 6.20: Time history of air content ρ_a, in kg/m^3, at (1) 5, (2) 10, (3) 20, and (4) 30 mm from the fire-exposed surface according to: (A) (2.8), (B) (3.3), (C) (2.12), (D) (3.4), (E) (3.29) for water vapour and (3.32) for air, and (F) (3.29) for both water vapour and air.

From the results above, the smaller the diffusivity, the smaller the unrealistic air content, even though the corrected results remain unrealistic (Section 5.6). As discussed in Chapter 5, reducing the molecular diffusivity by a relatively large number, say 10 or 20, as in Tenchev *et al.* (2001a and b), may lead to seemingly realistic results for a particular set of initial data; however, this does not make the use of molecular diffusivity any more reasonable for concrete.

When concrete diffusivity (3.16) is adopted, the air content *never* increases above the initial value of 1.18 kg/m^3. In fact, at the beginning of the fire, the air near the exposed surface can be totally expelled from concrete by the water vapour. The air content is minimum when and where the vapour content is maximum. It remains smaller than its initial value wherever the vapour content is greater than its initial value. After 60 minutes of exposure, the air content does not reach its initial value until the vapour content decreases to its initial value at a distance of about 130 mm from the exposed surface.

The same natural behaviour also appears in the time history. As soon as the water vapour increases, the air content decreases, and continues to decrease as long as the vapour content increases until it reaches its minimum value when the vapour content reaches its maximum value. At 5 mm from the exposed surface, the air disappears after 5 minutes of exposure when the vapour content reaches a value of about 4.5 kg/m^3. The air remains absent while the water vapour content continues to increase to its maximum value of 6 kg/m^3 after about 8 minutes of exposure. It appears only when the vapour content decreases to the same value of about 4.5 kg/m^3 after 12 minutes of exposure. Then, the air content gradually increases as the vapour content decreases. After 60 minutes of exposure, the vapour content is still greater than its initial value, and thus the air content is still smaller than its initial value. The air content is not expected to return to its initial value until the water vapour content decreases to its initial value.

Similar behaviour is observed at a distance of 10 mm from the exposed surface. It is interesting, however, to note that the values of the increasing air content at 10 mm, when the vapour content decreases after reaching a maximum, are smaller than those at 5 mm. This is because the values of the decreasing vapour content at 10 mm are greater than those at 5 mm. Similarly, the values of the increasing air content at 20 mm from the surface are smaller than those at 10 mm for the same reason. At a distance of 20 mm from the exposed surface, the air does not totally disappear, because it is more difficult to expel all the air when the distance to the surface increases.

When concrete diffusivity of vapour (3.29) is used for air as well, a similar behaviour is observed, but the values of the air content in the over-saturated zone are smaller than the real values, because the diffusivity used for air (3.29) is greater than the real one (3.32) and thus greater amounts of air can escape. On the other hand, the values of the air content in the dry zone are greater than the real values; the air is not completely expelled from concrete anywhere except near the exposed surface after 5 minutes of exposure, since the diffusivity (3.29) used for air is greater than the real one (3.32), and thus greater amounts of air can diffuse into the dry zone from the regions inside and from the environment where the concentration of air is greater than that in the dry zone. The time history is similar to the real case, but the greater diffusivity of air results in the minimum values of the air content being greater than the real values, and does not disappear at 10 mm from the exposed surface, because greater amounts of air can diffuse into the regions of minimum air content.

6.6 AIR PRESSURE

The air content must not exceed the initial air content; any increase in the air content above its initial value cannot be justified. On the other hand, the air pressure is not only a function of the air content, but also a function of the temperature, and thus it may slightly exceed the initial air pressure depending on the temperature. Nevertheless, the pore pressure must be mainly due to water vapour pressure rather than air pressure, and thus the air pressure must not be much greater than the initial air pressure. From (5.7) and (5.8), it is clear that the initial water vapour pressure is negligible and that the initial air pressure is almost equal to the standard atmospheric pressure, i.e. ${}^{0}P_a \approx 0.1$ MPa. From (5.3), and noting that the temperature at which the maximum pore pressure occurs is about 200°C, the very maximum air pressure that may occur is $P_a = 0.16$ MPa when the air content is at its initial value of 1.18 kg/m^3. Furthermore, as discussed before in this chapter, the air content should be smaller than its initial value whenever the water vapour content is greater than its value, and thus the maximum air pressure should be smaller than 0.16 MPa.

The distribution of the air pressure as determined by the six types of diffusion is presented in Figs. 6.1-6.6 and 6.21. The time history is shown in Figs. 6.1-6.6 and 6.22. The variation of the air pressure relative to that of the water vapour pressure is almost similar to the variation of the air content relative to that of the water vapour content.

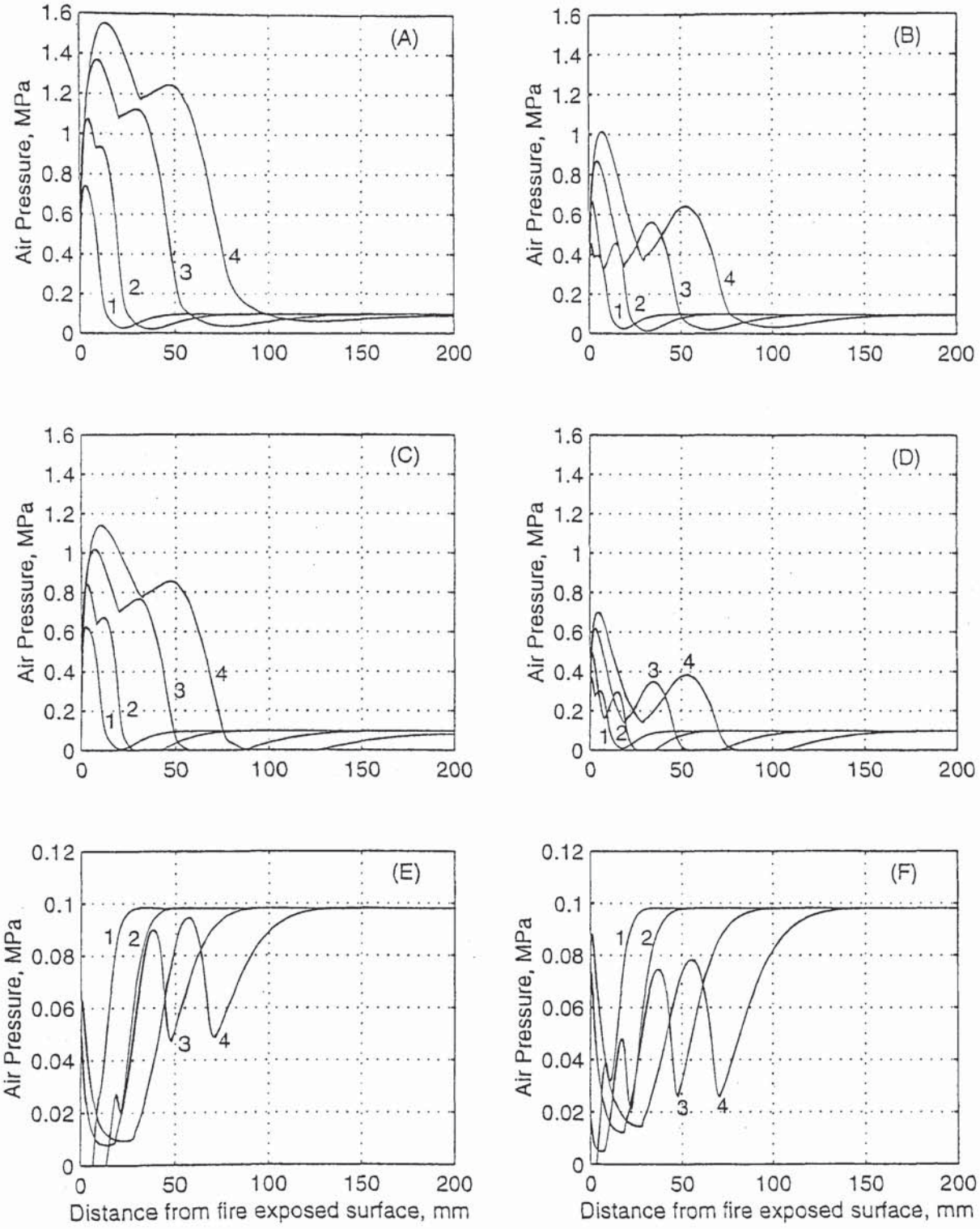

Fig. 6.21: Distribution of air pressure P_a, in MPa, after (1) 5, (2) 10, (3) 30, and (4) 60 minutes of exposure to fire according to: (A) (2.8), (B) (3.3), (C) (2.12), (D) (3.4), (E) (3.29) for water vapour and (3.32) for air, and (F) (3.29) for both water vapour and air.

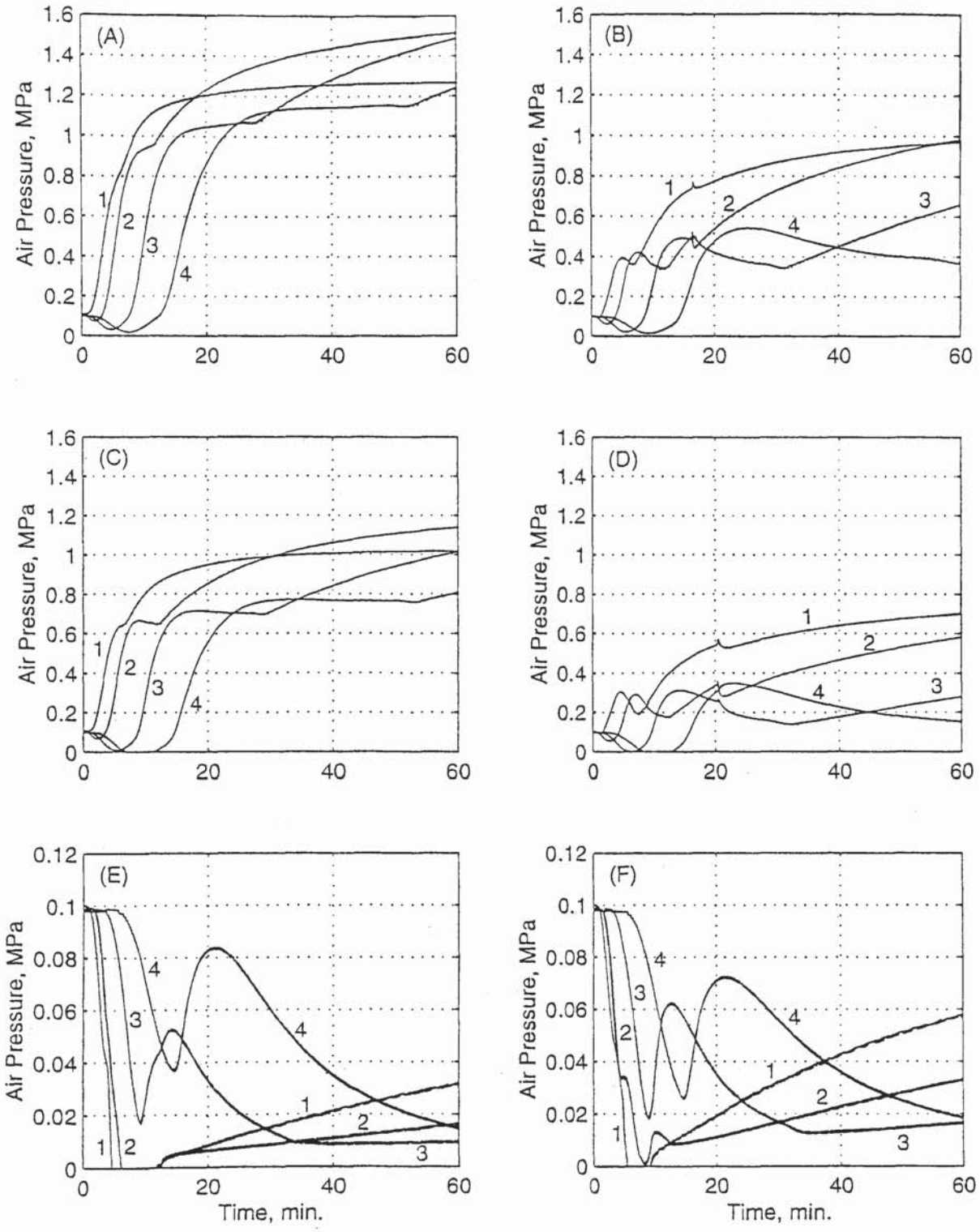

Fig. 6.22: Time history of air pressure P_a, in MPa, at (1) 5, (2) 10, (3) 20, and (4) 30 mm from the fire-exposed surface according to: (A) (2.8), (B) (3.3), (C) (2.12), (D) (3.4), (E) (3.29) for water vapour and (3.32) for air, and (F) (3.29) for both water vapour and air.

When (2.8) is used, the air pressure in the dry zone increases at a rate that is higher than the rate of increase of vapour pressure, and reaches values that are even greater than the maximum vapour pressure. For example, after 60 minutes of exposure to fire, the air pressure increases from its initial value of 0.1 MPa at the exposed surface to 1.6 MPa at 10 mm from the surface where the vapour pressure is only 0.5 MPa. When (3.3) in which the tortuosity is taken into account is adopted, the values of the air pressure are smaller than those obtained with (2.8), but the air pressure can be as high as 1 MPa in the dry zone. (2.12) leads to values of the air pressure that are smaller than those obtained from the corresponding (2.8) in which the tortuosity is neglected, but are greater than those obtained from (3.3) in which the tortuosity is considered. (3.4) in which the tortuosity is taken into account provides the smallest, and thus the best, values of the air pressure achieved with the molecular diffusivity equations used. Nevertheless, the air pressure can be as high as 0.7 MPa.

When concrete diffusivity (3.16) is used, the variation of the air pressure, in general, is similar to that of the air content. However, it can be seen that, due to the temperature, the air pressure can be closer to its initial value than the air content to the initial air content. Nevertheless, the air pressure remains smaller than, or equal to, its initial value of less than 0.1 MPa anywhere at all times. Of course, at locations where the air content is zero, the air pressure is zero. Also, the air pressure is minimum when the vapour pressure is at its maximum value. For example, after 60 minutes of exposure to fire, the air pressure is 0.01 MPa at 30 mm from the surface where the vapour pressure is at its maximum value of 1.5 MPa, and returns to its initial value of about 0.1 MPa at 130 mm from the surface where the air content is at the initial value of 1.18 kg/m^3. The time history shows that the air pressure is at its initial value when the vapour pressure is at its initial value, decreases when the vapour pressure increases, is minimum when the vapour pressure is maximum, and increases when the vapour pressure decreases after reaching a maximum.

The gradual increase in the air pressure, when the vapour pressure decreases after reaching a maximum, is more noticeable at 5 mm from the surface where the reduction in the vapour pressure is greater than that at 20 mm, since the reduction in the vapour pressure starts much earlier (after 8 minutes of exposure to fire).

Similarly, when (3.29) is used for both vapour and air, the variation of air pressure is similar to that of the air content. Although this assumption is unreal, it provides more realistic results than molecular diffusivity equations. The air pressure does not even exceed the initial value.

6.7 GASEOUS MIXTURE CONTENT

It may appear that the gaseous mixture content does not provide any additional information on the performance of the six different diffusivity equations, since the gaseous mixture content is merely the sum of the contents of water vapour and air. However, comparing the water vapour and air contents with the gaseous mixture content provides a clearer picture of the ratios of water vapour and air contents relative to their sum. The oscillations that appear in the air content distribution and time history do not appear in the gaseous mixture distribution and time history. The gaseous mixture content must be close to the water vapour content at high temperature, and must be close to the air content at low temperature. The results of this section are also particularly important in determining the effect of the variation of the diffusivities of water vapour and air as will be explained in the following section when the results of the pore pressure are discussed.

The distribution of the gaseous mixture content resulting from the six types of diffusion under consideration is presented in Figs. 6.1-6.6 and 6.23. The time history is shown in Figs. 6.8-6.13 and 6.24. When (2.8) is used, more than 60% of the gaseous mixture content at any location, and after any time of exposure to fire, consists of air. For example, after 60 minutes of exposure, the gaseous mixture content at 50 mm from the exposed surface is 15.5 kg/m^3 of which only 4.5 kg/m^3 is water vapour; the remaining 11 kg/m^3 is air! Considering the tortuosity (3.3) leads to an improvement. The adoption of (2.12) leads to values of the gaseous mixture content that are between those obtained with the corresponding (2.8) and those obtained with (3.3). When (3.4) is used, after 60 minutes of exposure to fire, the gaseous mixture content at 50 mm from the exposed surface is 8.75 kg/m^3 of which 5.5 kg/m^3 is water vapour and 3.25 kg/m^3 is air, and thus (3.4) leads to the best, albeit unreasonable, results obtained with molecular diffusivity equations.

According to concrete diffusivity (3.16), after 60 minutes of exposure to fire, the gaseous mixture content at 50 mm from the exposed surface is about 5.5 kg/m^3 of which 4.75 kg/m^3 is water vapour and only 0.75 kg/m^3 is air. The fact that the gaseous mixture content must be very close to the water vapour content at locations where the temperature is greater than 100°C and must be very close to the air content at locations where the temperature is smaller than 100°C is clear, since the water vapour content is much greater than the air content at high temperatures and is much smaller than the air content at low temperatures. The difference between the sixth case and the real one cannot be visually recognized. This difference, however, appears very clearly in the air contents.

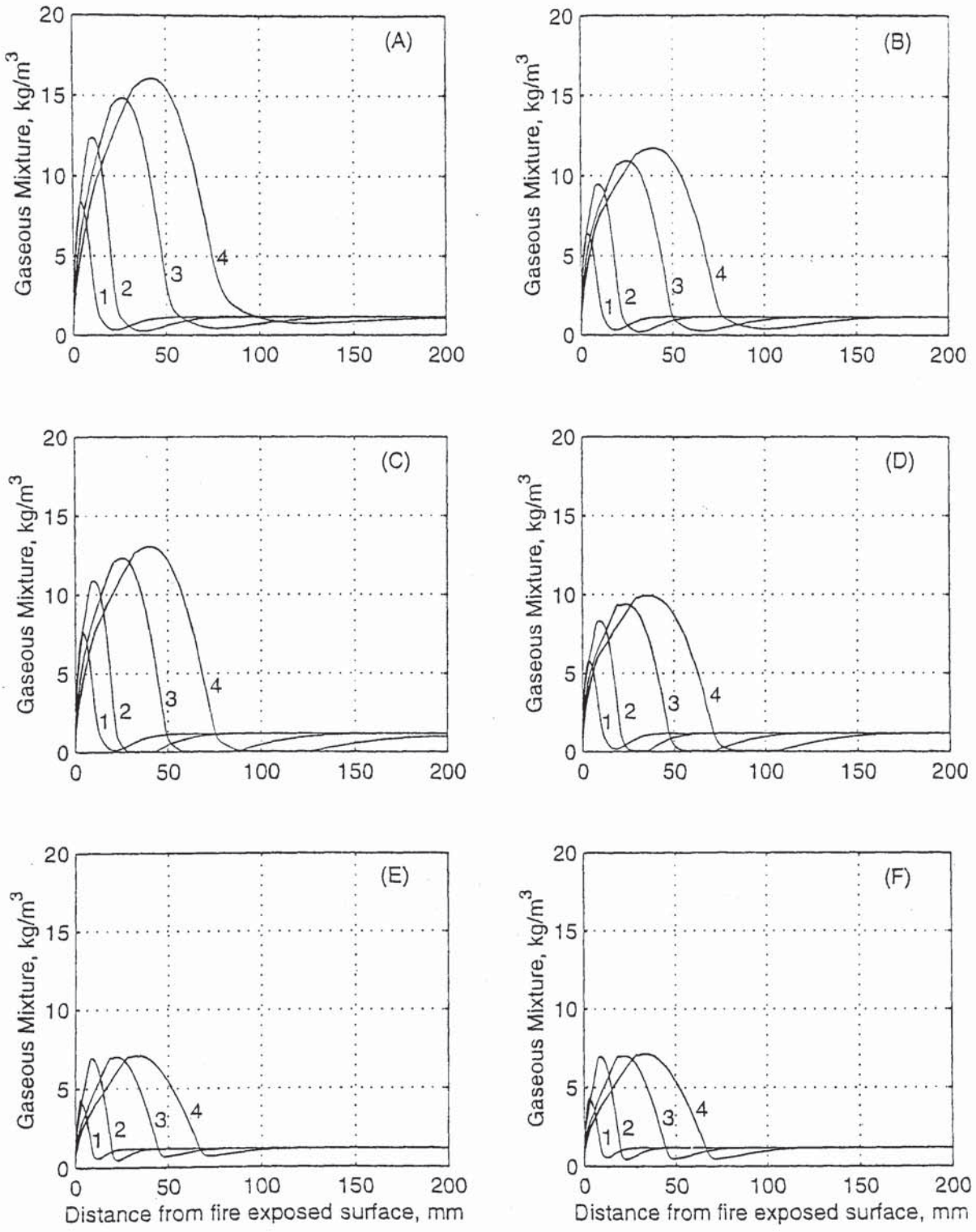

Fig. 6.23: Distribution of gaseous mixture ρ_g, in kg/m^3, after (1) 5, (2) 10, (3) 30, and (4) 60 minutes of exposure to fire according to: (A) (2.8), (B) (3.3), (C) (2.12), (D) (3.4), (E) (3.29) for water vapour and (3.32) for air, and (F) (3.29) for both water vapour and air.

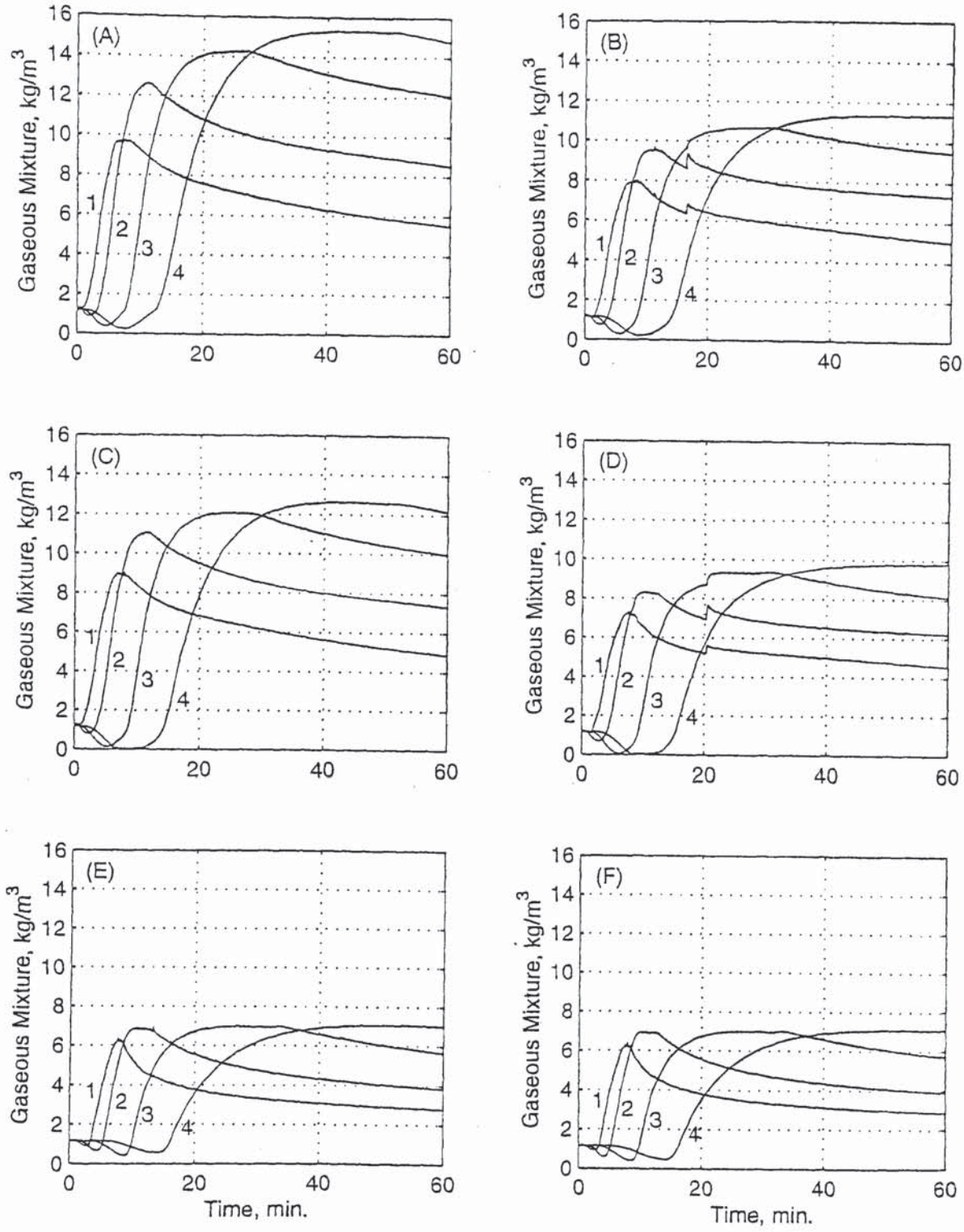

Fig. 6.24: Time history of gaseous mixture ρ_g, in kg/m^3, at (1) 5, (2) 10, (3) 20, and (4) 30 mm from the fire-exposed surface according to: (A) (2.8), (B) (3.3), (C) (2.12), (D) (3.4), (E) (3.29) for water vapour and (3.32) for air, and (F) (3.29) for both water vapour and air.

6.8 PORE PRESSURE

The distribution of the pore pressure for the six types of diffusion is presented in Figs. 6.1-6.6 and 6.25. The time history is shown in Figs. 6.8-6.13 and 6.26. (2.8) leads to pore pressures that consist of very significant proportions of air pressure compared with the water vapour pressure. For example, after 5 minutes of exposure to fire, the maximum pore pressure of 1.2 MPa consists of air pressure of 0.75 MPa, compared with only 0.45 MPa of water vapour pressure, i.e. more than 60% of the pore pressure is due to air pressure. After 60 minutes of exposure, the air pressure of 1.2 MPa represents 45% of the maximum pore pressure of 2.7 MPa, compared with the water vapour pressure of 1.5 MPa. When (3.3) is adopted, although the improvement in the performance of molecular diffusivity when the tortuosity is taken into account is clear, the significance of the air pressure remains. The performance of (2.12) is between that of (2.8) and that of (3.3). (3.4) provides the best performance obtained with molecular diffusivity equations; however, the air pressure still represents a significant proportion of the pore pressure. For example, after 5 minutes of exposure, the maximum pore pressure is 1 MPa consisting of 0.3 MPa of air pressure.

According to concrete diffusivity (3.16), after 5 minutes of exposure to fire, the maximum pore pressure is 0.8 MPa near the exposed surface, and is totally due to water vapour pressure. The air pressure at this location and time is zero since the air content is zero. After 10 minutes of exposure, the maximum pore pressure is about 1.4 MPa at a distance of about 10 mm from the exposed surface, and is also entirely due to water vapour pressure. Thereafter, the maximum pore pressure gradually increases very slightly. At locations where the temperature is equal to or greater than 100°C, the water vapour pressure remains the major source of pore pressure, while the air pressure is insignificant. For example, after 60 minutes of exposure, the maximum pore pressure occurs at a distance of about 30 mm from the exposed surface, and is very slightly greater than 1.5 MPa of which the air pressure is only 0.01 MPa.

When concrete diffusivity of water vapour (3.29) is used for air as well, the values of the maximum pore pressure are very slightly greater than the real values above, since the values of the air pressure at the evaporation front are slightly greater than the real ones. For example, after 5 minutes of exposure, the air pressure is 0.006 MPa, and thus the maximum pore pressure is very slightly greater than the real pore pressure, since the water vapour pressure remains at 1.5 MPa.

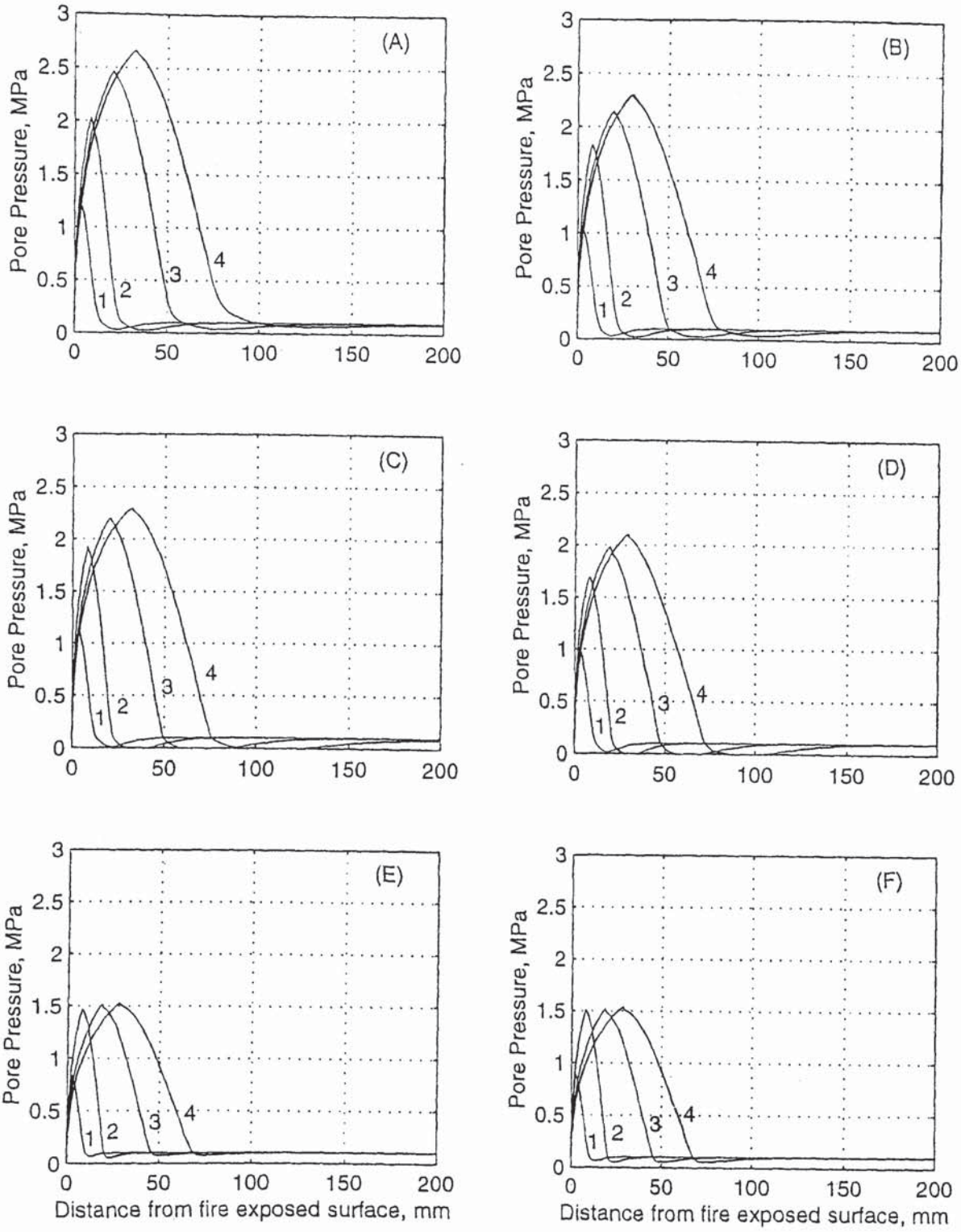

Fig. 6.25: Distribution of pore pressure P_g, in MPa, after (1) 5, (2) 10, (3) 30, and (4) 60 minutes of exposure to fire according to: (A) (2.8), (B) (3.3), (C) (2.12), (D) (3.4), (E) (3.29) for water vapour and (3.32) for air, and (F) (3.29) for both water vapour and air.

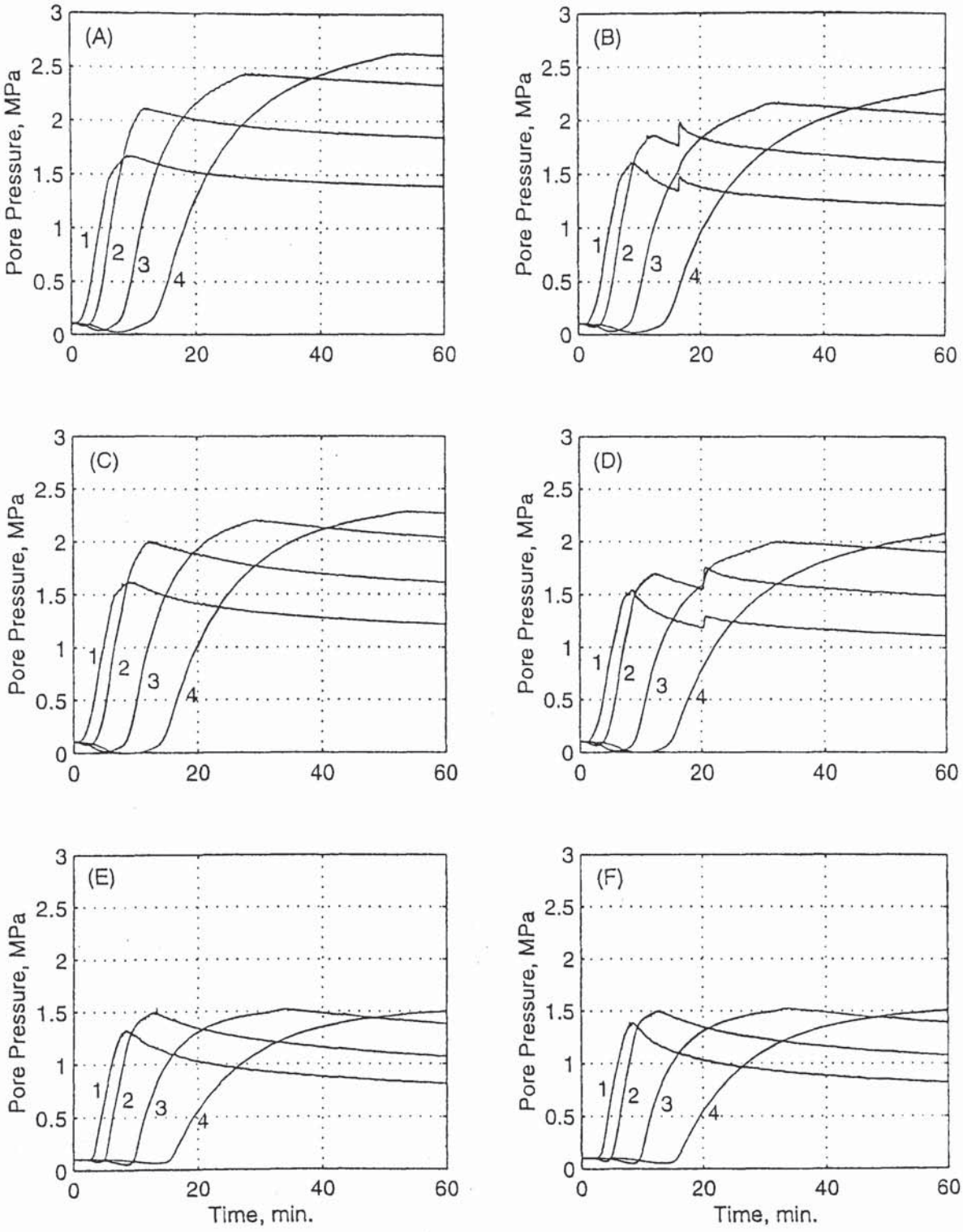

Fig. 6.26: Time history of pore pressure P_g, in MPa, at (1) 5, (2) 10, (3) 20, and (4) 30 mm from the fire-exposed surface according to: (A) (2.8), (B) (3.3), (C) (2.12), (D) (3.4), (E) (3.29) for water vapour and (3.32) for air, and (F) (3.29) for both water vapour and air.

The results of the gaseous mixture content (Fig. 6.23) and of the pore pressure (Fig. 6.25) re-confirm the hypothesis proposed in Section 3.4.6 that, whether or not the air significantly contributes to the increase of the pore pressure, the smaller the diffusivity, the smaller the gaseous mixture content, and thus the smaller the pore pressure. The hypothesis was confirmed in Chapter 5, and is re-confirmed by comparing Fig. 6.23(A), (B), (D), and (E), or (A), (C), (D), and (E), and Fig. 6.25(A), (B), (D), and (E), or (A), (C), (D), and (E). Thus, neglecting diffusion always results in the maximum underestimation of the pore pressure, while the use of molecular diffusivity always leads to the maximum overestimation of the pore pressure, although decreasing the molecular diffusivity results in a smaller overestimation of the pore pressure.

Also, similar the results of Chapter 5, the results of this chapter re-confirm that, since molecular diffusivity leads to an unrealistic air generation, the effect of decreasing the diffusivity, within limits, is to improve the results by increasing the vapour content, and thus increasing the vapour pressure, and decreasing the air content at a higher rate, and thus decreasing the air pressure, towards more realistic values with respect to the new decreased pore pressure, but, nevertheless, decreasing the diffusivity cannot lead to correct results.

6.9 FREE LIQUID WATER CONTENT

The distributions of the free water content for the six cases of diffusion are presented in Figs. 6.1-6.6 and 6.27. The time history is shown in Figs. 6.8-6.13 and 6.28. When (2.8) is adopted, the maximum free water content after 5 minutes of exposure to fire is 115 kg/m^3 at 10 mm from the fire-exposed surface. After 60 minutes of exposure, the maximum free water content is slightly less than 150 kg/m^3 at 60 mm from the surface. When (3.3) is adopted, it can be seen that taking the tortuosity into account leads to slightly greater amounts of free water in the over-saturated zone than those obtained with (2.8), since the vapour contents resulting from (3.3) are greater than those obtained with (2.8); thus, greater amounts of vapour can be condensed to free water in the over-saturated zone. When (2.12) is used, the amounts of the free water are between those obtained with (2.8) and those resulting from (3.3). (3.4) leads to amounts of free water that are the greatest obtained so far, because the amounts of water vapour that can be condensed to liquid water in the over-saturated zone are the greatest obtained from molecular diffusivity equations. The values of the maximum free water content, however, are only slightly greater than those obtained from (3.3).

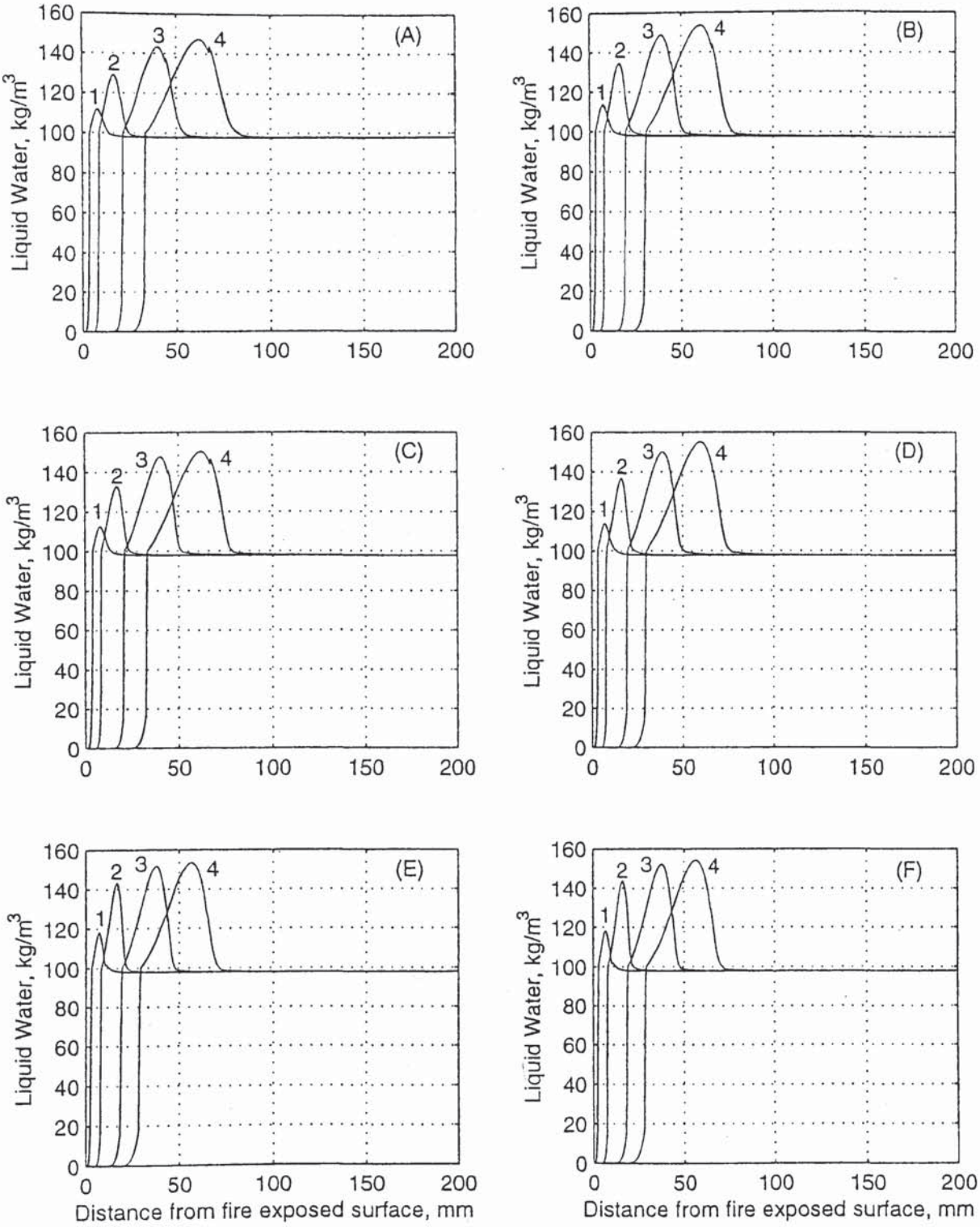

Fig. 6.27: Distribution of free liquid water $\varepsilon_l \rho_l$, in kg/m^3, after (1) 5, (2) 10, (3) 30, and (4) 60 minutes of exposure to fire according to: (A) (2.8), (B) (3.3), (C) (2.12), (D) (3.4), (E) (3.29) for water vapour and (3.32) for air, and (F) (3.29) for both water vapour and air.

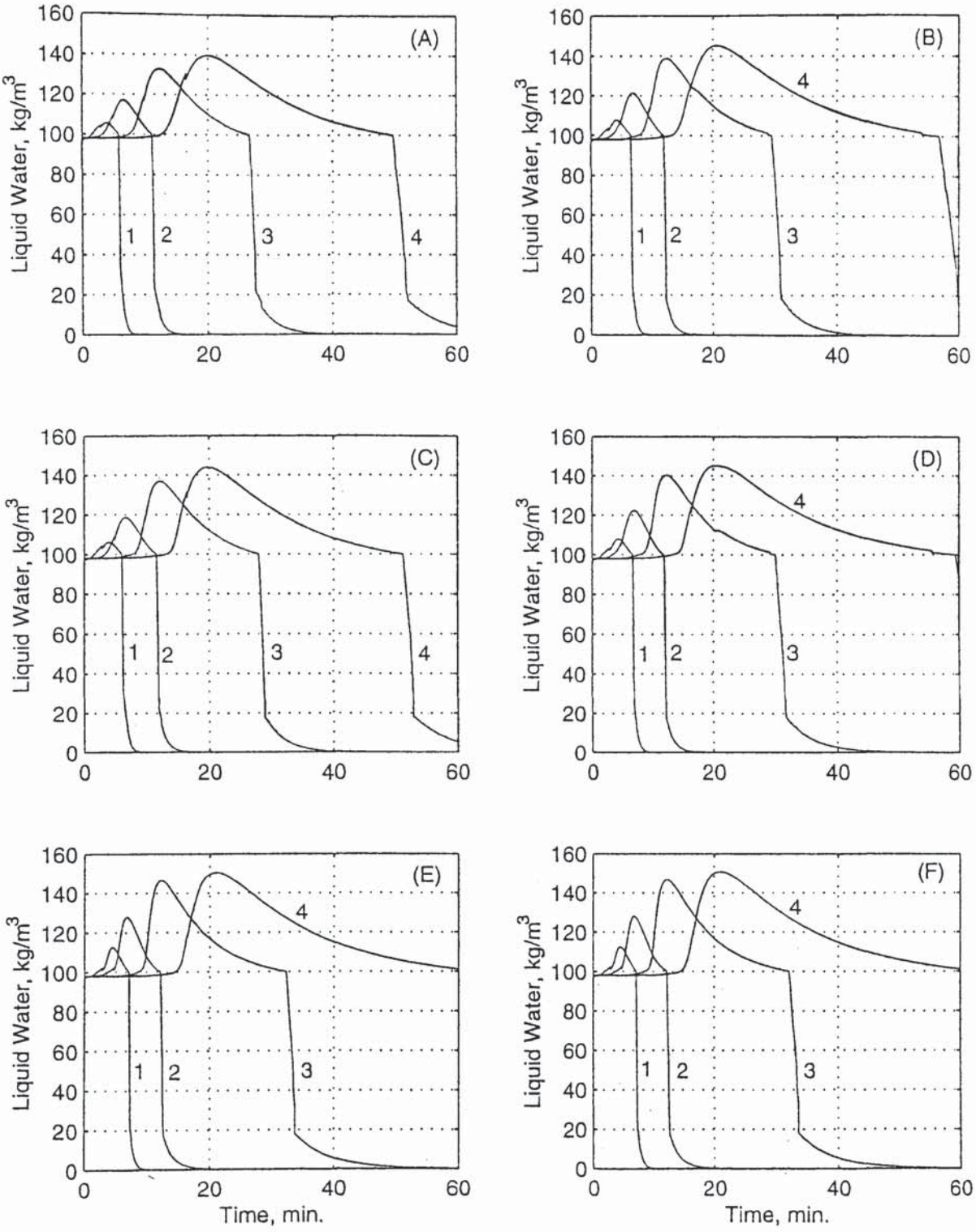

Fig. 6.28: Time history of free liquid water $\varepsilon_l \rho_l$, in kg/m^3, at (1) 5, (2) 10, (3) 20, and (4) 30 mm from the fire-exposed surface according to: (A) (2.8), (B) (3.3), (C) (2.12), (D) (3.4), (E) (3.29) for water vapour and (3.32) for air, and (F) (3.29) for both water vapour and air.

According to concrete diffusivity, at locations near the exposed surface and during the early stages of fire, the amounts of free water are slightly greater than those obtained from molecular diffusivity equations, because the amounts of water vapour are greater. For example, after 5 minutes of exposure to fire, the maximum free water content, at 10 mm from the exposed surface, is about 120 kg/m^3, compared with 115 kg/m^3 that results from (2.8), since the vapour content is 4.5 kg/m^3, compared with 2.5 kg/m^3 that results from (2.8). Also, after 10 minutes of exposure, the maximum free water content is greater than the maximum contents obtained with molecular diffusivity equations for the same reason. Thereafter, however, the rate of increase of the free water content is much smaller than that occurring with molecular diffusivity equations, since the vapour contents resulting from concrete diffusivity remain almost constant. Thus, the increase in the amounts of free water is only due to the longer periods available for condensation. On the other hand, when molecular diffusivity equations are used, the increase of free water is not only due to the longer periods available for condensation, but also due to the continuous increase in the vapour contents.

Therefore, beyond a certain distance from the exposed surface, the maximum amounts of free liquid water obtained from concrete diffusivity are smaller than those obtained from a molecular diffusivity equation. When Fig. 6.27(D) and 6.27(F) are compared, it can be seen that the critical distance at which the maximum free water content is the same when either (3.4) or (3.16) is adopted is about 40 mm from the exposed surface. At this distance, the maximum free water content is 150 kg/m^3 after 30 minutes of exposure to fire according to both (3.4) and (3.16).

The time history of the free water content according to concrete diffusivity (3.16) shows that the maximum amounts of free water are slightly greater than those obtained from (3.4) at all locations considered: 5, 10, 20, and 30 mm from the exposed surface. At 30 mm from the surface, the maximum free water is 150 kg/m^3, compared with 145 kg/m^3 that results from (3.4). This confirms that the distance of 30 mm from the exposed surface is within the range in which the amounts of free water obtained with concrete diffusivity are greater than those obtained with molecular diffusivity. The free water content obtained from molecular diffusivity is greater than that obtained from concrete diffusivity only when the distance from the exposed surface exceeds 40 mm.

The free water content when concrete diffusivity of air is assumed equal to that of water vapour (3.29) is the same as that resulting from the real diffusivities (3.29) and (3.32), since the distribution and time history of the water vapour content is the same.

6.10 VARIATION OF THE MEAN FREE PATH

In Chapter 3, it is found that the mean free path of water vapour molecules at ambient temperature and 1 atm is 1300 Å, and is 1600 Å at 100°C and 1 atm. Thus, it was argued that the type of diffusion, particularly in good concrete where capillary pores are segmented by gel pores, must be Knudsen diffusion. The following expression (2.6) was provided for the mean free path, in m (Cunningham and Williams, 1980, Cussler, 1997):

$$\lambda = \frac{kT}{\sqrt{2}\pi\sigma^2 P} \tag{6.1}$$

It is clear from (6.1) that the mean free path decreases when the pore pressure increases, and thus can no longer remain at 1600 Å when the free liquid water starts to evaporate at 100°C and the pore pressure starts increasing. Thus, when the pore pressure is at its maximum value, the mean free path may be reduced very significantly such that it may become much smaller than the mean pore diameter, and thus molecular diffusion may become the dominant type of diffusion.

However, at distances where the pore pressure is at its maximum value of about 1.5 MPa (according to concrete diffusivity), where the temperature is about 200°C, the mean free path of water vapour molecules calculated from (6.1) is 140 Å, while the mean pore diameter is 100 Å when the tortuosity is assumed equal to 3, and is 66 Å when the tortuosity is assumed equal to 2 (Section 3.5). Molecular diffusion does not dominate unless the mean free path is much smaller than the pore diameter. Moreover, the mean free path is reduced to 140 Å only locally where the pore pressure is at its maximum value. As the distance to the fire-exposed surface decreases, the temperature increases and the pore pressure decreases (Fig. 6.5). In fact, near the fire-exposed surface where the pore pressure is equal to the standard atmospheric pressure and the temperature is about 500°C after 60 minutes of exposure to fire, the mean free path is more than 3400 Å. Of course, as discussed in Chapter 3, this does not prevent water vapour molecules from diffusing to the environment.

At distances greater than that at which the maximum pore pressure occurs, the temperature gradually decreases. However, the pore pressure decreases at a much higher rate, and the mean free path increases until it reaches the value of 1600 Å at a distance of 70 mm from the fire-exposed surface where the pressure returns to its initial value and the temperature is just below 100°C, and

then decreases to the value of 1300 Å at a distance of about 120 mm where both the temperature and pressure are back to their initial values (Fig. 6.5).

6.11 CONCLUSIONS

- The use of molecular diffusivity equations in mathematical modelling of heat and mass transfer in heated concrete leads to unrealistic and unreasonable results. Molecular diffusivity equations lead to temperatures of the fire-exposed surface of up to 800°C. They also result in overestimating the pore pressure significantly; they lead to maximum pore pressures up to 2.7 MPa of which the water vapour pressure is 1.5 MPa while the air pressure is 1.2 MPa! Considering the tortuosity with molecular diffusivity results in a smaller overestimation of the pore pressure. Nevertheless, the contribution of the air to the increase of the pore pressure remains significant, and thus unreasonable.

- The results of concrete diffusivity are realistic and reasonable. Experimental evidence indicates that the surface temperatures of concrete when spalling occurs fall in the range of 250-420°C (Akhtaruzzaman and Sullivan, 1970; Connolly, 1995; Jumpannen, 1998; Khoury, 2000). This is an indication of the reasonableness and realism of concrete diffusivity, since it leads to maximum surface temperatures, when the maximum pressures occur, that are much closer to this range of temperatures than those obtained with different molecular diffusivity equations even when the tortuosity is taken into account. Also, the maximum pore pressure of slightly greater than 1.5 MPa is almost entirely due to the build up of water vapour pressure of 1.5 MPa. When the maximum pore pressure occurs, the air, and thus the air pressure, is almost zero, since the water vapour displaces some, or even all, of the air.

- The type of diffusion remains to be Knudsen diffusion in concrete exposed to fire even when the pore pressure is at its maximum value, since the mean free path of water vapour molecules remains greater than the mean pore diameter.

Concrete walls of different thickness exposed to fire on two sides will be investigated in Chapter 7. Based on the findings reached in this chapter, only concrete diffusivity will be adopted hereinafter.

CHAPTER 7

CONCRETE WALLS IN FIRE

7.1 INTRODUCTION

In Chapter 2, it was observed that the mechanism of explosive spalling is debateable, and that some researchers, e.g. Bažant and Thonguthai (1978) and Ahmed and Hurst (1997), compare the pressure with the strength of concrete at high temperature and argue that the pressure cannot be the main cause of spalling because the calculated as well as the measured magnitudes of the pressure are not high enough. At the same time, however, it was noted that comparison should be made between the forces. Furthermore, the difficulties, and thus the unreliability, of pore pressure measurements were demonstrated. Moreover, the invalidity of the assumptions related to diffusion in mathematical modelling, and thus the unreliability of the calculated pressures that is clear from the large differences in the results of different models, was illustrated in Chapters 3, 5, and 6.

The problem was solved with the development of concrete diffusivity, and, assuming that all assumptions are reasonable, it was found that a maximum pore pressure of 1.3 MPa occurs at a distance of 5 mm from the fire-exposed surface after 8 minutes of exposure to fire, and a maximum pressure of 1.5 MPa occurs at 10 mm from the surface after 12 minutes of exposure. Nevertheless, these values of the maximum pore pressure, their locations, and the corresponding times of exposure may or may not make the mechanism of explosive spalling less debateable.

However, as was stated by Purkiss (1996), explosive spalling is affected by five factors: moisture content, concrete porosity, stress conditions, aggregate type, and section profile and cover. As far as the fifth factor is concerned, Purkiss stated that explosive spalling is exacerbated in thin sections, partly because the depth of spalling is a greater proportion of the section dimension and thus proportionally worse, and partly due to the fact that there is less of a cool reservoir for moisture to migrate towards. Purkiss' explanation of the fact that spalling is exacerbated in heated thin sections implies that it is believed that greater pressures may occur in thin sections than those occurring in thick ones. Nevertheless, no attempt seems to have been made to investigate heated thin sections in detail. In particular, the maximum pore pressures that can occur in heated thin sections, their locations, and the corresponding times of exposure to heat have not been estimated quantitatively.

Thus, one of the major objectives of this study is to investigate the effect of thickness of heated concrete sections. Furthermore, Purkiss' explanation has led to the more general objective of investigating the effect of totally eliminating the cool zone, in which the thickness is only one of three factors. The reduction of the cool zone is affected by three factors: thickness, time of exposure, and type of exposure, i.e. whether the section is exposed to fire from one or more sides.

The cool zone is defined as that within which the temperature is less than 100°C, and thus the free water in the cool zone does not evaporate extensively. Therefore, eliminating the cool zone means that the temperature is equal to or greater than 100°C everywhere in the section. Thus, in a concrete wall exposed to fire from both sides, eliminating the cool zone requires that the temperature along the centreline of the wall cross-section is equal to or greater than 100°C. It should be noted that the results for the elimination of the cool zone (if any) will only hold if spalling does not occur.

Based on the findings reached so far in this study, only concrete diffusivity will be used.

7.2 EFFECT OF THICKNESS

Concrete walls with different thickness exposed to fire from both sides are considered in descending order as follows: 400, 150, 100, 75, 50, and 25-mm-thick walls exposed to fire for 240, 120, 60, 60, 60, and 60 minutes, respectively. The 75, 50, and 25-mm-thick walls are examined in order to determine the overall behaviour pattern whilst recognising the impracticality of these sizes.

7.2.1 400-mm-Thick Walls

Fig. 7.1 shows the time history of various parameters at distances of 5, 20, 40, 60, 80, and 100 mm from any of the two exposed surfaces of a 400-mm-thick wall exposed to fire for 240 minutes. The distribution after 5, 10, 30, 120, and 240 minutes of exposure is illustrated in Fig. 7.2. The cool zone is reduced after 240 minutes of exposure, but is not totally eliminated; the temperature along the centreline is about 60°C. The pore pressure at the centreline is equal to the standard atmospheric pressure. At a distance of 40 mm from the exposed surface, the maximum pore pressure does not exceed 1.6 MPa where the temperature is about 200°C. The magnitudes of the maximum pore pressure are 1.5, 1.55, and 1.6 MPa after 30, 120, and 240 minutes of exposure to fire, respectively.

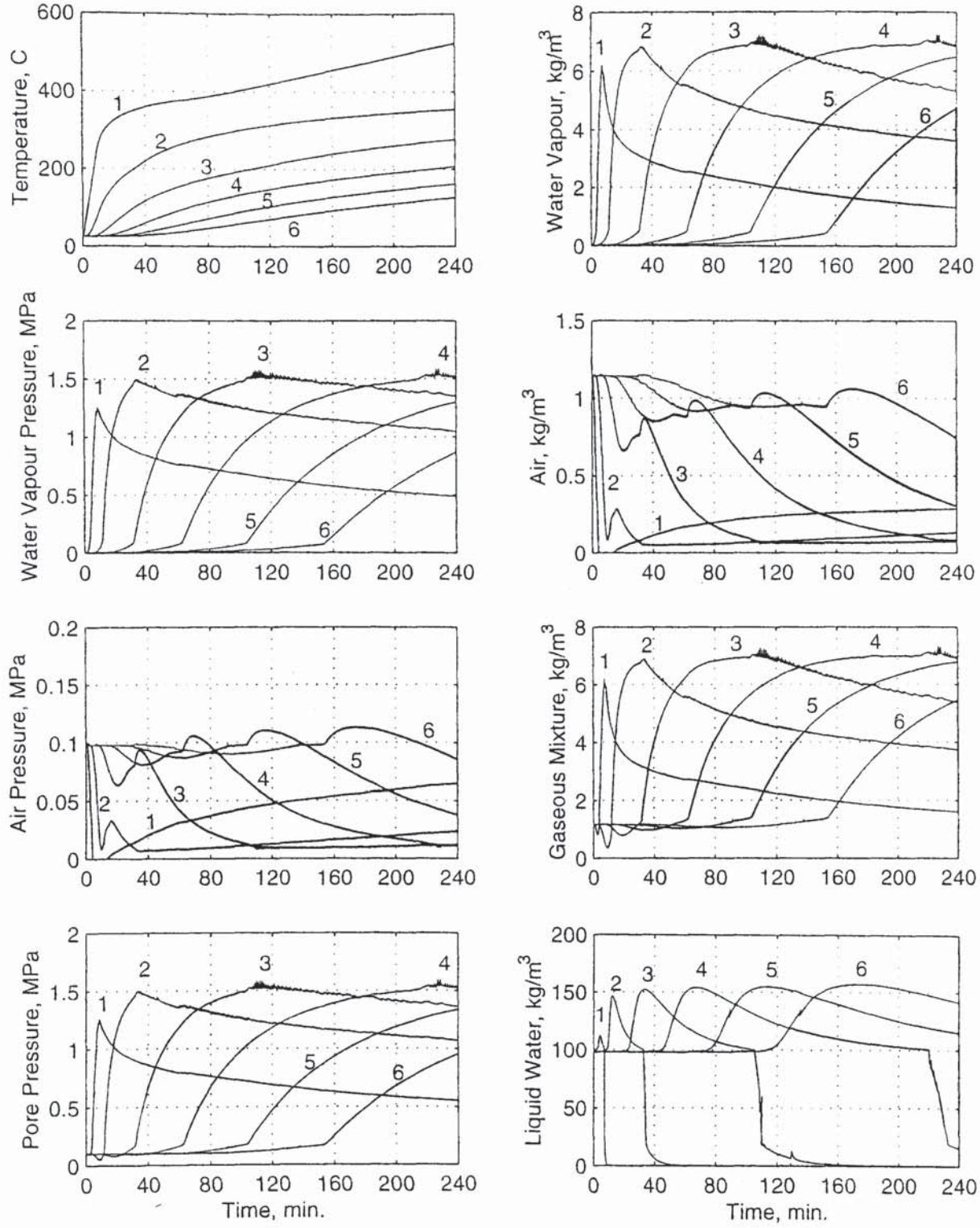

Fig. 7.1: Time history of T, in °C, ρ_v, in kg/m^3, P_v, in MPa, ρ_a, in kg/m^3, P_a, in MPa, ρ_g, in kg/m^3, P_g, in MPa, and $\varepsilon_l \rho_l$, in kg/m^3, at (1) 5, (2) 20, (3) 40, (4) 60, (5) 80, and (6) 100 mm from any of the fire-exposed surfaces of a 400-mm-thick concrete wall exposed to fire from both sides for 240 minutes.

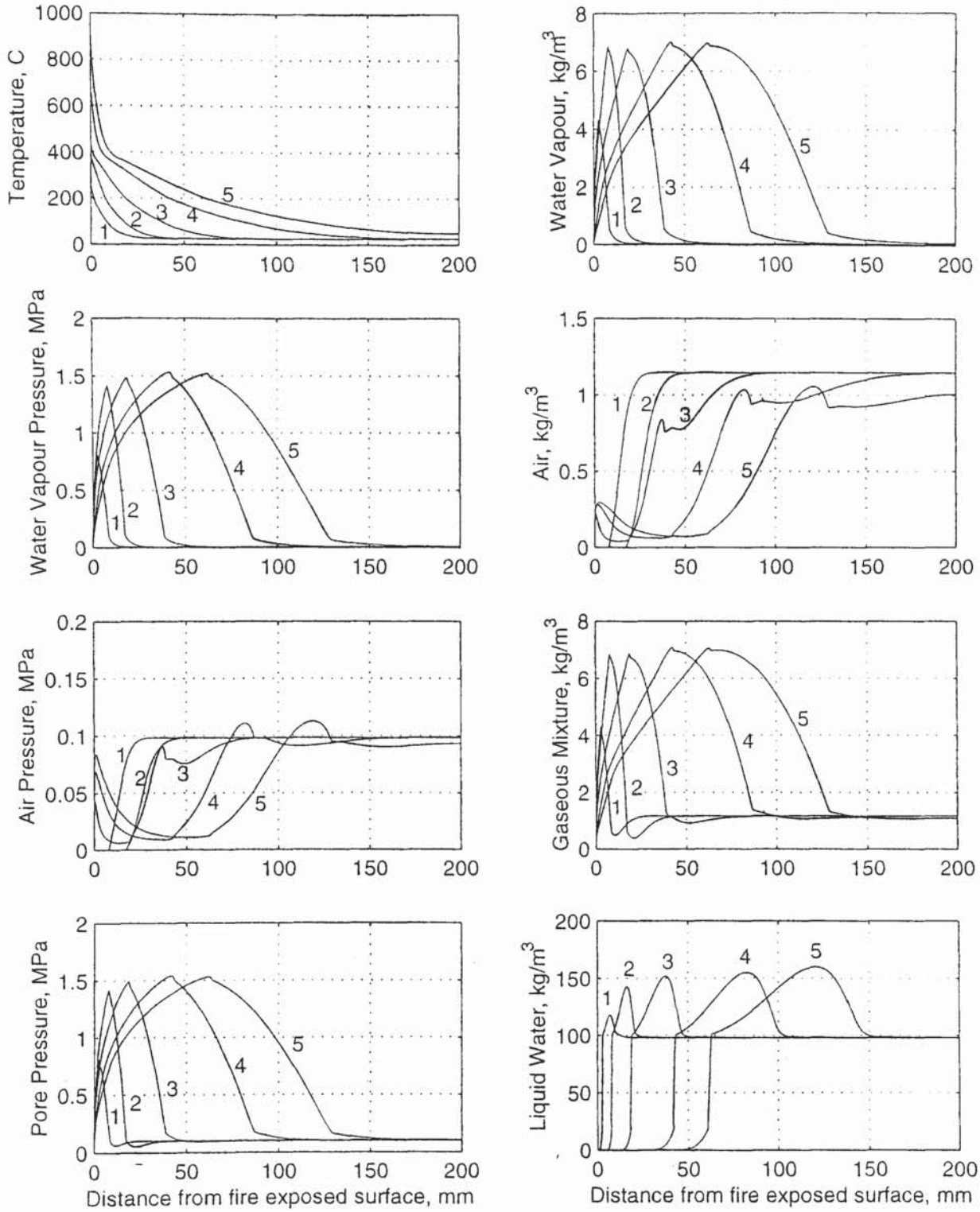

Fig. 7.2: Distribution of T, in °C, ρ_v, in kg/m^3, P_v, in MPa, ρ_a, in kg/m^3, P_a, in MPa, ρ_g, in kg/m^3, P_g, in MPa, and $\varepsilon_l \rho_l$, in kg/m^3, after (1) 5, (2) 10, (3) 30, (4) 120, and (5) 240 minutes of exposure to fire in a 400-mm-thick concrete wall exposed to fire from both sides for 240 minutes.

7.2.2 150-mm-Thick Walls

Fig. 7.3 shows the time history of various parameters at distances of 12.5, 25, 37.5, 50, 62.5, and 75 mm from any of the fire-exposed surfaces of a 150-mm-thick concrete wall exposed to fire from both sides for 120 minutes. The distribution after 20, 40, 60, 80, 100, and 120 minutes of exposure to fire is illustrated in Fig. 7.4. Fig. 7.3 shows that, after 60 minutes of exposure to fire, the cool zone is greatly reduced but is not totally eliminated; the temperature along the centreline of the wall section, i.e. at 75 mm from both surfaces, is just below 100°C. The maximum pore pressure is 1.5 MPa at a distance of 12.5 mm from the exposed surface after about 17 minutes of exposure to fire. Since the temperature along the centreline is less than 100°C after 60 minutes of exposure, the free water has not started to evaporate extensively at that location, and thus the pore pressure is only about 0.1 MPa.

However, after about 65 minutes of exposure to fire, the cool zone is eliminated from the section; the temperature starts exceeding 100°C along the centreline of the wall, and the pore pressure starts increasing at a high rate at that particular time. The pore pressure continues to increase until it reaches a very maximum value of 4.3 MPa after 115 minutes of exposure to fire when the temperature is about 200°C.

Fig. 7.4 shows that the maximum pore pressure is only slightly greater than 1.5 MPa at about 27 mm from the surface after 60 minutes of exposure. That the temperature is just below 100°C along the centreline after 60 minutes of exposure to fire is also evident. Again, after 115 minutes of exposure to fire, the maximum pore pressure is 4.3 MPa along the centreline of the wall section where the temperature is about 200°C. It can also be seen from the distribution of the pore pressure that, when the pore pressure is at its very maximum value in the middle of the section, the pore pressure at any location is the very maximum that can occur at that location. If the wall is reinforced, and the cover is 25 mm, the cover will be subjected to 2.9 MPa of pressure after 115 of exposure to fire. However, spalling occurs within the first 30 minutes of exposure to fire. Furthermore, after 115 minutes of exposure to fire, the 150-mm-thick wall is unlikely to remain intact, due to the loss of strength.

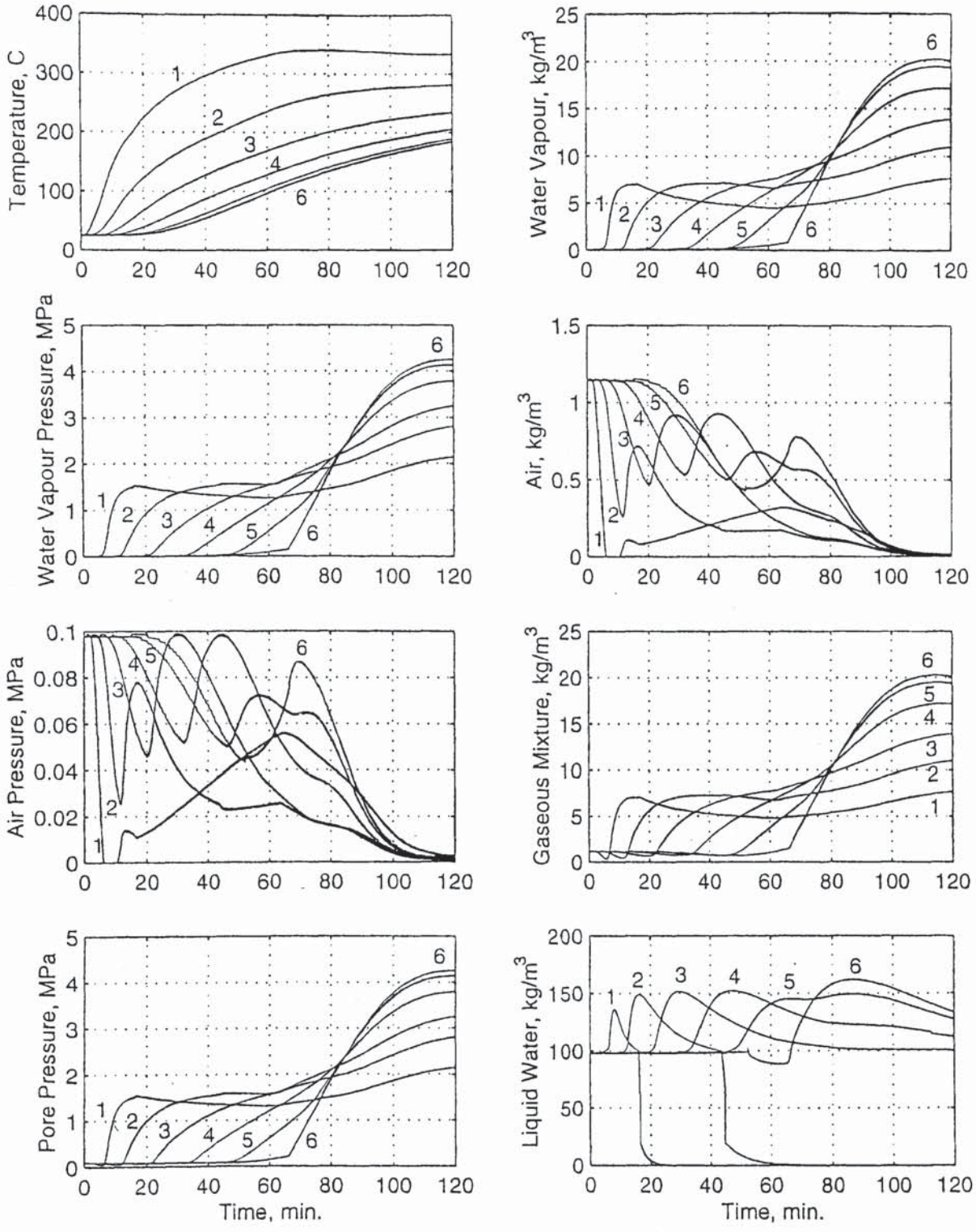

Fig. 7.3: Time history of T, in °C, ρ_v, in kg/m^3, P_v, in MPa, ρ_a, in kg/m^3, P_a, in MPa, ρ_g, in kg/m^3, P_g, in MPa, and $\varepsilon_l \rho_l$, in kg/m^3, at (1) 12.5, (2) 25, (3) 37.5, (4) 50, (5) 62.5, and (6) 75 mm from any of the fire-exposed surfaces of a 150-mm-thick concrete wall exposed to fire from both sides for 120 minutes.

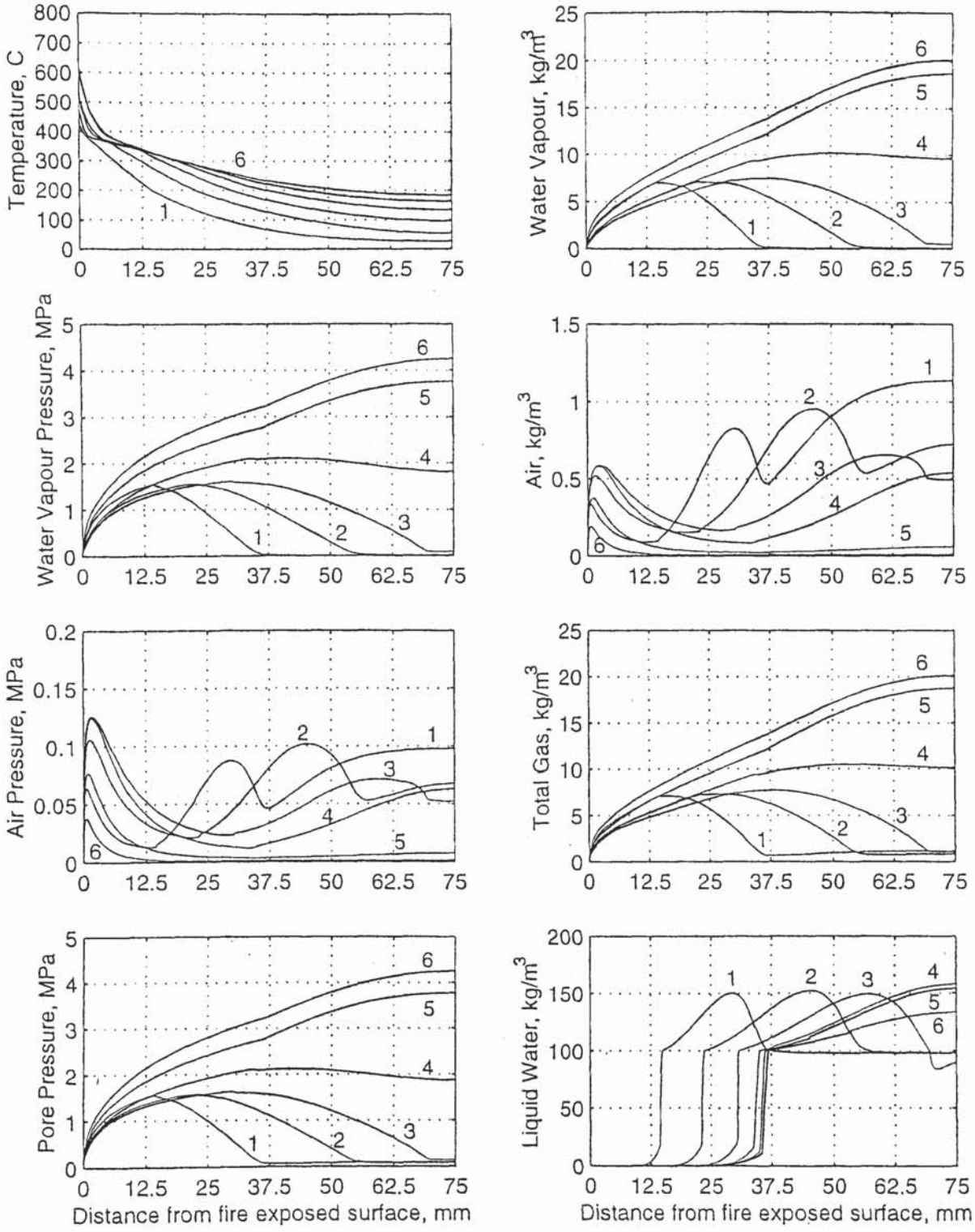

Fig. 7.4: Distribution of T, in °C, ρ_v, in kg/m^3, P_v, in MPa, ρ_a, in kg/m^3, P_a, in MPa, ρ_g, in kg/m^3, P_g, in MPa, and $\varepsilon_l \rho_l$, in kg/m^3, after (1) 20, (2) 40, (3) 60, (4) 80, (5) 100, and (6) 115 minutes of exposure to fire in a 150-mm-thick concrete wall exposed to fire from both sides for 120 minutes.

7.2.3 100-mm-Thick Walls

The time history of various parameters at distances of 10, 20, 30, 40, and 50 mm from any of the exposed surfaces of a 100-mm-thick wall exposed to fire from both sides is presented in Fig. 7.5. Fig. 7.6 shows the distribution after 10, 20, 30, 40, 55, and 60 minutes of exposure. Fig. 7.5 shows that, after 30 minutes of exposure to fire, the cool zone is greatly reduced, but is not eliminated, since the temperature along the centreline is just below 100°C. Up to about 32 minutes of exposure, the maximum pressure is about 1.5 MPa at 20 mm from the exposed surface. The temperature reaches 100°C at the centreline, and thus the cool zone is eliminated from the entire section, after 32 minutes of exposure to fire. However, after 55 minutes of exposure, the maximum pore pressure is 3.5 MPa along the centreline of the wall cross-section where the temperature is nearly 200°C.

Fig. 7.6 demonstrates that, after 55 minutes of exposure to fire, the pore pressure at any distance from the surface is greater than the maximum pressure that can be obtained at the same distance when there is a cool zone, and is the very maximum pressure that can occur at that distance. That the maximum pore pressure is 3.5 MPa along the centreline of the wall cross-section where the temperature is nearly 200°C after 55 minutes of exposure to fire is also evident.

7.2.4 75-mm-Thick Walls

The time history of various parameters at 6.25, 12.5, 18.75, 25, 31.25, and 37.5 mm from the exposed surface of a 75-mm-thick wall exposed to fire from both sides is demonstrated in Fig. 7.7. Fig. 7.8 shows the distribution after 10, 20, 33, 50, and 60 minutes of exposure. During the first 20 minutes, the pore pressures are the same as those obtained in the 400-mm-thick wall. Fig. 7.7 shows that the temperature at the centreline reaches 100°C, and thus the cool zone is eliminated, after 20 minutes. Then, the pore pressure along the centreline starts increasing at a very high rate. The very maximum pore pressure that can occur in the 75-mm-thick wall is about 3.4 MPa. It occurs along the centreline after about 33 minutes of exposure to fire when the temperature is nearly 200°C. Like the 100-mm-thick wall, the pore pressure along the centreline starts decreasing after reaching its maximum value when the time of exposure is 33 minutes, and continues to decrease until the time of exposure is 50 minutes. However, when the time of exposure exceeds 50 minutes, the pore pressure starts increasing again, and continues to increase until the time of exposure reaches 60 minutes. This behaviour is unrealistic, and will be discussed in Section 7.4.

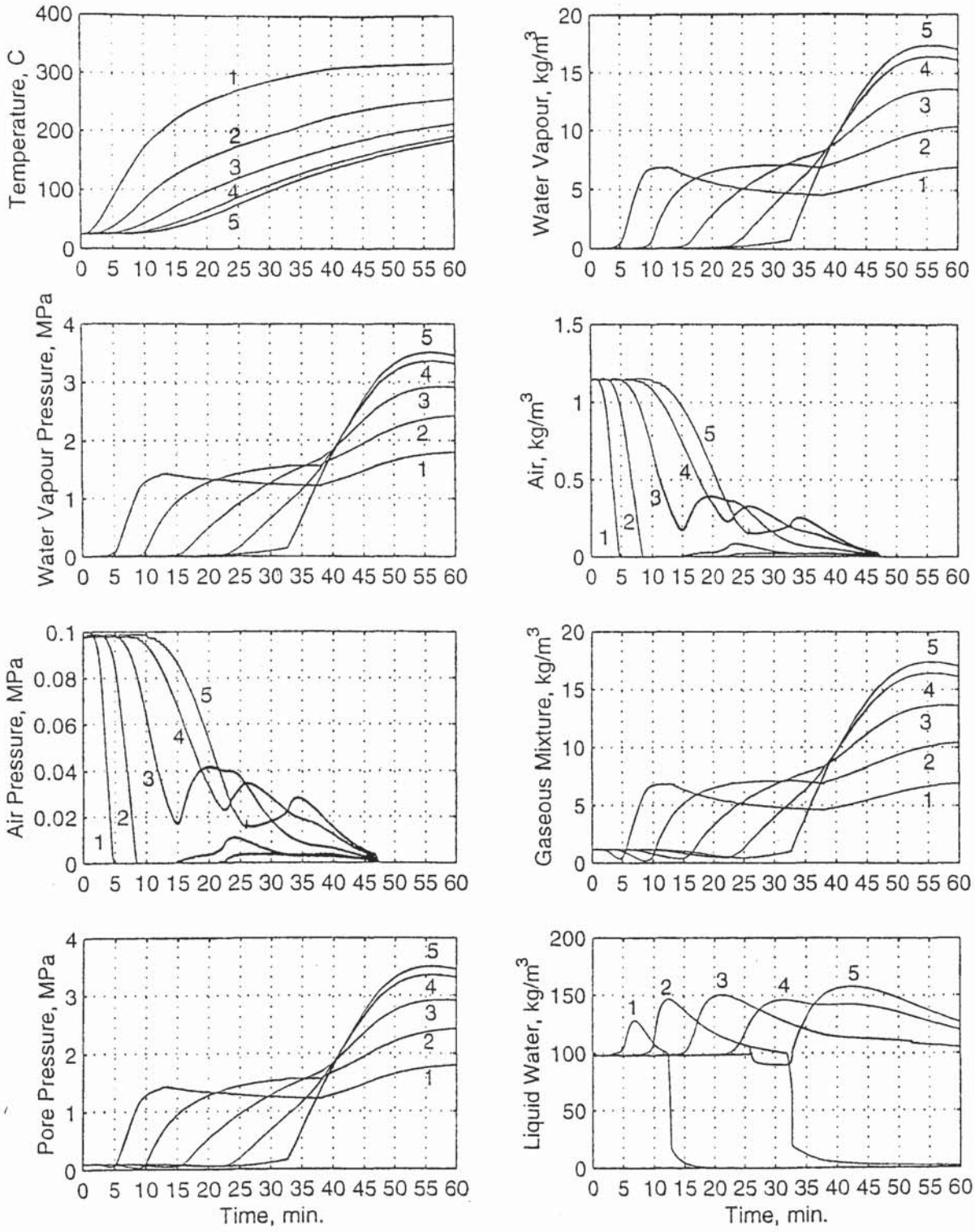

Fig. 7.5: Time history of T, in °C, ρ_v, in kg/m^3, P_v, in MPa, ρ_a, in kg/m^3, P_a, in MPa, ρ_g, in kg/m^3, P_g, in MPa, and $\varepsilon_l \rho_l$, in kg/m^3, at (1) 10, (2) 20, (3) 30, (4) 40, and (5) 50 mm from any of the fire-exposed surfaces of a 100-mm-thick concrete wall exposed to fire from both sides for 60 minutes.

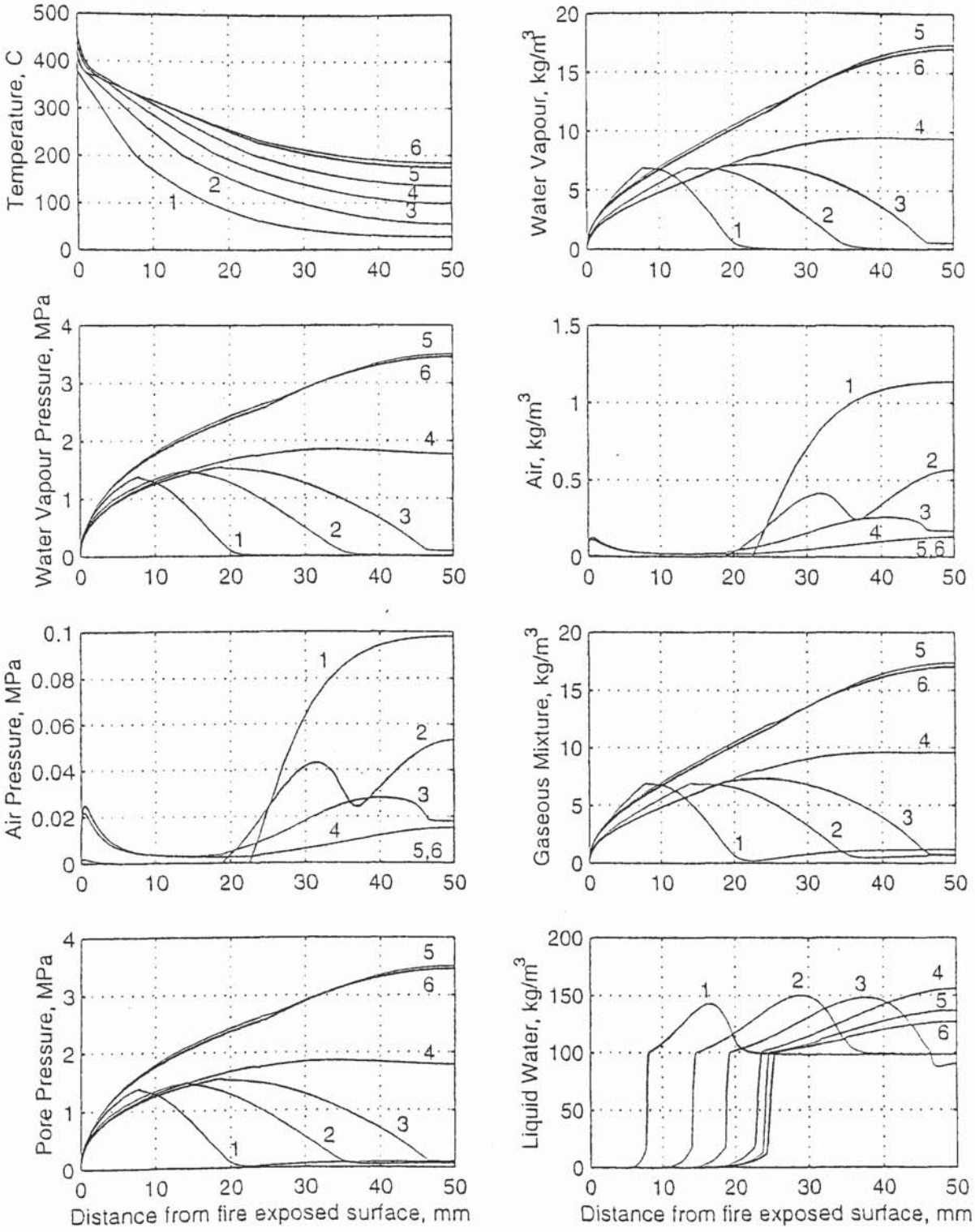

Fig. 7.6: Distribution of T, in °C, ρ_v, in kg/m^3, P_v, in MPa, ρ_a, in kg/m^3, P_a, in MPa,ρ_g, in kg/m^3, P_g, in MPa, and $\varepsilon_l \rho_l$, in kg/m^3, after (1) 10, (2) 20, (3) 30, (4) 40, (5) 55, and (6) 60 minutes of exposure to fire in a 100-mm-thick concrete wall exposed to fire from both sides for 60 minutes.

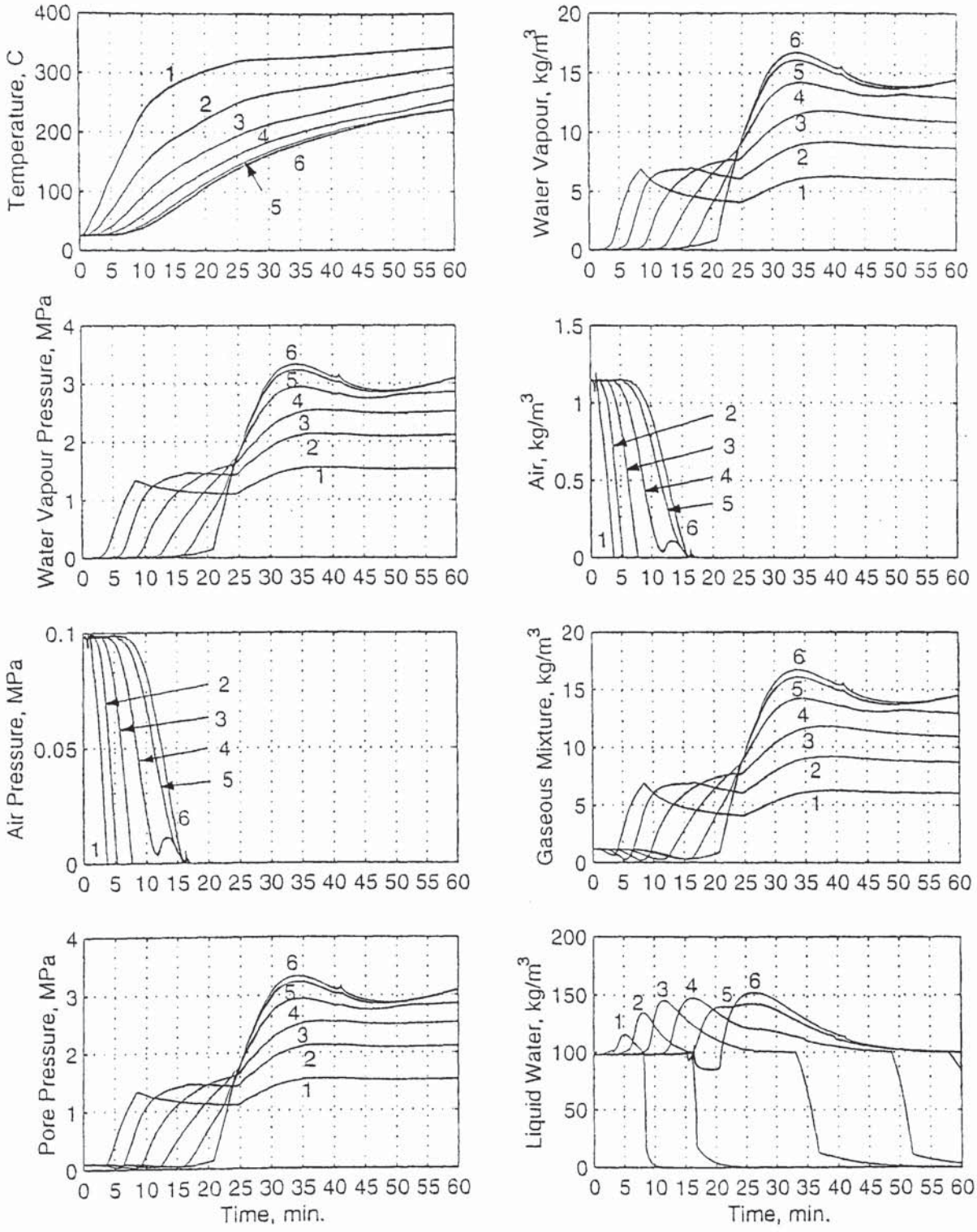

Fig. 7.7: Time history of T, in °C, ρ_v, in kg/m^3, P_v, in MPa, ρ_a, in kg/m^3, P_a, in MPa, ρ_g, in kg/m^3, P_g, in MPa, and $\varepsilon_l \rho_l$, in kg/m^3, at (1) 6.25, (2) 12.5, (3) 18.75, (4) 25, (5) 31.25, and (6) 37.5 mm from any of the fire-exposed surfaces of a 75-mm-thick concrete wall exposed to fire from both sides for 60 minutes.

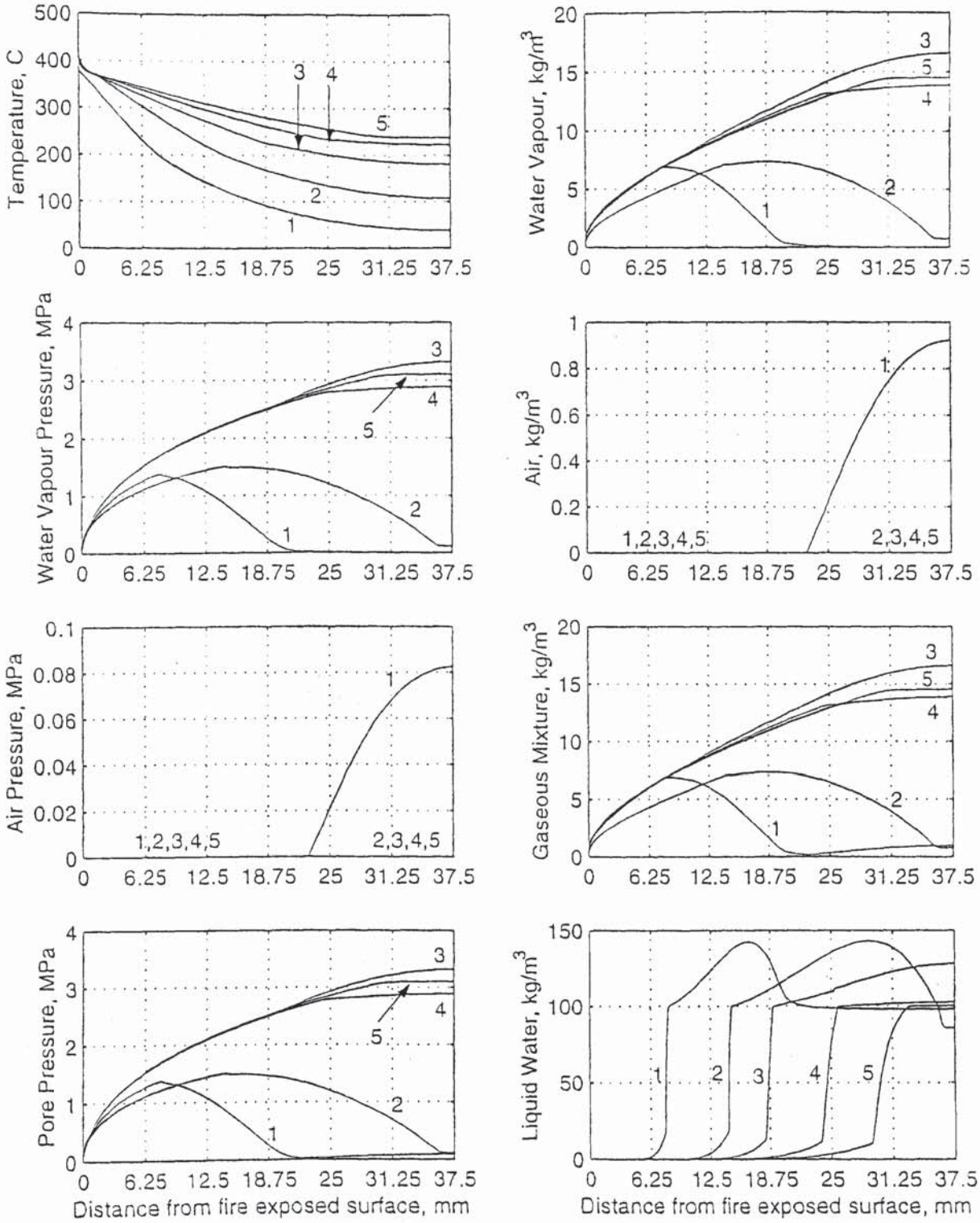

Fig. 7.8: Distribution of T, in °C, ρ_v, in kg/m^3, P_v, in MPa, ρ_a, in kg/m^3, P_a, in MPa, ρ_g, in kg/m^3, P_g, in MPa, and $\varepsilon_l \rho_l$, in kg/m^3, after (1) 10, (2) 20, (3) 33, (4) 50, and (5) 60 minutes of exposure to fire in a 75-mm-thick concrete wall exposed to fire from both sides for 60 minutes.

7.2.5 50-mm-Thick Walls

The time history of various parameters in a 50-mm-thick wall exposed to fire from both sides at distances of 5, 10, 15, 20, and 25 mm from the exposed surfaces is illustrated in Fig. 7.9. Fig. 7.10 shows the distribution after 5, 10, 15, 17, 25, and 40 minutes of exposure. The cool zone is eliminated after 12 minutes, and the maximum pore pressure is 1.5 MPa at a distance of 10 mm from the surface after 12 minutes. After 17 minutes, the very maximum pore pressure is 3.1 MPa. Similar to the results of the 75-mm-thick wall compared with those of the 100-mm-thick wall, the very maximum pore pressure is lower than that obtained in the middle of the 75-mm-thick wall. The other peak of 3.2 MPa that occurs after 33 minutes is not relevant as noted when the 75-mm-thick wall was considered. However, the sudden drop in the pressure when the free water completely evaporates after 35 minutes is reasonable, but there should have been a gradual decrease in the pore pressure for 18 minutes (between 17 and 35 minutes), rather than the unjustifiable increase from 2.7 MPa to 3.2 MPa. The results are valid for the first 24 minutes. They are also reasonable after 35 minutes and thereafter. The pressure at any distance from the exposed surface is the very maximum that can occur at that distance when the very maximum pressure of 3.1 MPa occurs at the centreline.

7.2.6 25-mm-Thick Walls

Fig. 7.11 shows the time history of various parameters at distances of 2.5, 5, 7.5, 10, and 12.5 mm from the exposed surfaces of a 25-mm-thick wall exposed to fire from both sides for 60 minutes. Fig. 7.12 illustrates the distribution after 5, 8, 10, 12, and 15 minutes of exposure. There is a cool zone along the centreline up to 5 minutes of exposure, and the temperature along the centreline reaches 100°C, and thus the cool zone is eliminated, after 5 minutes. When the temperature reaches 100°C at the centreline, the pore pressure increases at a very high rate. After 8 minutes, the very maximum pore pressure is 2.5 MPa. Then, the pore pressure decreases. The second increase of the pressure from 2.4 MPa to 2.75 MPa is unrealistic (as noted for the 75 mm wall). Again, when the very maximum pressure occurs along the centreline, the pore pressure at any distance from any of the exposed surfaces is the very maximum that can occur at that distance.

From the results of this section, the effect of time of exposure to fire is evident; provided that spalling does not occur, when the time of exposure increases, a greater very maximum pore pressure occurs in the middle of a thicker section exposed to fire from opposite sides.

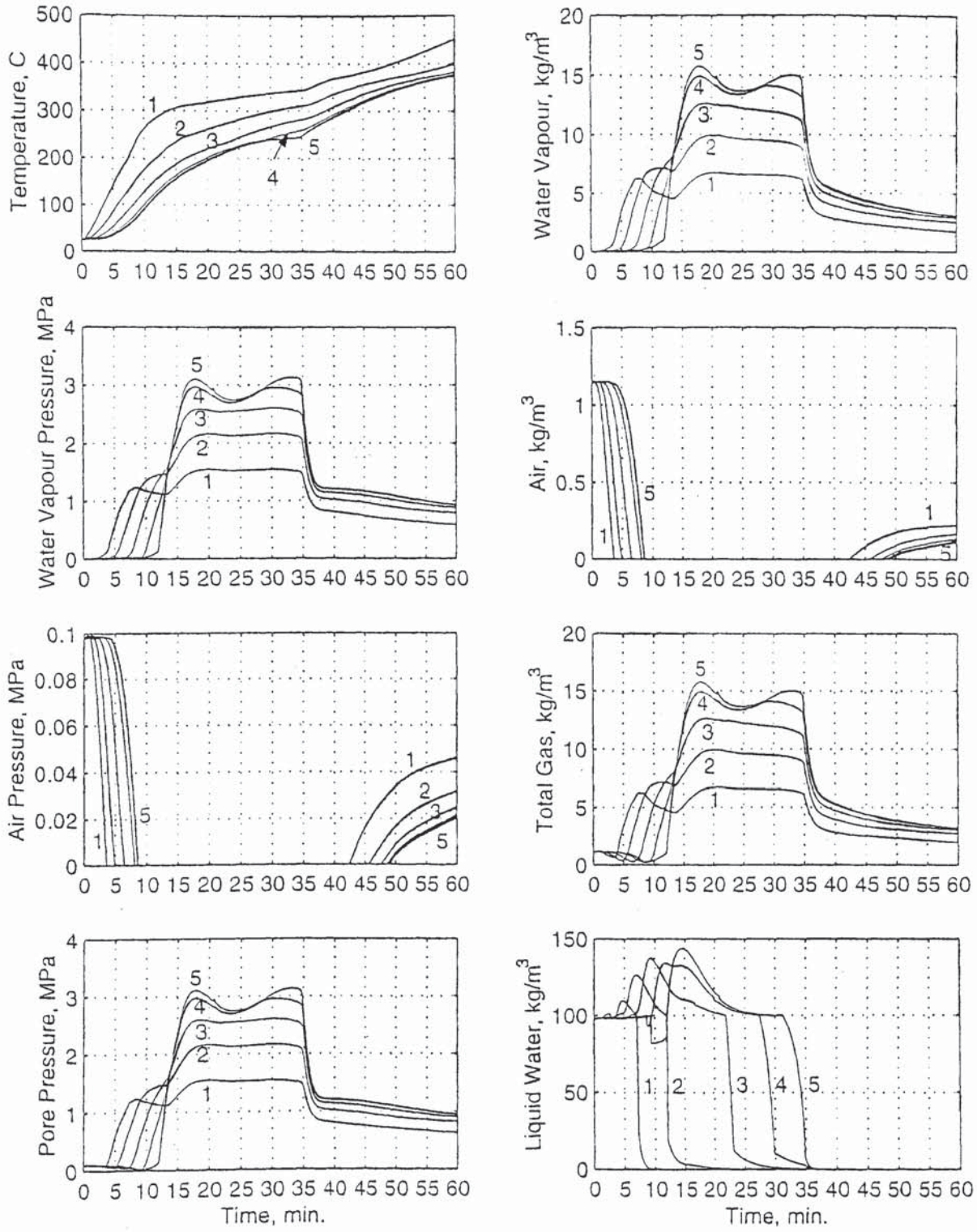

Fig. 7.9: Time history of T, in °C, ρ_v, in kg/m^3, P_v, in MPa, ρ_a, in kg/m^3, P_a, in MPa, ρ_g, in kg/m^3, P_g, in MPa, and $\varepsilon_l \rho_l$, in kg/m^3, at (1) 5, (2) 10, (3) 15, (4) 20, and (5) 25 mm from any of the fire-exposed surfaces of a 50-mm-thick concrete wall exposed to fire from both sides for 60 minutes.

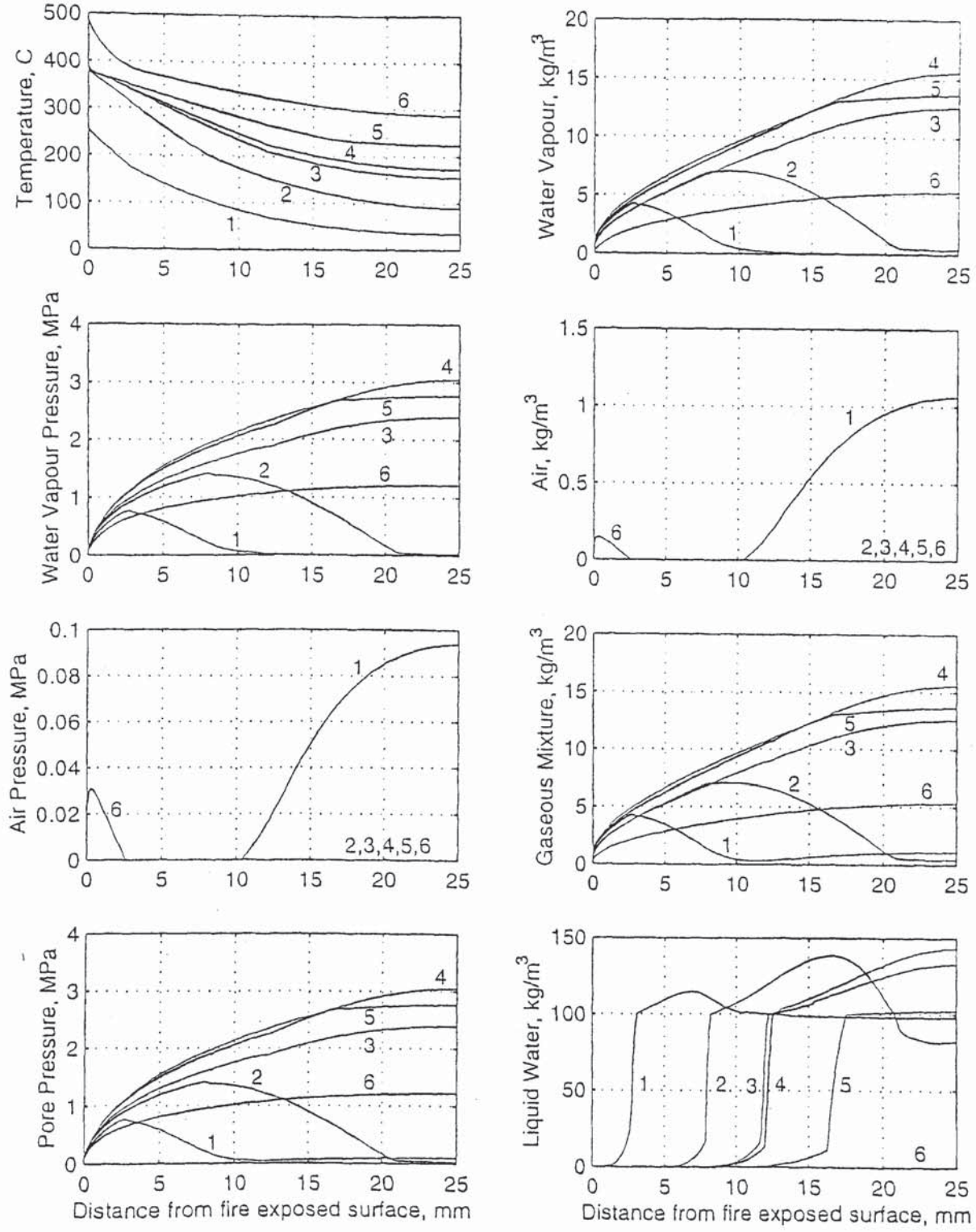

Fig. 7.10: Distribution of T, in °C, ρ_v, in kg/m^3, P_v, in MPa, ρ_a, in kg/m^3, P_a, in MPa, ρ_g, in kg/m^3, P_g, in MPa, and $\varepsilon_l \rho_l$, in kg/m^3, after (1) 5, (2) 10, (3) 15, (4) 17, (5) 25, and (6) 40 minutes of exposure to fire in a 50-mm-thick concrete wall exposed to fire from both sides for 60 minutes.

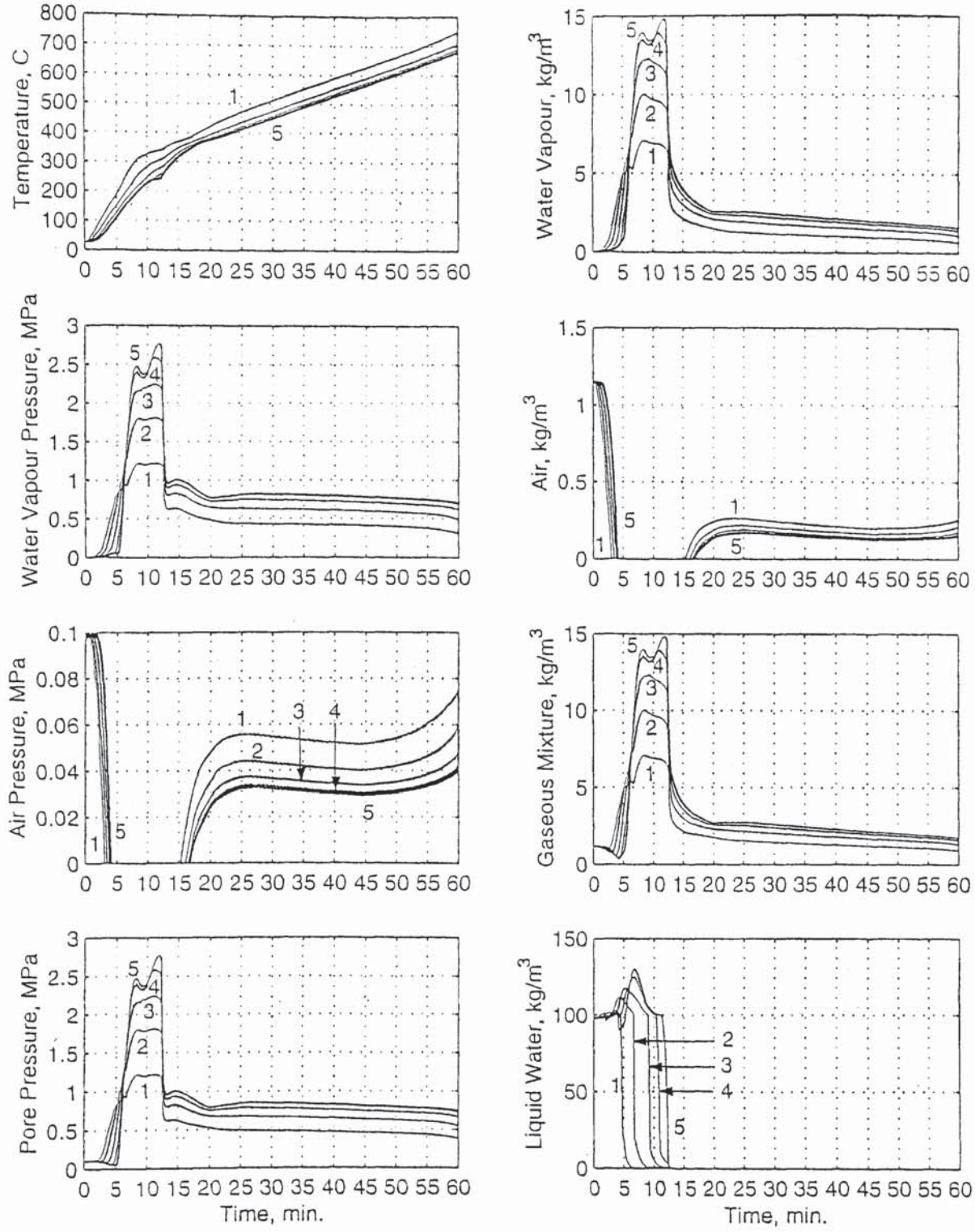

Fig. 7.11: Time history of T, in °C, ρ_v, in kg/m^3, P_v, in MPa, ρ_a, in kg/m^3, P_a, in MPa, ρ_g, in kg/m^3, P_g, in MPa, and $\varepsilon_l \rho_l$, in kg/m^3, at (1) 2.5, (2) 5, (3) 7.5, (4) 10, and (5) 12.5 mm from any of the fire-exposed surfaces of a 25-mm-thick concrete wall exposed to fire from both sides for 60 minutes.

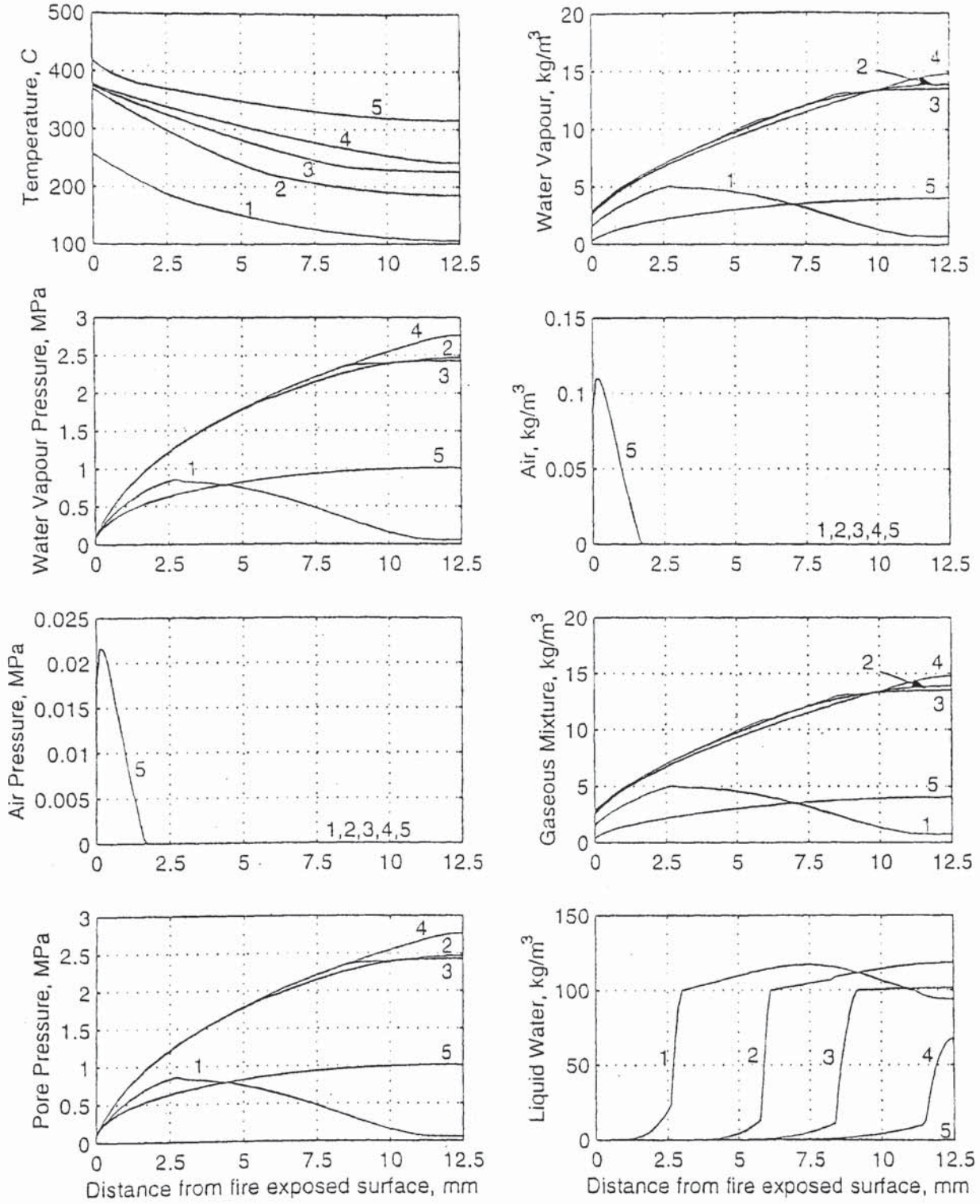

Fig. 7.12: Distribution of T, in °C, ρ_v, in kg/m^3, P_v, in MPa, ρ_a, in kg/m^3, P_a, in MPa, ρ_g, in kg/m^3, P_g, in MPa, and $\varepsilon_l \rho_l$, in kg/m^3, after (1) 5, (2) 8, (3) 10, (4) 12, and (5) 15 minutes of exposure to fire in a 25-mm-thick concrete wall exposed to fire from both sides for 60 minutes.

7.3 EFFECT OF TYPE OF EXPOSURE TO FIRE

As far as spalling is concerned, exposure of a concrete wall to fire from one side, or three sides of a column, could be the severest case, since the non-exposed surface is less cracked, and thus is less permeable for the water vapour to be released to the environment. However, as far as the magnitude of the pressure is concerned, exposure to fire from one side is the least severe case a concrete member can be subjected to. Nevertheless, apart from Tenchev and Khalafallah (2000) and Tenchev *et al.* (2001a and b), it appears that most, if not all, researchers, e.g. Bažant and Thonguthai (1979), Šelih *et al.* (1994), Šelih and Sousa (1996), and Ahmed and Hurst (1997), who are concerned with the magnitude of the pressure determine the pressure in sections exposed to heat from one side only. Furthermore, it appears that all researchers consider only thick heated sections.

However, as far the magnitude of the pressure is concerned, it does not make any difference whether the cool zone is eliminated from the section exposed to fire from one side or whether the section is thick or thin. The maximum pressure that can occur in unsealed walls exposed to fire from one side cannot exceed the maximum pressure that can occur when there is a cool zone since, when the cool zone is eliminated and the temperature of the non-exposed surface reaches 100°C, the water vapour produced from the evaporating water at the non-exposed surface is released to the environment and the maximum pressure starts decreasing until it becomes equal to the standard atmospheric pressure when it reaches the surface, i.e. when the entire free water evaporates.

Šelih *et al.* and Šelih and Sousa considered 200-mm-thick walls exposed to fire from one side according to ASTM E-119 the failure criterion of which is that the temperature at the unexposed surface is 139°C, and thus considered walls in which the cool zone is eliminated. Nevertheless, they calculated maximum pressures that do not exceed 1.3 MPa. Also, it can be seen from the results of Ahmed and Hurst (Figs. 2.22 and 2.24) that the maximum pressure of 0.75 is reached when the cool zone is eliminated after 120 minutes of exposure to fire while exposure to fire for 180 and 240 minutes results in maximum pressures of 0.65 and 0.55 MPa, respectively.

7.4 DISCUSSION

The durations of fires encountered in tunnels are significantly longer than those encountered in buildings which are normally up to 2 h (Khoury, 2000). For example, the durations of the Great Belt Tunnel fire (Tait and Hoj, 1996) and the Channel Tunnel fire (Coats, 1996) were 7 and 9 h, respectively. Nevertheless, it appears that, even in a tunnel fire, the 400-mm-thick wall behaves as if each fire-exposed face bounds a semi-infinite continuum since, after 4 h of exposure to fire, a substantial cool zone towards which water vapour can migrate remains and the maximum pore pressure does not exceed 1.6 MPa. Similarly, heating of unsealed concrete members on one side only cannot produce pore pressures greater than those occurring when there is a cool zone, since the water vapour cannot increase further when the temperature of the non-exposed side reaches 100°. Both cases cannot produce pore pressures of significantly high magnitude to produce spalling. Thus, regardless of the assumptions regarding diffusion, if spalling occurs on a thick member whether under one or two sided heating or on a thin member heated on one side, then such spalling must be due to high thermal stresses.

On the other hand, from the results of the 150-25 mm thick walls, the first, and most important, observation is:

The maximum pore pressures in heated concrete sections can be more than twice those calculated by different researchers and thought to be the maximum that can occur so far. These "very maximum" pore pressures occur at the centres of concrete sections exposed to heat from opposite sides after certain periods of time.

The following hypothesis is proposed to explain this observation:

Following the elimination of the cool zone at the centre of a concrete section exposed to fire from opposite sides for a certain period of time, the water vapour contents, and thus vapour and pore pressures, from the opposite sides of the section are *accumulated* at the centre of the section as the two evaporation fronts approach each other. The maximum water vapour contents, vapour pressures, and pore pressures from both sides of the section *reach* the centre after some time, and are *accumulated*.

At first, it may appear difficult to explain why these very maximum values of the water vapour content and vapour and pore pressures are *more* than twice those obtained when there is a cool zone. From the hypothesis proposed above, and due to the exposure to fire being from both sides, these very maximum values may be expected to be the sum of the maximum values obtained from the two peaks as they approach each other at the centreline. Thus, they may be expected to be exactly twice the maximum values obtained when there is a cool zone. However, it should be noted that, when the two peaks reach the centreline of a wall section (or the centroid of a column section), the temperature at that location is about 200°C, and thus the free water at the over-saturated centre is already evaporating. Thus, the maximum water vapour content in the middle is the sum of the maximum vapour contents from the two evaporation fronts plus an additional amount of water vapour that results from the evaporation of the free water in the over-saturated centre. Consequently, the very maximum pore pressure at the centre is more than two times greater than the maximum value obtained when there is a cool zone.

It appears that, unless it is strongly believed that the pressure cannot be the main cause of explosive spalling regardless of its magnitude, this finding may make the mechanism of explosive spalling in thin sections less debateable. It leads to the conclusion that the pore pressure, along with the reduced tensile strength of concrete at high temperature, can be the main cause of explosive spalling in thin members, since spalling is exacerbated in these members where very maximum pressures occur, and thus the relation between the pressure and explosive spalling seems obvious. Furthermore, some researchers argue that the magnitudes of the pressure cited so far are simply not high enough to cause tensile failure. Obviously, this first observation, and thus the ratio of the very maximum pressure to the maximum pressure that can occur when there is a cool zone, is independent of the model used. Thus, if concrete sections heated on opposite sides for periods of time long enough for the peaks to reach the centres were considered, Bažant and Thonguthai (1978) would have calculated a pressure as high as that (2.5 MPa) calculated by Bažant and Thonguthai (1979) that was considered high enough to cause spalling, Bažant and Thonguthai (1979) would have calculated a very maximum pressure of nearly 6 MPa, and Tenchev *et al.* (2001b) would have calculated a very maximum pressure of about 5 MPa.

The second most important observation, which confirms the validity of the hypothesis proposed, is:

A very maximum pore pressure can occur in a concrete section of *any* thickness exposed to fire from opposite sides, depending on the time of exposure to fire.

The third observation is:

When the very maximum pore pressure that can occur in a heated concrete section is reached at the centre of the section, the pore pressure at any location is the very maximum that can occur at that location.

This is one of the most important observations since, in reinforced concrete sections, it is the value of the pressure at the reinforcement, rather than that in the middle of a heated wall or that at the centroid of a heated column, that is of the greatest concern. In 100-mm-thick reinforced concrete walls, for example, if the concrete cover is 25 mm, the cover will be subjected to 2.7 MPa of pressure after 55 minutes of exposure to fire.

It is also observed that there is a critical time for heated concrete sections exposed to heat from opposite sides after which the cool zone is eliminated and after which the maximum pore pressure that can occur when there is a cool zone is no longer a maximum, and there is a maximum time at which the very maximum pore pressure that can occur in a heated concrete section is reached. The critical and maximum times are a function of the thickness.

For 150 mm-thick walls, the critical time at which the cool zone is eliminated, and at which the sum of the pore pressures from both sides of the wall starts exceeding the maximum value that can be obtained when there is a cool zone, is about 65 minutes of exposure to fire, and the maximum time at which the very maximum pore pressure occurs is 115 minutes.

Denoting the critical time as t_{crit} and the maximum time as t_{max}, the critical and maximum times for the 150-mm-thick wall are $t_{crit} \approx 65$ minutes and $t_{\max} \approx 115$ minutes.

For 100 mm-thick walls, $t_{crit} \approx 32$ minutes and $t_{\max} \approx 55$ minutes. An important observation is that, after 55 minutes of exposure of the 100-mm-thick wall to fire, the pore pressure starts decreasing after reaching its very maximum magnitude; after 60 minutes, the pore pressure is slightly smaller than the very maximum pressure obtained after 55 minutes. This is expected since, after 55 minutes, the free water in the over-saturated centreline of the wall is evaporating, and is decreasing until the entire free water evaporates. Thus, when the peaks from the two sides reach the centreline while the source of water vapour, i.e. the free water, in the over-saturated centreline is already decreasing, the pore pressure must start decreasing after reaching the very maximum, and cannot increase again.

The very maximum pore pressure is lower than that obtained in the middle of the 150-mm-thick wall, because the time available for condensation of water vapour is smaller than that available in the 150 mm-thick wall, and thus the maximum free water content available for evaporation in the over-saturated centreline of the 100-mm-thick wall is smaller than that in the over-saturated centreline of the 150-mm-thick wall.

For 75-mm-thick walls, $t_{crit} \approx 20$ minutes and $t_{max} \approx 33$ minutes. Like the 100-mm-thick wall, the water vapour content, and thus vapour and pore pressures, along the centreline starts decreasing after reaching its maximum value when the time of exposure is 33 minutes, and continue to decrease until the time of exposure is 50 minutes. However, when the time of exposure exceeds 50 minutes, the vapour content and vapour and pore pressures start increasing again, and continue to increase until the time of exposure reaches 60 minutes. This behaviour is unrealistic. As explained in the case of the 100-mm-thick wall, the decrease of the pore pressure after reaching its very maximum value at the middle of the section is expected. However, when the peaks from the two sides of the wall reach the centreline, the free water at the centreline is already decreasing. Thus, the vapour content, and hence vapour and pore pressures, cannot increase again; it must start decreasing. The reason for these unrealistic results when the time of exposure to fire exceeds the time required for the peaks to reach the middle of the section is unclear.

For 50-mm-thick walls, $t_{crit} \approx 12$ minutes and $t_{max} \approx 17$ minutes, and, for 25-mm-thick walls, $t_{crit} \approx 5$ minutes and $t_{max} \approx 8$ minutes. After 5 minutes of exposure of the 25-mm-thick wall to fire, the maximum pore pressure that can be obtained when there is a cool zone is 0.9 MPa at a distance of about 2.5 mm from the either of the fire-exposed surfaces. This maximum pressure is smaller than the maximum pressure of 1.5 that can be obtained in thicker sections when there is a cool zone, since the critical, and even the maximum, time is smaller than that (12 minutes) required for the maximum pressure of 1.5 MPa to occur when there is a cool zone.

From these results, the ratio between t_{max} and t_{crit} lies between 1.4 and 1.8. Also, regression analysis leads to the following expressions for the variation of t_{crit} and t_{max}, in min, with thickness a, in mm:

$$t_{crit} = 2.278 + 6.218 \times 10^{-2} a + 2.37 \times 10^{-3} a^2 \qquad (7.1a)$$

for which the correlation coefficient $R = 0.9998$ ($R^2 = 0.9997$), and

$$t_{max} = 3.825 + 3.873 \times 10^{-2} a + 4.688 \times 10^{-3} a^2 \qquad (7.1b)$$

for which the correlation coefficient $R = 0.99995$ ($R^2 = 0.9999$).

The variation of t_{crit} and t_{max} according to (7.1) is shown in Fig. 7.13.

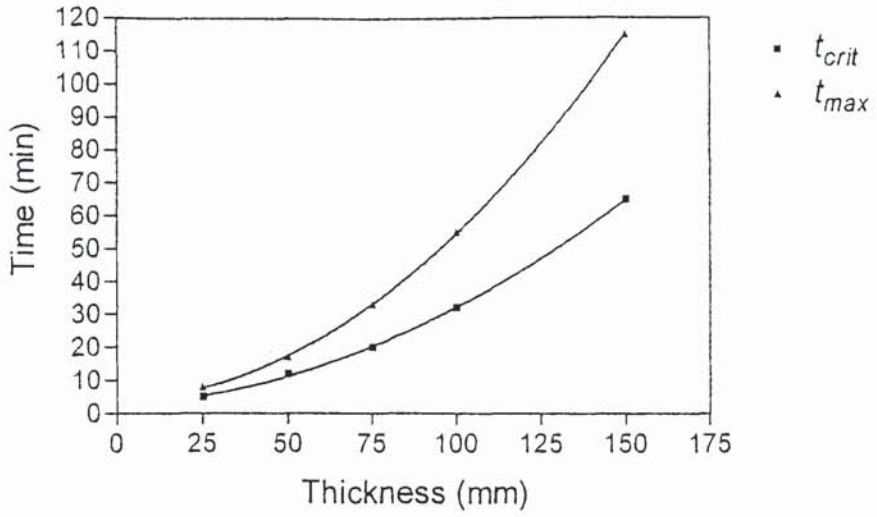

Fig. 7.13: Variation of critical and maximum times with thickness of wall.

If it is assumed that the variations of t_{crit} and t_{max} are proportional to the square of thickness only, then the following expressions are obtained:

$$t_{crit} = 4.492 + 0.0027 a^2 \qquad (7.2a)$$

for which the coefficient of correlation $R = 0.9994$ ($R^2 = 0.9989$), and

$$t_{max} = 5.2 + 0.0049 a^2 \qquad (7.2b)$$

for which the correlation coefficient $R = 0.9999$ ($R^2 = 0.9998$).

The variations of t_{crit} and t_{max} with the square of thickness of the wall according to (7.2) are demonstrated in Fig. 7.14.

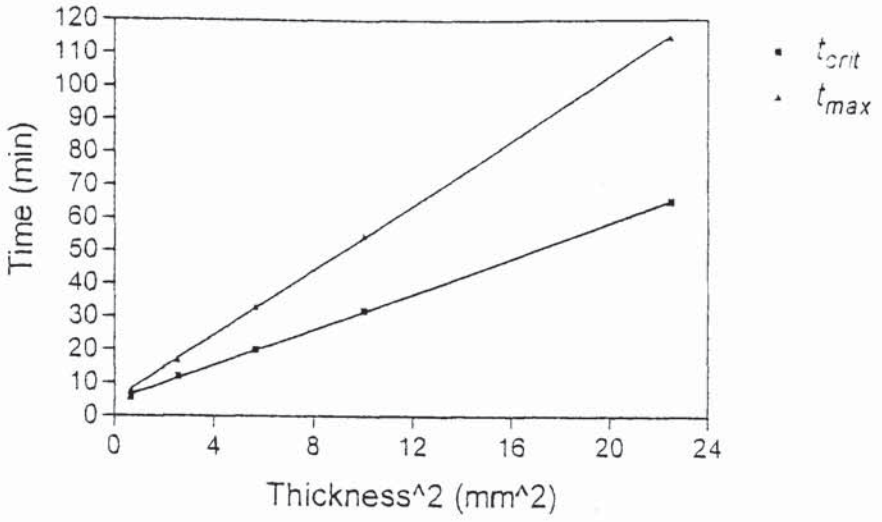

Fig. 7.14: Variation of critical and maximum times with square of thickness of wall

It may be argued that, theoretically, the critical and maximum times should be zero when the thickness is zero, and thus the constants in (7.1) and (7.2) should have been zero. However, extrapolating to the case where no wall exists ($a = 0$) is meaningless as there can be no diffusion; a very thin wall must suffer diffusion, and thus t_{crit} and t_{max} must be greater than zero. Thus, (7.1) and (7.2) are valid for all practical values of a. However, it is suggested that when a approaches zero, i.e. for very small a, t_{crit} and t_{max} will decrease sharply with a.

From the results obtained for the very maximum pore pressures, the fourth observation is:

The magnitude of the very maximum pore pressure is a function of the thickness.

The key results are tabulated in Table 7.1. From these results, nonlinear regression analysis leads to the following expression for the variation of the very maximum pressure P_{max}, in MPa, with thickness of the wall a, in mm:

$$P_{max} = 1.29 + 6.305 \times 10^{-2} a - 6.52 \times 10^{-4} a^2 + 2.435 \times 10^{-6} a^3 \qquad (7.3)$$

for which the correlation coefficient $R = 0.9998$ ($R^2 = 0.9995$).

Wall Thickness, in mm.	Maximum pressure, in MPa.	Temperature, in °C	Depth, in mm.	Time, in min.
400	1.6	200	60	230
150	4.3	200	75	115
100	3.5	200	50	55
75	3.4	200	37.5	33
50	3.1	200	25	17
25	2.5	200	12.5	8

Table 7.1: Key results in 400-25 mm thick concrete walls exposed to fire from both sides including: wall thickness and maximum pore pressure along with the temperature, depth, and time at which it occurs.

The variation of P_{max} with a according to (7.3) is shown in Fig. 7.15.

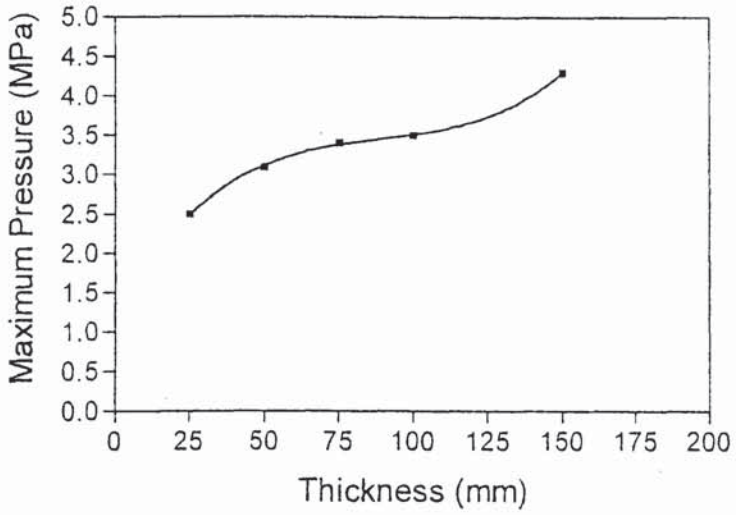

Fig. 7.15: Variation of the very maximum pore pressure, in MPa, with thickness, in mm.

However, a linear variation of the very maximum pore pressure with thickness appears to be more reasonable; linear regression leads to the following expression:

$$P_{max} = 2.292 + 0.01335a \tag{7.4}$$

for which the correlation coefficient $R = 0.9814$ ($R^2 = 0.9631$). The variation of the very maximum pressure with thickness according to (7.4) is shown in Fig. 7.16.

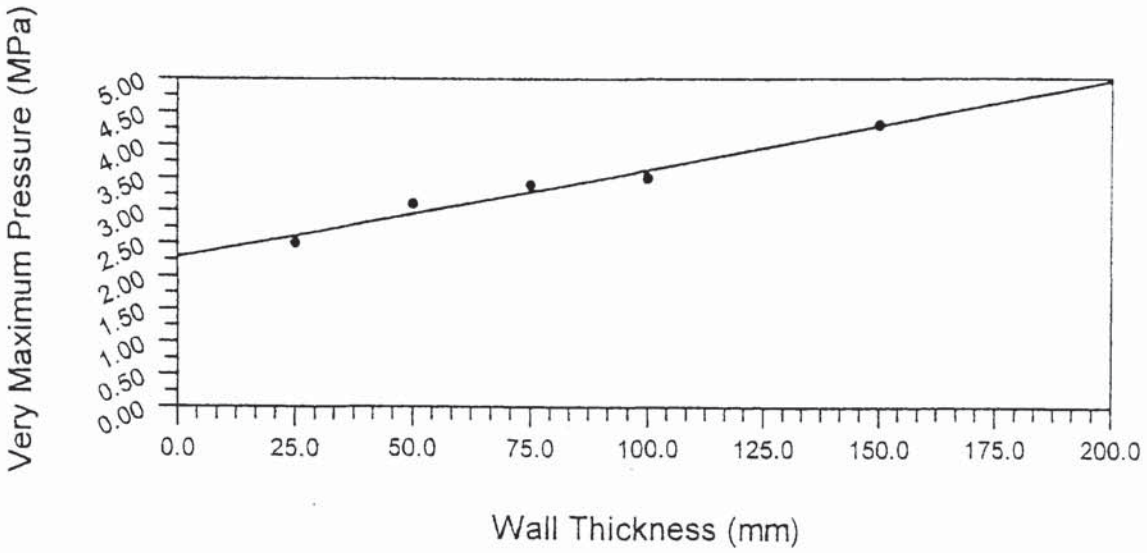

Fig. 7.16: Linear variation of the very maximum pore pressure with wall thickness.

Again, it may be argued that, theoretically, the pore pressure should be equal to the standard atmospheric pressure when the thickness of the wall is zero, and thus the constants in (7.3) and (7.4) should have been 0.101 MPa. Based on the same argument above, (7.3) and (7.4) are valid for all practical values of a, and it is suggested that, for very small a, P_{max} will decrease sharply with a.

The maximum values of the pore pressure are reached when the temperature is nearly 200°C. This is because the water at a certain distance only *starts* to evaporate when the temperature reaches 100°C at that distance after a certain time of exposure to fire, and the vapour content, and thus vapour and pore pressures, starts increasing at that particular time; the water continues to evaporate, and the vapour content and vapour and pore pressures continue to increase until they reach their maximum values after some time when the temperature at that distance reaches nearly 200°C. Of course, in systems without walls, the water remains at 100°C until it evaporates completely, since the pressure remains atmospheric. In heated concrete, however, the temperature of the water continues to increase while the water continues to evaporate due to the increase of the pressure.

The tensile strength of concrete declines with increase in temperature (Eurocode 2 1-2, 2000; Khoury, 2000). According to EC 2, the tensile strength starts decreasing linearly when the temperature reaches 100°C, and is practically zero at 600°C. Thus, at 200°C, the tensile strength is 80% of that at ambient temperature. Hence, considering the magnitudes of the pore pressure in thin members with two sided heating and the reduced strength, it appears that spalling in thin members exposed to fire from both sides is pore pressure spalling. It is also evident that the increased

susceptibility of pore pressure spalling occurring in thin members heated on opposite sides is due to the lack of a cool zone towards which water vapour can migrate, which leads to the accumulation of vapour from the two sides and thus to very maximum pressures occurring in these members.

It is important to note that, if spalling of a layer of, say, 10 mm of concrete occurs before the very maximum pressure that can occur at that distance is reached, then the thickness of the remaining section is reduced, and the very maximum pressure that corresponds to the new thickness may be higher than that required to cause spalling; thus, successive spalling is likely to occur. On the other hand, if spalling of the layer occurs only when the very maximum pressure is reached, then the likelihood of spalling of another layer occurring is smaller, since the new very maximum pressure that corresponds to the smaller thickness is smaller than that required to cause spalling. Also, if spalling removes a relatively large proportion of the section, as in explosive spalling, the boundary conditions change, and a very maximum pressure that corresponds to the new configuration is probably unlikely.

It should be noted that the same maximum pore pressure of about 1.5 MPa occurs in unsealed concrete slabs exposed to fire. However, spalling is less likely to occur in areas of sagging moment, e.g. at and near mid-span, due to the relatively large sizes and proportion of the cracks that allow the water vapour to be released to the environment, and is more likely to occur in areas of hogging moment, e.g. near fixed supports, due to the smaller sizes and proportion of the cracks which lessen the release of water vapour to the environment.

7.5 CONCLUSIONS

- The build up of pore pressure is low in thick concrete members whether under one or two sided heating, since there is a substantial cool zone towards which moisture can migrate; this is a similar solution to the semi-infinite continuum. Similarly, heating of unsealed concrete members on one side only cannot produce pore pressures of significantly high magnitude to produce spalling, since the water vapour cannot be built up further when the temperature of the non-exposed side reaches 100°C; this is the reason why the numerous investigators who have examined one sided heating, irrespective of the assumptions regarding diffusion, have only computed low pore pressures. Thus, if spalling occurs on a thick member whether under one or two sided heating or on a thin member heated on one side only, then such spalling must be due to high thermal stresses.

- For concrete walls heated on both sides, the time t_{crit} after which the maximum pore pressure starts exceeding the maximum pressure that can be reached when there is a cool zone and, on the assumption of no spalling, the time t_{max} at which the pore pressure reaches a very maximum value at the centreline are proportional to the square of the wall thickness.

- The ratio between t_{max} and t_{crit} lies between 1.4 and 1.8.

- The temperature at the location of the maximum pore pressure is about 200°C. Thus, the tensile strength at that position is 80% of the tensile strength at ambient temperature. Therefore, if spalling occurs in thin walls where there is an early build up in pore pressure, then this is more deleterious as the section suffers a high relative reduction in cross-section. If further spalling occurs, due to either continued pore pressure build up or high thermal stresses, then local, or worse global, failure could ensue.

- The reason for the enhanced propensity of pore pressure spalling occurring in thin walls with two sided heating has been conclusively demonstrated to be due to the lack of a "cool zone" towards which moisture can migrate.

- The maximum pore pressures computed in 400, 150, 100, 75, 50, and 25 mm thick walls exposed to fire on two sides are 1.6, 4.3, 3.5, 3.4, 3.1, and 2.5 MPa after 230, 115, 55, 33, 17, and 8 minutes of exposure to fire, respectively.

Having examined the heating of walls of various thicknesses from two opposite sides and drawn conclusions concerning the maximum pore pressure and time to spalling, it will be instructive to carry out a similar exercise on square columns heated on all four sides. This will be performed in the next chapter.

CHAPTER 8

CONCRETE COLUMNS IN FIRE

8.1 INTRODUCTION

As mentioned in Chapter 7, one of the major objectives of this study is to investigate the effect of thickness of concrete sections exposed to fire. In that chapter, walls of different thicknesses exposed to fire were investigated. In this chapter, 400×400, 300×300, 200×200, 100×100, 50×50, and 25×25 mm columns subjected to fire on all four sides for 60 minutes will be examined. Similar to the 75, 50, and 25-mm-thick walls, the 50×50 and 25×25 mm columns are included in order to determine the overall behaviour pattern whilst recognising the impracticality of these sizes.

Furthermore, now that a tenable expression that determines the diffusivities of gases in heated concrete has been developed, another major objective is to determine the actual maximum pressures that can occur in columns. The magnitudes of various parameters along a *diagonal* will be examined, since the temperatures along a diagonal between two adjacent sides exposed to fire are naturally higher than those occurring along the normal to the centreline of a wall or the centroidal x or y-axis of a column, and thus the maximum pressures are expected to be higher in columns; Fig. 2 of Appendix E confirms this fact. The time of exposure will be limited to 60 minutes, since spalling usually occurs within the first 30 minutes of exposure.

For the 400×400 mm column, a previous work (Tenchev and Khalafallah, 2000) (Appendix E) in which molecular diffusivity was adopted will be depended on. For the remaining columns, concrete diffusivity will be used. It is important to note that, in order to define a location along the diagonal, the origin is considered at the middle of the left hand side of the section, and, for convenience, only the x-coordinates of points along the diagonal will be given in the distribution. For example, the upper left corner of a 300×300 mm column is the point (0, 150), but will be denoted as 0 in Fig. 8.2, while the centroid, i.e. the point (150,0) will be denoted as 150 in Fig. 8.2.

8.2 EFFECT OF THICKNESS

8.2.1 400×400 mm Columns

From Fig. 2 (Appendix E), it can be seen that, within 60 minutes of exposure to fire, the 400×400 mm column is a thick section in which the temperature and pore pressure at the centroid C are equal to ambient after 60 minutes of exposure. The maximum pressures after 20 and 60 minutes of exposure are approximately 2.5 and 3 MPa, respectively. Since molecular diffusivity was adopted in this previous work, and depending on the investigations carried out in Chapters 3 and 6 in which it was demonstrated that the real diffusivity in concrete is smaller than molecular diffusivity and that the pore pressures resulting from concrete diffusivity are smaller than those resulting from molecular diffusivity, it is evident that the computed magnitude of the maximum pressure (3 MPa) that can occur in thick columns after 60 minutes of exposure to fire is overestimated. Thus, other thick sections (300×300 and 200×200 mm) exposed to fire on all four sides for 60 minutes will now be examined using concrete diffusivity.

8.2.2 300×300 mm Columns

Fig. 8.1 shows the time history of various parameters at distances of 10.6, 21.2, 42.4, 63.6, and 84.9 mm from the upper left corner along the diagonal of a 300×300 mm column exposed to fire on all four sides for 60 minutes. The distribution of various parameters along the diagonal after 5, 10, 20, 30, and 60 minutes of exposure is illustrated in Fig. 8.2. Within 60 minutes of exposure to fire, the 300×300 mm column is a thick section in which, after 60 minutes, the temperature at the centroid is that of the ambience and the pore pressure at the centroid does not exceed the standard atmospheric pressure. It is evident that, when concrete diffusivity is used, the maximum pore pressures along the diagonal after 5, 10, 20, and 30 minutes of exposure are 1.4, 1.9, 2.2, and 2.2, respectively. These results appear to be realistic. However, the pore pressure of 1.8 MPa after 60 minutes is unrealistic, as the pressure after 30 minutes is 2.2 MPa. As discussed in Chapter 4, since concrete diffusivity is adopted, this section requires a denser mesh than the 40×40 elements mesh used, which is computationally expensive and impractical. The results of the next thick column (200×200 mm) examined in Section 8.2.3 should confirm whether or not the pressure of 2.2 MPa is the maximum that can occur in thick columns exposed to fire when concrete diffusivity is used.

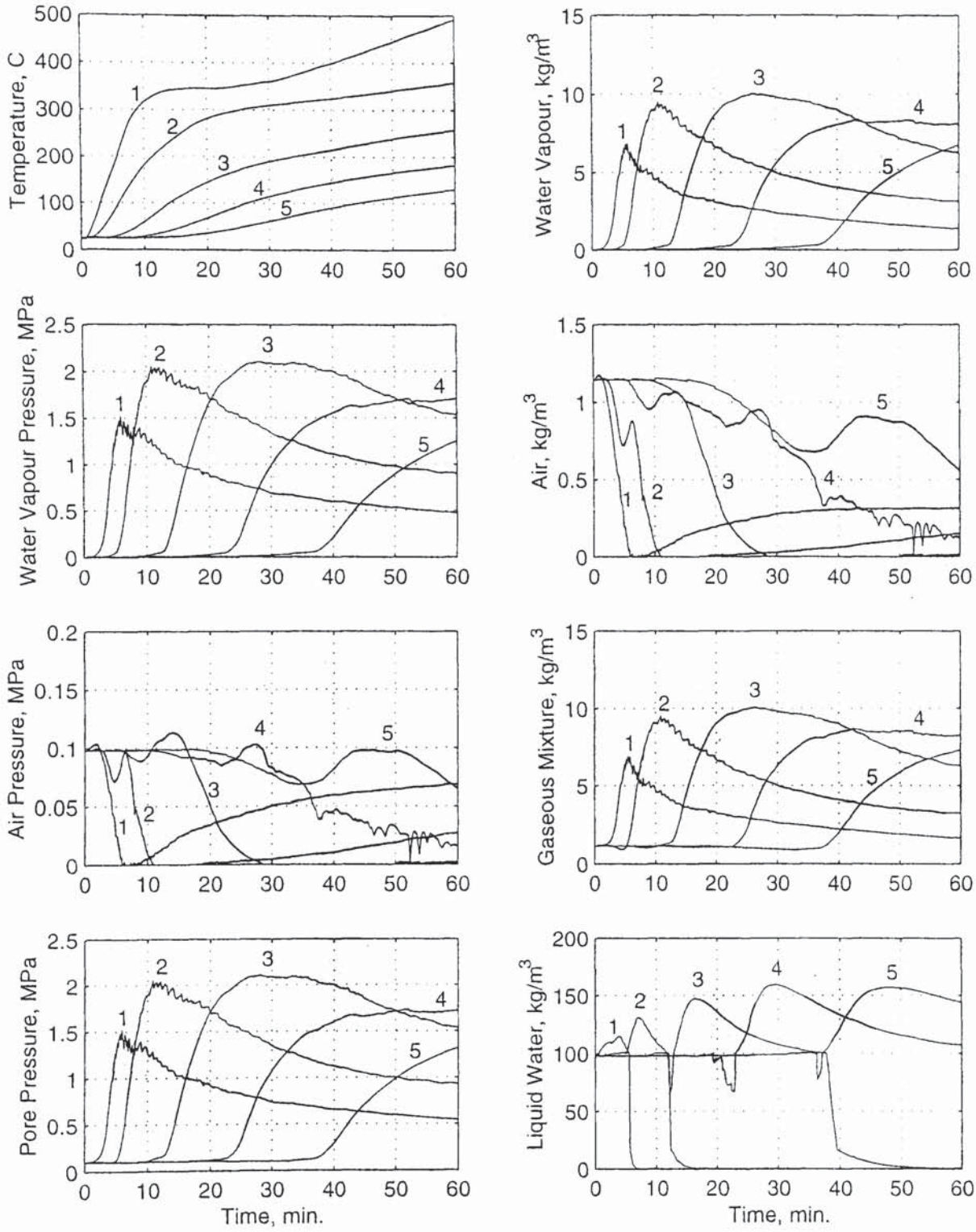

Fig. 8.1: Time history of T, in °C, ρ_v, in kg/m^3, P_v, in MPa, ρ_a, in kg/m^3, P_a, in MPa, ρ_g, in kg/m^3, P_g, in MPa, and $\varepsilon_l \rho_l$, in kg/m^3, at distances of (1) 10.6, (2) 21.2, (3) 42.4, (4) 63.6, and (5) 84.9 mm starting from a cross-section's corner along a diagonal of a 300×300 mm column exposed to fire on all four sides for 60 minutes.

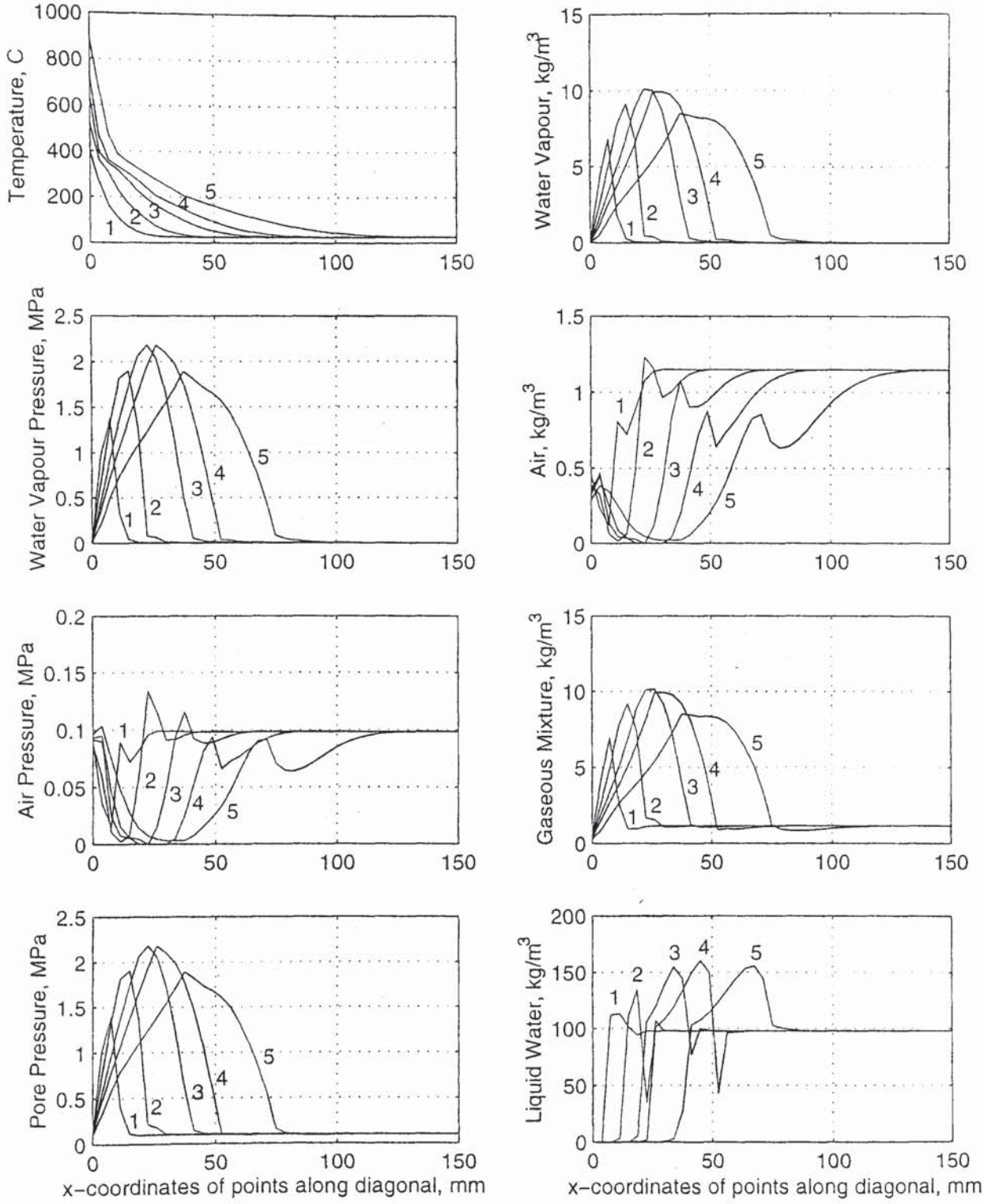

Fig. 8.2: Distribution of T, in °C, ρ_v, in kg/m^3, P_v, in MPa, ρ_a, in kg/m^3, P_a, in MPa, ρ_g, in kg/m^3, P_g, in MPa, and $\varepsilon_l \rho_l$, in kg/m^3, after (1) 5, (2) 10, (3) 20, (4) 30, and (5) 60 minutes of exposure along a diagonal of a 300×300 mm column exposed to fire on all four sides for 60 minutes; only x-coordinates of points along diagonal are shown.

8.2.3 200×200 mm Columns

The time history of various parameters at distances of 14.1, 28.3, 42.4, 56.6, and 70.7 mm from a corner along the diagonal of a 200×200 mm column exposed to fire on all four sides for 60 minutes is illustrated in Fig. 8.3. Fig. 8.4 shows the distribution of various parameters along the diagonal after 5, 10, 30, and 60 minutes of exposure. Fig. 8.4 confirms that, within 60 minutes of exposure to fire, the 200×200 mm column is a thick section in which, after 60 minutes, the temperature at the centroid is lower than 100°C and the pore pressure at the centroid does not exceed the standard atmospheric pressure. It also shows that, when concrete diffusivity is used, the maximum pore pressures along a diagonal after 5, 10, 30, and 60 minutes of exposure to fire are 1.4, 2.1, 2.2, and 2.2 MPa, respectively. These results confirm that, when concrete diffusivity is used, the maximum pressure that can occur in thick columns exposed to fire is about 2.2 MPa.

8.2.4 100×100 mm Columns

Fig. 8.5 shows the time history of various parameters at distances of 7.1, 14.1, 28.3, 42.4, 56.6, and 70.7 mm (the centroid) from a corner along the diagonal of a 100×100 mm column exposed to fire on all four sides for 60 minutes. The distribution of various parameters along a diagonal after 5, 10, 20, 35, and 60 minutes of exposure is illustrated in Fig. 8.6. From the time history of temperature, it can be seen that the cool zone is eliminated from the entire section when the temperature at the centroid reaches 100°C after about 24 minutes of exposure to fire; this is the critical time for the 100×100 mm column. Before the critical time is reached, the maximum pore pressure does not exceed 2.2 MPa. This re-confirms that, when concrete diffusivity is adopted, the maximum pressure that can be reached in thick columns exposed to fire on all four sides is 2.2 MPa. Also, Fig. 8.6 illustrates that the maximum pore pressure after 20 minutes of exposure is 2.2 MPa at the point (20,30) (shown as 20), i.e. at 28.3 mm along a diagonal.

The very maximum pore pressure that can occur at the centroid of this column is 4 MPa after 35 minutes of exposure; this is the maximum time for the 100×100 mm column.

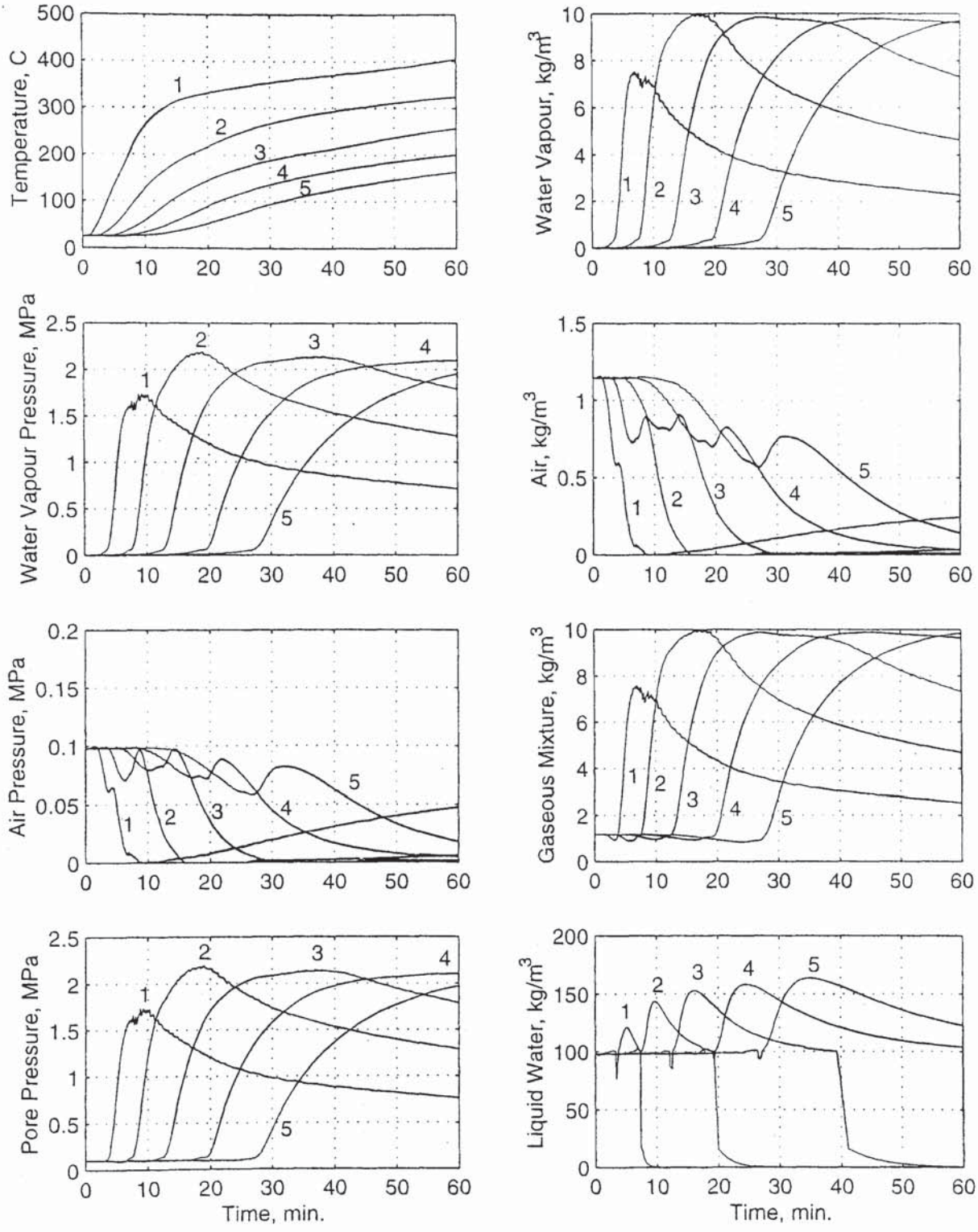

Fig. 8.3: Time history of T, in °C, ρ_v, in kg/m^3, P_v, in MPa, ρ_a, in kg/m^3, P_a, in MPa, ρ_g, in kg/m^3, P_g, in MPa, and $\varepsilon_l \rho_l$, in kg/m^3, at distances of (1) 14.1, (2) 28.3, (3) 42.4, (4) 56.6, and (5) 70.7 mm starting from a cross-section's corner along a diagonal of a 200×200 mm column exposed to fire on all four sides for 60 minutes.

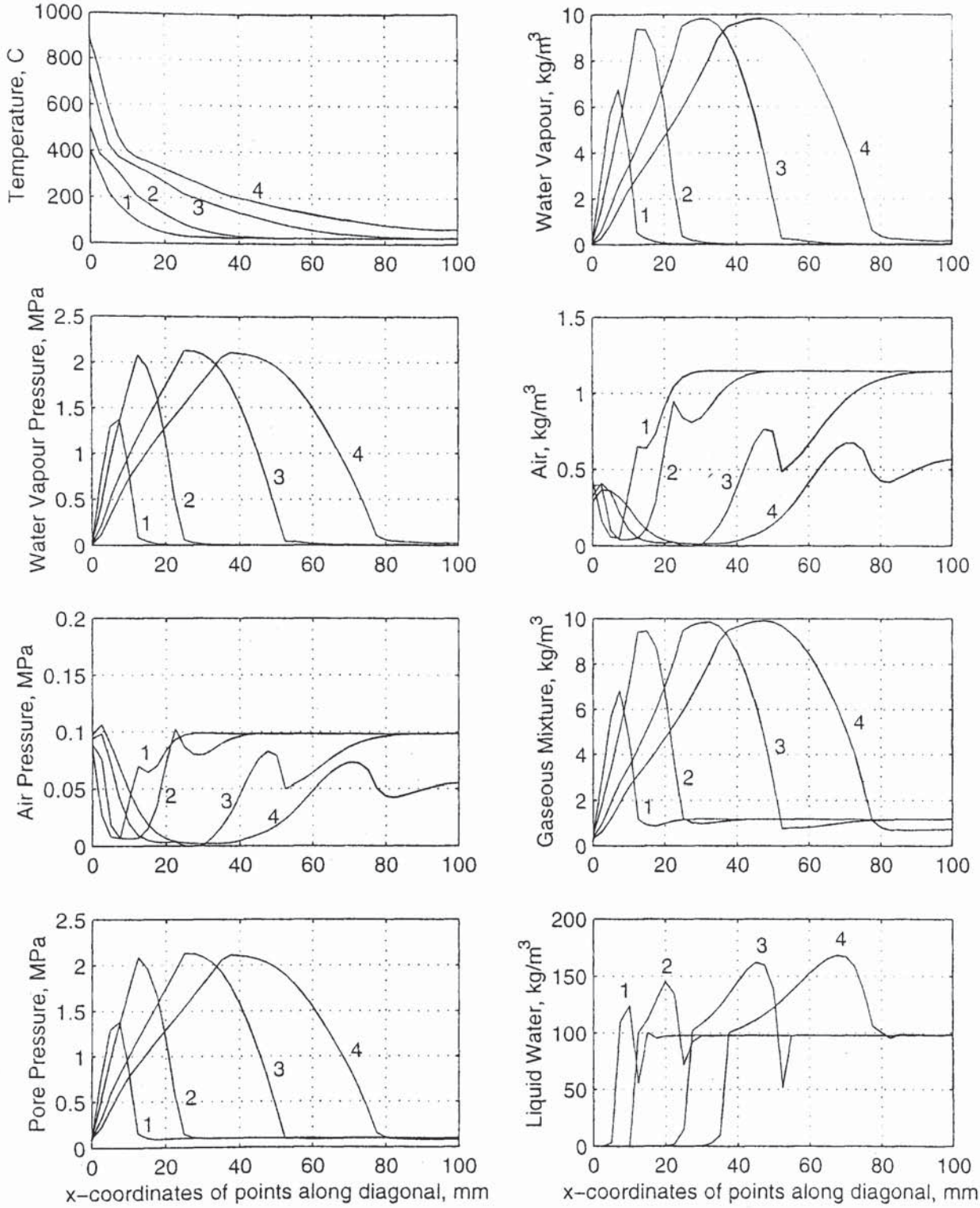

Fig. 8.4: Distribution of T, in °C, ρ_v, in kg/m^3, P_v, in MPa, ρ_a, in kg/m^3, P_a, in MPa, ρ_g, in kg/m^3, P_g, in MPa, and $\varepsilon_l \rho_l$, in kg/m^3, after (1) 5, (2) 10, (3) 30, and (4) 60 minutes of exposure to fire along a diagonal of a 200×200 mm column exposed to fire on all four sides for 60 minutes; only x-coordinates of points along diagonal are shown.

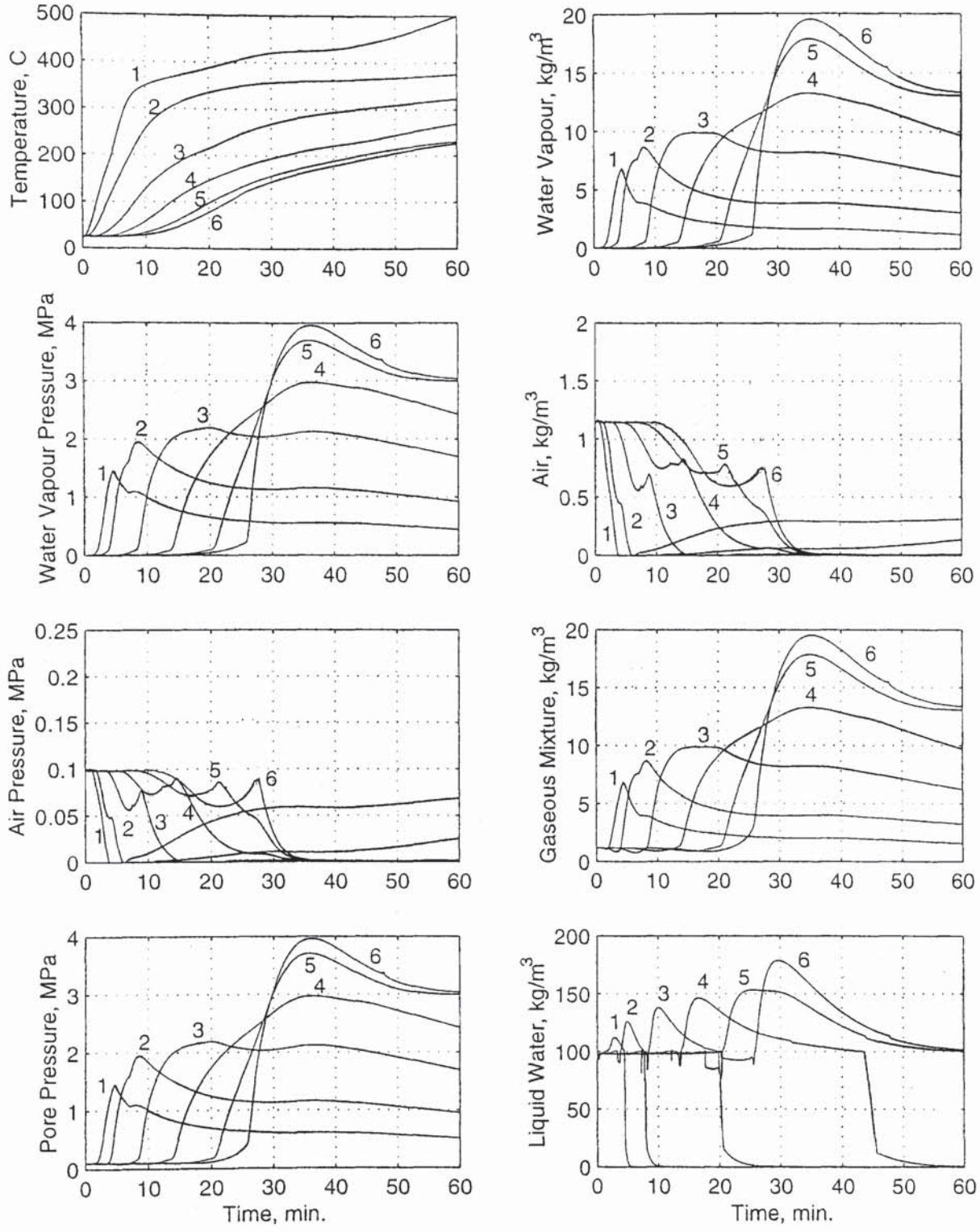

Fig. 8.5: Time history of T, in °C, ρ_v, in kg/m^3, P_v, in MPa, ρ_a, in kg/m^3, P_a, in MPa, ρ_g, in kg/m^3, P_g, in MPa, and $\varepsilon_l \rho_l$, in kg/m^3, at distances of (1) 7.1, (2) 14.1, (3) 28.3, (4) 42.4, (5) 56.6, and (6) 70.7 mm (the centroid) starting from a corner along a diagonal of a 100×100 mm column exposed to fire on all four sides for 60 minutes.

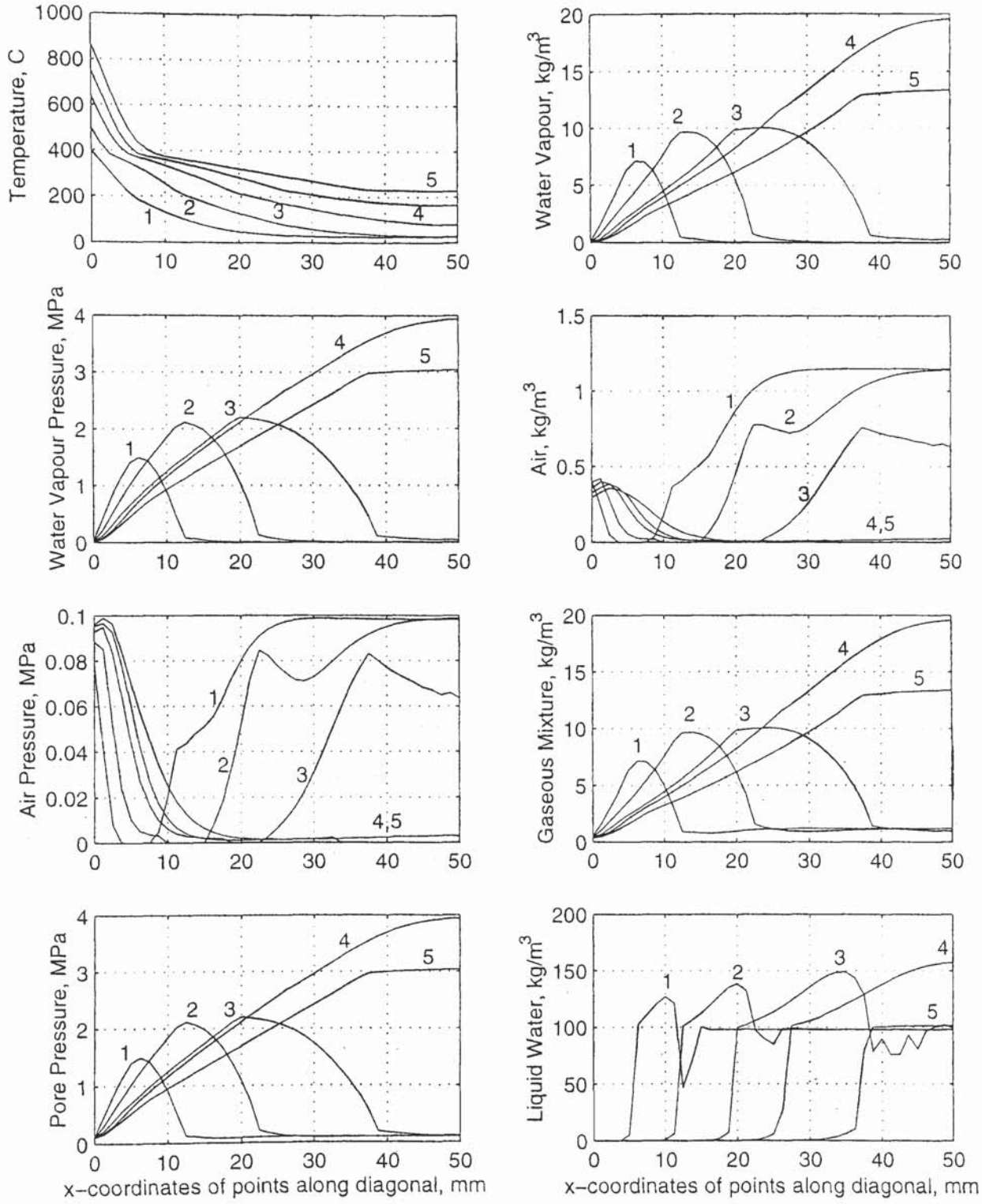

Fig. 8.6: Distribution of T, in °C, ρ_v, in kg/m^3, P_v, in MPa, ρ_a, in kg/m^3, P_a, in MPa, ρ_g, in kg/m^3, P_g, in MPa, and $\varepsilon_l \rho_l$, in kg/m^3, after (1) 5, (2) 10, (3) 20, (4) 35, and (5) 60 minutes of exposure to fire along a diagonal of a 100×100 mm column exposed to fire on all four sides for 60 minutes; only x-coordinates of points are shown.

8.2.5 50×50 mm Columns

The time history of various parameters at distances of 7.1, 14.1, 21.2, 28.3, and 35.4 mm (the centroid) from a corner along the diagonal of a 50×50 mm column exposed to fire on all four sides for 60 minutes is illustrated in Fig. 8.7. Fig. 8.8 shows the distribution of various parameters along the diagonal after 5, 10, 12, 25, and 60 minutes of exposure to fire. Fig. 8.7 illustrates that the cool zone is eliminated after 8 minutes of exposure to fire (the critical time), and the pore pressure at the centroid starts increasing at a very high rate and reaches a very maximum magnitude of 3.7 MPa after 12 minutes (the maximum time). Fig. 8.8 shows that, after 10 minutes, the maximum pressure is 2.5 MPa at 12.5 mm along the diagonal, which is greater than 2.2 MPa that occurs when there is a cool zone since this time of exposure is greater than the critical time of 8 minutes.

8.2.6 25×25 mm Columns

Fig. 8.9 illustrates the time history of various parameters at distances of 3.5, 7.1, 10.6, 14.1, and 17.7 mm (the centroid) from a corner along the diagonal of a 25×25 mm column exposed to fire on all four sides for 60 minutes. Fig. 8.10 shows the distribution of various parameters along the diagonal after 3, 5, 8, 10, and 30 minutes of exposure to fire. The time history shows that the cool zone is eliminated after about 3 minutes of exposure to fire (the critical time). The very maximum pore pressure at the centroid of the 25×25 mm column is 2.6 MPa, and occurs after 5 minutes of exposure to fire (the maximum time). As discussed in Chapter 7, the second increase of the very maximum water vapour pressure, and thus the very maximum pore pressure, from 2.6 MPa after 5 minutes to 2.9 MPa after 8 minutes, even though the very maximum water vapour content decreased from 14 kg/m^3 after 5 minutes to 13 kg/m^3 after 8 minutes, is unrealistic and not relevant.

Similar to the observation discussed in Chapter 7, from the results of the 100×100, 50×50, and 25×25 mm columns, the effect of time of exposure to fire is evident; provided that spalling does not occur, when the time of exposure increases, a greater very maximum pore pressure occurs in the middle of a thicker section exposed to fire from opposite sides.

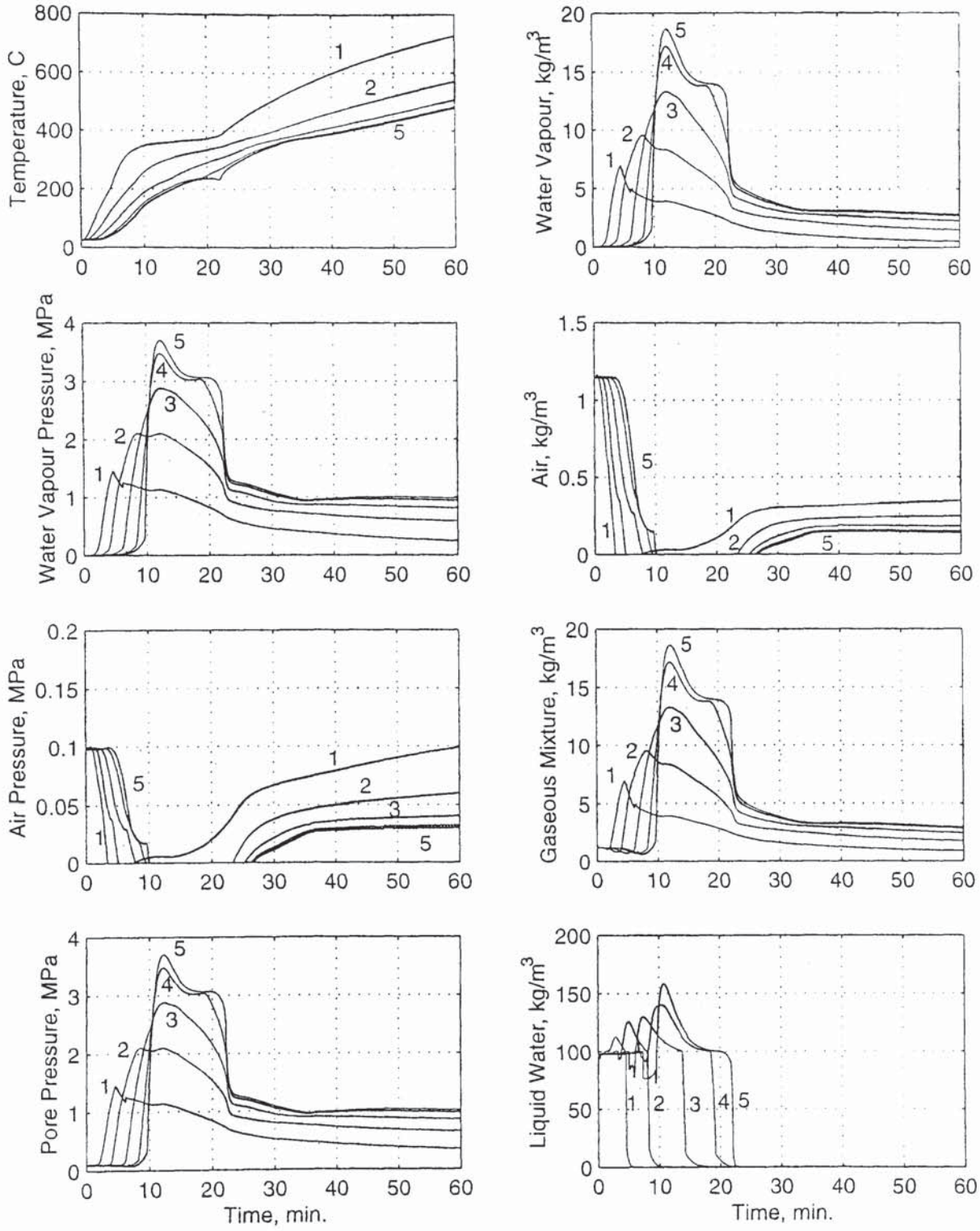

Fig. 8.7: Time history of T, in °C, ρ_v, in kg/m^3, P_v, in MPa, ρ_a, in kg/m^3, P_a, in MPa, ρ_g, in kg/m^3, P_g, in MPa, and $\varepsilon_l \rho_l$, in kg/m^3, at distances of (1) 7.1, (2) 14.1, (3) 21.2, (4) 28.3, and (5) 35.4 mm (the centroid) starting from a corner along a diagonal of a 50×50 mm column exposed to fire on all four sides for 60 minutes.

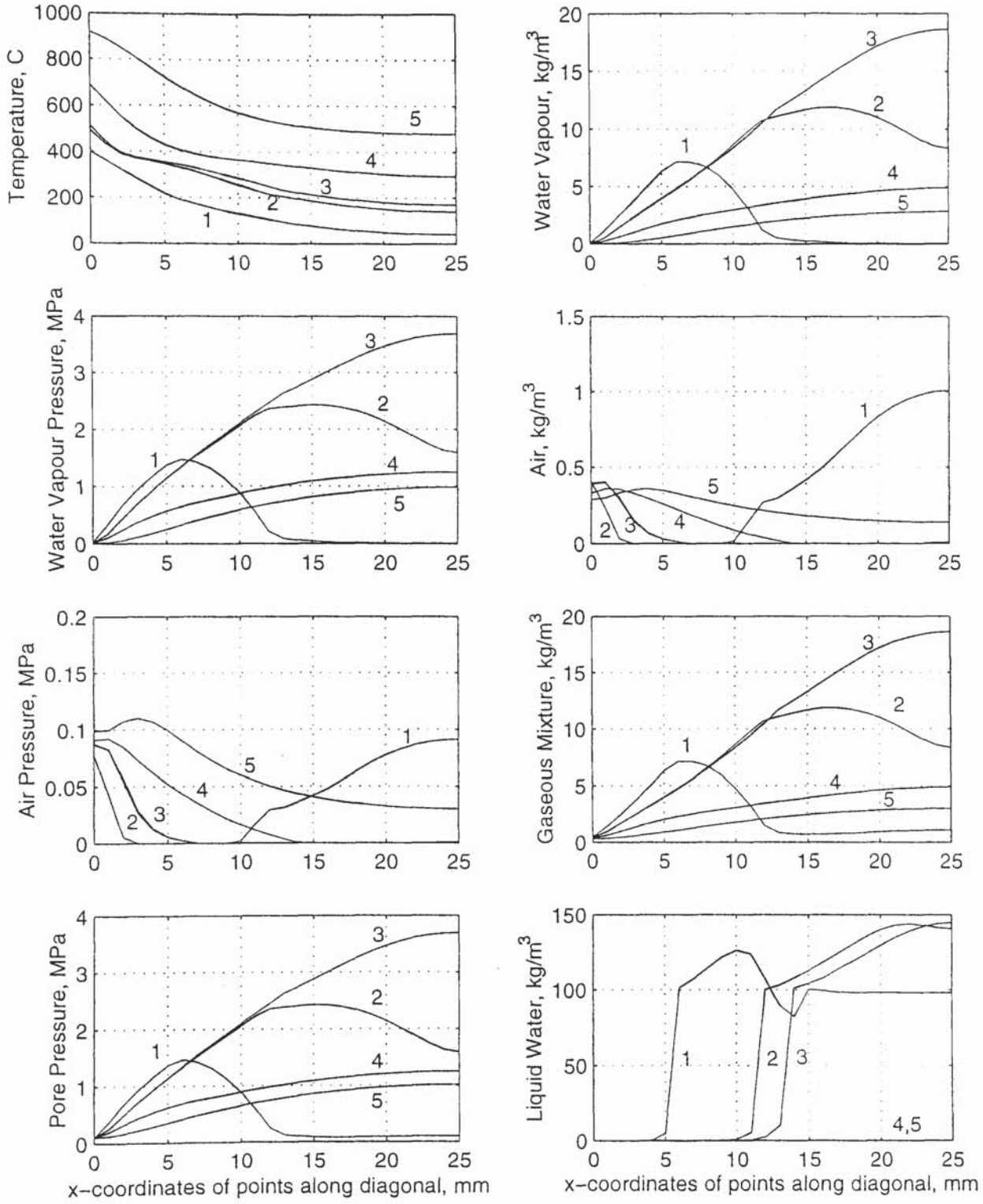

Fig. 8.8: Distribution of T, in °C, ρ_v, in kg/m^3, P_v, in MPa, ρ_a, in kg/m^3, P_a, in MPa, ρ_g, in kg/m^3, P_g, in MPa, and $\varepsilon_l \rho_l$, in kg/m^3, after (1) 5, (2) 10, (3) 12, (4) 25, and (5) 60 minutes of exposure to fire along a diagonal of a 50×50 mm column exposed to fire on all four sides for 60 minutes; only x-coordinates of points are shown.

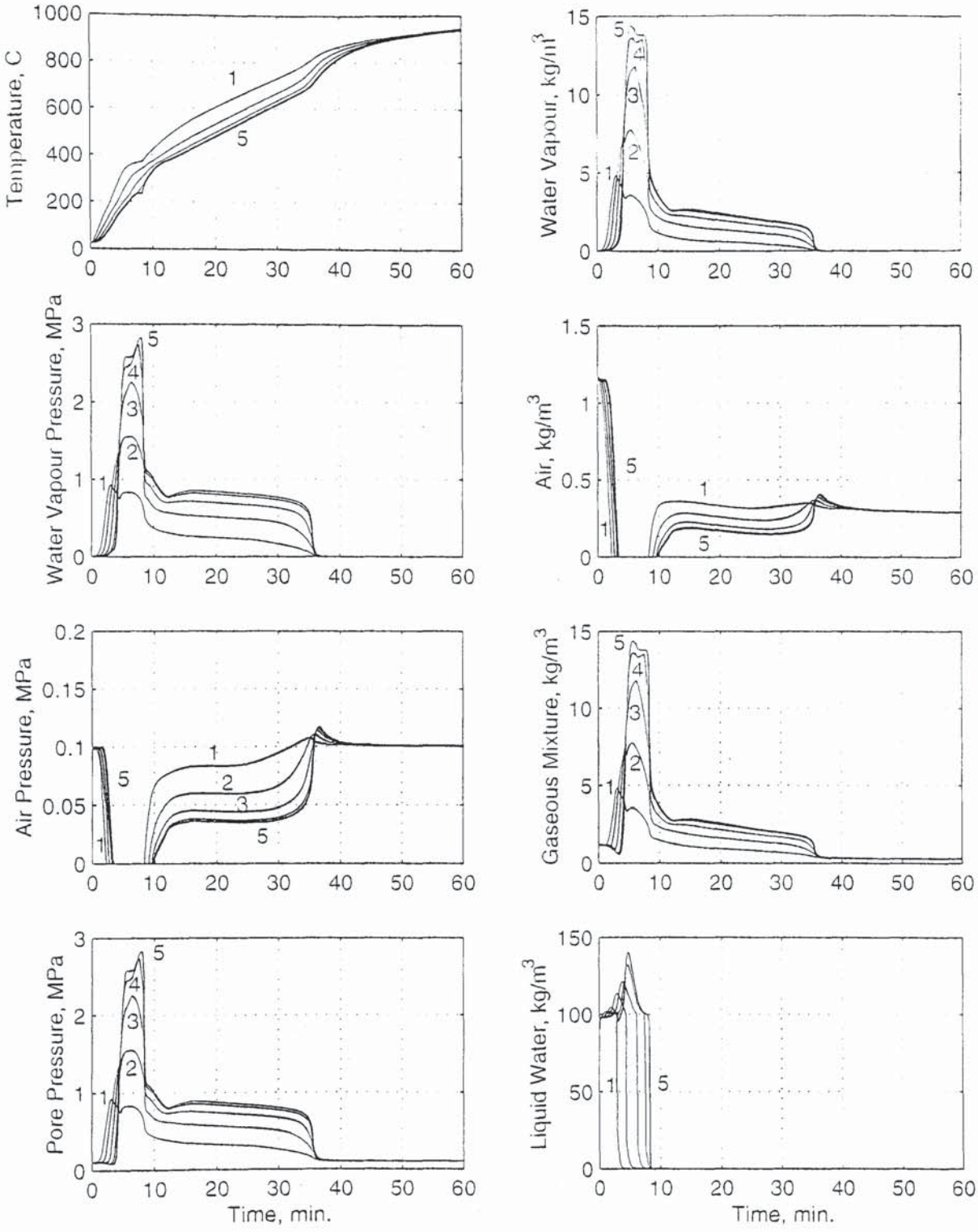

Fig. 8.9: Time history of T, in °C, ρ_v, in kg/m^3, P_v, in MPa, ρ_a, in kg/m^3, P_a, in MPa, ρ_g, in kg/m^3, P_g, in MPa, and $\varepsilon_l \rho_l$, in kg/m^3, at distances of (1) 3.5, (2) 7.1, (3) 10.6, (4) 14.1, and (5) 17.7 mm (the centroid) starting from a corner along a diagonal of a 25×25 mm column exposed to fire on all four sides for 60 minutes.

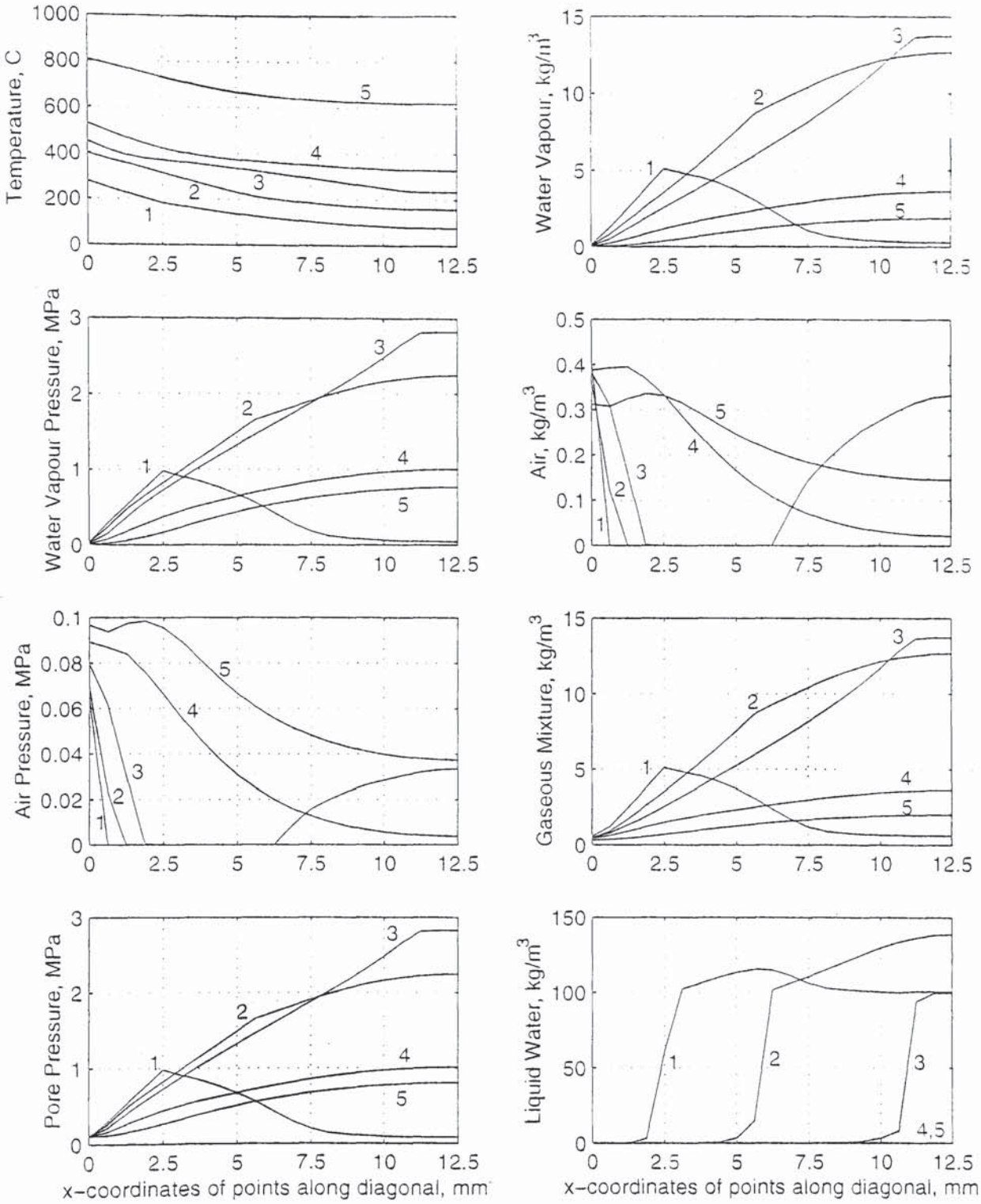

Fig. 8.10: Distribution of T, in °C, ρ_v, in kg/m^3, P_v, in MPa, ρ_a, in kg/m^3, P_a, in MPa, ρ_g, in kg/m^3, P_g, in MPa, and $\varepsilon_l \rho_l$, in kg/m^3, after (1) 3, (2) 5, (3) 8, (4) 10, and (5) 30 minutes of exposure to fire along a diagonal of a 25×25 mm column exposed to fire on all four sides for 60 minutes; only x-coordinates of points are shown.

8.3 EFFECT OF TYPE OF EXPOSURE TO FIRE

As discussed in Chapter 7, as far as spalling is concerned, exposure of a wall to fire from one side, or three sides of a column, could be the severest case, since the non-exposed surface is less cracked, and thus is less permeable for the vapour to be released to the environment. However, as far as the magnitude of the pressure is concerned, exposure of a thick column to fire from one, two, three, or all four sides does not make any difference (the maximum pressure is 2.2 MPa), whilst heating a thin column on all four sides is the severest case.

8.4 DISCUSSION

From the results obtained in this Chapter, it appears that exposure of unsealed columns to fire on one side cannot produce pressures of significantly high magnitude to produce spalling, since the pressure cannot exceed that of 1.5 MPa that can occur in thick walls, and thus, if spalling occurs on such a column, then such spalling must be due to high thermal stresses. On the other hand, exposure of thick unsealed columns to fire on two adjacent, three, or four sides produces maximum pressures of about 2.2 MPa along a diagonal, and thus, considering the reduced tensile strength at high temperatures, *corner* (but not surface or explosive) spalling is likely to be due to high pore pressure.

Also, the results of the 100×100, 50×50, and 25×25 mm columns confirm the first observation of Chapter 7 that the maximum pressures in heated sections can be more than twice those calculated by different researchers and thought to be the maximum that can occur so far, and that these very maximum pressures occur at the centres of sections exposed to heat from opposite sides after certain periods of time. Furthermore, these results confirm the second observation of Chapter 7 that a very maximum pressure can occur in a concrete section of *any* thickness exposed to fire from opposite sides, depending on the time of exposure to fire.

An important finding is that the third observation of Chapter 7, i.e. when the very maximum pressure is reached at the centre, the pressure at any location is the very maximum that can occur at that location, is applicable to locations along the centroidal x- and y-axes of a column (as an example, the distribution along the centroidal x-axis of the 100×100 column is shown in Fig. 8.11), but *not* to locations along the diagonals.

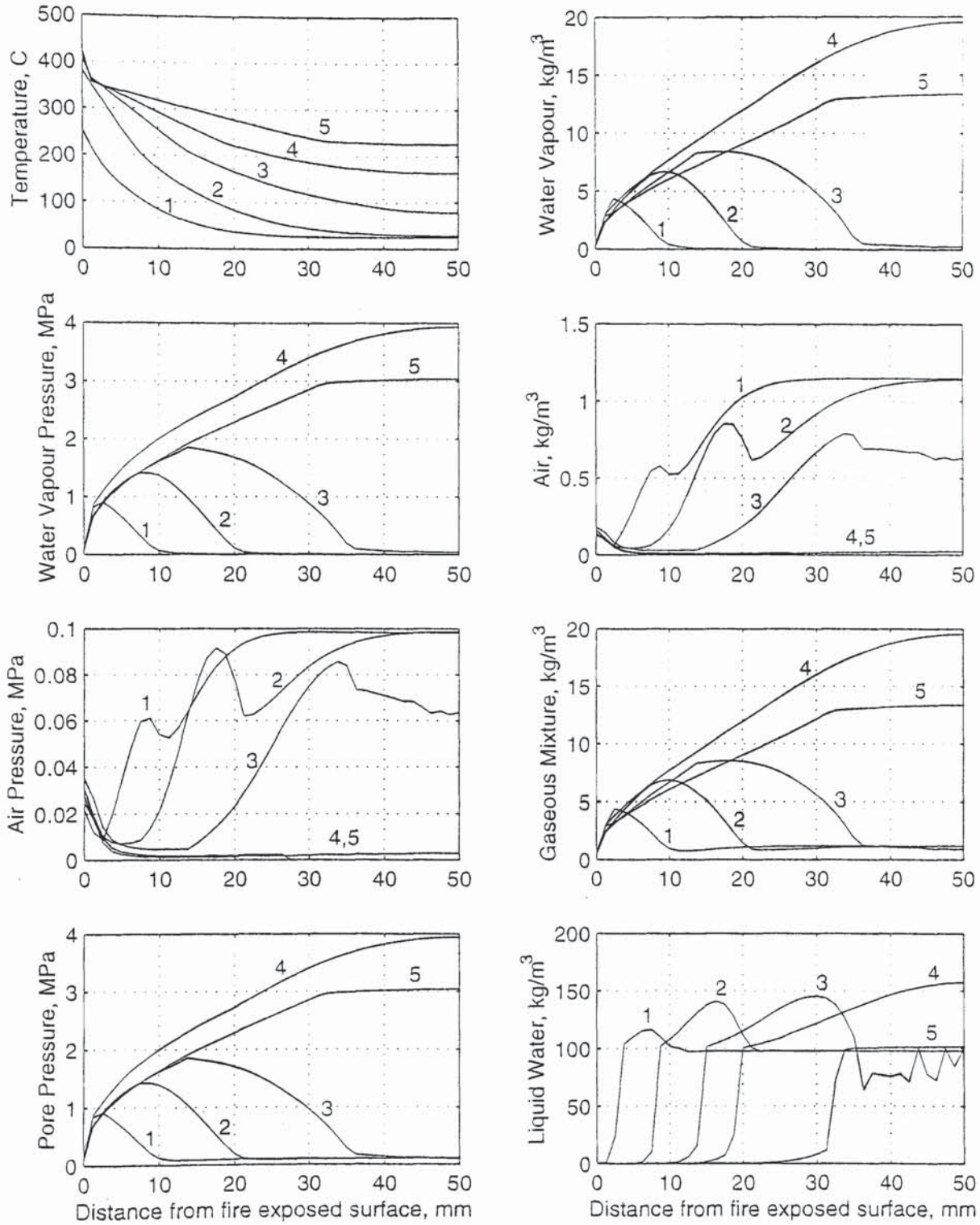

Fig. 8.11: Distribution of T, in °C, ρ_v, in kg/m^3, P_v, in MPa, ρ_a, in kg/m^3, P_a, in MPa, ρ_g, in kg/m^3, P_g, in MPa, and $\varepsilon_l \rho_l$, in kg/m^3, after (1) 5, (2) 10, (3) 20, (4) 35, and (5) 60 minutes of exposure to fire along the centroidal x-axis of a 100×100 mm column exposed to fire on all four sides for 60 minutes.

However, it is important to note that, when the very maximum pressure is reached at the centroid of a column, the maximum pressures at locations along the centroidal axes are the highest that can occur at similar locations along any other axis including the diagonal. For example, after 10 minutes of exposure to fire, the maximum pressure is 2.1 MPa at the point (13, 37) along the diagonal of the 100×100 mm column (Fig. 8.6), but the very maximum pressure at the same distance of 13 mm along the x-axis is 2.3 MPa (Fig. 8.11).

The critical times for the 100×100, 50×50, and 25×25 mm columns are 24, 8, and 3 minutes, respectively, and the maximum times are 35, 12, and 5 minutes, respectively. Thus, as for walls, the ratio between t_{max} and t_{crit} is between 1.46 and 1.67. Regression analysis leads to the following expressions for the variation of t_{crit} and t_{max}, in min, with size a, in mm:

$$t_{crit} = 0.08a + 0.0016a^2 \tag{8.1a}$$

for which the correlation coefficient $R = 1$, and

$$t_{max} = 1 + 0.1a + 0.0024a^2 \tag{8.1b}$$

for which the correlation coefficient $R = 1$. The variation of t_{crit} and t_{max}, in min, with size of column a, in mm, is shown in Fig. 8.12.

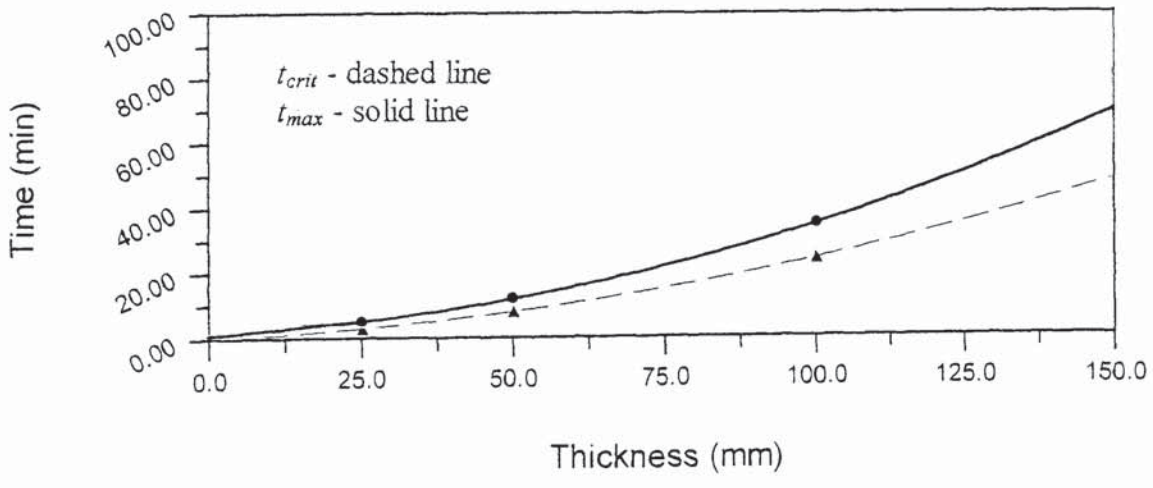

Fig. 8.12: Variation of critical and maximum times with size of column.

If it is assumed that the variations of t_{crit} and t_{max} are proportional to the square of column size, then the following expressions are obtained:

$$t_{crit} = 2 + 0.00221a^2 \tag{8.2a}$$

for which the correlation coefficient $R = 0.9992$, and

$$t_{max} = 3.5 + 0.00316a^2 \tag{8.2b}$$

for which the correlation coefficient $R = 0.9994$. The variation of t_{crit} and t_{max} with square of thickness according to (8.2) is shown in Fig. 8.13.

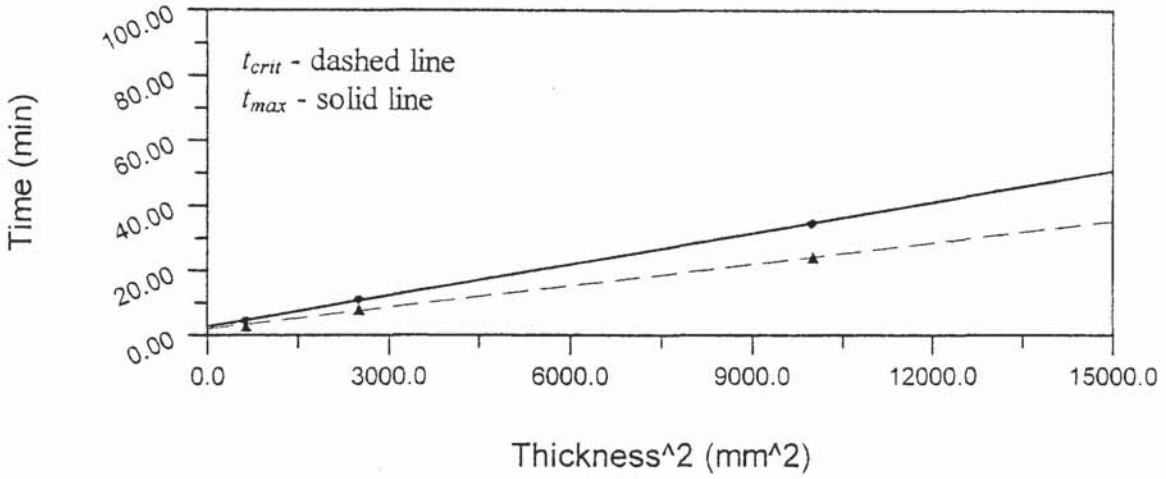

Fig. 8.13: Variation of critical and maximum times with square of size of column

Similar to walls, (8.1) and (8.2) are valid for practical column sizes, and it is suggested that, for very small sizes, t_{crit} and t_{max} will decrease sharply with a; it is interesting to note that (8.1a) leads to $t_{crit} = 0$ when $a = 0$.

The key results are tabulated in Table 8. From the results for the 100×100, 50×50, and 25×25 mm columns, the fourth observation discussed in Chapter 7, i.e. the magnitude of the very maximum pressure is a function of the thickness, is applicable to columns as well. The variation of the very maximum pressure with thickness is shown in Fig. 8.14 for which the following expression for the variation of P_{max}, in MPa, with a, in mm, is valid:

$$P_{max} = \frac{4.01}{1 + 3.524e^{-0.075a}} \tag{8.3}$$

for which the correlation coefficient $R = 1$.

Column size, in mm	Maximum pressure, in MPa	Temperature, in °C	Depth, in mm	Time, in min
300×300	2.2	200	20	20
200×200	2.2	200	20	20
100×100	4	160	50	35
50×50	3.7	160	25	12
25×25	2.6	160	12.5	8

Table 8.1: Key results for 300×300, 200×200, 100×100, 50×50, and 25×25 mm columns exposed to fire on all four sides including: column size and maximum pore pressure along with the temperature, depth, and time at which it occurs.

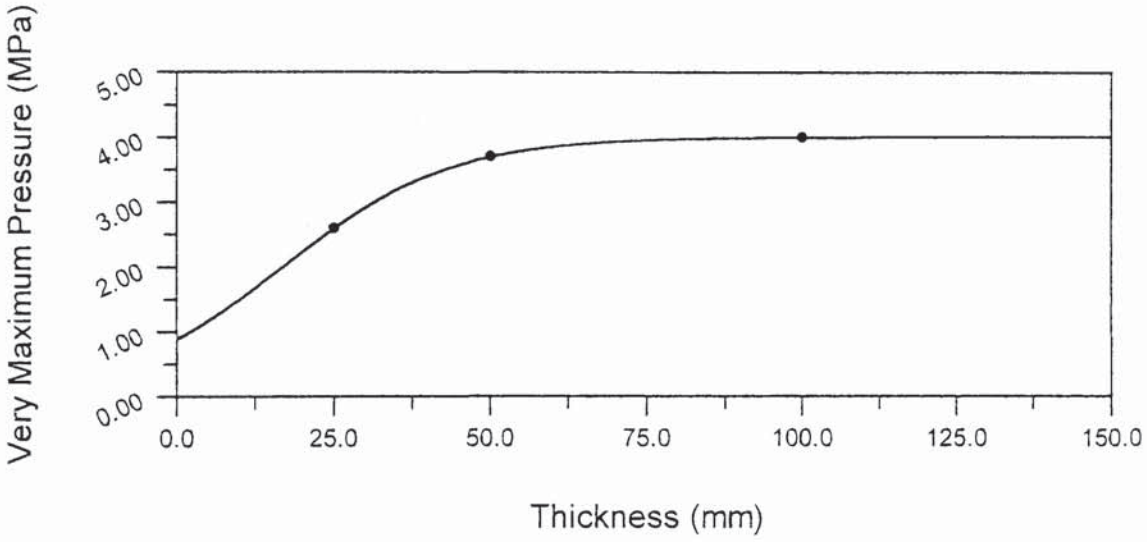

Fig. 8.14: Variation of the very maximum pore pressure with size of column.

However, similar to walls, it seems that a linear variation of the very maximum pressure with size of column as shown in Fig. 8.15 is the most reasonable, and thus the following expression is proposed:

$$P_{max} = 2.45 + 0.017a \tag{8.4}$$

for which the correlation coefficient R = 0.8733.

Similar to (7.4) for walls, (8.4) is valid only for practical column sizes, and it is suggested that, for very small a, P_{max} will decrease sharply with a.

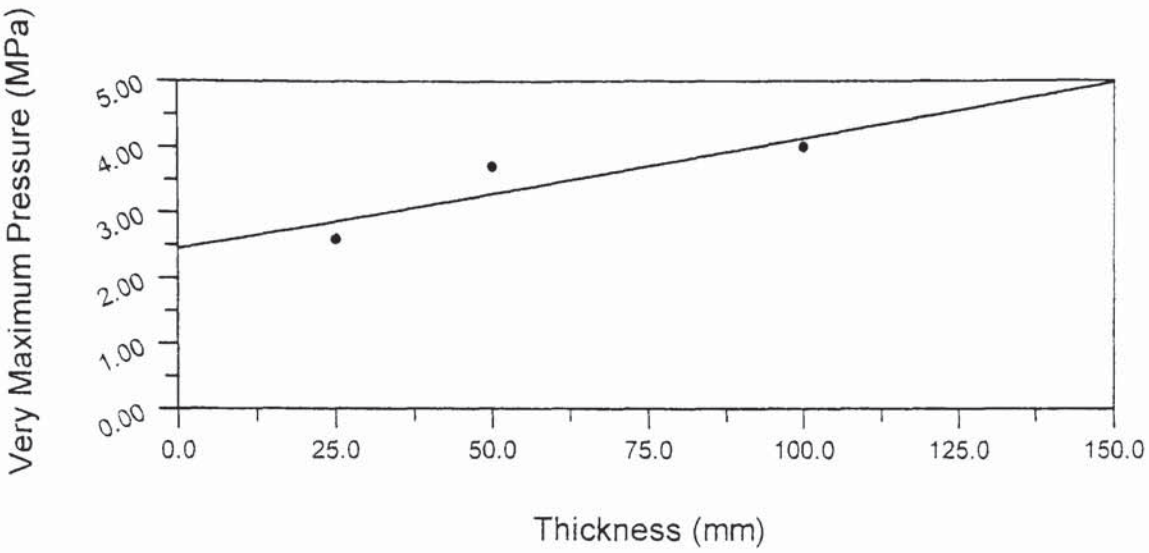

Fig. 8.15: Linear variation of the very maximum pore pressure with size of column.

The computed pressures in thin columns along with the reduced tensile strength re-confirm that spalling in thin members heated on opposite sides is very likely to be pore pressure spalling. They also provide further evidence that the increased susceptibility of pore pressure spalling occurring in thin members exposed to fire on opposite sides is due to the lack of a cool zone towards which vapour can migrate, which results in the accumulation of vapour from two opposite, three, or four sides and thus to very maximum pressures occurring at the centres of these members.

8.5 COMPARISON: WALLS AND COLUMNS IN FIRE

When the results for columns are compared with those for walls, it is evident that the cool zones are eliminated and very maximum pressures occur in columns heated on four sides *faster* than they do in walls heated on both sides; the critical and maximum times are 24 and 35 minutes for 100×100 mm columns compared with 32 and 55 minutes for 100-mm-thick walls, since vapour travels to the centroids of columns from four sides compared with two in walls. Also, the maximum pressure that can occur in thick columns and the very maximum pressures that can be reached in thin ones are higher than those occurring in walls of similar thicknesses; the very maximum pressure in a 100×100 mm column is 4 MPa compared with 3.5 MPa in a 100-mm-thick wall. Thus, it is evident that pore pressure spalling occurs in thin columns heated on three or all four sides sooner than it does in thin walls heated on both sides; for example, if a 25×25 mm column is heated on all four sides, the very maximum pressure occurs after 5 minutes of exposure to fire whilst, in a 25-mm-thick wall, the very maximum pressure occurs after 8 minutes of exposure to fire from both sides.

8.6 CONCLUSIONS

- The build up of pore pressure in thick concrete columns exposed to fire on two adjacent, three, or four sides is likely to produce corner spalling, but not surface or explosive spalling. Thus, if surface or explosive spalling occurs on a thick column under one, two, three, or four sided heating, then such spalling must be due to high thermal stresses.

- It has again been demonstrated that the reason for the enhanced propensity of pore pressure spalling occurring in thin members is the lack of a cool zone towards which vapour can migrate.

- Pore pressure spalling occurs in thin columns exposed to fire on three or all four sides sooner than it does in thin walls exposed to fire on both sides.

- It is reconfirmed that the temperature at the location of the maximum pressure is about 200°C, and thus the tensile strength is around 80% of the strength at ambient temperature. If spalling occurs in a thin column, the column suffers a high relative reduction in cross-section and, if further spalling occurs, local or even global failure could occur.

- For concrete columns heated on two opposite, three, or four sides, and on the assumption of no spalling, the time t_{crit} after which the maximum pressure starts exceeding the maximum pressure that can occur when there is a cool zone and the time t_{max} at which the pressure reaches a very maximum value at the centroid are proportional to the size of the column.

- The ratio between t_{max} and t_{crit} for columns heated on all four sides lies between 1.5 and 1.7 with an average of 1.6 (as for walls).

- The maximum pore pressures computed in 300×300, 200×200, 100×100, 50×50, and 25×25 mm columns exposed to fire on all four sides are 2.2, 2.2, 4, 3.7, and 2.6 MPa after 20, 20, 35, 12, and 5 minutes of exposure to fire, respectively.

CHAPTER 9

CONCLUSIONS AND FURTHER WORK

Spalling can be a very serious problem that occurs on concrete members exposed to high temperatures. The mechanisms proposed to explain spalling suggest that it is due to thermal stresses, high pore pressures, or both. As far as thermal stresses are concerned, estimates have been made using elastic theory. Also, constitutive models for heated concrete have been investigated, and models for predicting thermal stresses have been developed. However, the theory seems not to agree with the experimental observations.

On the other hand, the magnitudes of the pressure in heated concrete are difficult to predict. Consequently, the measured as well as the calculated magnitudes of the pressure show large variations. The reason, or at least one of the reasons, for the variation of the computed magnitudes of the pressure is that, in mathematical modelling of heat and mass transfer in heated concrete, diffusion of water vapour in concrete has been quietly debatable, and thus two approaches have been adopted; diffusion of water vapour is neglected in the first approach, but is considered in the second one. Evidently, only one of the two approaches is correct (diffusion either occurs or does not), and thus only the results of one approach can be reliable. Furthermore, researchers who consider diffusion either assume that the diffusivity is constant or depend on molecular diffusivity equations intended for systems devoid of walls.

Another aspect is that spalling is exacerbated in thin concrete sections exposed to high temperatures (Purkiss, 1996), but no detailed investigation has been undertaken to examine heated thin sections.

In this study, therefore, the validity (or invalidity) of the assumptions related to diffusion of water vapour through concrete in mathematical modelling has been investigated. Also, an equation that determines the effective diffusivity of any gas in concrete at any temperature has been developed and its realism has been ensured. Furthermore, thin concrete sections exposed to fire have been examined in detail. The mathematical model used has been checked in order to ensure that it leads to the correct solution of the governing equations. The conclusions reached and recommendations for further work are now discussed.

9.1 CONCLUSIONS

9.1.1 Main Conclusions

- The basic assumption that diffusion of water vapour does not occur in concrete is invalid, since it is confirmed by many researchers that diffusion, known as Knudsen diffusion, of different gases *does* occur through micropores in porous media. Neglecting diffusion leads to a significant underestimation of the pore pressure. It leads to a maximum pore pressure of less than 1 MPa in thick unsealed normal-concrete sections exposed to fire, compared with the maximum pore pressure of 1.5 MPa computed when a tenable newly developed diffusivity equation is used.

- In the second approach in which diffusion is considered, assuming that the diffusivities of water vapour and air are constant is incorrect, since the diffusivity in heated concrete, i.e. Knudsen diffusivity, varies with temperature, mean pore diameter, and tortuosity. Also, assuming that the diffusivities of water vapour and air in concrete are molecular is unreasonable since, unlike Knudsen diffusivity, molecular diffusivity has a stronger dependence on the temperature, varies with the pressure, and does not vary with the mean pore diameter. The use of molecular diffusivity leads to unrealistic results and to a significant overestimation of the pore pressure. It leads to maximum pore pressures up to 2.7 MPa of which the water vapour pressure is 1.5 MPa while the air pressure is 1.2 MPa.

- The first effective diffusivity equation for heated concrete, named concrete diffusivity, (3.16) has been developed that determines the effective diffusivity of any gas in concrete at any temperature. One of the most important advantages of concrete diffusivity is that the variable tortuosity is implicitly included in the equation.

- The fact that the maximum pressure of 1 MPa computed when the diffusivity approaches zero is about the same as that cited by researchers who neglect diffusion implies that different assumptions, other than diffusion, adopted in the model used are equivalent to those adopted by researchers who neglect diffusion. Thus, assuming that *all* assumptions are now reasonable, it has been concluded that the maximum pore pressures of 1.5 and 2.2 MPa computed with concrete diffusivity seem to be the realistic magnitudes of the pore pressure that can occur in unsealed thick normal-concrete walls and columns (along diagonals) exposed to fire, respectively.

- The build up of pore pressure is low in thick concrete walls whether under one or two sided heating, since there is a substantial cool zone towards which moisture can migrate; this is a similar solution to the semi-infinite continuum. Similarly, heating of unsealed members on one side only cannot produce pressures of significantly high magnitude to produce spalling, since the water vapour cannot be built up further when the temperature of the non-exposed side reaches 100°C. On the other hand, the build up of pressure in thick columns exposed to fire on two adjacent, three, or four sides is likely to produce corner, but not surface or explosive, spalling. Thus, if surface and/or explosive spalling occur on a thick member whether under one, two, three or four sided heating or on a thin member heated on one side only, then such spalling must be due to high thermal stresses.

- The reason for the enhanced propensity of pore pressure spalling occurring on thin walls with two sided heating and on small columns heated on two opposite, three, or four sides has been conclusively demonstrated to be due to the lack of a "cool zone" towards which water vapour can migrate.

9.1.2 Subsidiary Conclusions

- In order to confirm that the model leads to the correct numerical solution, and thus ensure the correctness of the results, an arbitrary set of unknowns was chosen that is different from the original one, the corresponding equations were derived, the model was modified, and results for different problems were computed. The results were found virtually identical to those obtained with the original set, which ensures the reliability of the results.

- The validity of concrete diffusivity has been ensured, since it leads to maximum pore pressures between those obtained from the extreme assumptions that diffusion does not occur in concrete and that diffusion in concrete is molecular, and since the maximum pore pressure of 1.5 MPa computed with concrete diffusivity is almost entirely due to the build up of water vapour pressure of 1.5 MPa. Also, concrete diffusivity leads to maximum surface temperatures, when the maximum pressures occur, that are much closer to the experimental range of surface temperatures of 250-420°C measured when spalling occurs than those obtained with different molecular diffusivity equations.

- A by-product of concrete diffusivity is the development of a new equation (3.35) that determines the mean pore diameter in heated concrete.

- It has been found that the type of diffusion remains to be Knudsen diffusion in concrete exposed to fire even when the pore pressure is at its maximum value, since the mean free path of water vapour molecules that is inversely proportional to the pressure remains greater than the mean pore diameter.

- One of the major shortcomings of most mathematical models of heat and mass transfer in heated concrete in which diffusion is considered is that the tortuosity in concrete is neglected. Considering the tortuosity with molecular diffusivity results in a smaller overestimation of the pore pressure. Nevertheless, the contribution of the air to the increase of the pore pressure remains significant, and thus unreasonable.

- Another major shortcoming of most models is the assumption that the intrinsic permeability remains constant at all temperatures. The permeability increases when the porosity increases due to dehydration of bound water. This assumption leads to an overestimation of the pore pressure, since the smaller the permeability, the greater the water vapour content that cannot escape. Variable intrinsic permeability has been used in this study.

- For walls heated on both sides and columns heated on two opposite, three, or four sides, the time t_{crit} after which the maximum pore pressure starts exceeding the maximum pressure that can be reached when there is a cool zone and, on the assumption of no spalling, the time t_{max} at which the pore pressure reaches a very maximum value at the centre are proportional to the square of the thickness. The ratio between t_{max} and t_{crit} lies between 1.4 and 1.8 with an average of 1.6. Also, a linear variation of the very maximum pore pressure with thickness seems to be the most reasonable.

- Pore pressure spalling occurs in small columns exposed to fire on three or all four sides *sooner* than it does in thin walls exposed to fire on both sides. Also, the very maximum pressures in small columns are higher than those in walls of similar thicknesses.

- The temperature at the location of the maximum pore pressure is about 200°C. Thus, the tensile strength at that position is around 80% of the tensile strength at ambient temperature. Therefore, if spalling occurs on a thin wall or a small column where there is an early build up in

pore pressure, then this is more deleterious as the section suffers a high relative reduction in cross-section. If further spalling occurs, due to either continued pore pressure build up or high thermal stresses, then local, or worse global, failure could ensue.

- The maximum pore pressures computed in 400, 150, 100, 75, 50, and 25-mm-thick walls exposed to fire on two sides are 1.5, 4.3, 3.5, 3.4, 3.1, and 2.5 MPa after 240, 115, 55, 33, 17, and 8 minutes of exposure to fire, respectively. The maximum pressures computed in 300×300, 200×200, 100×100, 50×50, and 25×25 mm columns exposed to fire on all four sides are 2.2, 2.2, 4, 3.7, and 2.6 MPa after 20, 20, 35, 12, and 5 minutes of exposure to fire, respectively.

9.2 FURTHER WORK

This study has called attention to some developments that need to be carried out in the area of heat and mass transfer in concrete subjected to high temperatures in order to determine the real pore pressures that can occur in heated concrete, and thus, with the determination of thermal stresses, a better assessment of the causes of spalling can be made. It also highlighted the fact that a similar approach can be adopted to investigate the behaviour of other materials exposed to high temperatures. Recommendations for future work are now discussed.

Determination of the free water in the mathematical model used in this study, and apparently in all other models, is based on the sorption isotherms of Bažant and Thonguthai (1978), due to the lack of a different approach. The sorption isotherms, however, determine the total moisture, i.e. the free water and the water vapour. It has been assumed that the sorption isotherms could be used to approximately estimate the free water content since, when there is free water in concrete, the mass of the free water is much greater than that of vapour. However, the vapour content, and thus vapour and pore pressures, depends on the free water content. Thus, the results of the vapour content and vapour and pore pressures are overestimated. Considering the ratios of water vapour to free water, the overestimation ranges from about 5% in thick sections to approximately 10% in thin sections. A different approach for determining the free water needs to be developed in order to determine, or at least approach the determination of, the real pore pressures that can occur in heated concrete.

Mathematical modelling and the developments made in this study are applicable to other materials, e.g. soil, wood, and masonry, subjected to high temperatures although masonry has additional

problems caused by the mortar bed and internal voids. Mathematical models of heat and mass transfer in soil were developed (Chapter 2), but, due to the lack of a diffusivity equation that is specific for soil, researchers had to rely on Krischer and Rohnalter's molecular diffusivity (2.8). It appears that diffusion in soil may not be mainly Knudsen, but the assumption that it is entirely molecular cannot be justified. Thus, from pore size distribution studies, the proportion of pores that are smaller the mean free path of water vapour molecules can be determined, and then the same approach adopted in this study can be used to derive an effective diffusivity equation for these pores whilst molecular diffusivity (with an appropriate tortuosity factor) is limited to pores larger the mean free path. Similar developments need to be carried out for wood and masonry.

For w/c ratios greater than 0.38, in order to approach the real results for pores greater than the mean free path, if any, an experimental study needs to be carried out to determine the variable tortuosity that is a function of the variable pore size distribution at temperatures greater than 100°C when the porosity increases, and thus the pore size distribution changes, due to dehydration of bound water.

The real results for heated materials such as concrete, wood, masonry, and soil can be further approached by determining the exact locations of the evaporation front from the actual pressures at which water starts boiling based on thermodynamics (Çengel and Boles, 1998) from which the curve below was drawn and the corresponding expression was derived that can be implemented in mathematical modelling of heat and mass transfer in porous media:

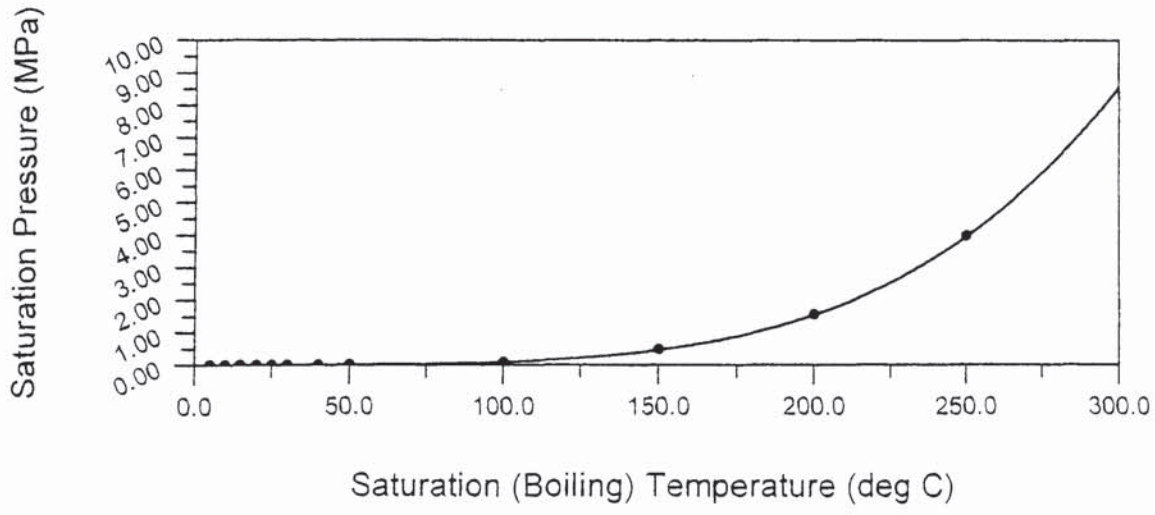

Water-Vapour Saturation Curve

$$P_{sat} = 3.1\times10^{-5} - 1.088\times10^{-4}T_{sat} + 1.142\times10^{-5}T_{sat}^{2} - 1.424\times10^{-7}T_{sat}^{3} + 1.411\times10^{-9}T_{sat}^{4}$$

for which the correlation coefficient $R = 0.9999$.

REFERENCES

Abbot, M.M. and Van Ness, H.C. (1976), 'Thermodynamics', McGraw-Hill, Suffolk.

Abdel-Rahman, A.K. and Ahmed, G.H. (1996), 'Computational Heat and Mass Transport in Concrete Walls Exposed to Fire', *Numer. Heat Transfer Part A*, Vol. 29, pp. 373-395.

Abrams, M.S. and Gustaferro, A.H. (1968), 'Fire endurance of concrete slabs as influenced by thickness, aggregate type, and moisture', *Research Department Bulletin 223*, PCA.

Ahmed, G.N. and Huang, C.L. (1990), 'Modelling of concrete slabs under fire', *Chemical Engineer Communication*, **91**, pp. 241-253.

Ahmed, G.N. and Hurst, J.P. (1997), 'Coupled Heat and Mass Transport Phenomena in Siliceous Aggregate Concrete Slabs Subjected to Fire', *Fire and Materials*, Vol. 21, pp. 161-168.

Akhtaruzzaman, A.A. and Sullivan, P.J. (1970), 'Explosive spalling of concrete exposed to high temperature', PhD thesis, Imperial College, London.

Anderberg, Y. (1976), 'Fire exposed hyperstatic concrete structures – An experimental and theoretical study', Bulletin 55, Division of Structural Mechanics and Concrete Construction, Lund Institute of Technology, Sweden.

Anderberg, Y. (1997), 'Spalling Phenomena of HPC and OC', in L. T. Phan, N. J. Carino, D. Duthinh, and E. Garboczi (eds.), *Proc. Int. Workshop on Fire Performance of High-Strength Concrete, NIST Spec. Publ. 919*, National Institute of Standards and Technology, Gaithersberg, MD, pp. 69-73.

ASTM (1989), 'Standard test methods for fire tests of building construction and materials', ASTM Standard E-119, ASTM, Philadelphia, Pa.

Atkison, A. and Nickerson, A.K. (1984), 'The Diffusion of Ions through Water-Saturated Cement'. *J. Materials Science*, Vol. 19, pp. 3068-3078.

Austin, S., Robins, P., and Richards, M. (1992), 'Jetblast temperature resistant concrete for harrier aircraft pavements', *The Structural Engineer*, **70(23/24)**, pp. 427-432.

Bathe, Klaus-Jürgen (1996), 'Finite Element Procedures', Prentice Hall, New Jersey.

Bažant, Z.P. (1997), 'Analysis of Pore Pressure, Thermal Stress and Fracture in Rapidly Heated Concrete', *Proceedings, International Workshop on Fire Performance of High-Strength Concrete*, NIST, Gaithersburg, MD, February 13-14, NIST Special Publication 919, eds. L.T. Phan, N.J. Carino, D. Duthinh, and E. Garboczi, pp. 155-164.

Bažant, Z.P. and Kaplan, M.F. (1996), 'Concrete at High Temperatures: Material Properties and Mathematical Models', Longman Group, Essex.

Bažant, Z.P. and Najjar, L.J. (1972), 'Nonlinear Water diffusion in Nonsaturated Concrete', *Materials and Structures*, Paris, France, Vol.5, pp. 3-20.

Bažant, Z.P. and Thonguthai, W. (1978), 'Pore Pressure and Drying of Concrete at High Temperature', *Journal of the Engineering Mechanics Division*, Proceedings of the American Society of Civil Engineers, Vol. 104, No. EM5, pp. 1059-1079.

Bažant, Z.P. and Thonguthai, W. (1979), 'Pore Pressure in Heated Concrete Walls: Theoretical Prediction', *Magazine of Concrete Research*, Vol. 31, No. 107, pp. 67-76.

Bažant, Z.P., Chern, J.C., and Thonguthai, W. (1981), 'Finite element program for moisture and heat transfer in heated concrete', *Nuclear Engineering and Design*, **68**, pp. 61-70.

Ben Nasrallah, S. and Perre, P. (1988), 'Detailed Study of a Model of Heat and Mass Transfer During Convective Drying of Porous Media', *International Journal of Heat and Mass Transfer*, Vol. 31, No. 5, pp. 957-967.

Bird, R.B., Stewart, W.E., and Lightfoot, E.N. (1960), 'Transport Phenomena', John Wiley and Sons, New York.

Bolton, A. (1994), 'Island strife', *New Civil Engineer*, 6th October, pp. 14-21.

Bremer, F. (1967), 'Multi-layer (Double-wall) prestressed concrete pressure vessel', *Nuclear Engineering and Design*, **5**, 183-190.

BS 476:Part 20:1987, 'Fire tests on building materials and structures', British Standards Institution, London.

BS 1881:Part 117:1983, 'Methods for determination of tensile splitting strength', British Standards Institution, London.

Burganos, V.N. and Sotirchos, S.V. (1987), 'Diffusion in Pore Networks: Effective Medium Theory and Smooth Field Approximation', *Journal of the American Institute of Chemical Engineers (AIChE Journal)*, Vol. 33, No. 10, pp. 1678-1689.

Carniglia, S.C. (1986), 'Construction of the Tortuosity Factor from Porosimetry', *Journal of Catalysis*, **102**, pp. 401-418.

Çengel, Y.A. (1998), 'Heat Transfer-A Practical Approach', McGraw Hill, Boston.

Çengel, Y.A. and Boles, M.A. (1998), 'Thermodynamics-An Engineering Approach', 3rd Edition, McGraw-Hill, Boston.

Chapman, D.A. (1976), 'A Study of the Movement of Moisture in and from Concrete at Elevated and Non-Uniform Temperatures', PhD Thesis, University of London, January, 1976.

Chapman, D.A. and England, G.L. (1977), 'Effects of Moisture Migration on Shrinkage, Pore Pressure and Other Concrete Properties', *Transactions, Fourth International Conference on Structural Mechanics in Reactor Technology, San Francisco*. Editors: B.A. Boley and T.A. Jaeger. Brussels, Commission of European Communities. Paper M5/3.

Chen, P. and Pei, D.C.T. (1989), 'A mathematical model of drying processes', Vol. 32, No. 2, pp. 297-310.

Coates, J. (1996), 'Chunnel: They have been told', Construction News No. 6494, 5 December, pp. 1.

Comite Euro-International du Beton (1990), 'CEB-FIP Model Code 1990', *Bulletin d'Information.* No. 195, 196, Lausanne.

Concrete Society (1987), 'Permeability Testing of Site Concrete: A Review of Methods and Experience', Technical Report No. 31, August 1988, *Report of a Concrete Society Working Party*, London.

Connoly, R.J. (1995), 'The Spalling of Concrete in Fires', PhD Thesis, University of Aston in Birmingham.

Connoly, R.J. (1997), 'The Spalling of Concrete', *Fire Engineering Journal*, pp. 38-40.

Connolly, R.J., Kirby, J.A., and Barnes, N. (1994), 'A parametric study of the influence of boundary conditions in using THELMA', BRE Note 149/94, Building Research Establishment, Watford.

Consolazio, G.R., McVay, M.C., and Rish III, J.W. (1997), 'Measurement and Prediction of Pore Pressure in Cement Mortar Subjected to Elevated Temperature', *Proceedings, International Workshop on Fire Performance of High-Strength Concrete,* NIST, Gaithersburg, MD, February 13-14, NIST Special Publication 919, eds. L.T. Phan, N.J. Carino, D. Duthinh, and E. Garboczi, pp. 125-148.

Copier, W.J. (1979), 'Spalling of normalweight and lightweight concrete on exposure to fire', Report **24(2)**, Heron, Holland.

Cunningham, R.E. and Williams, R.J.J. (1980), 'Diffusion in Gases and Porous Media', Plenum Press, New York.

Cussler, E.L. (1997), 'Diffusion Mass Transfer in Fluid Systems', Cambridge University Press, Cambridge.

Dayan, A. and Gluekler, E.L. (1982), 'Heat and mass transfer within an intensely heated concrete slab', *Int J. Heat Mass Transfer*, Vol. 25, No. 10, pp. 1461-1467.

Dhatt, G., Jacquemier, M., and Kadje, C. (1986), 'Modelling of Drying Refractory Concrete', *Drying 86, Proceedings of the 5th International Symposium on Drying*, McGill University, pp. 94-104.

deVries, D.A. (1958), 'Simultaneous Transfer of Heat and Moisture in Porous Materials', *Trans. Am. Geophys. Union*, Vol. 39, pp. 909-916.

Dougill, J.W. (1971), 'The effect of high temperature on concrete with reference to thermal spalling', PhD Thesis, Imperial College, London.

Dougill, J.W. (1972), 'Modes of failure of concrete panels exposed to high temperatures', *Magazine of Concrete Research*, **24(79)**, pp. 71-76.

Ehm, H. (1966), 'Contribution to calculation of fire loaded beam type reinforced concrete elements', PhD Thesis, Technical University of Braunschweig, Germany.

Ellingwood, B.R. (1991), 'Impact of fire exposure on heat transmission in concrete slabs', *J. Struct. Engrg.*, ASCE, **117(6)**, pp. 1870-1875.

England, G. (1971), 'Migration of moisture and pore pressures in heated concrete', *Proceedings of First International Conference on Structural Mechanics in Reactor Technology*, **3 (H)**, Berlin, pp. 22-26.

England, G., Greathead, R., and Khan, S. (1991), 'Influence of high temperature on water content, permeability and pore pressures in concrete', *Transactions of Structural Mechanics in Reactor Technology*, **H(02/1)**, Japan, 31-36.

Eurocode 2 (2000), 'Design of concrete structures-Part 1:General Rules-Structural fire design', European Standard prEN 1992-1-2 (1st informal draft), January 2000, CEN, European Committee for Standardization, Brussels.

Feng, C. and Stewart, W.E. (1973), 'Practical Models for Isothermal Diffusion and Flow of Gases in Porous Solids', *Industrial and Engineering Chemistry Fundamentals*, Vol. 12, No. 2, pp. 143-147.

Gary, M. (1916), 'Fire tests on reinforced concrete buildings', Verlag Wilhelm Ernst und Sohn, Heft 11, Germany.

Gong, Z. and Mujumdar, A. (1993), 'A Model for Kiln-Drying of Refractory Concrete Slabs', Drying Technology, Vol. 11, No. 7, pp. 1617-1693.

Gong, Z. and Mujumdar, A.S. (1995a), 'The Influence of an Impermeable Surface on Pore Steam Pressure During Drying of Refractory Concrete Slabs', *Int. J. Heat Mass Transfer*, Vol. 38, No. 7, pp. 1297-1303.

Gong, Z. and Mujumdar, A.S. (1995b), 'A Two Dimensional Finite Element Model for Kiln-Drying of Refractory Concrete', *Drying Technology*, Vol. 13, No. 3, pp. 585-605.

Gong, Z., Song, B., and Mujumdar, A. (1991), 'Numerical Simulation of Drying of Refractory Concrete', *Drying Technology*, Vol. 9, No.2, pp. 479-500.

Häupl, P., Grunewald, J., and Fechner, H. (1997), 'Coupled heat, air, and moisture transfer in building structures', Int. J. Heat Mass Transfer, Vol.40, No. 7, pp. 1633-1642.

Harada, K. and Terai, T. (1991), 'Heat and mass transfer in an intensely heated mortar wall', *Proceedings of 3rd International Symposium on Fire Safety Science*, Edinburgh, 781-790.

Harmathy, T.Z. (1965), 'Effect of Moisture on the Fire Endurance of Building Elements', *ASTM Publication STP 385*, American Society of Testing and Materials, pp. 74-95.

Harmathy, T.Z. (ed.) (1986), 'Evaluation and Repair of Fire Damage to Concrete', aci SP-92, American Concrete Institute, Detroit.

Hassenjaeger, (1935), 'The behaviour of concrete and reinforced concrete in fire and the design of expansion joints in reinforced concrete construction', PhD Thesis, Technical University of Braunschweig, Germany.

Hognestad, E.,Hanson, N., and Mc Henry, D. (1955), 'Concrete stress distribution in ultimate strength design', *Journal of American Concrete Institution*, **52**, 455-479.

Incropera, F.P. and De Witt, D.P. (1996), 'Fundamentals of Heat and Mass Transfer', John Wiley & Sons, New York.

Irudayaraj, J. and Wu, Y. (1994), 'Finite element analysis of coupled heat, mass, and pressure transfer in porous biomaterials', *Numerical Heat Transfer*, Part A, **26**, pp. 337-350.

ISO 834 (1975), 'Fire resistance tests-elements of building construction', International Organization for Standardization, Switzerland.

ISO 834:Part 1:1987, 'Elements of building construction-General requirements for fire resistance testing', British Standards Institution, London.

Johnson, M.F.L. and Stewart, W.E. (1965), 'Pore Structure and Gaseous Diffusion in Solid Catalysts', *Journal of Catalysis*, **4**, 248-252.

Jumpannen, U-M (1989), 'Effect of strength on fire behaviour of concrete', *Nordic Concrete Research* Publication No. 8.

Khoury, G.A. (2000), 'Effect of fire on concrete and concrete structures', *Prog. Struct. Engng. Mater.*, **2**, 429-447.

Kodres, C.A. (1996), 'Moisture-Induced Pressures in Concrete Airfield Pavements', *Journal of Materials in Civil Engineering*, Vol. 8, No. 1, pp. 41-50.

Künzel, H.M. and Kiessl K. (1997), 'Calculation of heat and moisture transfer in exposed building components', *Int. J. Heat Mass Transfer*, Vol. 40, No. 1, pp. 159-167.

Lawrence, C.D. (1984), 'Transport of Oxygen Through Concrete', *British Ceramic Society Meeting on Chemistry and Chemically-Related Properties of Cement*, London, pp. 277-293.

Li, L.Y. and Page, C.L. (2000), 'Finite element modelling of chloride removal from concrete by an electrochemical method', *Corrosion Science*, **42**, pp. 2145-2165.

Lie, T.T. (1984), 'A procedure to calculate fire resistance of structural members', *Fire Technology*, **14(1)**, pp. 28-85.

Logan, D.L. (1993), 'A First Course in the Finite Element Method', PWS Publishing Company, Boston.

Luikov, A.V. (1975), 'Systems of differential equations of heat and mass transfer in capillary porous bodies', *Int. J. Heat Mass Transfer*, Vol. 18, pp. 1-14.

Majumdar, P. and Marchertas, A. (1997), 'Heat, Moisture Transport, and Induced Stresses in Porous Materials Under Rapid Heating', *Numerical Heat Transfer*, Part A, Vol. 32, pp. 111-130.

Majumdar, P., Gupta, A., and Marchertas, A. (1994), 'Moisture Propagation and Resulting Stress in Heated Porous Media', *Advances in Heat Transfer, Engineering Systems Design and Analysis*, Vol. 1, ASME Publication, pp. 81-91.

Majumdar, P., Gupta, A., and Marchertas, A. (1995), 'Moisture Propagation and Resulting Stress in Heated Concrete Walls', *Nuclear Engineering and Design*, Vol. 156, pp. 147-158.

Malhotra, H.L. (1984), 'Spalling of Concrete in Fires', Technical Note 118, Construction Industry Research and Information Association (CIRIA), London.

Malhotra, H.L. (1986), 'A survey of fire protection developments for buildings', in *'Design of Structures against Fire'*, (eds. R.D. Anchor, H.L. Malhotra, and J.A. Purkiss), Elsevier Applied Science, London, pp. 1-13.

Malhotra, H.L. (1987), 'Fire Safety in Buildings', BRE, Garston.

Marrero, T.R. and Mason, E.A. (1972), 'Gaseous Diffusion Coefficients', *Journal of Phys. Chem. Ref. Data 1*, pp. 3-118.

McGovern, J.A. (1996), 'The Essence of Engineering Thermodynamics', Prentice Hall, London.

Meyer-Ottens, C. (1972), 'The Question of spalling of concrete structural elements of standard concrete under fire loading', PhD Thesis, Technical University of Braunschweig, Germany.

Mustapha, K.N. (1994), 'Parametric Study of the Behaviour of Reinforced Concrete Columns in Fire', PhD Thesis, University of Aston in Birmingham.

Nekrasov, K.D., Zhukov, V.V., and Shevchenko, V.I. (1967), 'Investigation of heating of large blocks of refractory concrete from one side', *Refractories* (Translated from Ogneupony), 6, 21-22, New York.

Neville, A.M. (1995), 'Properties of Concrete', Longman, Essex.

Nisugi, N., Kono, T., and Sugawara, M. (1959), 'Fire resistance of prestressed concrete beams', Journal of Japanese Society of Civil Engineers, **44 (9)**, pp. 16-20.

Papadakis, V.G., Vayenas, C.G., and Fardis, M.N. (1991), 'Physical and Chemical Characteristics Affecting the Durability of Concrete', *ACI Materials Journal*, Vol. 8, No.2, pp. 186-196.

Phillips, J.R. and deVries, D.A. (1957), 'Moisture Movement in Porous Materials Under Temperature Gradients', *Trans. Am. Geophys. Union*, Vol. 38, pp. 222-232.

Powers, T.C. and Brownyard, T.L. (1948), 'Studies of the Physical Properties of Hardened Portland Cement Pastes', Research Laboratory of the Portland Cement Association, Bulletin 22.

Pruess, K. (1987), 'TOUGH User's Guide', Earth Sciences Division, Lawrence Berkeley Laboratory, University of California, Berkeley, CA 94720, Document LBL-20700.

Purkiss, J.A. (1996), 'Fire Safety Engineering Design of Structures', Butterworth-Heinemann, Oxford.

Rogers, G.F. and Mayhew, Y.R. (1991), 'Thermodynamics and transport properties of fluids', Fourth Edition, Basil Blackwell Ltd., Oxford.

Saito, H. (1965), 'Explosive spalling of prestressed concrete in fire', Occasional Report No. 22, Building Research Institute, Japan.

Scheidegger, A.E. (1974), 'The physics of flow through porous media', University of Toronto Press, Toronto.

Schneider, U. (1986), 'Modelling of concrete behaviour at high temperatures', In Design of structures against fire (eds. Anchor, R.D., Malhotra, H.L., and Purkiss, J.A.), Elsevier Applied Science Publishers, London, pp. 53-69.

Šelih, J., Sousa, A.C.M, and Bremmer, T.W. (1994), 'Moisture and Heat Flow in Concrete Walls Exposed to Fire', *Journal of Engineering Mechanics, ASCE*, Vol. 120, No. 10, pp. 2028-2043.

Šelih, J. and Sousa, A.C.M. (1996), 'Heat Transfer and Thermal Stress Calculation in Fire-Exposed Concrete Walls', *Advanced Computing in Heat Transfer*, 265-274.

Sertmehemetoglu, Y. (1977), 'On the mechanism of spalling of concrete under fire conditions', PhD Thesis, Kings College, London.

Shorter, G.W. and Harmathy, T.Z. (1965), 'Moisture Clog Spalling', In *Proceedings of Institution of Civil Engineers*, **20**, 75-90.

Skalny, J. and Mindess, S., (eds.) (1991), 'Materials Science of Concrete I', The American Ceramic Society, Westerville, Ohio.

Skalny, J. and Mindess, S., (eds.) (1991), 'Materials Science of Concrete II', The American Ceramic Society, Westerville, Ohio.

Skalny, J. and Mindess, S., (eds.) (1991), 'Materials Science of Concrete III', The American Ceramic Society, Westerville, Ohio.

Skelland, A.H.P. (1974), 'Diffusional Mass Transfer', John Wiley & Sons, New York.

Schneider, U. (1985), 'Properties of materials at high temperatures-concrete', International Union of Testing and Research Laboratories for Materials and Structures (RILEM), Kassel University Press, Germany.

Tait, J.C. and Hoj, N.P. (1996), 'Storebaelt eastern railway tunnel: Dania tunnel boring machine fire-analysis and recovery', *Proceedings of the Institution of Civil Engineers: Supplement*, **114** Special Issue 1, pp. 40-48.

Tenchev, R.T. and Khalafallah, B.H. (2000), 'Numerical analysis of pore pressure and thermal stresses in intensely heated concrete columns', Concrete Communication Conference 2000, *Proceedings of the 10th BCA Annual Conference on Higher Education and the Concrete Industry'*, 29-30 June, Birmingham, pp. 255-266.

Tenchev, R.T., Li, L.Y., and Purkiss, J.A. (2001a), 'Finite element analysis of coupled heat and moisture transfer in concrete subjected to fire', *Numerical Heat Transfer*, Part A, **39**, pp. 685-710.

Tenchev, R.T., Li, L.Y., Purkiss, J.A., and Khalafallah, B.H. (2001b), 'Finite element analysis of coupled heat and mass transfer in concrete when it is in a fire', *Magazine of Concrete Research*, **53**, No. 2, April, pp. 117-125.

Thelanderson, S. (1974), 'Effect of high temperatures on tensile strength of concrete', Report by Division of Structural Mechanics and Concrete Technology, Lund Institute of Technology, Sweden.

Thomas, H.R. and He, Y. (1997), 'A Coupled Heat-Moisture Transfer Theory for Deformable Unsaturated Soil and Its Algorithmic Implementation', International Journal for Numerical Methods in Engineering, Vol. 40, pp. 3421-3441.

Thomas, H.R. and Missoum, H. (1999), 'Three-Dimensional Coupled Heat, Moisture, and Air Transfer in a Deformable Unsaturated Soil' International Journal for Numerical Methods in Engineering, Vol. 44, pp. 919-943.

Ulm, F.J., Coussy, O., and Bažant, Z.P. (1999a), 'The "Channel" Fire. I: Chemoplastic Softening in Rapidly Heated Concrete', *J. Engineering Mechanics*, ASCE, Vol. 125, No. 3, pp. 272-282.

Ulm, F.J., Coussy, O., and Bažant, Z.P. (1999b), 'The "Channel" Fire. II: Analysis of Concrete Damage', *J. Engineering Mechanics*, ASCE, Vol. 125, No. 3, pp. 283-289.

Wakao, N. and Smith, J.M. (1962), 'Diffusion in Catalyst Pellets', *Chemical Engineering Science*, Vol. 17, pp. 825-834.

Wang, Y., Li, L.Y., and Page, C.L. (2000), 'Efficiency Investigation of Chloride Removal from Concrete by Using an Electrochemical Method', *Concrete Communication Conference 2000, Proceedings of the 10th BCA Annual Conference on Higher Education and the Concrete Industry, 29-30 June, Birmingham*, pp. 223-235.

Zhukov, V.V. (1975), 'Explosive failure of concrete during a fire', (in Russian), Translation No. DT 2124, Joint Fire Research Organisation, Borehamwood.

Zhukov, V.V. (1994), 'Forecast of a brittle failure of concrete by fire', Scientific Research Institute for Concrete and Reinforced Concrete, Moscow.

Zienkiewicz, O.C. and Taylor, R.L. (1991), 'The Finite Element Method-Volume 2: Solid and Fluid Mechanics , Dynamics, and Non-linearity', McGraw-Hill, London.

Zienkiewicz, O.C. and Taylor, R.L. (1994), 'The Finite Element Method-Volume 1: Basic Formulation and Linear Problems', McGraw-Hill, London.

Zou, Y., Rajapakse, R.K.N.D., and Graham, J. (1998), 'Coupled Heat-Moisture-Air Transfer in Deformable Unsaturated Media', *Journal of Engineering Mechanics*, ASCE, Vol. 124, No. 10, pp. 1090-1099.

APPENDIX A

DERIVATION OF EQUATIONS FOR SET T, P_G, P_V

A.1 GOVERNING EQUATIONS

The system of differential equations for heat and mass transfer in concrete under transient heating conditions is derived from the basic laws of conservation of mass and energy.

A.1.1 Conservation of Free Water

Conservation of mass of free liquid water is

$$\frac{\partial \bar{\rho}_L}{\partial t} = -\nabla \cdot J_L - \dot{E} + \frac{\partial \bar{\rho}_D}{\partial t} \tag{A.1}$$

where $\bar{\rho}_L$ is the mass of free liquid water per unit volume of concrete, in kg/m^3, J_L is the mass flux of free water per unit area of concrete, in kg/m^{2}s, $\dot{E}$ is the rate of evaporation of free water per unit volume of concrete, in kg/m^{3}s, and $\bar{\rho}_D$ is the mass of the chemically bound water released by dehydration per unit volume of concrete, in kg/m^3.

A.1.2 Conservation of Water Vapour

Conservation of mass of water vapour in the gaseous mixture of water vapour and air is

$$\frac{\partial}{\partial t}(\varepsilon_G \rho_V) = -\nabla \cdot J_V + \dot{E} \tag{A.2}$$

where ε_G is the volume fraction of the gaseous mixture of water vapour and air, ρ_V is the mass of water vapour per unit volume of the gaseous mixture, in kg/m^3, and J_V is the mass flux of water vapour per unit area of concrete, in kg/m^{2}s.

A.1.3 Conservation of Air

Conservation of mass of air in the gaseous mixture is

$$\frac{\partial}{\partial t}(\varepsilon_G \rho_A) = -\nabla \cdot J_A \tag{A.3}$$

where ρ_A is the mass of air per unit volume of the gaseous mixture, in kg/m^3, and J_A is the mass flux of air per unit area of concrete, in kg/m^{2}s.

A.1.4 Conservation of Energy

Conservation of energy is

$$\left(\overline{\rho C}\right)\frac{\partial T}{\partial t} = -\nabla \cdot \left(-k_{eff}\nabla T\right) - \left(\overline{\rho C v}\right)\cdot \nabla T - \lambda_E \dot{E} - \lambda_D \frac{\partial \bar{\rho}_D}{\partial t} \tag{A.4}$$

where $\overline{\rho C}$ is the effective heat capacity of concrete, in J/(m^3·°C), T is the temperature, in °C, k_{eff} is the effective thermal conductivity of concrete (Abdel-Rahman and Ahmed, 1996), in J/(m^2·s·°C/m), $\overline{\rho C v}$ is the vector of energy transport by material fluid flow, in J/(m^2·s·°C), λ_E is the latent heat of evaporation (Çengel, 1998), in J/kg, and λ_D is the specific heat of dehydration of the chemically bound water (Bažant and Kaplan, 1996), in J/kg.

A.2 SYSTEM OF DIFFERENTIAL EQUATIONS

From (A.1)-(A.4), the following system of three differential equations is derived:

$$\frac{\partial}{\partial t}(\varepsilon_G \rho_A) = -\nabla \cdot J_A \tag{A.5a}$$

Summation of (A.1) and (A.2) yields

$$\frac{\partial}{\partial t}(\varepsilon_G \rho_V) + \frac{\partial \bar{\rho}_L}{\partial t} - \frac{\partial \bar{\rho}_D}{\partial t} = -\nabla \cdot (J_V + J_L) \tag{A.5b}$$

The rate of evaporation of free water $\dot{E}$ $\left(= -\nabla \cdot J_L - \frac{\partial \bar{\rho}_L}{\partial t} + \frac{\partial \bar{\rho}_D}{\partial t} \right)$, as determined from (A.1), is substituted in (A.4) to yield

$$\left(\overline{\rho C}\right)\frac{\partial T}{\partial t} - \lambda_E \frac{\partial \bar{\rho}_L}{\partial t} + (\lambda_D + \lambda_E)\frac{\partial \bar{\rho}_D}{\partial t} = \nabla\left(k_{eff}\nabla T\right) + \lambda_E \nabla \cdot J_L - \left(\overline{\rho C v}\right)\nabla T \qquad \text{(A.5c)}$$

For the set of unknown variables T, P_G, P_V, the system of coupled transient differential equations that is suitable for a finite element solution is:

$$C_{AT}\frac{\partial T}{\partial t} + C_{AP}\frac{\partial P_G}{\partial t} + C_{AV}\frac{\partial P_V}{\partial t} = \nabla \cdot \left(K_{AT}\nabla T + K_{AP}\nabla P_G + K_{AV}\nabla P_V\right) \qquad \text{(A.6a)}$$

$$C_{MT}\frac{\partial T}{\partial t} + C_{MP}\frac{\partial P_G}{\partial t} + C_{MV}\frac{\partial P_V}{\partial t} = \nabla \cdot \left(K_{MT}\nabla T + K_{MP}\nabla P_G + K_{MV}\nabla P_V\right) \qquad \text{(A.6b)}$$

$$C_{TT}\frac{\partial T}{\partial t} + C_{TP}\frac{\partial P_G}{\partial t} + C_{TV}\frac{\partial P_V}{\partial t} = \nabla \cdot \left(K_{TT}\nabla T + K_{TP}\nabla P_G + K_{TV}\nabla P_V\right) \qquad \text{(A.6c)}$$

A.3 DERIVATION OF COEFFICIENTS

A.3.1 Water Vapour Flux

Total mass flux of water vapour including Fick's law of diffusion is:

$$J_V = \varepsilon_G \rho_V v_G - \varepsilon_G \rho_G D_{VA}\nabla\left(\frac{\rho_V}{\rho_G}\right) \qquad \text{(A.7)}$$

where v_G is the mass-average velocity of the gaseous mixture, in m/s, ρ_G is the mass of the gaseous mixture per unit volume of the gaseous mixture, in kg/m^3, and D_{VA} is the diffusion coefficient (or diffusivity) of water vapour through air, in m^2/s.

The mass-average velocity v_G is defined by Darcy's law as

$$v_G = -\frac{KK_G}{\mu_G}\nabla P_G \qquad \text{(A.8)}$$

where K is the intrinsic permeability of concrete, in m^2, K_G is the relative permeability of the gaseous mixture through concrete (Scheidegger, 1974), μ_G is the dynamic viscosity of the gaseous mixture (Çengel, 1998), in kg/ms, and P_G is the pore pressure of the gaseous mixture, in Pa. Thus,

$$-J_V = \frac{KK_G}{\mu_G}\varepsilon_G \rho_V \nabla P_G + \varepsilon_G \rho_G D_{VA} \nabla\left(\frac{\rho_V}{\rho_G}\right) \tag{A.9}$$

Ideal gas law (Çengel, 1998):

$$P_A = R_A \rho_A T \tag{A.10a}$$

$$P_V = R_V \rho_V T \tag{A.10b}$$

from which

$$\rho_A = \frac{P_A}{R_A T} \tag{A.11a}$$

$$\rho_V = \frac{P_V}{R_V T} \tag{A.11b}$$

Partial pressures and partial densities (Çengel, 1998):

$$P_G = P_A + P_V \tag{A.12a}$$

$$\rho_G = \rho_A + \rho_V \tag{A.12b}$$

Using (A.10)-(A.12),

$$\nabla\left(\frac{\rho_V}{\rho_G}\right) = \frac{\rho_G \nabla\rho_V - \rho_V \nabla\rho_G}{\rho_G^2} = \frac{(\rho_A + \rho_V)\nabla\rho_V - \rho_V \nabla(\rho_A + \rho_V)}{\rho_G^2}$$

$$= \frac{\rho_A \nabla\rho_V - \rho_V \nabla\rho_A}{\rho_G^2} \tag{A.13}$$

$$\nabla\rho_A = \nabla\left(\frac{P_A}{R_A T}\right) = \nabla\left(\frac{P_G - P_V}{R_A T}\right) = \nabla\left(\frac{P_G}{R_A T}\right) - \nabla\left(\frac{P_V}{R_A T}\right)$$

$$= \frac{T\nabla P_G - P_G \nabla T}{R_A T^2} - \frac{T\nabla P_V - R_V \rho_V T \nabla T}{R_A T^2}$$

$$= \left(\frac{R_V \rho_V}{R_A T} - \frac{P_G}{R_A T^2}\right)\nabla T + \left(\frac{1}{R_A T}\right)\nabla P_G + \left(-\frac{1}{R_A T}\right)\nabla P_V \tag{A.14}$$

$$\nabla\rho_V = \nabla\left(\frac{P_V}{R_V T}\right) = \frac{T\nabla P_V - P_V \nabla T}{R_V T^2} = \frac{\nabla P_V - R_V \rho_V \nabla T}{R_V T}$$

$$= \left(-\frac{\rho_V}{T}\right)\nabla T + (0)\nabla P_G + \left(\frac{1}{R_V T}\right)\nabla P_V \qquad \text{(A.15)}$$

Substituting (A.14) and (A.15) in (A.13) yields

$$\nabla\left(\frac{\rho_V}{\rho_G}\right) = \frac{\rho_V}{\rho_G^2 T}\left(\frac{P_G}{R_A T} - \rho_A - \frac{R_V}{R_A}\rho_V\right)\nabla T + \left(-\frac{\rho_V}{\rho_G^2 R_A T}\right)\nabla P_G$$

$$+ \frac{1}{\rho_G^2 T}\left(\frac{\rho_A}{R_V} + \frac{\rho_V}{R_A}\right)\nabla P_V \qquad \text{(A.16)}$$

Thus,

$$-J_V = \frac{\varepsilon_G \rho_V}{\rho_G T} D_{VA}\left(\frac{P_G}{R_A T} - \rho_A - \frac{R_V}{R_A}\rho_V\right)\nabla T$$

$$+ \varepsilon_G \rho_V \left(\frac{KK_G}{\mu_G} - \frac{1}{\rho_G R_A T} D_{VA}\right)\nabla P_G$$

$$+ \frac{\varepsilon_G}{\rho_G T} D_{VA}\left(\frac{\rho_A}{R_V} + \frac{\rho_V}{R_A}\right)\nabla P_V \qquad \text{(A.17)}$$

or

$$-J_V = K_{VT}\nabla T + K_{VP}\nabla P_G + K_{VV}\nabla P_V \qquad \text{(A.18)}$$

where

$$K_{VT} = \frac{\varepsilon_G \rho_V}{\rho_G T} D_{VA}\left(\frac{P_G}{R_A T} - \rho_A - \frac{R_V}{R_A}\rho_V\right) \qquad \text{(A.19a)}$$

$$K_{VP} = \varepsilon_G \rho_V \left(\frac{KK_G}{\mu_G} - \frac{1}{\rho_G R_A T} D_{VA}\right) \qquad \text{(A.19b)}$$

$$K_{VV} = \frac{\varepsilon_G}{\rho_G T} D_{VA}\left(\frac{\rho_A}{R_V} + \frac{\rho_V}{R_A}\right) \qquad \text{(A.19c)}$$

A.3.2 Air Flux

Total mass flux of air including Fick's law of diffusion:

$$J_A = \varepsilon_G \rho_A v_G - \varepsilon_G \rho_G D_{AV} \nabla\left(\frac{\rho_A}{\rho_G}\right) \tag{A.20}$$

where D_{AV} is the diffusivity of air through water vapour in the gaseous mixture, in m^2/s.

Applying Darcy's law (A.8) yields

$$-J_A = \frac{KK_G}{\mu_G} \varepsilon_G \rho_A \nabla P_G + \varepsilon_G \rho_G D_{AV} \nabla\left(\frac{\rho_A}{\rho_G}\right) \tag{A.21}$$

$$\nabla\left(\frac{\rho_A}{\rho_G}\right) = \nabla\left(\frac{\rho_G - \rho_V}{\rho_G}\right) = -\nabla\left(\frac{\rho_V}{\rho_G}\right) \tag{A.22}$$

Thus,

$$\begin{aligned} -J_A = {} & \frac{\varepsilon_G \rho_V}{\rho_G T} D_{AV}\left(\rho_A + \frac{R_V}{R_A}\rho_V - \frac{P_G}{R_A T}\right)\nabla T \\ & + \varepsilon_G\left(\rho_A \frac{KK_G}{\mu_G} + \frac{\rho_V}{\rho_G R_A T} D_{AV}\right)\nabla P_G \\ & + \left[-\frac{\varepsilon_G}{\rho_G T} D_{AV}\left(\frac{\rho_A}{R_V} + \frac{\rho_V}{R_A}\right)\right]\nabla P_V \end{aligned} \tag{A.23}$$

or

$$-J_A = K_{AT}\nabla T + K_{AP}\nabla P_G + K_{AV}\nabla P_V \tag{A.24}$$

where

$$K_{AT} = \frac{\varepsilon_G \rho_V}{\rho_G T} D_{AV}\left(\rho_A + \frac{R_V}{R_A}\rho_V - \frac{P_G}{R_A T}\right) \tag{A.25a}$$

$$K_{AP} = \varepsilon_G\left(\rho_A \frac{KK_G}{\mu_G} + \frac{\rho_V}{\rho_G R_A T} D_{AV}\right) \tag{A.25b}$$

$$K_{AV} = -\frac{\varepsilon_G}{\rho_G T} D_{AV}\left(\frac{\rho_A}{R_V} + \frac{\rho_V}{R_A}\right) \tag{A.25c}$$

A.3.3 Water Flux

Mass flux of water:

$$J_L = \bar{\rho}_L v_L \tag{A.26}$$

where v_L is the absolute velocity of liquid water, in m/s, that is defined by Darcy's law as

$$v_L = -\frac{KK_L}{\mu_L}\nabla P_L \tag{A.27}$$

where K_L is the relative permeability of free liquid water through concrete (Scheidegger, 1974), μ_L is the dynamic viscosity of liquid water (Çengel, 1998), in kg/ms, and P_L is the pressure of free liquid water (Dayan and Gluekler, 1982), in Pa.

Thus,

$$-J_L = \bar{\rho}_L \frac{KK_L}{\mu_L}\nabla P_L \tag{A.28}$$

Assuming that the influence of the capillary pressure is accounted for by K_L, and thus $P_L = P_G$, then

$$-J_L = \bar{\rho}_L \frac{KK_L}{\mu_L}\nabla P_G \tag{A.29}$$

or

$$-J_L = K_{LT}\nabla T + K_{LP}\nabla P_G + K_{LV}\nabla P_V \tag{A.30}$$

where

$$K_{LT} = K_{LV} = 0 \tag{A.31a}$$

$$K_{LP} = \bar{\rho}_L \frac{KK_L}{\mu_L} \tag{A.31b}$$

A.3.4 Moisture (Liquid Water and Water Vapour) Flux

Adding (A.18) and (A.30) yields

$$-(J_V + J_L) = (K_{VT} + K_{LT})\nabla T + (K_{VP} + K_{LP})\nabla P_G + (K_{VV} + K_{LV})\nabla P_V \tag{A.32}$$

or

$$-(J_V + J_L) = K_{MT}\nabla T + K_{MP}\nabla P_G + K_{MV}\nabla P_V \tag{A.33}$$

where

$$K_{MT} = \frac{\varepsilon_G \rho_V}{\rho_G T} D_{VA}\left(\frac{P_G}{R_A T} - \rho_A - \frac{R_V}{R_A}\rho_V\right) \tag{A.34a}$$

$$K_{MP} = \varepsilon_G \rho_V \left(\frac{KK_G}{\mu_G} - \frac{1}{\rho_G R_A T} D_{VA}\right) + \bar{\rho}_L \frac{KK_L}{\mu_L} \tag{A.34b}$$

$$K_{MV} = \frac{\varepsilon_G}{\rho_G T} D_{VA}\left(\frac{\rho_A}{R_V} + \frac{\rho_V}{R_A}\right) \tag{A.34c}$$

A.3.5 K_{TT}, K_{TP}, and K_{TV}

K_{TT}, K_{TP}, and K_{TV} are determined from the right hand side of (A.5c). They are:

$$K_{TT} = k_{eff} \tag{A.35a}$$

$$K_{TP} = -\lambda_E \bar{\rho}_L \frac{KK_L}{\mu_L} \tag{A.35b}$$

$$K_{TV} = 0 \tag{A.35c}$$

K_{TP} required substitution for $\nabla J_L\left(= \nabla\left(-\bar{\rho}_L (KK_L/\mu_L)\nabla P_G\right)\right)$ obtained from differentiating (A.29) in (A.5c).

A.3.6 Time Derivatives

A.3.6.1 $\frac{\partial}{\partial t}(\varepsilon_G \rho_A)$

$$\frac{\partial}{\partial t}(\varepsilon_G \rho_A) = \varepsilon_G \frac{\partial \rho_A}{\partial t} + \rho_A \frac{\partial \varepsilon_G}{\partial t} \tag{A.36}$$

$$\begin{aligned}\frac{\partial \rho_A}{\partial t} &= \frac{\partial}{\partial t}\left(\frac{P_A}{R_A T}\right) = \frac{\partial}{\partial t}\left(\frac{P_G - P_V}{R_A T}\right) = \frac{\partial}{\partial t}\left(\frac{P_G}{R_A T}\right) - \frac{\partial}{\partial t}\left(\frac{P_V}{R_A T}\right) \\ &= \frac{1}{R_A T^2}\left(T\frac{\partial P_G}{\partial t} - P_G\frac{\partial T}{\partial t} - T\frac{\partial P_V}{\partial t} + P_V\frac{\partial T}{\partial t}\right) \\ &= \left[\frac{1}{R_A T^2}(P_V - P_G)\right]\frac{\partial T}{\partial t} + \left(\frac{1}{R_A T}\right)\frac{\partial P_G}{\partial t} + \left(-\frac{1}{R_A T}\right)\frac{\partial P_V}{\partial t}\end{aligned} \tag{A.37}$$

Porosity:

$$P_{or} = \varepsilon_L + \varepsilon_G \tag{A.38}$$

from which

$$\varepsilon_G = P_{or} - \varepsilon_L \tag{A.39}$$

Thus,

$$\frac{\partial \varepsilon_G}{\partial t} = \frac{\partial P_{or}}{\partial t} - \frac{\partial \varepsilon_L}{\partial t} \tag{A.40}$$

The porosity is a function of the dehydrated water volume fraction:

$$P_{or} = {}^0P_{or} + \varepsilon_D \tag{A.41}$$

where

$$\varepsilon_D = \frac{\bar{\rho}_D}{\rho_L} \tag{A.42}$$

where $\bar{\rho}_D$ is the bound water released by dehydration (Bažant and Kaplan, 1996):

$$\bar{\rho}_D = f(\rho_{cem}, T) \tag{A.43}$$

Thus,

$$\frac{\partial P_{or}}{\partial t} = \frac{\partial P_{or}}{\partial T}\frac{\partial T}{\partial t} \tag{A.44}$$

Volume fraction of free water:

$$\varepsilon_L = \frac{\bar{\rho}_L}{\rho_L} \tag{A.45}$$

From the sorption isotherms (Bažant and Thonguthai, 1978):

$$\bar{\rho}_L = f\left(\rho_{cem}, T, \frac{P_V}{P_{sat}}\right) \tag{A.46}$$

Thus,

$$\frac{\partial \varepsilon_L}{\partial t} = \frac{\partial \varepsilon_L}{\partial T}\frac{\partial T}{\partial t} + \frac{\partial \varepsilon_L}{\partial P_V}\frac{\partial P_V}{\partial t}$$

$$= \frac{1}{\rho_L}\frac{\partial \bar{\rho}_L}{\partial T}\frac{\partial T}{\partial t} + \frac{1}{\rho_L}\frac{\partial \bar{\rho}_L}{\partial P_V}\frac{\partial P_V}{\partial t} \tag{A.47}$$

Substitution of (A.44) and (A.47) in (A.40) yields

$$\frac{\partial \varepsilon_G}{\partial t} = \left(\frac{\partial P_{or}}{\partial T} - \frac{1}{\rho_L}\frac{\partial \bar{\rho}_L}{\partial T}\right)\frac{\partial T}{\partial t} + (0)\frac{\partial P_G}{\partial t} + \left(-\frac{1}{\rho_L}\frac{\partial \bar{\rho}_L}{\partial P_V}\right)\frac{\partial P_V}{\partial t} \tag{A.48}$$

Substitution of (A.37) and (A.48) in (A.36) gives

$$\frac{\partial}{\partial t}(\varepsilon_G \rho_A) = \left[\frac{\varepsilon_G}{R_A T^2}(P_V - P_G) + \rho_A \frac{\partial P_{or}}{\partial T} - \frac{\rho_A}{\rho_L}\frac{\partial \bar{\rho}_L}{\partial T}\right]\frac{\partial T}{\partial t}$$

$$+\left(\frac{\varepsilon_G}{R_A T}\right)\frac{\partial P_G}{\partial t}$$

$$+\left(-\frac{\rho_A}{\rho_L}\frac{\partial \bar{\rho}_L}{\partial P_V} - \frac{\varepsilon_G}{R_A T}\right)\frac{\partial P_V}{\partial t} \tag{A.49}$$

or

$$\frac{\partial}{\partial t}(\varepsilon_G \rho_A) = C_{AT}\frac{\partial T}{\partial t} + C_{AP}\frac{\partial P_G}{\partial t} + C_{AV}\frac{\partial P_V}{\partial t} \tag{A.50}$$

where

$$C_{AT} = \frac{\varepsilon_G}{R_A T^2}(P_V - P_G) + \rho_A \frac{\partial P_{or}}{\partial T} - \frac{\rho_A}{\rho_L}\frac{\partial \bar{\rho}_L}{\partial T} \tag{A.51a}$$

$$C_{AP} = \frac{\varepsilon_G}{R_A T} \tag{A.51b}$$

$$C_{AV} = -\frac{\rho_A}{\rho_L}\frac{\partial \bar{\rho}_L}{\partial P_V} - \frac{\varepsilon_G}{R_A T} \tag{A.51c}$$

A.3.6.2 $\frac{\partial}{\partial t}(\varepsilon_G \rho_V)$

$$\frac{\partial}{\partial t}(\varepsilon_G \rho_V) = \varepsilon_G \frac{\partial \rho_V}{\partial t} + \rho_V \frac{\partial \varepsilon_G}{\partial t} \tag{A.52}$$

$$\frac{\partial \rho_V}{\partial t} = \frac{\partial}{\partial t}\left(\frac{P_V}{R_V T}\right) = \frac{1}{R_V T^2}\left(T\frac{\partial P_V}{\partial t} - P_V \frac{\partial T}{\partial t}\right)$$
$$= \left(-\frac{\rho_V}{T}\right)\frac{\partial T}{\partial t} + (0)\frac{\partial P_G}{\partial t} + \left(\frac{1}{R_V T}\right)\frac{\partial P_V}{\partial t} \tag{A.53}$$

Substitution of (A.48) and (A.53) in (A.52) yields

$$\frac{\partial}{\partial t}(\varepsilon_G \rho_V) = \left[\rho_V\left(-\frac{\varepsilon_G}{T} + \frac{\partial P_{or}}{\partial T} - \frac{1}{\rho_L}\frac{\partial \bar{\rho}_L}{\partial T}\right)\right]\frac{\partial T}{\partial t} + (0)\frac{\partial P_G}{\partial t}$$
$$+ \left(\frac{\varepsilon_G}{R_V T} - \frac{\rho_V}{\rho_L}\frac{\partial \bar{\rho}_L}{\partial P_V}\right)\frac{\partial P_V}{\partial t} \tag{A.54}$$

A.3.6.3 Moisture: $\frac{\partial}{\partial t}(\varepsilon_G \rho_V) + \frac{\partial \bar{\rho}_L}{\partial t} - \frac{\partial \bar{\rho}_D}{\partial t}$

From (A.46),

$$\frac{\partial \bar{\rho}_L}{\partial t} = \left(\frac{\partial \bar{\rho}_L}{\partial T} \right) \frac{\partial T}{\partial t} + (0) \frac{\partial P_G}{\partial t} + \left(\frac{\partial \bar{\rho}_L}{\partial P_V} \right) \frac{\partial P_V}{\partial t} \tag{A.55}$$

From (A.43),

$$\frac{\partial \bar{\rho}_D}{\partial t} = \left(\frac{\partial \bar{\rho}_D}{\partial T} \right) \frac{\partial T}{\partial t} + (0) \frac{\partial P_G}{\partial t} + (0) \frac{\partial P_V}{\partial t} \tag{A.56}$$

Thus, from (A.54)-(A.56),

$$\frac{\partial}{\partial t}(\varepsilon_G \rho_V) + \frac{\partial \bar{\rho}_L}{\partial t} - \frac{\partial \bar{\rho}_D}{\partial t} = \left[\rho_V \left(-\frac{\varepsilon_G}{T} + \frac{\partial P_{or}}{\partial T} - \frac{1}{\rho_L} \frac{\partial \bar{\rho}_L}{\partial T} \right) + \frac{\partial \bar{\rho}_L}{\partial T} - \frac{\partial \bar{\rho}_D}{\partial T} \right] \frac{\partial T}{\partial t}$$

$$+ (0) \frac{\partial P_G}{\partial t} + \left[\frac{\varepsilon_G}{R_V T} + \left(1 - \frac{\rho_V}{\rho_L} \right) \frac{\partial \bar{\rho}_L}{\partial P_V} \right] \frac{\partial P_V}{\partial t} \tag{A.57}$$

or

$$\frac{\partial}{\partial t}(\varepsilon_G \rho_V) + \frac{\partial \bar{\rho}_L}{\partial t} - \frac{\partial \bar{\rho}_D}{\partial t} = C_{MT} \frac{\partial T}{\partial t} + C_{MP} \frac{\partial P_G}{\partial t} + C_{MV} \frac{\partial P_V}{\partial t} \tag{A.58}$$

where

$$C_{MT} = \rho_V \left(-\frac{\varepsilon_G}{T} + \frac{\partial P_{or}}{\partial T} - \frac{1}{\rho_L} \frac{\partial \bar{\rho}_L}{\partial T} \right) + \frac{\partial \bar{\rho}_L}{\partial T} - \frac{\partial \bar{\rho}_D}{\partial T} \tag{A.59a}$$

$$C_{MP} = 0 \tag{A.59b}$$

$$C_{MV} = \frac{\varepsilon_G}{R_V T} + \left(1 - \frac{\rho_V}{\rho_L} \right) \frac{\partial \bar{\rho}_L}{\partial P_V} \tag{A.59c}$$

A.3.6.4 Energy: $\left(\overline{\rho C}\right)\frac{\partial T}{\partial t} - \lambda_E \frac{\partial \bar{\rho}_L}{\partial t} + (\lambda_D + \lambda_E)\frac{\partial \bar{\rho}_D}{\partial t}$

Using (A.55) and (A.56),

$$\left(\overline{\rho C}\right)\frac{\partial T}{\partial t} - \lambda_E \frac{\partial \bar{\rho}_L}{\partial t} + (\lambda_D + \lambda_E)\frac{\partial \bar{\rho}_D}{\partial t} = \left[\left(\overline{\rho C}\right) - \lambda_E \frac{\partial \bar{\rho}_L}{\partial T} + (\lambda_D + \lambda_E)\frac{\partial \bar{\rho}_D}{\partial T}\right]\frac{\partial T}{\partial t}$$

$$+ (0)\frac{\partial P_G}{\partial t} + \left(-\lambda_E \frac{\partial \bar{\rho}_L}{\partial P_V}\right)\frac{\partial P_V}{\partial t} \qquad \text{(A.60)}$$

or

$$\left(\overline{\rho C}\right)\frac{\partial T}{\partial t} - \lambda_E \frac{\partial \bar{\rho}_L}{\partial t} + (\lambda_D + \lambda_E)\frac{\partial \bar{\rho}_D}{\partial t} = C_{TT}\frac{\partial T}{\partial t} + C_{TP}\frac{\partial P_G}{\partial t} + C_{TV}\frac{\partial P_V}{\partial t} \qquad \text{(A.61)}$$

where

$$C_{TT} = \left(\overline{\rho C}\right) - \lambda_E \frac{\partial \bar{\rho}_L}{\partial T} + (\lambda_D + \lambda_E)\frac{\partial \bar{\rho}_D}{\partial T} \qquad \text{(A.62a)}$$

$$C_{TP} = 0 \qquad \text{(A.62b)}$$

$$C_{TV} = -\lambda_E \frac{\partial \bar{\rho}_L}{\partial P_V} \qquad \text{(A.62c)}$$

APPENDIX B

MODIFICATIONS

B.1 MODIFICATIONS FOR IMPLEMENTING CONCRETE DIFFUSIVITY

The heart of the model is a subroutine called "SUBROUTINE RvPgT" (RvPgT stands for the primary unknown variables ρ_V, P_G, and T) in which all material properties, e.g. diffusivity of air D_{AV}, diffusivity of water vapour D_{VA}, effective heat capacity of concrete $\overline{\rho C}$, effective thermal conductivity of concrete k_{eff}, latent heat of evaporation of the free water λ_E, specific heat of dehydration of the chemically bound water λ_D, relative permeability of the gaseous mixture through concrete K_G, dynamic viscosity of the gaseous mixture μ_G, relative permeability of free liquid water through concrete K_L, dynamic viscosity of liquid water μ_L, are defined and thus determined. Furthermore, in this subroutine, the coefficients related to the mass matrix, i.e. (19) in Appendix C, and those related to the stiffness matrix, i.e. (20) in Appendix C), are defined and thus determined.

In the very first version of the model (the one used in this study), Krischer and Rohnalter's molecular diffusivity was adopted, that is,

$$D = 5.893 \times 10^{-6} \frac{T^{2.3}}{P_g} \tag{2.8}$$

and thus the model was designed such that $D_{AV} = D_{VA}$.

Thus, the modifications related to the implementation of concrete diffusivity were made to the Fortran statements that define D_{AV} and D_{VA}, and to the Fortran statements that define the coefficients in which the diffusivities appear.

The parts of the original Fortran listing (in bold) related to the diffusivities and coefficients in subroutine RvPgT are listed below. Statements are numbered for convenience only. Also, for convenience, and in order to avoid unnecessary repetition, coefficients that must be modified in this

section as well as those that need to be modified in the following Section B.2 are included in this listing. By referring to Appendix C, it can be seen that the terms that appear in the listing are self-explained. For example, **DAV** $(\equiv D_{AV})$ is diffusivity of air through water vapour, **Pg** $(\equiv P_G)$ is pore pressure, **Tkelv** $(\equiv T)$, is absolute temperature, in K, **epsG** $(\equiv \varepsilon_G)$ is gaseous mixture volume fraction, **roTilV** (and **roV**) $\left(\equiv \tilde{\rho}_V\right)$ is water vapour content, **roG** $(\equiv \rho_G)$ is gaseous mixture content, **roVroG** $\left(\equiv \tilde{\rho}_V / \rho_G\right)$ is the ratio of water vapour content to gaseous mixture content, **Tkelv2** $\left(\equiv T^2\right)$ is the square of absolute temperature, **sK** $(\equiv K)$ is intrinsic permeability, and **akvT** $(\equiv K_{VT})$ is the first coefficient on the right hand side of (B1f) of Appendix C.

.

Certain Fortran statements not related to these modifications

.

*************Material properties**

(1) **if (Pg.gt.0.) DAV = 5.893d-6*(Tkelv**2.3d0)/Pg**

(2) **DAV = DAV*epsG**

(3) **DVA = DAV**

.

Other Fortran statements related to defining, and thus determining, other properties

.

*************Coefficients used in 'Stiffness' matrix integrals**

(4) **roVroG = 0.d0**

(5) **roAroG = 0.d0**

(6) **if (roG.ne.0.d0) roVroG = roTilV/roG**

(7) **if (roG.ne.0.d0) roAroG = roTilA/roG**

(8) **akvT = DVA*roVroG*Pg/RA/Tkelv2**

(9) **akvP1 = sK*rKG/dmuG*roTilV**

(10) **akvP2 = DVA*roVroG/RA/Tkelv**

(11) **akvP = akvP1 - akvP2**

(12) **akvr1 = DVA*roAroG**

(13) **akvr2 = DVA*roVroG*RV/RA**

(14) **akvr = akvr1 + akvr2**

(15) **aklP = roTilL*sK*rKL/dmuL**

(16) **akAT = - akvT**

(17) **akAP1 = sK*rKG/dmuG*roTilA**

(18) **akAP2 = akvP2**

(19) **akAP = akAP1+akAP2**

(20) **akAr = -akvr**

(21) **akWT = akvT**

(22) **akWP = akvP+aklP**

(23) **akWr = akvr**

(24) **akTT = effK**

(25) **akTP = -amda*aklP**

.

Statements related to determination of derivative of bound water release **dDbdT** $\left(\equiv \partial \bar{\rho}_D / \partial T\right)$

.

**********Coefficients used in 'Mass' matrix**

(26) **acTT = amda*roL*deGdT + rC + amdaD*dDbdT**

(27) **acTr = amda*roL*deGdrV**

(28) **acWT = (roTilV-roL)*deGdT**

(29) **acWr = (roTilV-roL)*deGdrV + epsG**

(30) **acAT1 = roTilA*deGdT**

(31) **acAT2 = epsG*Pg/RA/Tkelv2**

(32) **acAT = acAT1 – acAT2**

(33) **acAP = epsG/RA/Tkelv**

(34) **acAr1 = roTilA*deGdrV**

(35) **acAr2 = epsG*RV/RA**

(36) **acAr = acAr1 - acAr2**

.

Other non-relevant statements

.

The first modification was to replace the Fortran statements that define molecular diffusivity with statements that define concrete diffusivity.

Concrete diffusivity of water vapour is:

$$D_{Conc,V} = 1.5 \times 10^{-7} \varepsilon_g P_{or}^{0.8} T^{0.5} \tag{3.29}$$

and concrete diffusivity of air is:

$$D_{Conc,A} = 1.18 \times 10^{-7} \varepsilon_g P_{or}^{0.8} T^{0.5} \tag{3.32}$$

Thus, Statements (1)-(3) were replaced with the following two statements:

DAV = 1.18d-7*epsG*(Por8.d-1)*(Tkelv**5.d-1)**
DVA = 1.5d-7*epsG*(Por8.d-1)*(Tkelv**5.d-1)**

If the same approach of using the partial diffusivities used in the model were adopted, then the partial concrete diffusivity of water vapour is

$$D'_{Conc,V} = 1.5 \times 10^{-7} P_{or}^{0.8} T^{0.5} \tag{3.28}$$

and the partial concrete diffusivity of air is

$$D'_{Conc,A} = 1.18 \times 10^{-7} P_{or}^{0.8} T^{0.5} \tag{3.31}$$

Then, Statements (1)-(3) would have been replaced with the following statements:

DAV = 1.18d-7*(Por8.d-1)*(Tkelv**5.d-1)**
DVA = 1.5d-7*(Por8.d-1)*(Tkelv**5.d-1)**
DAV = DAV*epsG
DVA = DVA*epsG

As seen in (B1f) (Appendix C), the diffusivity of water vapour through air D_{VA} is one of the variables in the first coefficient K_{VT} that is defined by Statement (8). On the other hand, the first coefficient K_{AT} on the right hand side of (B2c) is a function of the diffusivity of air through water vapour D_{AV} (other variables are the same as those in K_{VT}). Consequently, since $D_{AV} = D_{VA}$ when molecular diffusivity is adopted, Statement (16) is valid. However, when concrete diffusivity is to be adopted, $D_{AV} \neq D_{VA}$, and thus $K_{AT} \neq -K_{VT}$. Thus, to implement concrete diffusivity, Statement (16) was modified as follows:

akAT = -akvT*DAV/DVA

Similarly, the difference between the second term of the coefficient K_{VP} in (B1e) and that of the coefficient K_{AP} in (B2c) is only in the diffusivity, and thus Statement (18) is valid when the diffusivity is assumed to be molecular, but is invalid when concrete diffusivity is to be adopted. Thus, Statement (18) was replaced with the following statement:

akAP2 = akvP2*DAV/DVA

Finally, when the diffusivity is assumed to be molecular, and thus $D_{AV} = D_{VA}$, the third coefficient K_{AV} in (B2d) is equal to minus K_{VV} in (B1e), and thus Statement (20) is valid. However, to implement concrete diffusivity, this statement had to be replaced with:

akAr = -akvr*DAV/DVA

The last three modifications made to Statements (16), (18), and (20) are *permanent*, and made the model workable with any type of diffusivity and any set of unknown variables; all that needed to adopt different diffusivities is to modify the first part of the listing that is related to defining the diffusivities, i.e. Statements (1)-(3).

B.2 MODIFICATIONS FOR IMPLEMENTING SET T, P_G, P_V

As discussed in Section 4.4, only the modifications related to the coefficients C_{TV}, C_{AT}, C_{AV}, C_{MT}, C_{MV}, K_{AT}, K_{AV}, K_{MT}, and K_{MV} will be described. Reference will be made to the listing in Section B.1.

The first statement to be modified was Statement (8) **akvT** $(\equiv K_{VT})$. Considering (A.19a), this statement had to be replaced with the following statement:

akvT=DVA*roVroG/Tkelv*(Pg/RA/Tkelv – roTilA - RV/RA*roTilV)

Consequently, the necessary modifications to K_{MT} $(= K_{VT} + K_{LT})$ to conform to (A.34a) has been completed, since $K_{LT} = 0$ (A.31a), and thus Statement (21) **akWT** $(\equiv K_{MT})$ remains unchanged.

The next modification was made to Statement (12) **akvr1** that is the first term of K_{VV} in (B1e) of Appendix C. Considering the first term of K_{VV} in (A.19c), i.e. $\varepsilon_G D_{VA} \rho_A / (\rho_G TR_V)$, this statement was replaced with the following:

akvr1 = DVA*roAroG/Tkelv/RV

Then, modifications had to be made to Statement (13) **akvr2** that is the second term of K_{VV} in (B1e) of Appendix C. From the second term of K_{VV} in (A.19c), i.e. $\varepsilon_G D_{VA} \rho_V / (\rho_G TR_A)$, this statement was replaced with the following:

akvr2 = DVA*roVroG/Tkelv/RA

Statement (14) **akvr** $(\equiv K_{VV})$ remains unchanged even though K_{VV} is different for each set of unknown variables, since the modifications were made to the individual terms **akvr1** and **akvr2** above. Consequently, the necessary modifications to K_{MV} $(= K_{VV} + K_{LV})$ to conform to (A.34c) have been made, since $K_{LV} = 0$ (A.31a), and thus Statement (23) **akWr** $(\equiv K_{MV})$ remains unchanged.

The modifications made to Statement (16) **akAT** $(\equiv K_{AT})$ in Section B.1 took care of the necessary modifications required to conform to the new K_{AT} (A.25a), since, as in the original set of unknown variables, $K_{AT} = -K_{VT}(D_{AV} / D_{VA})$, while K_{VT} has been already modified in this section. Similarly, the modifications made to Statement (20) **akAr** $(\equiv K_{AV})$ in Section B.1 took care of the necessary modifications required to conform to the new K_{AV} (A.25c), since $K_{AV} = -K_{VV}(D_{AV} / D_{VA})$, while K_{VV} has been modified in this section.

This completes the modifications necessary for the coefficients K_{AT}, K_{AV}, K_{MT}, and K_{MV}.

Next, Statement (27) **acTr** $(\equiv C_{TV})$ was modified to the following:

acTr = amda*roL*deGdPv

This statement may require some explanation. From (A.62c), it can be seen that $C_{TV} = -\lambda_E\left(\partial \bar{\rho}_L / \partial P_V\right)$, while the statement above implies that $C_{TV} = \lambda_E \rho_L (\partial \varepsilon_G / \partial P_V)$. Both forms are equivalent. The form expressed by the statement was obtained with some mathematical manipulations as follows:

From (A.38):

$$\varepsilon_L = P_{or} - \varepsilon_G \tag{B.1}$$

or

$$\bar{\rho}_L = \rho_L (P_{or} - \varepsilon_G) \tag{B.2}$$

Then,

$$\frac{\partial \bar{\rho}_L}{\partial P_V} = \rho_L \frac{\partial P_{or}}{\partial P_V} - \rho_L \frac{\partial \varepsilon_G}{\partial P_V} \tag{B.3}$$

But, from (A.41), P_{or} is a function of ε_D (A.42) that is a function of $\bar{\rho}_D$ (A.43) that is *not* a function of P_V, and thus $\partial P_{or} / \partial P_V = 0$. Hence,

$$\frac{\partial \bar{\rho}_L}{\partial P_V} = -\rho_L \frac{\partial \varepsilon_G}{\partial P_V} \tag{B.4}$$

Thus,

$$C_{TV} = -\lambda_E \frac{\partial \bar{\rho}_L}{\partial P_V} = \lambda_E \rho_L \frac{\partial \varepsilon_G}{\partial P_V} \tag{B.5}$$

The next modifications were made to Statement (28) **acWT** $(\equiv C_{MT})$ that had to be modified to conform to (A.59a) as follows:

acWT = (roTilV-roL)*deGdT – epsG*roTilV/Tkelv

This statement may need some explanation. The mathematical formula that corresponds to this statement is:

$$C_{MT} = (\rho_V - \rho_L)\frac{\partial \varepsilon_G}{\partial T} - \frac{\varepsilon_G \rho_V}{T} \tag{B.6}$$

while (A.59a) is $C_{MT} = \rho_V \left(\frac{\partial P_{or}}{\partial T} - \frac{\varepsilon_G}{T} \right) + \left(1 - \frac{\rho_V}{\rho_L} \right) \frac{\partial \bar{\rho}_L}{\partial T} - \frac{\partial \bar{\rho}_D}{\partial T}$.

The compact form (B.6) expressed by the statement was obtained with the following mathematical manipulations:

From (A.38),

$$\frac{\partial P_{or}}{\partial T} = \frac{\partial \varepsilon_G}{\partial T} + \frac{1}{\rho_L} \frac{\partial \bar{\rho}_L}{\partial T} \tag{B.7}$$

Also, the dehydrated water $\bar{\rho}_D = \rho_L \varepsilon_D$, and thus

$$\frac{\partial \bar{\rho}_D}{\partial T} = \rho_L \frac{\partial \varepsilon_D}{\partial T} \tag{B.8}$$

From (A.41),

$$\varepsilon_D = P_{or} - {}^0P_{or} \tag{B.9}$$

Using (B.7),

$$\frac{\partial \varepsilon_D}{\partial T} = \frac{\partial P_{or}}{\partial T} = \frac{\partial \varepsilon_G}{\partial T} + \frac{1}{\rho_L}\frac{\partial \bar{\rho}_L}{\partial T} \tag{B.10}$$

Thus,

$$\frac{\partial \bar{\rho}_D}{\partial T} = \rho_L \frac{\partial \varepsilon_G}{\partial T} + \frac{\partial \bar{\rho}_L}{\partial T} \tag{B.11}$$

Substitution of (B.7) and (B.11) for $\partial P_{or}/\partial T$ and $\partial \bar{\rho}_D/\partial T$, respectively, in (A.59a) leads to (B.6).

Next, Statement (29) **acWr** $(\equiv C_{MV})$ had to be modified to conform to (A.59c) as follows:

acWr = (roTilV-roL)*deGdPv + epsG/RV/Tkelv

Then, Statement (31) **acAT2** was modified to conform to the first term on the right hand side of (A.51a) as follows:

acAT2 = epsG*(Pg-Pv)/RA/Tkelv2

Thus, Statement (32) **acAT** $(\equiv C_{MA})$ remains unchanged, since the necessary modifications were made to Statement (31) **acAT2** above.

Next, Statement (34) **acAr1** that is the first term on the right hand side of (A.51c) was modified. This term was expressed differently by applying (B.4) as follows:

$$-\frac{\rho_A}{\rho_L}\frac{\partial \bar{\rho}_L}{\partial P_V} = \rho_A \frac{\partial \varepsilon_G}{\partial P_V} \tag{B.12}$$

Thus, Statement (34) was modified to the following:

acAr1 = roTilA*deGdPv

Finally, Statement (35) **acAr2** that is the second term on the right hand side of (A.51c) was modified as follows:

acAr2 = epsG/RA/Tkelv

Thus, the necessary modifications to C_{MV} were complete, and hence Statement (36) **acAr** $(\equiv C_{MV})$ remains unchanged.

B.3 IMPLEMENTING TORTUOSITY AND OTHER DIFFUSIVITY EQUATIONS

In order to implement Krischer and Rohnalter's molecular diffusivity with the tortuosity considered, i.e.

$$D_{e,VA} = 5.893\times10^{-6}\frac{\varepsilon_g}{\tau}\frac{T^{2.3}}{P_g} \tag{3.3}$$

where the tortuosity $\tau = 3$, Statement (1) was modified as follows:

if (Pg.gt.0.) DAV = 5.893d-6*(Tkelv2.3d0)/Pg/3.d0**

from which ε_g is excluded, since it is introduced by Statement (2).

To implement molecular diffusivity according to Chapman-Enskog theory, i.e.

$$D_{VA} = 5.6\times10^{-4}\frac{T^{1.5}}{P_g} \tag{2.12}$$

Statement (1) was modified as follows:

if (Pg.gt.0.) DAV = 5.6d-4*(Tkelv1.5d0)/Pg**

To implement molecular diffusivity according to Chapman-Enskog theory with the tortuosity considered, i.e.

$$D_{e,VA} = 5.6\times10^{-4}\frac{\varepsilon_g}{\tau}\frac{T^{1.5}}{P_g} \tag{3.4}$$

Statement (1) was modified as follows:

if (Pg.gt.0.) DAV = 5.6d-4*(Tkelv1.5d0)/Pg/3.d0**

from which ε_g is excluded, since it is introduced by Statement (2).

B.4 IMPLEMENTING VARIABLE INTRINSIC PERMEABILITY

To implement (4.5), i.e. $K={}^0K\left(\frac{P_{or}}{{}^0P_{or}}\right)^3\left(\frac{1-{}^0P_{or}}{1-P_{or}}\right)^2$, the following statement was introduced in its proper location in the program:

sK = 8.d-17*(Por/Por0)3*((1-Por0)/(1-Por))**2**

where **8.d-17** $\left(\equiv 8\times10^{-17}\right)$ is the mean value of the initial intrinsic permeability ${}^0K$, in m^2, at ambient temperature.

APPENDIX C

(For convenience of readers, the governing equations used in the mathematical model developed by Tenchev *et al.* (2001a) along with the equations to which reference was made in Appendix B are presented in this appendix.)

APPENDIX D

APPENDIX E

(The paper was published in Concrete Communication Conference 2000, *Proceedings of the 10th BCA Annual Conference on Higher Education and the Concrete Industry'*, 29-30 June, Birmingham, pp. 255-266.)